2011

Synthesis of a Library of Sulfated Small Molecules

Shrenik Mehta
Virginia Commonwealth University

SYNTHESIS OF A LIBRARY OF SULFATED SMALL MOLECULES

A Thesis submitted in partial fulfillment of the requirements for the degree of Master of Science at Virginia Commonwealth University.

by

SHRENIK C. MEHTA
Bachelor of Pharmacy, Mumbai Educational Trust Institute of Pharmacy, India, 2009

Director: UMESH R. DESAI
PROFESSOR, DEPARTMENT OF MEDICINAL CHEMISTRY

Virginia Commonwealth University
Richmond, Virginia
July 2011

Acknowledgement

I would like to thank Dr. Desai for his support and encouragement throughout this period. The past two years have been a great learning experience and I will carry the lessons with me throughout my life. I would like to specially thank Dr. Rajesh Karuturi and Rami Al-Horani, as they have taught me all that I know about organic chemistry today. I would like to thank my committee members, Dr. Martin Safo and Dr. Julio Alvarez for taking time off from their busy schedules to read my thesis. I would thank all our research group members, Rio, Akul, Preetpal, Tim, Aiye, May, Malaika and Pooja for making this journey a memorable one. Last but not the least, I would like to thank my friends and family for their support and encouragement.

Table of Contents

Page

List of Tables

Page

List of Figures

Page

Abstract

SYNTHESIS OF A LIBRARY OF SULFATED SMALL MOLECULES

By Shrenik Mehta

A Thesis submitted in partial fulfillment of the requirements for the degree of Master of Science at Virginia Commonwealth University.

Virginia Commonwealth University, 2011

Major Director: Umesh R. Desai
Professor, Department of Medicinal Chemistry

The discovery of heparin in 1916 resulted in a huge impact on the practice of medicine. Heparin has played a major role in alleviating thrombotic disorders and has also exhibited effects on almost every major system in the human body. Over the past few decades, more and more heparin-protein interactions have come to light. It is implicated to modulate several important processes such as cell growth and differentiation, inflammatory response, viral infection mechanism etc. More interesting is the observation that these interactions are considerably specific with regard to oligosaccharide sequences which have specific spatially oriented sulfate groups modulating the responses. However, due to the complex nature of these interactions and lack of effective computational capabilities, predicting these interactions is challenging.

An alternative approach to modulating heparin-protein interactions would be to screen a library of molecules having a diverse distribution of the negative charges and screen them against various proteins of interest to obtain valuable information about the binding/selectivity requirements. This approach would not only yield molecules with potential clinical viability, but may also yield molecules that help decipher native mechanisms regulating proteins, which is called chemical biology in today's terms. Since the difficulties associated with carbohydrate synthesis are well known, well characterized highly sulfated oligosaccharide library screening is considered nearly impossible. Thus, the main aim of this project was to develop an effective method for the synthesis of a library of variably sulfated, non-carbohydrate molecules. The library would contain varying in the number of sulfate groups, offer positional variants of the sulfate groups and provide molecules of varying length so as to afford structural diversity necessary to mimic the heparin sequences.

Previous attempts in our laboratory to synthesize such a library encountered two major problems: 1) dimerization of polyphenols due to difficult protection / deprotection strategies and 2) ineffective purification of highly water soluble sulfated molecules. To overcome the problem of protection-deprotection, "click" chemistry has been used in this work for dimerization of polyphenols without any protective groups. To overcome the second problem, a non-aqueous method of purification of highly sulfated molecules was developed, which is the first such report.

As a proof of concept, a small library of 14 sulfated monomers and dimers and 8 non-sulfated dimers was generated. The protocol for dimerization of free polyphenolic molecules in has been established to use “click” chemistry for coupling the monomers without the need to protect the free hydroxyl groups. Thus by circumventing the inefficient protection-deprotection protocol, there is a tremendous improvement in yields, ease of purification and characterization and greater productivity allowing the synthesis of more number of molecules in a relatively shorter span of time. By masking the charge of the sulfate using an appropriate counter-ion and owing to the inherent lipophilicity of the aromatic scaffold, these highly charged molecules could be purified using normal phase silica gel chromatography. This method reduced the purification time from previous over 48 hours with the aqueous method to approximately 15 minutes. Further, this purification protocol may be possibly automated so as to truly generate a large library of variably sulfated non-carbohydrate molecules for the first time.

Screening this library of 22 sulfated and unsulfated molecules against three enzymes of the coagulation cascade – factors IIa, Xa and XIa – has provided a wealth of information with regard to engineering specificity for recognition of these enzymes. The screening led to the identification of **CS3** which inhibited factor XIa with an IC 50 of ~ 5 μM and other enzymes with an IC 50 of > 500 μM as a lead candidate with high selectivity. The success of this strategy bodes well for understanding the heparin-protein interactions at a molecular level.

Chapter 1 Introduction

1.1 Discovery and development of heparin

The year 1916 marked the discovery of heparin by a medical student Jay McLean. This historic event took place in Dr. William Howell's laboratory at Johns Hopkins University.[1] Over the next few decades, a lot of work was done on this new entity. The components of heparin were identified to be uronic acid and glucosamine in 1928 and 1935-1936 by Howell and Jorpes - Bergstrom respectively.[2] However, it was not until 1940, that evidence for presence of a high sulfation pattern in heparin was provided by Jorpes and Charles.[3] In 1968, Perlin et al. finally confirmed that *L*-iduronic acid was the uronic acid in heparin.[4] Thus, it was concluded, that heparin is a highly sulfated polysaccharide consisting of repeating iduronic acid and glucosamine units linked in a 1-4 manner **(Figure 1)**. In spite of it being discovered almost 20 years ago, it was not until 1935 that sufficiently purified heparin could be obtained for testing its efficacy against post-operative thrombosis and thrombo-embolic disease in human subjects.[5,6] This preparation, credited to the effort of Charles and Scott in Toronto and Jorpes in Stockholm, however, occasionally led to fever, chills, joint pain and other short term side effects.[6] With better purification techniques, better understanding of the coagulation cascade and development of fractionated heparin in the form of low molecular weight heparin (LMW) heparin has formed an important part of drug therapy worldwide.[7]

Figure 1 **General structure of heparin** (Figure adapted from Henry, B. L.; Desai, U. R. Recent developments in the direct inhibition of coagulation proteinases-inhibitors of the initiation phase. *Cardiovasc. Hematol. Agents Med. Chem.* **2008,** *6,* 323-336).

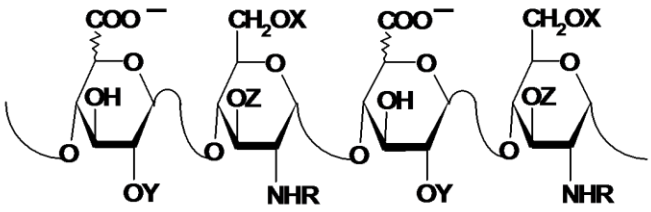

X, Y and Z = –H or $–OSO_3^-$;R = $–COCH_3$ or $–OSO_3^-$
Heparin (M_W = ~15,000 Da); LMW-heparin (M_W = ~5,000 Da)

1.2 Heparin-protein interactions

Heparin is well known for its interactions with the proteins of the blood coagulation cascade. However, heparin and its derivatives have been shown to interact with a number of other proteins as well. In the circulatory system, heparin binds to and activates the antithrombin mediated inhibition of factor Xa, factor XIa and thrombin which are essential protein in the coagulation cascade. The end result of this inhibition is delaying of the clotting process. Heparin is also well known to affect various growth factors such as fibroblast growth factor (FGF), vascular endothelial growth factor (VEGF), endothelial factor (EF) and it is thus implicated as an anti-cancer agent. Its role in inflammatory processes is attributed to its interactions with endotoxin, tissue necrosis factor-α (TNF-α), neutrophils, adhesion molecules expressed on endothelial and leukocyte cell surface etc. Finally, preventing viral binding and internalization by recognizing viral coat proteins, heparin exhibits anti-viral properties **(Figure 2).**

Figure 2 Heparin-protein interactions. (Figure adapted from Capila, I.; Linhardt. R. J. Heparin-protein interactions. *Angew. Chem. Int. Ed.* **2002,** *41*, 390-412.)

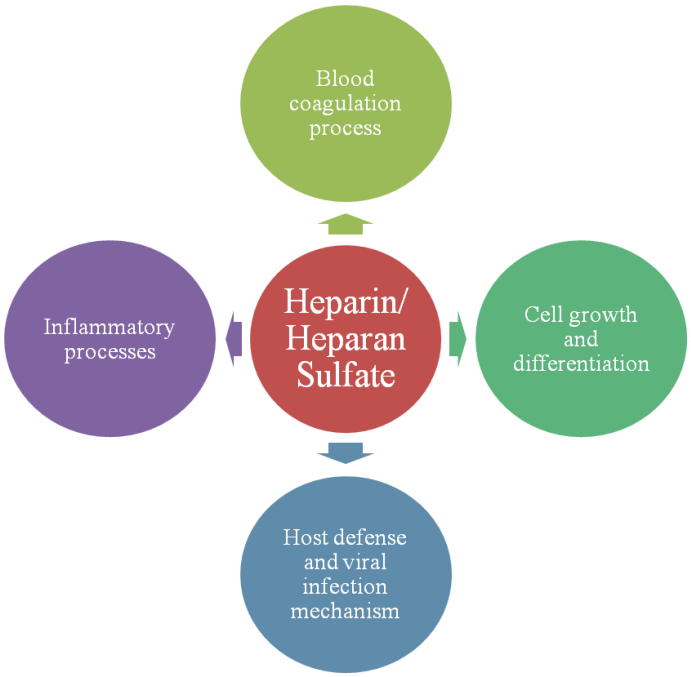

1.2.1 Regulation of proteases

Heparin-antithrombin III is the first and most well studied heparin-protein interaction. The potency of heparin as an anticoagulant is mainly due to its ability to accelerate the antithrombin III mediated inhibition of thrombin and factor Xa. Serine protease inhibitors (SERPIN) form inactive complexes with serine proteases, which are then cleared from the body. More than 40 proteins belong to the serpin family. Antithrombin (AT) is one such protein.[8] The mechanism by which this antithrombin mediated inhibition of serine protease occurs is called the serpin mouse trap mechanism. The reactive center loop (RCL) of antithrombin contains P1-P1' residues which bind to

the target serine protease. The P1-P1' bond is scissile and as soon as the Michaelis-Menten complex (E:AT) is formed, this bond is cleaved. This results in the formation of the acyl-enzyme intermediate (E-AT), whose rearrangement leads to subsequent disruption of the catalytic triad of the enzyme (E*-AT*). Mutational changes in AT may lead to competition from a parallel pathway known as the substrate pathway. This leads to hydrolysis of the acyl-enzyme intermediate (E-AT), thus releasing the active enzyme (E) and the cleaved inhibitor (ATc) **(Figure 3).** In the presence of heparin, there is a 10^2-10^6 fold increase in the rate of inhibition of fIIa, fXa, and fXIa.[9,10]

The pentasaccharide sequence of heparin containing 5 residues DEFGH interacts with AT **(Figure 4).** Depending on the length of sequence binding, AT can inhibit the proteases by two mechanisms. Once the pentasaccharide is recognized by the AT, it leads to a change in conformation of the partially inserted RCL, followed by its accelerated cleavage.[9,11,12] The second mechanism is the bridging mechanism, where binding of the AT to UFH is followed by non-specific binding of thrombin along the polysaccharide chain. The Michaelis-Menten complex (E: AT) is then formed by the diffusion of thrombin along the chain **(Figure 5).** [13]

Figure 3 A representation of the AT inhibition mechanism for serine proteases

(Figure is adapted from Desai, U. R. New antithrombin based anticoagulants. *Med. Res. Rev*. **2004,** *24*, 151-181).

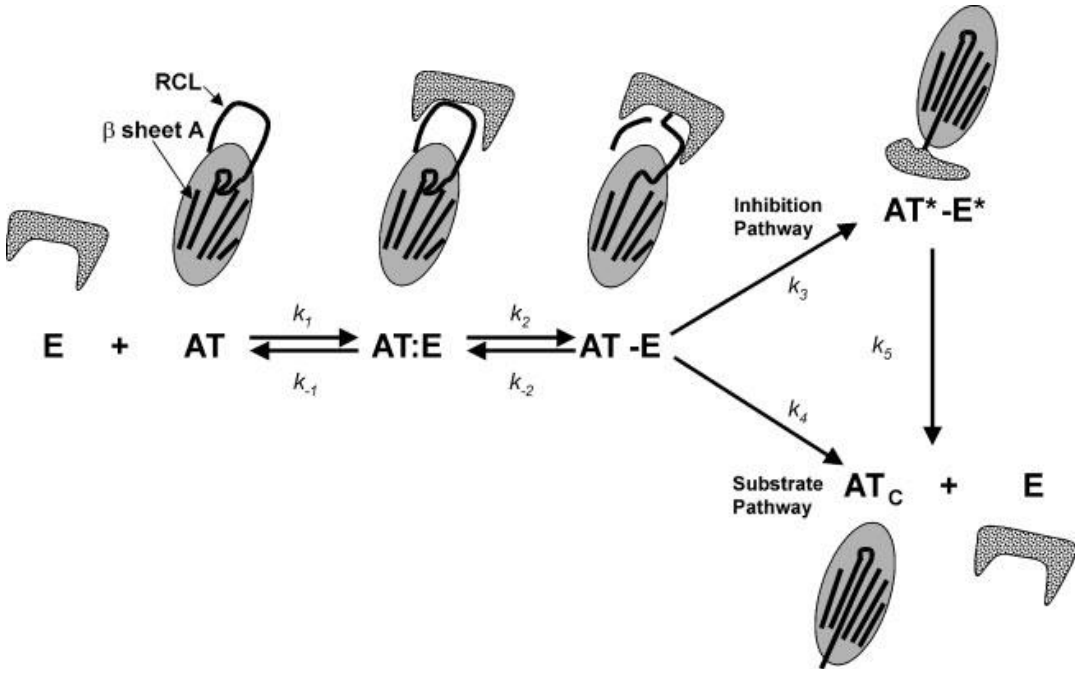

Figure 4 The pentasaccharide binding sequence

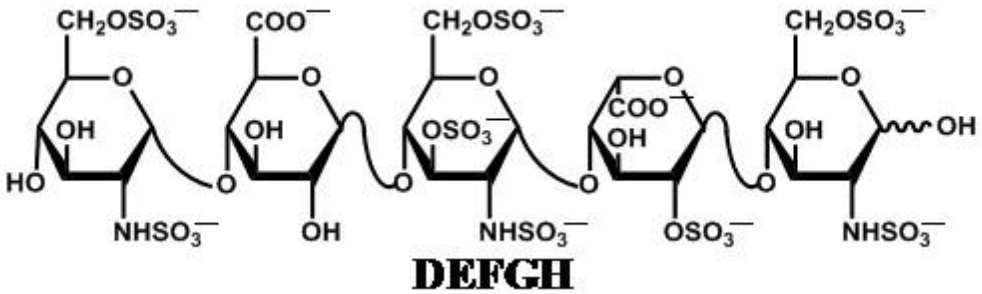

Figure 5 The mechanisms of antithrombin inhibition of proteases in the presence of heparin (Figure adapted from Desai, U. R. New antithrombin based anticoagulants. *Med. Res. Rev.* **2004,** *24*, 151-181).

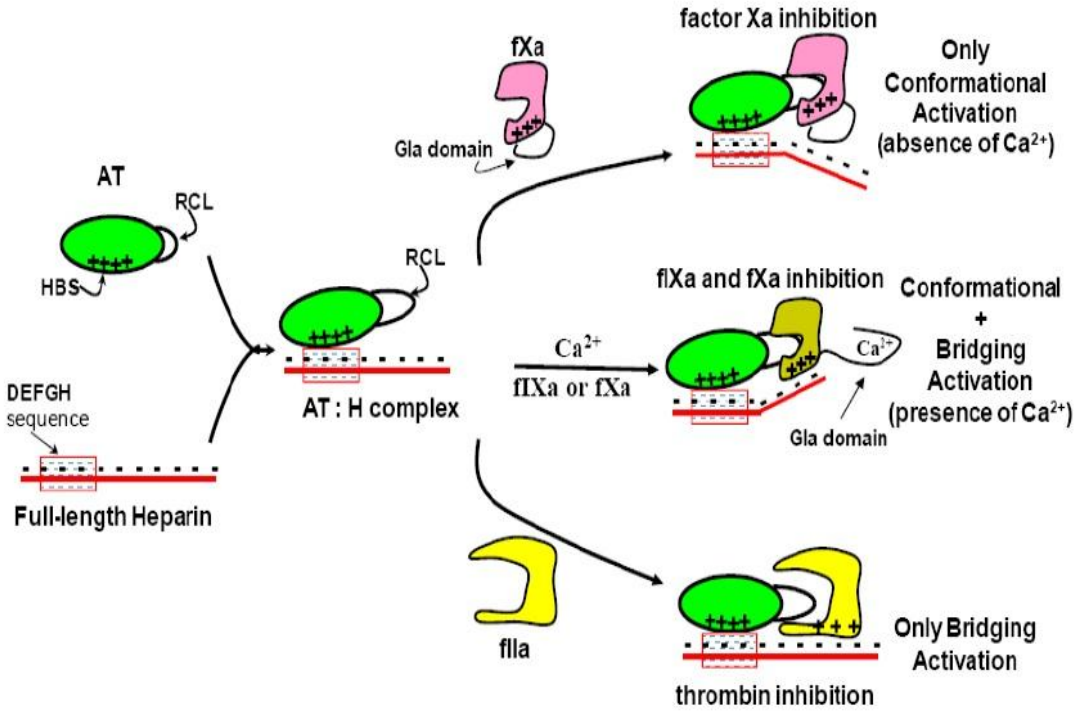

1.2.2 Regulation of cell growth factors

Growth factors or fibroblast growth factors (FGF's) are a group of 23 proteins that are implicated in a variety of physiological processes such as cell proliferation, differentiation, morphogenesis and angiogenesis.[14] Since the first evidence of inhibition of vascular smooth muscle cell growth by heparin in 1977, followed by the advent of heparin-agarose columns to purify growth factors in 1984, heparin and heparan sulfate's (HS) roles in cell growth and regulation are now well established facts.[15,16] Heparin and cell surface HS play a dual role in stabilizing the binding of FGF to the fibroblast growth factor receptor (FGFR) and also promoting dimerization and subsequent of the FGFRs.[17] Besides, the affinity of vascular endothelial growth factor (VEGF) and epidermal growth factor (EGF) are also enhanced by HS and heparin.[18,19] In addition, heparin and HS have the ability to directly affect receptor signaling and in turn modulate cell growth, independently without the involvement of protein ligands such as growth factors by direct interaction with 'heparin receptors.[20] Considering the close modulation of cell signaling and growth, their involvement in cancer is fairly intuitive and their role in tumorigenisis, angiogenesis and metastasis is well documented.[21,22]

1.2.3 Regulation of inflammatory processes

The existence of a subtle relationship between thrombosis and inflammatory diseases both in the vascular and cardiovascular systems.[23] A well known representation of this phenomenon is the attainment of a hypercoagulable state due to generation of tissue factor (TF). This generation of tissue factor is the final outcomes of the various downstream pro-inflammatory responses due to exposure to interleukins or *E. coli*

endotoxin. We can thus conclude that coagulation and inflammation may be regulated by common molecules. The anti-inflammatory actions of heparin and HS are well documented.[24, 25] This anti-inflammatory effect has been attributed to a number of interactions including but not limiting to endotoxin, tissue necrosis factor-α (TNF-α), neutrophils, adhesion molecules expressed on endothelial and leukocyte cell surface etc.[26-28] Clinically, heparin has displayed the potential to be therapeutic in managing ulcerative colitis and Chron's disease.[29,30] Surprisingly, during the course of these studies, no hemorrhagic complications were observed. It is thus hypothesized that heparin's anti-inflammatory effect may be distinct from its anticoagulant effect.

1.2.4 Role in viral infection mechanism

The most important step in the pathogenesis of a virus is the initial attachment of the virus to the target cell surface.[2] This initial binding of the viral envelope to specific receptors on the cell surface are followed by the internalization of the viron by fusion of the viral envelope with the cell membrane. Since HS are found on most cell surfaces, their role in viral binding and entry is not surprising.[31] The importance of heparin and HS is further emphasized by the reduced binding of viruses to cells both in the absence of cell surface HS and in the presence of heparanases (enzymes cleaving HS).[32] Thus, in the presence of soluble heparin or HS, viral infections are reduced as they bind to the virus and prevent it from binding and internalizing into the cell. This fact has been exploited to inhibit a number of viruses. Heparin shows anti-HIV activity by binding to the V3 loop which contains the viral surface glycoprotein gp120. It does not prohibit the virus from binding to the CD4 cells, but does not allow membrane fusion to take place.[33] It has been

well demonstrated that viral entry of herpes simplex virus (HSV) both 1 and 2, along with other viruses of the herpes family such as human cytpmegalovirus (CMV), human herpes virus (HMV) and varicella zoster virus (VZV) require HS for the initial binding to host cell surface.[34] Thus, molecules similar to heparin and HS hold potential anti-viral activity by preventing viral entry into the cell. This has been previously demonstrated in our laboratory where a sulfated lignins, which could possibly be mimics of HS, displayed viral inhibition.[35]

1.3 Predicting heparin-protein interactions

As more and more heparin binding proteins (HBP) were discovered, the value of understanding these highly specific interactions was highlighted. The idea was that if the proteins which interact with heparin could be predicted, based on these specific interactions, it would be easier to exploit heparin, in terms of synthetic mimics for its use therapeutically. A summary of the various heparin-binding proteins is presented in **Table 1**.[2]

HBP	Physiological Role	Oligosaccharide size	K_d	Function of heparin
AT III	Coagulation cascade	5-mer	20 nM	Enhances activity
FGF-1	Cell proliferation, differentiation, angiogenesis etc.	4-mer to 6-mer	-	Activates signal transduction
IL-8	Pro-inflammatory cytokine	18-mer to 20-mer	6 μM	Promotes
HIV-1 gp120	Viral entry into cell	10-mer	0.3 μM	Inhibits
HSV	Viral entry and fusion	Oligosaccharide	20 μM	Inhibits

Cardin and Weintraub first investigated and tried to establish the general requirements for such heparin-protein interactions in 1989.[36] Their study comprised of a comparative correlation between the heparin binding domains of four proteins, viz. apolipoprotein B, apolipoprotein E, vitronectin and platelet factor 4. They concluded that, besides having high sequence homology, these proteins displayed common motifs. They hypothesized that heparin binding proteins should display the following two motifs. The first motif, XBBXBX ('B' stands for basic and 'X' for hydropathic amino acid residues) should be present in the β-strand conformation while the second motif XBBBXXBX should be folded in an α-helix. For the von Willebrand factor, another heparin binding protein, a third motif, XBBBXXBBBXXBBX was proposed by Sobel and coworkers.[37] These motifs were thought to play the role of probes to identify and possibly give information about the important binding requirements of heparin to various proteins. But, with discovery of more and more heparin binding proteins, these hypothesis could not be applied to all these proteins. The fundamental drawback in this method was that it concentrated on the sequence proximity of the basic residues. In reality, however, the spatial orientation is more important as the protein folding may bring residues which are far away in terms of sequence, closer together. Conversely, the heparin chain should also have specific sequences and orientations to recognize and bind to specific proteins. Heparin and HS both have sulfo and carboxyl groups displayed at regular intervals and the defined orientations of these charged groups bestows it with this high level of specificity and affinity. There are numerous examples as evidence for this spatial specificity. The 3-*O*-sulfo group of the pentasaccharide unit of heparin is most essential

for its high affinity for antithrombin.[38] Specificity within the same family of proteins has also been observed. 6-*O*-sulfo groups are not directly required for binding of FGF-2 to heparin but they are extremely important for FGF-1.[39] Thus, considering the importance of heparin-protein interactions, there lacks a suitable method to provide information about these interactions.

1.4 The need for a library of small sulfated molecules

Ionic interactions predominate the variety of ways in which heparin interacts with proteins. The spatially defined sulfo and carboxyl groups form ion pairs with specific positively charged basic amino acid residues of the protein. As we saw earlier, a number of methods to study these interactions have been tried and failed. But, it is extremely essential to get more information about theses interactions as it will prove to be extremely valuable in terms of designing better, more selectively therapeutics. Thus, if we have a library of molecules differing in number and spatial orientation of sulfate groups, it would provide us with a great deal of information about these interactions. As easy as it sounds, obtaining a 'library' of compounds is not an easy task. The scaffold must be chosen such that it has minimum synthetic complications. The yields should be high, there should be ease of purification and characterization and most importantly, the cost should be low.

1.5 Difficulties in synthesizing an oligosaccharide library

The most intuitive thing to do in this case would be to try and obtain a library of diverse sulfated oligosaccharides. However, the synthesis of oligosaccharides fail in every single requirement for library generation mentioned in the above paragraph. Even

nature for that matter, which is known for its selectivity and precision, makes saccharides in an apparent haphazard manner using a wide variety of enzymes in competition to produce a wide variety of products.[41] Also, the absence of any information carrier encoding for a specific saccharide structure makes it impossible to adapt techniques popular for protein synthesis for synthesizing these oligosaccharide libraries.[42] Additionally, saccharides are usually branched rather than linear. Two types of linkages, viz. α or β can be used to connect the monomers gives rise to a new stereogenic center with each coupling reaction. The presence of a large number of functional groups of similar reactivities (hydroxyl and amino) necessitate the development of highly selective protection and deprotection strategies.[43] Furthermore, with every glycosidic linkage, the complexity of the protection-deprotection strategy increases. The complexity of such synthesis becomes evident by the fact that greater than 15 million possible tetrasaccharides can be synthesized from the nine monosaccharides found in humans. Enzymatic synthesis of oligosaccharides was highly revered as a solution to all these problems associated with oligosaccharides. Making extensive protection-deprotection redundant, enzymes provide stereo and regioselectivity. It is thus easier to control the anomeric configurations and all this under extremely mild reaction conditions. Yet, the prohibitive cost and scarce availability of these enzymes and substrates are a major roadblock in this approach.[44] Low yields coupled with inability to accept unnatural sugars as substrates makes oligosaccharide libraries a unrealistic proposition.[45]

Despite these difficulties, groups have attempted synthesis of oligosaccharide libraries. In general three approaches are very popular for this purpose. The first method

is ‘random glycosylation’ which involves non-selective coupling of a fucosyl donor to create three sub-libraries of α-fucosylated disaccharides **(Scheme 1)**. This method yields an equiproportionate mixture of all possible trisaccharides in a single step. This method is known for its simplicity as it does not involve any complex protecting group manipulations. But, screening and hit identification is an extremely complex process as the samples are mixtures of molecules with identical molecular weight.[51] Another popular strategy is the ‘split and mix’ strategy. Mixtures of trisaccharide libraries of α/β linkage at every glycosidic linkage can be prepared. The method involves glycosylation of a monomer to form dimers with two possible linkages, which is split and reacted with two monomers to further from two possible products each **(Scheme 2)**. In this way a mixture of 16 trisaccharides can be obtained.[52] The third strategy is a ‘two-directional’ glycosylation strategy using solid support. One of the The C6 hydroxyl group of a monosaccharide is immobilized on solid support and glycosylated with three different monomers to produce three different dimers. Another hydroxyl group is then deprotected, followed by a second set of glycosylation reactions with three monomers **(Scheme 3)**. Thus, a mixture of 12 trisaccharides is obtained.[53] Although a number of other methods have also been tried and published, these three are the most popular methods. As we can see from the results, a large number of molecules can be obtained through this method, however, the mixtures are extremely difficult to separate and characterize.[43]

Scheme 1 Random glycosylation

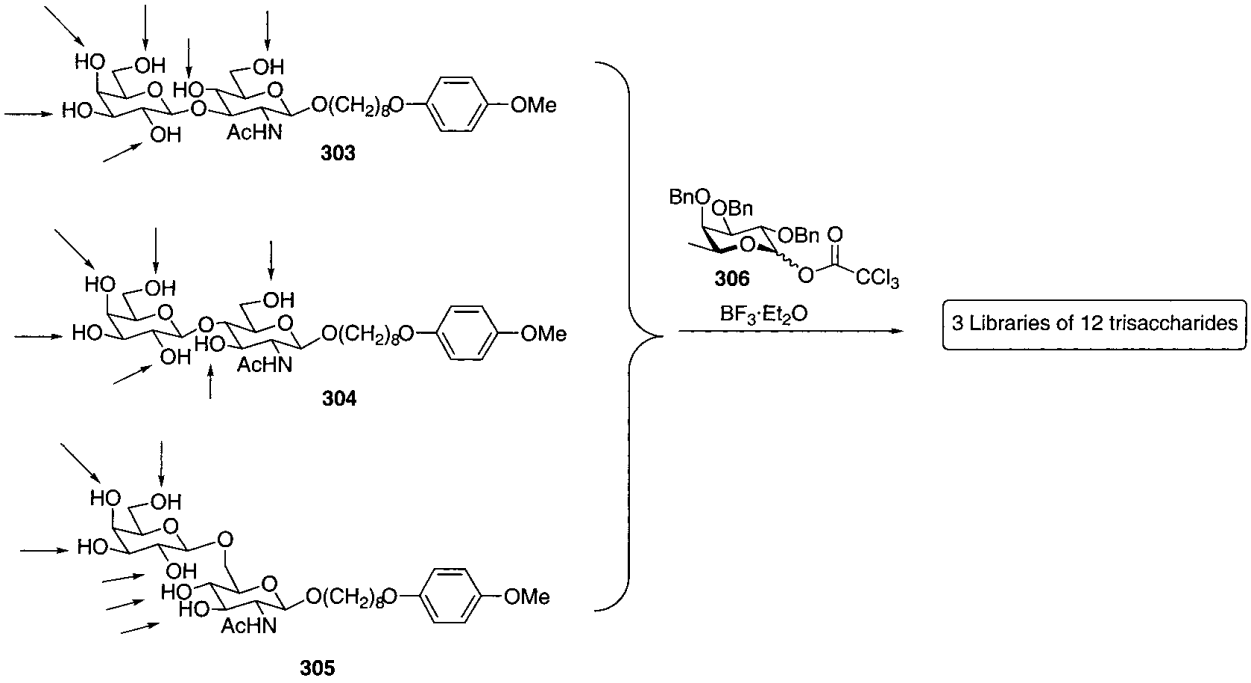

Scheme 2 Split and mix

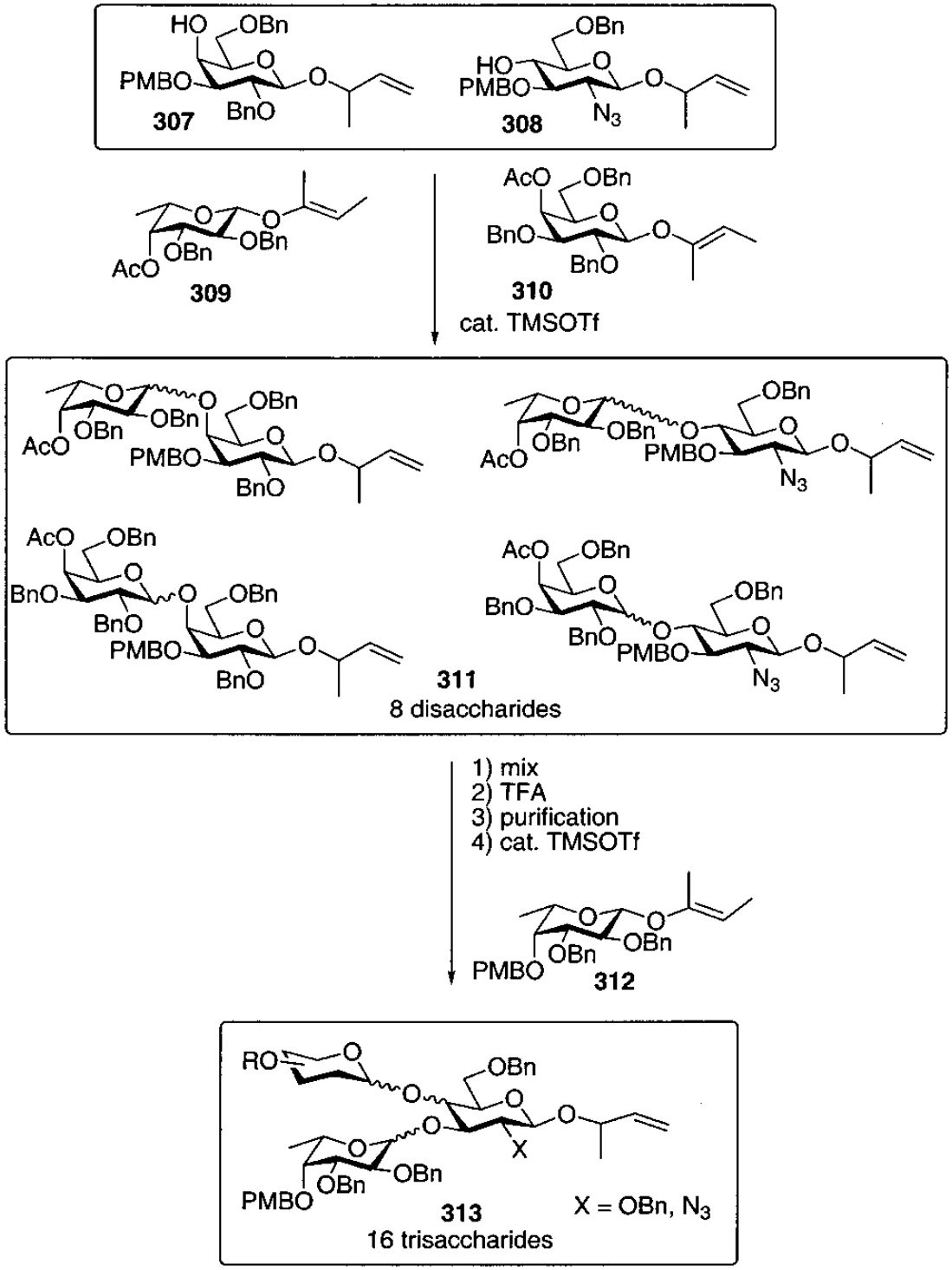

Scheme 3 Two directional glycosylation using solid support

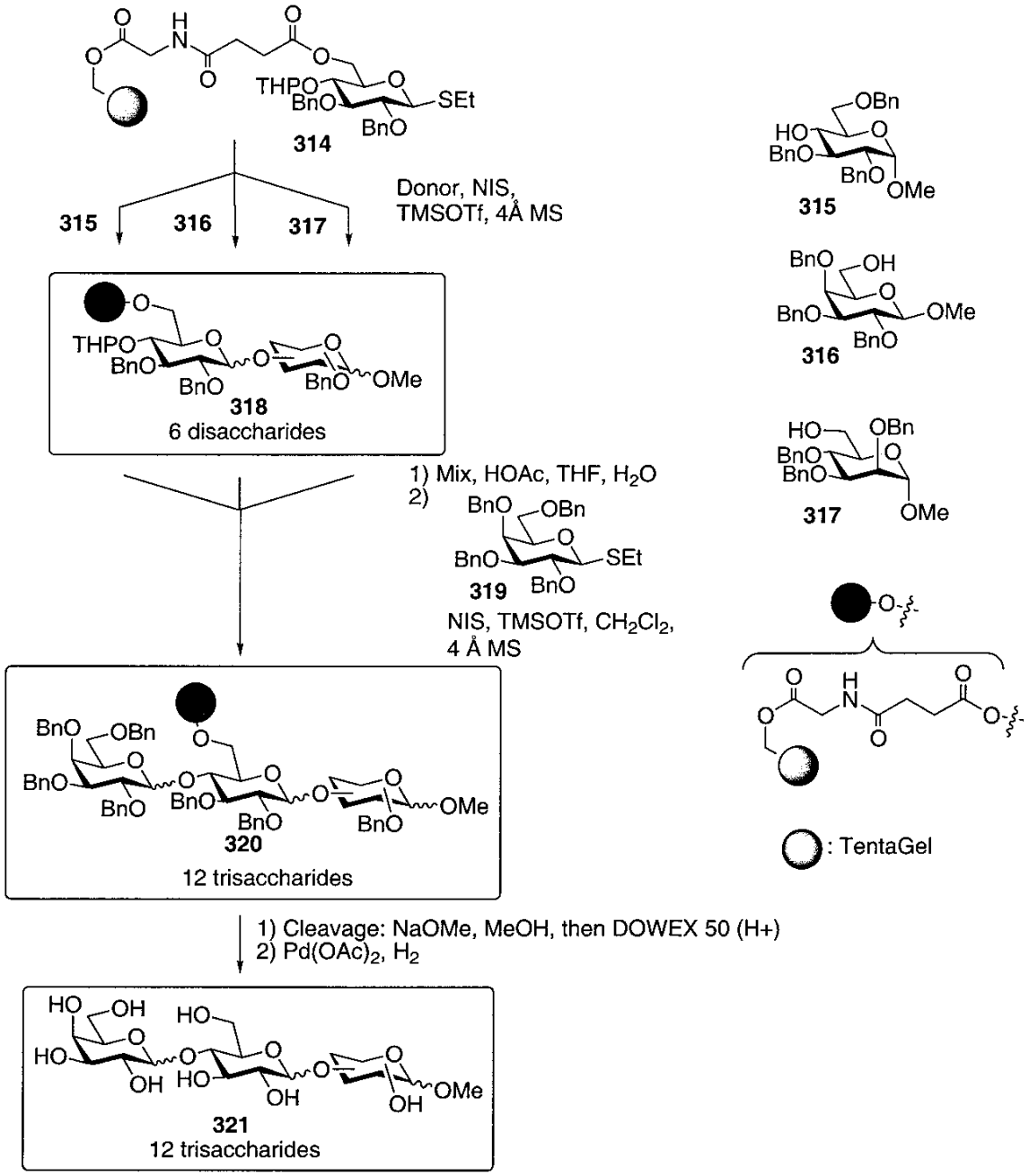

Furthermore, synthesis of a sulfated oligosaccharide library as heparin mimics adds another dimension of complexity to this already convoluted synthetic protocol. The hydroxyl groups that undergo sulfation in the end have to be selectively protected while those hydroxyl groups which will be further used to couple other monomers have to remain free.[54] This is extremely difficult to achieve considering the similar reactivities of these hydroxyl groups. Also, the formation of the oligosaccharide itself requires selective protection and deprotection strategies, thus the total number of different protecting groups used in a single monomer can be as high as five different agents.[55] In addition, the amine group, further requires a different protecting group, usually an azide.[56]

1.6 Alternate approach: Synthesis of a non-carbohydrate sulfated library

Considering the above mentioned difficulties, it would seem like a good idea to try and synthesize diverse polysulfated compounds on an aromatic backbone. The wide range of reactions, the simple purification and characterization, the simplification of structure in terms of stereochemistry and the possibility of selecting a suitable scaffold having hydroxyl groups of different reactivities will probably makes this strategy synthetically more feasible.

However, even this synthesis is riddled with many problems. The first problem was that which scaffold would effectively mimic the polysaccharide scaffold. However, previous studies in our lab concluded that the flavonoid backbone was a good representative scaffold to work on.[46] With the aim of obtaining structural diversity, it was very important to make flavonoid dimers or biflavonoids. This proved to be a major hurdle and obtaining the dimerized polyphenol with sufficient purity and yield was an

extremely difficult task. For the sulfation reaction, the difficulty in achieving a per sulfated molecule increases as the number of sulfate groups increase. However, the real difficulty lies in purification of these highly charged species. Aqueous chromatographic techniques such as size exclusion chromatography are used to purify these molecules and this results in great loss of time and yields. Thus, weighing both the options, the synthesis of a library based on the aromatic scaffold, in spite of having its share of difficulties seems plausible.

1.7 The sulfation reaction

Sulfation is a single step reaction, however the change in the physico-chemical properties of molecules after sulfation is extremely drastic making such chemistry extremely difficult. Besides the solubility issues, presence of inorganic salts is also a problem.[47] Drastic reduction in the functional group transformations after sulfation, sensitivity to acidic conditions and high temperature and the necessity of using high quantities of starting material make this an extremely challenging task.[48] However, given the importance of the sulfate group in biological as well as other applications several new methods have been developed to make this reaction more efficient. One of the initial instances of chemical sulfation was demonstrated in 1965 by use of sulfuric acid. However, as obvious as it seems, this method suffered from a number of drawbacks such as scaffold degradation, dehydration, non-selective sulfation.[48] Subsequently dicyclohexylcarbodiimide-mediated sulfation and protection-deprotection strategies for sulfation where the sulfate is masked and introduced into the scaffold and eventually deprotected have been developed.[49,50] However, the most effective method for sulfation,

developed by Raghuraman et al, has been a microwave assisted sulfation method using sulfurtrioxide complexed with base such as triethylamine. The hypothesis is that ionic conduction because of coupling of the microwaves with the sulfates may produce significant rate enhancements. This protocol can tolerate a wide range of functional groups such as amides, esters, aldehydes as well as alkenes. Besides the significant enhancement in yields (~70-95%) and short reaction duration (30 mins) makes this perfect for library synthesis.[47]

1.7 Specific aims

In order to synthesize a library of small sulfated molecules, the following synthetic difficulties have to be overcome.

1. Choosing a scaffold similar to the flavonoids, however offering greater synthetic ease.
2. Dimerization of molecules with high yields and easy purification
3. Developing alternate means to purify sulfated molecules with enhanced yields.

To overcome the synthetic difficulty associated with the flavonoid scaffold, the quinazolinone scaffold was selected. These two scaffolds share identical geometry, however, the presence of the amide hydrogen in the quinazolinone makes manipulation of the scaffold easy for subsequent dimerization **(Figure 6)**.

Figure 6. Comparison of the flavone and quinazolinone scaffold

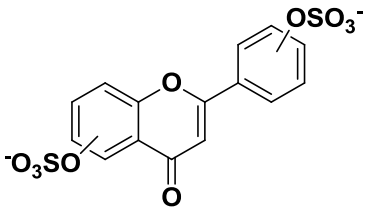

Sulfated flavone

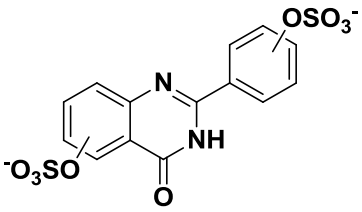

Sulfated quinazolinone

Previously a number of strategies have been tried to dimerize the molecules. However, all these techniques required deprotection after dimerization to yield the polyphenol. This proved to be an extremely difficult step as the result was a complex mixture of partially deprotected molecules which was impossible to purify. The next logical step was to devise a way to dimerize the monomers without having to protect them, thus in turn removing the need for deprotection. The answer lied in one of the most popular reactions of recent times. Click chemistry consists of a copper catalyzed reaction where an azide containing monomer and an alkyne containing monomer are coupled by the formation of a triazole. The beauty of this reaction is that it can be carried out in the presence of free hydroxyl groups under mild conditions in good yields. Thus the problematic deprotection step is bypassed. Thus, the second aim is to establish a protocol for click based dimerization of the quinazolinone monomers and subsequently, optimize the reaction conditions to afford maximum yield.

The next problem is associated with the purification of sulfated molecules. Traditionally since these are water soluble, aqueous chromatographic methods such as size exclusion chromatography have been used to purify these molecules. This led to a

substantial loss in yields. Also, since the fractions collected are so dilute, it is essential to start with large quantities to ensure detection and subsequent collection. This created a high synthetic burden. Due to the highly charged nature of these molecules, non-aqueous purification techniques are never considered. However, if we closely study the structure of these scaffolds, there is actually a higher percentage of lipophilic groups. Thus, the charge can be masked effectively, non-aqueous purification may be possible for these molecules. So the third aim will be to try using non-aquous purification techniques for the sulfated molecules and try and eventually try and achieve this using flash chromatography in order to save time, maximize yields and afford small sample size.

The last and final aim will be to screen this library for direct inhibition of thrombin, factor Xa, factor XIa and indirect inhibition of factor Xa via antithrombin. First an initial screening using 500 μM concentration of the synthesized compounds will be performed and residual enzyme activity will be calculated. If any of the molecules show a 100% reduction in enzyme activity at this concentration, then the IC50 will be calculated for that molecule. Subsequently for any promising results, Michaelis-Menten kinetics experiment will be performed in order to get more information about the type of inhibition and binding site. Finally, the results for all the enzymes will be compared and correlated to obtain valuable information about the binding requirements, selectivity requirements etc.

Chapter 2 Synthesis and Biological Evaluation of Sulfated Quinazolinone Monomers, Dimers and Poly-Phenolic Dimers

2.1 Synthesis of the core quinazolinone scaffold

The quinazolinone core structure was formed by a condensation reaction between anthranilamide and suitably substituted benzaldehyde. Depending on the substitution on the benzaldehyde, different monomers viz. **1L, 1M, 1N, 1O, 1P, 1Q** and **1R** were formed respectively. The products were formed in 45 - 65 % yields which decreased with increasing number of free hydroxyl groups. Standard water-ethyl acetate work up led to significant precipitation which drastically reduced the yield. With an aim to prevent this loss during work up two strategies were tried. First, we tried to reduce the volume of the reaction mixture to 5 ml and directly subjected it to flash chromatography without any work up. The result was inefficient separation and no improvement in yields. Next was a 'hot' work up strategy . The reaction was monitored through TLC and once the reaction was complete, the temperature of the oil bath was reduced to 65° C. Water and ethyl acetate were added to this hot solution and stirred for 10 minutes. This hot solution was then transferred to a separating funnel, shaken vigorously and then separated immediately. The water layer was further given two more washing with hot ethyl acetate to ensure complete extraction of product. This procedure prevented precipitation and

increased the overall yield to 60%. Another problem encountered was in the separation of unreacted anthranilamide from the product as they both displayed similar R_f values. To counter this the substituted benzaldehyde was taken in slight excess (1.2 equivalents as compared to 1 equivalent of anthranilamide) to ensure consumption of all the anthranilamide.

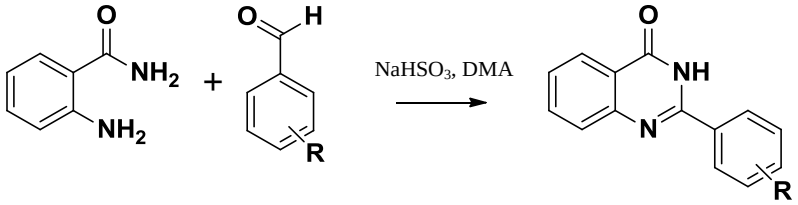

1

2A : 3-OH
2B : 3,5-OH
2C : 3-OCH_3, 4-OH
2D : 3-OH, 4-OCH_3
2E : 2-OCH_3, 3-OH, 4-OCH_3
2F : 2-OH, 4-OH
2G : 2,4,6-OH

1L : 3-OH
1M : 3,5-OH
1N : 3-OCH_3, 4-OH
1O : 3-OH, 4-OCH_3
1P : 3-OCH_3, 4-OH, 5-OCH_3
1Q : 2-OH, 4-OH
1R : 2,4,6-OH

2.1.2 Protection of quinazolinone monomer

When selecting the protecting group, four important qualities were considered, viz. stability of the protecting group during other reactions, ease of deprotection, easy purification and short reaction time. Initially, trimethyl silane (TMS) was used as it satisfies all the above conditions. However, in the subsequent reactions, TMS was not found to be stable to potassium carbonate. Thus, diphenyl t-butyl silyl (TBDPS) was tried, but it suffered from low yields. Acetyl was later found to be the most effective protecting group. It has a number of options for deprotection from extremely strong reagents like 3M hydrochloric acid, mild reagents like lithium hydroxide to extremely

selective agents like pyrrolidine. Reaction times are longer and yields relatively poorer as compared to TMS but better than TBDPS. As, the two most important condition were satisfied, acetyl was the protecting group of choice.

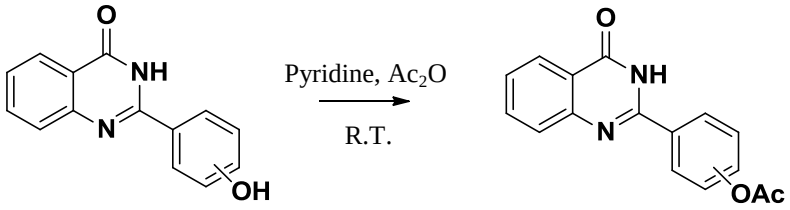

1L : 3-OH
1M : 3,5-OH
1N : 3-OCH_3, 4-OH

2L : 3-OAc
2M : 3,5-OAc
2N : 3-OCH_3, 4-OAc

2.1.3 Synthesis of propargylated quinazolinone monomer

This is a simple S_N2 type of reaction. The proton attached to '*N'* is fairly acidic as the charge is resonance stabilized by the carbonyl group. Thus, it can be readily abstracted using a base. This then acts as the nucleophile. In this case potassium carbonate was used as base. Dimethyl formamide (DMF), a polar aprotic solvent is used to prevent solvation of the nucleophile which could prevent it from displacing the leaving group, i.e. the bromide.

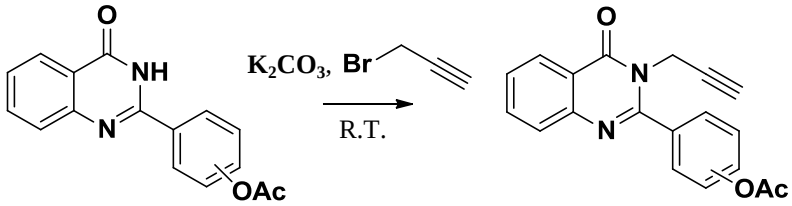

2L : 3-OAc
2M : 3,5-OAc
2N : 3-OCH_3, 4-OAc

3L : 3-OAc
3M : 3,5-OAc
3N : 3-OCH_3, 4-OAc

2.1.4 Deacetylation of propargylated quinazolinone monomer

Four different conditions were tried for this step. The results are summarized in the **Table 2** below. Note that deacetylation was observed in all four cases.

Reagent	Observed Result
3M HCl / Acetonitrile	Displacement of side chain
K_2CO_3 / Methanol	Displacement of side chain
Pyrrolidine (neat)	No displacement of side chain but low yield
Lithium hydroxide / THF	Complete deacetylation & no side chain displacement

First 3M HCl was used but significant deprotection was observed as side-products. Alkaline conditions such as potassium carbonate in methanol also yielded the same result. This phenomenon is thought to occur due to resonance stabilization of the propargyl cation which makes it a good leaving group.

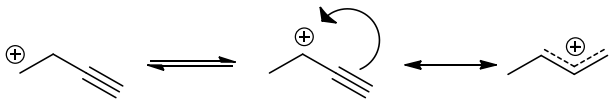

It was then hypothesized that using mild reagents might prevent this from occurring. Thus, lithium hydroxide in tetrahydrofuran (THF) was tried. As expected, the side-chain remained intact along with successful deacetylation. The only problem was that as the number of hydroxyl groups increased, the reaction time proved to be very long, 10 – 15 hours. Pyrrolidine which is used for selective deprotection of phenolic

acetyl groups was hence attempted. The reaction in neat pyrrolidine takes 1-2 minutes as reported.[57] However, the extraction in 3M HCl and ethyl acetate was not efficient and led to a huge loss in yield. Thus, we utilized lithium hydroxide in THF was used for preparative purposes.

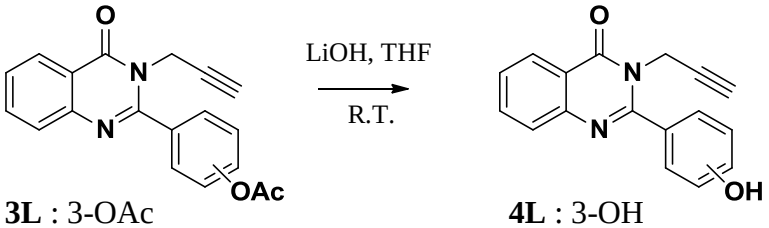

3L : 3-OAc
3M : 3,5-OAc
3N : 3-OCH_3, 4-OAc

4L : 3-OH
4M : 3,5-OH
4N : 3-OCH_3, 4-OH

2.1.5 Synthesis of quinazolinone with alkyl chloro side-chain

Similar to the propargylation reaction described in **2.3**, this is a true S_N2 type of reaction. The base used for abstraction of proton was potassium carbonate and solvent used was dimethyl formamide (DMF).

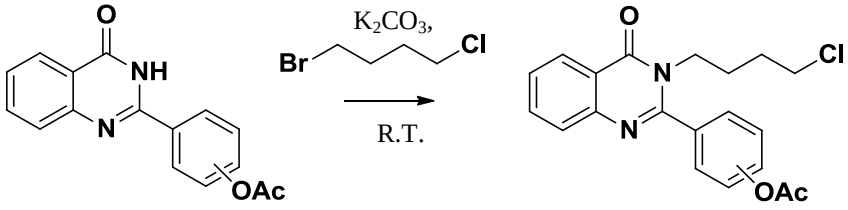

2L : 3-OAc
2M : 3,5-OAc
2N : 3-OCH_3, 4-OAc

5L : 3-OAc
5M : 3,5-OAc
5N : 3-OCH_3, 4-OAc

2.1.6 Conversion of chloro to azide

Two different parameters had to be explored in order to optimize this reaction - solvent and reaction temperature. The results of solvent manipulation are summarized in the **Table 3** below

Solvent	Outcome
Ethanol	No conversion along with deprotection
DMF	Complete conversion along with partial deprotection

When ethanol was used as solvent, the chloride could not be displaced, however, the acetyl protecting groups were lost. Using DMF as an aprotic polar solvent resulted in the formation of the azide, which was confirmed by its characteristic IR peak at 2100 cm^{-1}. But TLC and NMR indicated partial deprotection of the acetyl groups. Thus, to overcome this phenomenon, the effect of temperature on deacetylation in presence of azide was studied. The results are summarized in the **Table 4** below. Note that the yields are rough estimates based on TLC results.

Temperature	Outcome
100° C	Partial deprotection of acetyl group (60%)
90° C	Partial deprotection of acetyl group (60%)
80° C	Partial deprotection of acetyl group (50%)
70° C	Partial deprotection of acetyl group (20%)
60° C	No deprotection of acetyl group (0%)

When the reaction was carried out at 60° C, no deprotection of the acetyl group was observed. Also, since the next reaction has to be deprotection of the acetyl group, it was logical to exploit higher temperature for azide formation as well as acetyl deprotection in one step, thus improving synthetic efficiency. We tried to optimize the

reaction so as to achieve this, however, we were never able to achieve complete deacetylation. It is assumed that the excess azide is the nucleophile which leads to the deprotection of the acetyl. The equivalents of the azide, which may account for the deacetylation, were thus increased to account for all the acetyl moieties, but complete deprotection was never observed. A complex mixture of fully deprotected, mono and diacetyl products was formed and was difficult to separate. Hence, both reactions were carried out separately.

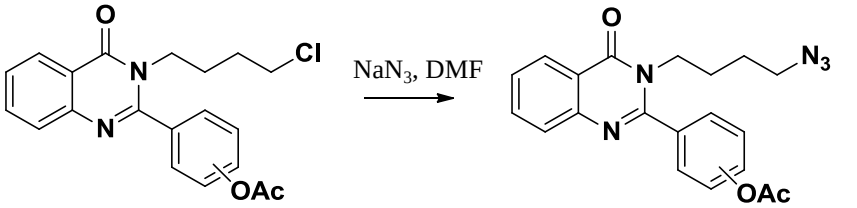

5L : 3-OAc
5M : 3,5-OAc
5N : 3-OCH_3, 4-OAc

6L : 3-OAc
6M : 3,5-OAc
6N : 3-OCH_3, 4-OAc

2.1.7 Partial and complete deprotection of quinazolinone azide

This was fairly simple to achieve as compared to the deacetylation of the propargylated monomer. The partially deprotected monomer was obtained using lithium hydroxide and THF in 3 hours.

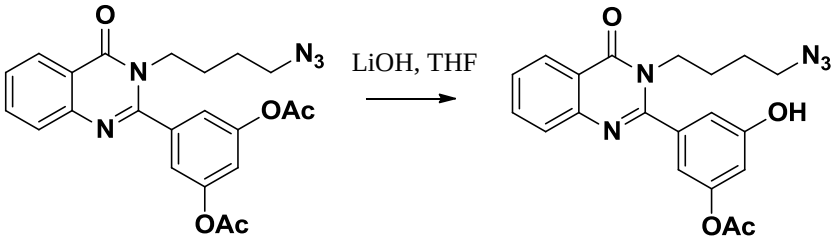

6M **7M**

Complete deprotection of quinazolinone monomer was achieved using 3M HCl.

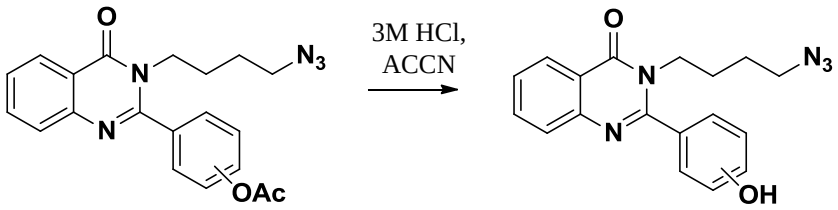

6L : 3-OAc
6M : 3,5-OAc
6N : 3-OCH_3, 4-OAc

7L : 3-OH
8M : 3,5-OH
7N : 3-OCH_3, 4-OH

2.1.8 Dimerization of quinazolinone monomers using click chemistry

A number of techniques have been adopted for dimerization of molecules. However, in case of polyphenols, it has been previously observed that protection-deprotection strategies prove to be a big hurdle in the formation of the final product.[58] The advantage of "Click" chemistry is that the final dimerization step can be performed in the presence of free hydroxyl groups. It is for this reason that the click chemistry approach was used for dimerization.

Click chemistry is a copper catalyzed regioselective cycloaddition reaction forming the 1,4 – regiomer selectively. A number of different solvent combinations along with catalyst equivalents were screened in order to optimize the reaction. The results are summarized in **Table 5** below:

Solvent Combination	Catalyst (CuSO4 : Na^+ Ascorbate)	Outcome
t- BuOH / Water (20:80)	0.3 eq : 0.5eq	No reaction
t- BuOH / Water (30:70)	0.3 eq : 0.5eq	No reaction
t-BuOH / Water (50:50)	0.3 eq : 0.5eq	No reaction
DMF / Water (30:70)	0.3 eq : 0.5eq	30 % yield
DMF / Water (50:50)	0.3 eq : 0.5eq	50 % yield
DMF / Water (50:50)	0.1 eq : 0.5 eq	80 % yield

Thus, copper catalyzed click reaction with 0.1 equivalents of copper sulfate and 0.5 equivalents of sodium ascorbate was used to dimerize the polyphenolic monomers without any protection. This reaction was performed at room temperature to ensure the formation of the 1,4 regioisomer exclusively.

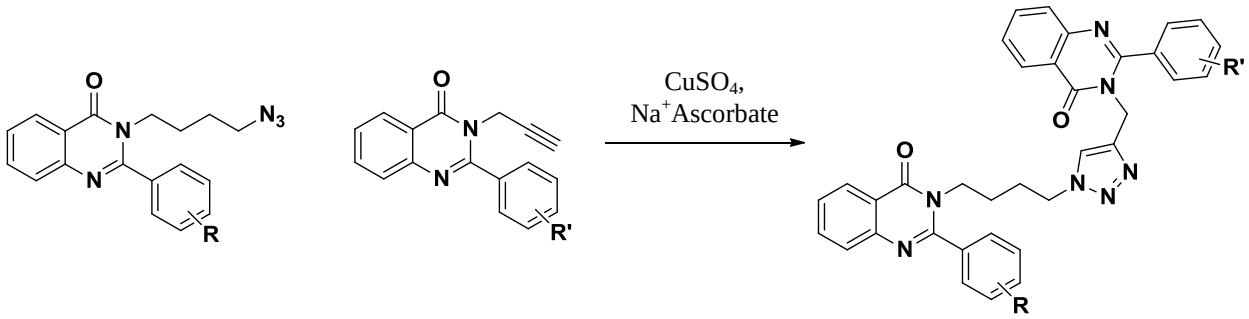

6L : 3-OAc
6M : 3,5-OAc
7L : 3-OH
7M : 3-OH, 5-OAc
8M : 3,5-OH
7N : 3-OCH_3, 4-OH

3L : 3-OAc
4L : 3-OH
4M : 3,5-OH
4N : 3-OCH_3, 4-OH

R / R'
C1 : 3-OAc / 3-OH
C2 : 3-OH / 3-OAc
C3 : 3-OH / 3-OH
C4 : 3-OAc, 5-OH / 3-OH
C5 : 3-OH, 5-OH / 3-OH
C6 : 3-OH / 3-OH, 5-OH
C7 : 3-OAc, 5-OAc / 3-OAc, 5-OAc
C8 : 3-OAc, 5-OH / 3-OH, 5-OH
C9 : 3-OH, 5-OH / 3-OH, 5-OH
C10 : 3-OMe, 4-OH / 3-OMe, 4-OH

2.1.9 Sulfation of quinazolinone monomers and dimers

Sulfation of the quinazolinone monomers and clicked dimers was achieved using microwave assisted sulfation reaction in the presence of a base, triethyl amine. For the first time, we report a non-aqueous method of purification for these sulfated molecules. Contrary to popular belief, these highly charged molecules can be purified using normal phase silica gel chromatography. In this case we used flash chromatography. Since the sulfation reaction is done in the presence of base triethyl amine, the counter ion for the sulfate group after the reaction is triethyl amine. We hypothesize, it is because of the charge masking effect of this group that the separation using flash chromatography is possible. The solvent system used to make this separation possible was dichloromethane/methanol (0-20%). This method of purification was used for molecules with up to four sulfate groups with great ease and efficiency. The development of this method of purification has increased efficiency and yields in the process of making sulfated organic molecules. Thus synthesizing a large library of sulfated organic molecules is now less of a time consuming, labor intensive process. Once purified, the counter ion was exchanged with sodium to form the more stable sodium salt of the sulfated organic molecules.

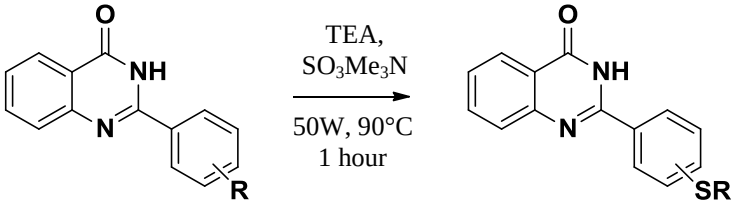

1L : 3-OH
1M : 3,5-OH
1N : 3-OCH_3, 4-OH
1O : 3-OH, 4-OCH_3
1P : 2-OCH_3, 3-OH, 4-OCH_3
1Q : 2-OH, 4-OH
1R : 2,4,6-OH

1S : 3-SO_3^-
2S : 3,5- SO_3^-
3S : 3-OCH_3, 4- SO_3^-
4S : 3- SO_3^-, 4-OCH_3
5S : 2-OCH_3, 3-SO_3^-, 4-OCH_3
6S : 2,4- SO_3^-
7S : 2,4,6- SO_3^-

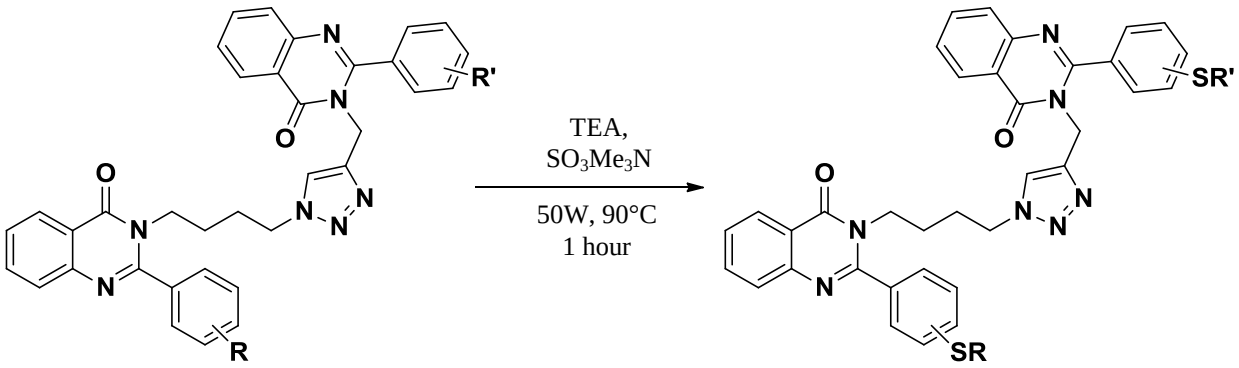

R / R'
C2 : 3-OH / 3-OAc
C3 : 3-OH / 3-OH
C4 : 3-OAc, 5-OH / 3-OH
C5 : 3-OH, 5-OH / 3-OH
C7 : 3-OAc, 5-OH / 3-OH, 5-OH
C8 : 3-OH, 5-OH / 3-OH, 5-OH
C9 : 3-OMe, 4-OH / 3-OMe, 4-OH

R / R'
CS2 : 3-SO_3^- / 3-OAc
CS3 : 3-SO_3^- / 3-SO_3^-
CS4 : 3-OAc, 5-SO_3^- / 3-SO_3^-
CS5 : 3,5-SO_3^- / 3-SO_3^-
CS7 : 3-OAc, 5-SO_3^- / 3,5-SO_3^-
CS8 : 3,5-SO_3^- / 3,5-SO_3^-
CS9 : 3-OMe, 4-SO_3^- / 3-OMe, 4-SO_3^-

2.2 Experimental section

2.2.1 General methods

Reagents/chemicals were purchased from Sigma-Aldrich (unless specified otherwise) and used as supplied. Analytical thin layer chromatography (TLC) was performed using UNIPLATE™ silica gel GHLF 250 μm pre-coated plates (ANALTECH, Newark, DE) with a fluorescence indicator (254 nm). Flash chromatography was performed using Combi Flash®Rf flash chromatographer (TELEDYNE ISCO, Lincon, NE) with pre-packed RediSep®Rf silica gel columns. Microwave-assisted sulfation reactions were performed using CEM-Discover (Matthews, NC) synthesizer in sealed reaction vessels (7 ml). The reaction condition was set to ramp to 90°C at 30 W and was maintained by cooling with nitrogen at 45 psi.

SP Sephadex-Na chromatography (cation exchange) was performed using flex columns (KIMBLE/KONTES, Vineland, NJ) of dimensions 75 × 1.5 cm. Cation exchange was performed using 30 fold excess of sodium ion equivalents. Samples were chromatographed at a controlled flow rate of 0.5 ml/min using water as eluent. Fractions of 5 ml each were collected and analyzed with a using thin layer chromatography (TLC) under conditions mentioned above.

^{1}H NMR and ^{13}C NMR were recorded on Bruker Ultrashield™ Plus-400MHz spectrometer in $CDCl_3$, DMSO-d_6, CD_3OD, $CO(CD_3)_2$ or D_2O. All signals were reported in ppm with residual $CDCl_3$, DMSO-d_6, CD_3OD, $CO(CD_3)_2$ or D_2O signals at 7.26, 2.50, 3.31, 2.05 and 4.79, respectively, as standards. The data is reported as chemical shifts (ppm), multiplicity (s = singlet, d = doublet, t = triplet, m = multiplet), coupling

constant(s) (Hz) and integration. ESI mass spectra were recorded using Waters Acquity triple quadrupole mass spectrometer. Samples were dissolved in either methanol or 5% formic acid in water and infused at a rate of 20µl /min. Mass scans were obtained in the range of 200-1200 amu at a scan rate of 400 amu/sec. Ionization conditions were optimized for each compound to maximize ionization of the parent ion. The capillary voltage was varied between 3.0 to 5.0 kV, while cone voltage ranged from 28 to 35 V. For all experiments, the extractor voltage was set to 3.0 V, the Rf lens voltage to 0.1 V, source block temperature to 150° C and desolvation temperature to 250° C.

Proteins – Human coagulation factors Xa, IIa (α-thrombin) and XIa were purchased from Haematologic Technologies (Essex Junction, VT). Stock solutions of proteins were prepared in 20 mM sodium phosphate buffer, pH 7.4, containing 100 mM NaCl and 2.5 mM $CaCl_2$ (thrombin and factor XIa) or 5 mM MES buffer, pH 7.4 (factor Xa). Chromogenic substrates Spectrozyme TH was purchased from American Diagnostica (Greenwich, CT) while substrate Chromogenix S-2765 (factor Xa) and Chromogenix S-2366 was from DiaPharma group, Inc (west Chester, Ohio).

Figure 7 General reaction scheme

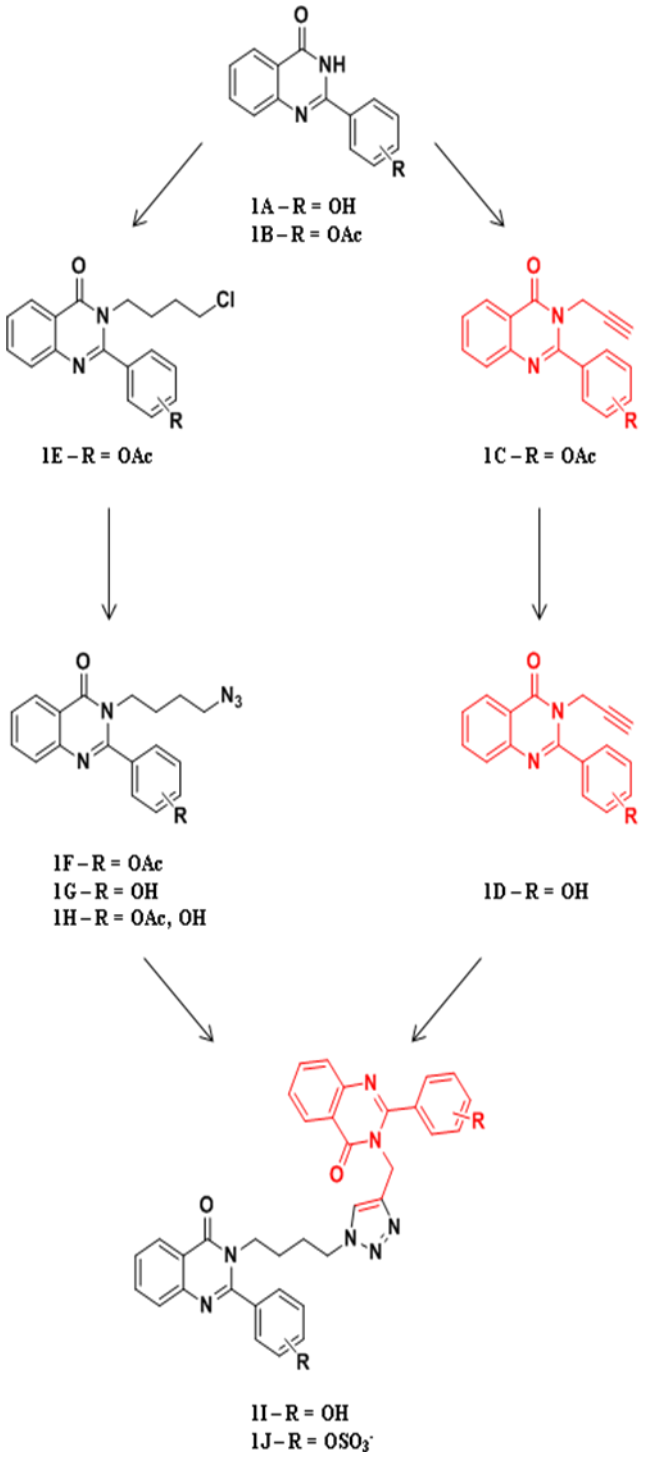

2.2.2 General procedure for synthesis of quinazolinone core structure

To a solution of anthranilamide **1** (1.0 equiv) in dimethyl acetamide were added the substituted benzaldehyde **2** (1.3 equiv) and sodium sulfate (1.0 equiv) in a single neck flask attached with a reflux condenser. The reaction mixture was vigorously stirred and heated to 145°C. After 24 hours, the hot mixture was extracted with water and ethyl acetate. The organic extract was dried (Na_2SO_4), concentrated *in vacuo* and purified using flash chromatography on silica gel (10-80% ethyl acetate in hexanes) to give **1A**.

2.2.3 General procedure for protection of quinazolinone core structure

1A was then acetylated to protect the free hydroxyl group(s) by solubilizing in dichloromethane followed by addition of pyridine (2.0 equiv per hydroxyl group) and acetic anhydride (1.0 equiv per hydroxyl group). This was vigorously stirred at room temperature and after 10 hours extracted using acidified water and dichloromethane. The organic layer was dried (Na_2SO_4), concentrated *in vacuo* and purified using flash chromatography on silica gel (10-50% ethyl acetate in hexanes) to give **1B**.

2.2.4 General procedure for synthesis of the propargylated quinazolinone monomer

To a solution of **1B** in dimethyl formamide add potassium carbonate (1.5 equiv). Allow this reaction mixture to stir for 2 minutes and add propargyl bromide (1.5 equiv). After vigorous stirring for 12 hours at room temperature, extraction using water and ethyl acetate is carried out. The organic layer was dried (Na_2SO_4), concentrated *in vacuo* and purified using flash chromatography on silica gel (10-25% ethyl acetate in hexanes) to give **1C**.

2.2.5 General procedure for deacetylation of the propargylated quinazolinone monomer

1C was deacetylated by solubilizing in THF followed by addition of lithium hydroxide. This reaction mixture was vigorously stirred for 12 hours after which **1D** was obtained by the extraction and purification method mentioned above.

2.2.6 General procedure for addition of chloro alkyl side chain to quinazolinone scaffold

To a solution of **1B** in dimethyl formamide was added potassium carbonate (1.0 equiv) and stirred for two minutes. This was followed by addition of 1-bromo-4-chlorobutane and vigorous stirring for 12 hours. Extraction and purification by the above mentioned method yields **1E**.

2.2.7 General procedure for conversion of chloro to azide

1E was then solubilized in dimethyl formamide in a flask attached to a reflux condenser and sodium azide (1.5 equiv) was added to it. The reaction mixture was vigorously stirred at 60°C to yield **1F** after extraction and purification. The formation of **1F** was confirmed using IR as azides show characteristic IR peak at 2100 cm^{-1}.

2.2.8 General procedure for deacetylation of quinazolinone azide monomer

1F was deacetylated by solubilizing in acetonitrile followed by addition of 3M HCl. This reaction mixture was refluxed at 80° C for 0.5 hours after which **1G** was obtained by the extraction and purification method mentioned above.

To obtain the partially deacetylated monomer **1H**, it was solubilized in THF, followed by the addition of LiOH. Vigorous stirring at room temperature for 6 hours afforded the product.

2.2.9 General procedure for dimerization of quinazolinone monomers using click chemistry

The monomers **1D** (1.0 equiv) and **1G/1H** (1.0 equiv) were solubilized in dimethylformamide. Freshly prepared solution of sodium ascorbate in water (0.5 equiv, 0.1 mM) was added and allowed to stir. After 2 minutes, freshly prepared copper sulfate solution in water (0.1 equiv, 0.1 mM) was added. The reaction mixture was stirred vigorously for 12 hours at room temperature followed by extraction and purification to yield the dimerized quinazolinone **1I**.

2.2.10 General procedure for sulfation and sodium exchange for monomers and clicked dimers

1I was solubilized in acetonitrile with tri-ethylamine (6 equiv per hydroxyl group) in a microwave reaction tube. Sulfur trioxide trimethyl amine (6 equiv per hydroxyl group) was added and the tube sealed. The reactions parameters for the microwave reactor were set according to the previously mentioned settings. After 45minutes the reaction mixture was transferred to a round bottom flask and volume reduced as much as possible under low pressure conditions at 25°C. The reaction mixture was then directly loaded on to a flash chromatography column and purified using dichloromethane and methanol solvent system (0-20%) to obtain the sulfated dimer **1J**. This is further

chromatographed using the cation exchange column mentioned previously to obtain the sodium salt.

2-(3-hydroxylphenyl)quinazolin-4(3*H*)-one (1L). Anthranilamide (2.5 g, 18.36 mmol) and 3-hydroxybenzaldehyde (2.91 g, 23.87 mmol) were dissolved in 25 ml DMA and reacted as per **2.2.2** to yield 2.39 g (67 % yield). Theoretical yield: 4.37 g. ^{1}H NMR (400MHz, DMSO-d6) δ 8.16-8.14 (1H, m), 7.86-7.82 (1H, m), 7.73 (1H, d, *J* = 8Hz), 7.60-7.58 (2H, m), 7.54-7.50 (1H, m), 7.34 (1H, t, *J* = 8), 6.99-6.97 (1H, m) **(Figure 8).** ^{13}C NMR (100MHz, DMSO-d6) δ 162.16, 157.45, 152.32, 148.67, 134.58, 133.99, 129.66, 127.41, 126.52, 125.80, 120.93, 118.48, 118.33, 114.51 **(Figure 53).** ESI (+ve) m/z calculated for $C_{14}H_{10}N_2O_2$ $[(M+H)^+]$ 239.24, found 239.14 **(Figure 93).**

3-(4-oxo-3,4-dihydroquinazolin-2-yl)phenyl acetate (2L). 1L (1.5 g, 6.29 mmol) was dissolved in 20 ml dichloromethane followed by addition of pyridine (1.01 ml, 12.60 mmol), acetic anhydride (1.2 ml, 12.60 mmol) and reacted as per **2.2.3** to yield 1.1 g (62 % yield). Theoretical yield: 1.76 g.

3-(4-oxo-3-(prop-2-yn-l-yl)-3,4-dihydroquinazolin-2-yl)phenyl acetate (3L). 2L (0.5 g, 1.78 mmol), potassium carbonate (0.36 g, 2.67 mmol) and propargyl bromide (0.3184g, 2.67 mmol) were dissolved in 5 ml dimethylformamide and reacted as per **2.2.4** to yield 0.4g (70 % yield). Theoretical yield: 0.57g. ^{1}H NMR (400MHz, $CDCl_3$) δ 8.41 (1H, d, *J* = 7.88), 8.23 (1H, t, *J* = 1.88), 8.14-8.12 (1H, m), 7.92 (1H, d, *J* = 8.4), 7.79-7.74 (1H, m), 7.49-7.43 (2H, m), 7.19-7.14 (1H, m), 5.26 (2H, d, *J* = 2.4), 2.49 (1H, t, *J* = 2.4), 2.28 (3H, s) **(Figure 9).** ESI (+ve) m/z calculated for $C_{19}H_{14}N_2O_3$ $[(M+Na)^+]$ 341.33, found 341.16 **(Figure 54).**

2-(3-hydroxyphenyl)-3-(prop-2-yn-1-yl)quinazolin-4(3*H*)-one (4L). 3L (0.3 g, 0.94 mmol), lithium hydroxide (0.079 g, 1.88 mmol) were dissolved in 4 ml THF and reacted as per **2.2.5** to yield 0.25 g (96 % yield). Theoretical yield: 0.26 g. ^{1}H NMR (400MHz, MeOD) δ 8.18-8.16 (1H, m), 8.03-7.95 (3H, m), 7.89-7.87 (1H, m), 7.61-7.57 (1H, m), 7.34 (1H, t, *J* = 7.92), 6.98-6.95 (1H, m), 5.36 (2H, d, *J* = 2.44), 3.04 (1H, t, *J* = 1.64) **(Figure 10).** ^{13}C NMR (100MHz, MeOD) δ 166.93, 161.29, 159.18, 158.75, 153.02, 140.37, 136.89, 136.17, 135.24, 131.12, 130.46, 128.73, 128.47, 128.11, 127.98, 127.65, 124.40, 122.32, 121.04, 118.88, 118.49, 116.34, 116.05, 115.92, 79.39, 79.16, 77.30, 76.68, 74.29, 55.42 **(Figure 55).**

3-(3-(4-chlorobutyl)-4-oxo-3,4-dihydroquinazolin-2-yl)phenyl acetate (5L). 1L (1.0 g, 3.56 mmol) was solubilized in 10 ml DMF. To this potassium carbonate (0.98 g, 7.09 mmol) along with 1-bromo-4-chlorobutane (0.62, 3.61 mmol) were added and reacted as per **2.2.6** to yield 1.1 g of **5L** (83 % yield). Theoretical yield: 1.32 g. ^{1}H NMR (400MHz, $CDCl_3$) δ 8.39 (1H, d, *J* = 7.92), 8.22 (1H, t, *J* = 2.04), 8.09-8.07 (1H, m), 7.90 (1H, d, *J* = 8.36), 7.77-7.72 (1H, m), 7.47-7.41 (1H, m), 7.16-7.13 (1H, m), 4.68 (2H, t, *J* = 5.92), 3.61 (2H, t, *J* = 6.36), 2.08-1.98 (4H, m). **(Figure 11).** ^{13}C NMR (100MHz, $CDCl_3$) δ 169.45, 166.67, 158.98, 151.83, 151.00, 139.91, 133.58, 129.31, 128.07, 126.63, 125.86, 123.65, 123.39, 121.49, 115.36, 66.11, 44.62, 29.59, 29.45, 26.22 **(Figure 56).** ESI (+ve) m/z calculated for $C_{20}H_{19}ClN_2O_3$ $[(M+Na)^+]$ 370.11, found 370.21 **(Figure 94).**

3-(3-(4-azidobutyl)-4-oxo-3,4-dihydroquinazolin-2-yl)phenyl acetate (6L). 5L (0.5g, 1.35 mmol) was solubilized in 6 ml DMF. To this sodium azide (0.14 g, 2.02 mmol) was added and reacted as per **2.2.7** to yield 0.4g of **6L** (78 % yield). Theoretical yield: 0.509

g. ^{1}H NMR (400MHz, $CDCl_3$) δ 8.38 (1H, d, *J* = 7.88), 8.21 (1H, t, *J* = 1.96), 8.07-8.05 (1H, m), 7.89 (1H, d, *J* = 8.36, 7.76-7.71 (1H, m), 7.46-7.41 (2H, m), 7.17-7.13 (1H, m), 4.65 (2H, t, *J* = 6.24), 3.34 (2H, t, *J* = 6.76), 2.27 (3H, s), 2.00-1.93 (2H, m), 1.84-1.81 (2H, m) **(Figure 12).** ^{13}C NMR (100MHz, $CDCl_3$) δ 169.49, 166.66, 158.96, 151.81, 150.99, 139.90, 133.60, 129.33, 128.06, 126.65, 126.36, 125.86, 123.67, 123.39, 121.49, 115.34, 66.22, 51.15, 26.10, 25.80, 21.21 **(Figure 57).** ESI (+ve) m/z calculated for $C_{20}H_{19}ClN_2O_3$ [$(M+Na)^+$] 400.40 found 400.21 **(Figure 95).**

3-(4-azidobutyl)-2-(3-hydroxyphenyl)quinazolin-4(*3H*)-one (7L). 6L (0.4g, 1.06 mmol) was solubilized in 2 ml acetonitrile followed by addition of 2 ml 3M HCl and reacted as per **2.2.8** to yield 0.34 g (95 % yield). Theoretical yield: 0.355 g. ^{1}H NMR (400MHz, $(CD_3)_2CO$) δ 8.55 (1H, s), 8.17-8.12 (3H, m), 7.94-7.92 (1H, m), 7.89-7.85 (1H, m), 7.59-7.55 (1H, m), 7.37 (1H, t, *J* = 7.88), 7.05-7.02 (1H, m) 4.74 (2H, t, *J* = 6.36), 3.49 (2H, t, *J* = 6.84), 2.09-2.04 (2H, m), 2.03-1.91 (2H, m) **(Figure 13).** ^{13}C NMR (100MHz, $CDCl_3$) δ 167.38, 160.37, 158.46, 152.67, 140.51, 134.55, 134.25, 130.50, 130.22, 129.93, 128.69, 128.36, 127.46, 127.17, 126.37, 124.43, 124.18, 120.97, 120.71, 120.39, 118.53, 118.08, 116.39, 116.09, 115.97, 115.79, 68.56, 67.17, 51.80, 26.75, 26.45 **(Figure 58).**

2-(3,5-dihydroxyphenyl)quinazolin-4(*3H*)-one (1M). Anthranilamide (2.0 g, 14.6 mmol) and 3,5-dihydroxybenzaldehyde (2.43 g, 11.59 mmol) were dissolved in 20 ml DMA and reacted as per **2.2.2** to yield 1.43 g (45 % yield). Theoretical yield: 3.13 g. ^{1}H NMR (400MHz, CD_3OD) δ 8.24-8.21 (1H, m), 7.85-7.52 (1H, m), 7.50 (1H, d, *J* = 1.2), 7.54-7.50 (1H, m), 6.95 (2H, d, *J* = 2.12), 6.51 (1H, t, *J* = 4.36) **(Figure 14).** ^{13}C NMR

(100MHz, $(CD_3)_2CO$) δ 162.75, 159.76, 159.33, 153.14, 150.17, 136.09, 135.24, 128.60, 127.23, 127.11, 122.41, 107.02 **(Figure 59).** ESI (+ve) m/z calculated for $C_{14}H_{10}N_2O_3$ $[(M+Na)^+]$ 277.24 found 277.12 **(Figure 96).**

5-(4-oxo-3,4-dihydroquinazolin-2-yl)-1,3-phenylene diacetate (2M). 1M (1.0 g, 3.93 mmol) was dissolved in 20 ml dichloromethane followed by addition of pyridine (1.27 ml, 15.73 mmol), acetic anhydride (1.49 ml, 15.73 mmol) and reacted as per **2.2.3** to yield 1.2 g (90 % yield). Theoretical yield: 1.33 g. ^{1}H NMR (400MHz, DMSO-d6) δ 12.51 (1H, s), 8.17-8.15 (1H, m), 7.93 (2H, d, *J* = 2.08), 7.88-7.84 (1H, m), 7.76 (1H, d, *J* = 7.72), 7.58-7.54 (1H, m), 7.28 (1H, t, *J* = 2.08), 2.33 (6H, s) **(Figure 15).**

5-(4-oxo-3-(prop-2-yn-1-yl)-3,4-dihydroquinazolin-2-yl)-1,3-phenylene diacetate (3M). 2M (0.4 g, 1.17 mmol), potassium carbonate (0.326 g, 2.35 mmol) and propargyl bromide (0.28 g, 2.35 mmol) were dissolved in 5 ml dimethylformamide and reacted as per **2.2.4** to yield 0.33g (75 % yield). Theoretical yield: 0.44g. ^{1}H NMR (400MHz, $CDCl_3$) δ 8.14-8.11 (3H, m), 7.91-7.89 (1H, m), 7.79-7.76 (1H, m), 7.50-7.46 (1H, m), 7.00 (1H, t, *J* = 2.16), 5.24 (2H, d, *J* = 2.44), 2.49 (1H, t, *J* = 2.44), 2.27 (6H, s) **(Figure 16).** ^{13}C NMR (100MHz, $CDCl_3$) δ 169.00, 165.62, 157.77, 151.85, 151.18, 140.30, 133.93, 128.11, 127.07, 123.52, 118.99, 117.55, 115.14, 115.04, 54.47, 21.15 **(Figure 60).** ESI (+ve) m/z calculated for $C_{21}H_{16}N_2O_5$ $[(M+Na)^+]$ 399.36 found 399.19 **(Figure 97).**

2-(3,5-dihydroxyphenyl)-3-(prop-2-yn-1-yl)quinazolin-4(*3H*)-one (4M). 3M (0.33 g, 0.75 mmol), lithium hydroxide (0.25 g, 6.06 mmol) were dissolved in 4 ml THF and reacted as per **2.2.5** to yield 0.20 g (90 % yield). Theoretical yield: 0.22 g. ^{1}H NMR

(400MHz, CH_3OD) δ 8.19 (1H, d, *J* = 0.68), 7.96-7.87 (2H, m), 7.62-7.58 (1H, m), 7.52 (2H, d, *J* = 2.28), 6.45 (1H, t, *J* = 2.28), 5.37 (2H, d, *J* = 0.24), 3.03 (1H, s) **(Figure 17).** ^{13}C NMR (100MHz, CH_3OD) δ 166.86, 161.34, 159.73, 152.99, 141.00, 135.22, 128.46, 128.31, 124.40, 116.07, 106.09, 77.00, 54.79 **(Figure 61).**

5-(3-(4-chlorobutyl)-4-oxo-3,4-dihydroquinazolin-2-yl)-1,3-phenylene diacetate (5M)

1M (0.42 g, 1.23 mmol) was solubilized in 5 ml DMF. To this potassium carbonate (0.34 g, 2.47 mmol) along with 1-bromo-4-chlorobutane (0.31, 1.84 mmol) were added and reacted as per **2.2.6** to yield 0.45 g of **5M** (84 % yield). Theoretical yield: 0.530 g. ^1H NMR (400MHz, $(CD_3)_2CO$) δ 8.20 (2H, d, *J* = 2.16), 8.12-8.10 (1H, m), 7.93-7.86 (2H, m), 7.60-7.56 (1H, m), 7.16 (1H, t, *J* = 2.24), 4.70 (2H, t, *J* = 6.04), 3.77 (2H, t, *J* = 6.32), 2.35 (6H, s), 2.12-2.10 (4H, m). **(Figure 18).** ^{13}C NMR (100MHz, $CDCl_3$) δ 169.64, 167.59, 158.63, 152.45, 152.38, 141.21, 134.85, 128.74, 128.03, 124.26, 119.68, 118.88, 116.10, 67.31, 45.70, 26.90, 21.15 **(Figure 62).** ESI (+ve) m/z calculated for $C_{22}H_{21}ClN_2O_5$ $[(M+Na)^+]$ 451.87, found 451.23 **(Figure 98).**

5-(3-(4-azidobutyl)-4-oxo-3,4-dihydroquinazolin-2-yl)-1,3-phenylene diacetate (6M).

5M (0.31g, 0.74 mmol) was solubilized in 3 ml DMF. To this sodium azide (0.072 g, 1.12 mmol) was added and reacted as per **2.2.7** to yield 0.31g of **6M** (96 % yield). Theoretical yield: 0.32 g. ^1H NMR (400MHz, $CDCl_3$) δ 8.13 (2H, d, *J* = 2.24), 8.08-8.05 (1H, m), 7.88 (1H, d, *J* = 8.2), 7.76-7.43 (1H, m), 7.47-7.43 (1H, m), 6.99 (1H, t, *J* = 6.52), 4.64 (2H, t, *J* = 6.24), 3.32 (2H, t, *J* = 6.76), 2.26 (6H, s), 2.00-1.93 (2H, m), 1.84-1.77 (2H, m) **(Figure 19).** ^{13}C NMR (100MHz, $CDCl_3$) δ 169.03, 166.70, 158.09, 151.80, 151.69, 140.60, 133.68, 133.59, 128.10, 128.00, 126.85, 126.69, 123.41, 118.91, 117.41,

115.42, 66.31, 66.23, 51.14, 26.07, 25.79, 21.16 **(Figure 63).** ESI (+ve) m/z calculated for $C_{22}H_{21}N_5O_5$ [$(M+Na)^+$] 458.43 found 458.29 **(Figure 99).**

3-(3-(4-azidobutyl)-4-oxo-3,4-dihydroquinazolin-2-yl)-5-hydroxyphenyl acetate (7M). 6M (0.15 g, 0.34 mmol) was solubilized in 2 ml THF followed by addition of LiOH (0.05 g, 0.034 mM) and reacted as per **2.2.8** to yield 0.1 g (74 % yield). Theoretical yield: 0.135 g. ^{1}H NMR (400MHz, $CDCl_3$) δ 8.12-8.09 (1H, m), 7.98-7.93 (2H, m), 7.85-7.79 (2H, m), 7.54-7.50 (1H, m), 6.78 (1H, t, *J* = 2.24), 6.68 (1H, s), 4.68 (2H, t, *J* = 6.28), 3.43 (2H, t, *J* = 6.76), 2.35 (3H, s), 2.07-2.00 (2H, m), 1.91-1.88 (2H, m) **(Figure 20).** ^{13}C NMR (100MHz, $CDCl_3$) δ 169.75, 166.59, 158.95, 156.90, 151.70,151.48, 140.42, 133.69, 127.73, 126.74, 123.38, 115.28, 113.80, 113.19, 111.56, 66.31, 51.13, 26.04, 25.74, 21.21 **(Figure 64).**

3-(4-azidobutyl)-2-(3,5-dihydroxyphenyl)quinazolin-4(*3H*)-one (8M). 6L (0.4g, 1.06 mmol) was solubilized in 2 ml acetonitrile followed by addition of 2 ml 3M HCl and reacted as per **2.2.8** to yield 0.34 g (95 % yield). Theoretical yield: 0.355 g. ^{1}H NMR (400MHz, $(CD_3)_2CO$) δ 8.55 (1H, s), 8.17-8.12 (3H, m), 7.94-7.92 (1H, m), 7.89-7.85 (1H, m), 7.59-7.55 (1H, m), 7.37 (1H, t, *J* = 7.88), 7.05-7.02 (1H, m) 4.74 (2H, t, *J* = 6.36), 3.49 (2H, t, *J* = 6.84), 2.09-2.04 (2H, m), 2.03-1.91 (2H, m) **(Figure 21).**

2-(4-hydroxy-3-methoxyphenyl)quinazolin-4(*3H*)-one (1N). Anthranilamide (2.0 g, 14.68 mmol) and 3-hydroxy-4-methoxybenzaldehyde (2.68 g, 17.61 mmol) were dissolved in 25 ml DMA and reacted as per **2.2.2** to yield 2.83 g (84 % yield). Theoretical yield: 3.33 g. ^{1}H NMR (400MHz, CH_3OD) δ 8.24-8.21 (1H, m), 7.85-7.83 (1H, m), 7.77-7.72 (2H, m), 7.60-7.57 (1H, m), 7.53-7.49 (1H, m), 6.96 (1H, d, *J* = 8.36),

4.00 (1H, s) **(Figure 22).** ^{13}C NMR (100MHz, CH_3OD) δ 162.38, 152.04, 149.93, 148.90, 147.45, 134.47, 127.10, 125.90, 125.78, 123.33, 121.45, 120.52, 115.38, 111.31, 55.75 **(Figure 65).** ESI (+ve) m/z calculated for $C_{15}H_{12}N_2O_3$ [$(M+H)^+$] 269.27, found 269.19 **(Figure 100).**

2-methoxy-4-(4-oxo-3,4-dihydroquinazolin-2-yl)phenyl acetate (2N). 1N (2.0 g, 7.45 mmol) was dissolved in 20 ml dichloromethane followed by addition of pyridine (1.17 g, 14.90 mmol), acetic anhydride (1.52 ml, 14.90 mmol) and reacted as per **2.2.3** to yield 1.5 g (54 % yield). Theoretical yield: 2.31 g. ^{1}H NMR (400MHz, DMSO-d6) δ 12.60 (1H, s), 8.18-8.16 (1H, m), 7.92 (1H, d, *J* = 1.88), 7.85-7.83 (2H, m), 7.76 (1H, d, *J* = 7.92), 7.53 (1H, t, *J* = 7.2), 7.28 (1H, d, *J* = 8.32), 3.92 (3H, s), 2.31 (3H, s) **(Figure 23).** ^{13}C NMR (100MHz, DMSO-d6) δ 168.30, 162.21, 151.52, 150.81, 148.62, 141.71, 134.61, 131.30, 127.50, 126.62, 125.82, 123.12, 120.92, 120.55, 112.01, 106.71, 56.07, 20.38 **(Figure 66).**

2-methoxy-4-(4-oxo-3-(prop-2-yn-1-yl)-3,4-dihydroquinazolin-2-yl)phenyl acetate (3N). 2N (0.18 g, 0.58 mmol), potassium carbonate (0.16 g, 1.16 mmol) and propargyl bromide (0.10 g, 0.87 mmol) were dissolved in 3 ml dimethylformamide and reacted as per **2.2.4** to yield 0.19g (95 % yield). Theoretical yield: 0.20g. ^{1}H NMR (400MHz, $CDCl_3$) δ 8.19 (1H, d, *J* = 1.8), 8.14-8.10 (2H, m), 7.91 (1H, d, *J* = 8.36), 7.77-7.73 (1H, m), 7.47-7.43 (1H, m), 7.09 (1H, d, *J* = 8.28), 5.23 (2H, d, *J* = 2.4), 3.92 (3H, s), 2.48 (1H, t, *J* = 2.4), 2.27 (3H, s) **(Figure 24).** ^{13}C NMR (100MHz, $CDCl_3$) δ 168.84, 165.46, 158.84, 152.01, 151.11, 141.94, 136.75, 133.80, 127.99, 126.71, 123.47, 121.39, 112.42,

78.22, 75.08, 56.04, 54.28, 20.74 **(Figure 67).** ESI (+ve) m/z calculated for $C_{20}H_{16}N_2O_4$ $[(M+Na)^+]$ 371.35 found 371.20 **(Figure 101).**

2-(4-hydroxy-3-methoxyphenyl)-3-(prop-2-yn-1-yl)quinazolin-4(*3H)*-one (4N). 3N (0.12 g, 0.34 mmol), lithium hydroxide (0.043 g, 1.03 mmol) were dissolved in 3 ml THF and reacted as per **2.2.5** to yield 0.09 g (90 % yield). Theoretical yield: 0.10 g. ^{1}H NMR (400MHz, $CO(CD_3)_2$) δ 8.26 (1H, d, *J* = 1.92), 8.21-8.15 (2H, m), 7.96-7.89 (2H, m), 7.61-7.57 (1H, m), 6.99 (1H, d, *J* = 8.32), 5.42 (2H, d, *J* = 2.44), 3.99 (3H, s), 3.18 (1H, s) **(Figure 25).** ^{13}C NMR (100MHz, $CO(CD_3)_2$) δ 166.15, 160.22, 153.05, 150.44, 148.31, 134.81, 130.58, 128.55, 127.23, 124.05, 123.26, 115.73, 115.33, 112.46, 79.35, 76.79, 56.60, 56.31, 55.08 **(Figure 68).**

4-(3-(4-chlorobutyl)-4-oxo-3,4-dihydroquinazolin-2-yl)-2-methoxyphenyl acetate (5N). 1N (0.27 g, 0.87 mmol) was solubilized in 3 ml DMF. To this potassium carbonate (0.24 g, 1.74 mmol) along with 1-bromo-4-chlorobutane (0.22, 1.30 mmol) were added and reacted as per **2.2.6** to yield 0.31 g of **5M** (91 % yield). Theoretical yield: 0.34 g. ^{1}H NMR (400MHz, $(CD_3)_2CO$) δ 8.27 (1H, d, *J* = 0.18), 8.23-8.20 (1H, m), 8.15-8.13 (1H, m), 7.99 (1H, d, *J* = 8.36), 7.84-7.80 (1H, m), 7.53-7.49 (1H, m), 7.19 (1H, d, *J* = 8.28), 4.72 (2H, t, *J* = 5.92), 4.02 (3H, s), 3.68 (2H, 6.32), 2.38 (3H, s), 2.15-2.11 (4H, m) **(Figure 26).** ^{13}C NMR (100MHz, $CDCl_3$) δ 168.84, 166.54, 159.11, 151.81, 151.11, 141.89, 137.03, 133.54, 130.43, 127.95, 127.75, 126.48, 123.39, 122.64, 121.88, 121.34, 115.19, 112.29, 111.65, 66.02, 65.88, 60.38, 56.06, 44.79, 44.66, 44.48, 29.25, 26.23, 20.74, 20.64 **(Figure 69).** ESI (+ve) m/z calculated for $C_{21}H_{21}ClN_2O_4$ $[(M+H)^+]$ 401.86, found 401.23 **(Figure 102).**

4-(3-(4-azidobutyl)-4-oxo-3,4-dihydroquinazolin-2-yl)-2-methoxyphenyl acetate (6N). 5N (0.2g, 0.49 mmol) was solubilized in 3 ml DMF. To this sodium azide (0.048 g, 0.99 mmol) was added and reacted as per **2.2.7** to yield 0.18g of **6N** (90 % yield). Theoretical yield: 0.203 g.

3-(4-azidobutyl)-2-(4-hydroxy-3-methoxyphenyl)quinazolin-4(*3H*)-one (7N). 6N (0.15g, 0.36 mmol) was solubilized in 2 ml acetonitrile followed by addition of 1.5 ml 3 M HCl and reacted as per **2.2.8** to yield 0.1 g (76 % yield). Theoretical yield: 0.13 g. ^{1}H NMR (400MHz, $CO(CD_3)_2$) δ 8.24 (1H, d, *J* = 1.84), 8.20-8.17 (2H, m), 7.93-7.86 (2H, m), 7.57 (1H, t, *J* = 7.52), 6.38 (1H, d, *J* = 8.28), 4.81 (2H, t, *J* = 6.32), 3.53 (2H, t, *J* = 6.8), 2.13-2.05 (4H, m) **(Figure 27).** ^{13}C NMR (100MHz, $CO(CD_3)_2$) δ 167.28, 160.46, 152.92, 150.33, 148.27, 134.51, 130.90, 128.49, 126.94, 1 24.21, 123.22, 115.70, 115.66, 112.36, 67.09, 56.32, 51.81 **(Figure 70).**

2-(3-hydroxy-4-methoxyphenyl)quinazolin-4(3*H*)-one (1O). Anthranilamide (1.0 g, 7.34mmol) and 3-hydroxy-4-methoxybenzaldehyde (1.45 g, 9.53 mmol) were dissolved in 20 ml DMA and reacted as per **2.2.2** to yield 1.1 g (57 % yield). Theoretical yield: 1.92 g

2-(4-hydroxy-3,5-dimethoxyphenyl)quinazolin-4(3*H*)-one (1P). Anthranilamide (0.5 g, 3.67 mmol) and 4-hydroxy-3,5-dimethoxybenzaldehyde (0.86 g, 4.40 mmol) were dissolved in 15 ml DMA and reacted as per **2.2.2** to yield 0.6 g (55 % yield). Theoretical yield: 1.09 g.

2-(2,4-dihydroxyphenyl)quinazolin-4(*3H*)-one (1Q). Anthranilamide (0.5 g, 3.67 mmol) and 4-hydroxy-3,5-dimethoxybenzaldehyde (0.67 g, 4.40 mmol) were dissolved in

15 ml DMA and reacted as per **2.2.2** to yield 0.62 g (66 % yield). Theoretical yield: 0.93 g

2-(2,4,6-trihydroxyphenyl)quinazolin-4(*3H*)-one (1R). Anthranilamide (0.5 g, 3.67 mmol) and 2,4,6-trihydroxybenzaldehyde (0.74 g, 4.77 mmol) were dissolved in 15 ml DMA and reacted as per **2.2.2** to yield 0.07 g (7 % yield). Theoretical yield: 0.99 g. ^{1}H NMR (400MHz, $CDCl_3$) δ 9.50 (1H, s), 8.22 (1H, d, *J* = 1.08), 8.21-7.66 (2H, m), 7.43-7.39 (1H, m), 6.10 (2H, s) **(Figure 28).**

3-(3-(4-(4-((2-(3-hydroxyphenyl)-4-oxoquinazolin-3(4*H*)-yl)methyl)-1*H*-1,2,3-triazol-1-yl)butyl)-4-oxo-3,4-dihydroquinazolin-2-yl)phenyl acetate (C1). 6L (0.224 g, 0.5935 mM) and **4L** (0.164 g, 0.5935 mM) were solubilized in DMF followed by addition of sodium ascorbate (0.06, 0.2967 mM) and $CuSO_4$ (0.044 mg, 0.1780 mM) and reacted as per **2.2.9** to yield 0.32 g (82 % yield). Theoretical yield: 0.38 g. ^{1}H NMR (400MHz, $CO(CD_3)_2$) δ 8.40 (1H, d, *J* = 7.88), 8.29-8.13 (5H, m), 7.88-7.76 (4H, m), 7.53-7.24 (6H, m), 7.06-7.04 (1H, m), 5.83 (2H, s), 4.60-4.55 (4H, m), 2.32 (3H, s), 2.19-2.16 (2H, m), 1.95-1.91 (2H, m) **(Figure 29).** ^{13}C NMR (100MHz, $CO(CD_3)_2$) δ 169.95, 167.36, 166.81, 163.15, 160.11, 159.33, 158.65, 152.69, 152.40, 152.20, 143.76, 140.55, 140.29, 134.66, 134.63, 130.34, 130.14, 128.65, 127.69, 127.50, 126.48, 125.18, 124.85, 124.19, 124.16, 122.37, 120.67, 118.71, 116.18, 115.91, 115.78, 67.09, 61.00, 50.59, 27.86, 26.55 **(Figure 71).** ESI (+ve) m/z calculated for $C_{37}H_{31}N_7O_5$ $[(M+H)^+]$ 654.69, found 654.44 **(Figure 103).**

3-(3-((1-(4-(2-(3-hydroxyphenyl)-4-oxoquinazolin-3(4*H*)-yl)butyl)-1*H*-1,2,3-triazol-4-yl)methyl)-4-oxo-3,4-dihydroquinazolin-2-yl)phenyl acetate (C2). 7L (0.224 g, 0.5935

mM) and **3L** (0.164 g, 0.5935 mM) were solubilized in DMF followed by addition of sodium ascorbate (0.06, 0.2967 mM) and $CuSO_4$ (0.044 mg, 0.1780 mM) and reacted as per **2.2.9** to yield 0.28 g (80 % yield). Theoretical yield: 0.38 g. ^{1}H NMR (400MHz, $CO(CD_3)_2$) δ 8.40 (1H, d, *J* = 7.88), 8.29-8.13 (5H, m), 7.88-7.76 (4H, m), 7.53-7.24 (6H, m), 7.06-7.04 (1H, m), 5.83 (2H, s), 4.60-4.55 (4H, m), 2.32 (3H, s), 2.19-2.16 (2H, m), 1.95-1.91 (2H, m) **(Figure 30).**

2-(3-hydroxyphenyl)-3-((1-4-(2-(3-hydroxyphenyl)-4-oxoquinazolin-3(4*H*)-yl)butyl)-1*H*-1,2,3-triazol-4-yl)methyl)quinazolin-4(3*H*)-one (3C). 7L (0.15 g, 0.4474 mM) and **4L** (0.14 g, 0.4474 mM) were solubilized in DMF followed by addition of sodium ascorbate (0.04, 0.2237 mM) and $CuSO_4$ (0.033 mg, 0.1342 mM) and reacted as per **2.5.9** to yield 0.2 g (74 % yield). Theoretical yield: 0.27 g. ^{1}H NMR (400MHz, DMSO d-6) δ 8.39 (1H, s), 8.13-8.02 (2H, m), 8.01-7.95 (2H, m), 7.94-7.91 (6H, m), 7.62-7.57 (2H, m), 7.36-7.31 (2H, m), 6.95-6.91 (2H, m), 5.83 (2H, s), 4.69 (2H, t, *J* = 4), 4.53 (2H, t, *J* = 8), 2.14-2.08 (2H, m), 1.91-1.88 (2H, m) **(Figure 31).** ^{13}C NMR (100MHz, DMSO d-6) δ 166.06, 165.61, 158.96, 158.82, 157.57, 157.52, 151.24, 151.10, 142.13, 138.74, 134.27, 134.10, 129.52, 129.45, 127.56, 127.52, 127.06, 126.95, 124.65, 123.21, 119.08, 118.99, 117.92, 117.83, 114.75, 114.71, 114.52, 114.40, 65.97, 59.90, 49.18, 48.56, 26.51, 25.30. **(Figure 72).** ESI (+ve) m/z calculated for $C_{35}H_{29}N_7O_4$ [$(M+H)^+$] 612.65, found 612.49 **(Figure 104).**

3-hydroxy-5-(3-(4-(4-((2-(3-hydroxyphenyl)-4-oxoquinazolin-3(4H)-yl)methyl)-1H-1,2,3-triazol-1-yl)butyl)-4-oxo-3,4-dihydroquinazolin-2-yl)phenyl acetate (4C). 7M (0.12 mg, 0.3126 mM) and **4L** (0.086 mg, 0.3126 mM) were solubilized in DMF

followed by addition of sodium ascorbate (0.031 mg, 0.1563 mM) and $CuSO_4$ (0.023 mg, 0.0937 mM) and reacted as per **2.2.9** to yield 0.16 g (76 % yield). Theoretical yield: 0.20 g. ^{1}H NMR (400MHz, MeOD) δ 8.06 (1H, s), 7.92-7.90 (1H, m), 7.86-7.81 (3H, m), 7.73 (2H, s), 7.69-7.63 (3H, m), 7.54-7.53 (1H, m), 7.35-7.31 (2H, m), 7.16 (1H, t, *J* = 7.84), 7.11 (1H, s), 6.81-6.78 (1H, m), 6.54 (1H, t, *J* = 2.24), 5.66 (2H, s), 4.43-4.39 (4H, m), 3.21-3.19 (2H, m), 2.16 (3H, s), 2.05-1.98 (2H, m), 1.79-1.72 (2H, m) **(Figure 32).** ^{13}C NMR (100MHz, MeOD) δ 171.18, 167.84, 167.31, 161.11, 160.38, 159.58, 158.77, 153.27, 152.92, 152.68, 144.47, 141.33, 140.37, 135.11, 134.98, 130.54, 128.45, 128.37, 128.03, 127.98, 125.90, 124.47, 124.43, 120.91, 118.83, 116.28, 116.11, 113.95, 113.86, 112.29, 67.37, 60.88, 30.68, 27.92, 26.80 **(Figure 73).** ESI (+ve) m/z calculated for $C_{37}H_{31}N_7O_6$ [$(M+H)^+$] 670.69, found 670.45 **(Figure 105).**

2-(3,5-dihydroxyphenyl)-3-(4-(4-((2-(3-hydroxyphenyl)-4-oxoquinazolin-3(4*H*)-yl)methyl)-1*H*-1,2,3-triazol-1-yl)butyl)quinazolin-4(3*H*)-one (5C). 8M (89 mg, 0.25 mM) and **4L** (79 mg, 0.2533 mM) were solubilized in DMF followed by addition of sodium ascorbate (30 mg, 0.1519 mM) and $CuSO_4$ (12.6 mg, 0.0506 mM) and reacted as per **2.2.9** to yield 0.12 g (72 % yield). Theoretical yield: 0.16 g. ^{1}H NMR (400MHz, MeOD) δ 8.32 (2H, t, *J* = 1.72), 8.13 (1H, s), 7.98-7.70 (6H, m), 7.42-7.34 (4H, m), 6.88 (2H, d, *J* = 8.72), 6.43 (1H. t, *J* = 2.28), 5.74 (2H, s), 4.51 (4H, t, *J* = 6.52), 2.16-2.09 (2H, m), 1.88-1.83 (2H, m) **(Figure 33).** ^{13}C NMR (100MHz, MeOD) δ 167.63, 167.11, 164.86, 161.49, 161.32, 159.68, 152.97, 152.64, 144.53, 141.20, 134.97, 134.83, 131.46, 130.26, 128.22, 127.90, 127.74, 127.32, 125.80, 124.45, 124.38, 116.28, 108.25, 106.09,

67.27, 60.77, 36.96, 31.67 **(Figure 74).** ESI (+ve) m/z calculated for $C_{35}H_{27}N_7O_5$ $[(M+H)^+]$ 628.65, found 628.46 **(Figure 106).**

2-(3,5-dihydroxyphenyl)-3-((1-(4-(2-(3-hydroxyphenyl)-4-oxoquinazolin-3(4H)-yl)butyl)-1H-1,2,3-triazol-4-yl)methyl)quinazolin-4(3H)-one (6C). 7M (0.08 mg, 0.2394 mM) and **4M** (0.07 mg, 0.2394 mM) were solubilized in DMF followed by addition of sodium ascorbate (0.023 g, 0.1197 mM) and $CuSO_4$ (0.017 g, 0.0718 mM) and reacted as per **2.2.9** to yield 0.09 g (60 % yield). Theoretical yield: 0.15 g. ^{1}H NMR (400MHz, MeOD) δ 8.14 (1H, s), 7.94-7.84 (4H, m), 7.79-7.69 (4H, m), 7.48 (2H, d, *J* = 2.24), 7.39-7.34 (2H, m), 7.25 (1H, t, *J* = 8.16), 6.90-6.88 (1H, m), 6.45 (1H, t, *J* = 2.28), 5.70 (2H, s), 4.49 (4H, t, *J* = 6.56), 2.13-2.08 (2H, m), 1.88-1.84 (2H, m) **(Figure 34).** ^{13}C NMR (100MHz, MeOD) δ 167.69, 167.10, 161.34, 161.02, 159.77, 158.62, 152.76, 152.60, 144.41, 141.01, 140.50, 135.00, 134.86, 130.45, 128.25, 128.17, 127.86, 127.77, 125.90, 124.39, 120.96, 118.71, 116.32, 116.06, 116.01, 108.20, 106.17, 67.30, 60.78, 51.25, 27.94, 26.82 **(Figure 75).** ESI (+ve) m/z calculated for $C_{35}H_{29}N_7O_5$ $[(M+H)^+]$ 628.65, found 628.42 **(Figure 107).**

5-(3-((1-(4-(2-(3,5-diacetoxyphenyl)-4-oxoquinazolin-3(4H)-yl)butyl)-1H-1,2,3-triazol-4-yl)methyl)-4-oxo-3,4-dihydroquinazolin-2-yl)-1,3-phenylene diacetate (7C). 6M (65 mg, 0.15 mM) and **4H** (56.18 mg, 0.15 mM) were solubilized in DMF followed by addition of sodium ascorbate (14.77 mg, 0.0746 mM) and $CuSO_4$ (11.15 mg, 0.0447 mM) and reacted as per **2.2.9** to yield 0.01 g (8.3 % yield). Theoretical yield: 0.1211 g. ^{1}H NMR (400MHz, MeOD) δ 8.27 (1H, s), 8.17-8.11 (5H, m), 8.02-7.87 (6H, m), 7.56-7.53 (2H, m), 7.08-7.04 (2H, m), 5.82 (2H, s), 4.60-4.50 (5H, m), 2.33 (12H, d, *J* = 8),

2.18-2.04 (2H, m), 1.87-1.84 (m, 2H) **(Figure 35).** ESI (+ve) m/z calculated for $C_{43}H_{37}N_7O_{10}$ [$(M+Na)^+$] 834.79, found 834.54 **(Figure 108).**

3-(3-(4-(4-((2-(3,5-dihydroxyphenyl)-4-oxoquinazolin-3(4H)-yl)methyl)-1H-1,2,3-triazol-1-yl)butyl)-4-oxo-3,4-dihydroquinazolin-2-yl)-5-hydroxyphenyl acetate (8C). **7M** (40.3 mg, 0.10 mM) and **4H** (30 mg, 0.1026 mM) were solubilized in DMF followed by addition of sodium ascorbate (12.18 mg, 0.0615 mM) and $CuSO_4$ (5.12 mg, 0.0205 mM) and reacted as per **2.2.9** to yield 0.04 g (57 % yield). Theoretical yield: 0.07 g. ^{1}H NMR (400MHz, MeOD) δ 8.12 (1H, s), 7.96 (2H, t, *J* = 8.84), 7.78-7.70 (5H, m), 7.56 (1H, t, *J* = 1.88), 7.40-7.39 (4H, m), 6.55 (1H, t, *J* = 2.2), 6.32 (1H, t, *J* = 2.24), 5.71 (2H, s), 4.73-4.44 (4H, m), 2.20 (3H, s), 2.09-2.05 (2H, m), 1.84-1.80 (2H, m) **(Figure 36).** ^{13}C NMR (100MHz, MeOD) δ 171.21, 167.97, 167.28, 161.21, 160.48, 159.81, 159.61, 153.29, 152.94, 152.76, 144.48, 141.36, 141.03, 135.13, 135.04, 128.48, 128.37, 128.11, 127.99, 125.99, 124.49, 116.35, 116.17, 113.95, 113.86, 112.29, 108.17, 106.15, 67.41, 60.84, 27.93, 26.84, 21.01 **(Figure 76).** ESI (+ve) m/z calculated for $C_{37}H_{31}N_7O_7$ [$(M+H)^+$] 686.68, found 686.51 **(Figure 109).**

2-(3,5-dihydroxyphenyl)-3-((1-(4-(2-(3,5-dihydroxyphenyl)-4-oxoquinazolin-3(4H)yl)butyl)-1H-1,2,3-triazol-4-yl)methyl)quinazolin-4(3H)-one (9C). **8M** (0.08 g, 0.2326 mM) and **4M** (0.068 g, 0.2326 mM) were solubilized in DMF followed by addition of sodium ascorbate (0.027 g, 0.1395 mM) and $CuSO_4$ (0.029 mg, 0.1163 mM) and reacted as per **2.2.9** to yield 0.06 g (40 % yield). Theoretical yield: 0.14 g. ^{1}H NMR (400MHz, MeOD) δ 8.19 (1H, s), 8.02-7.98 (3H, m), 7.82-7.78 (4H, m), 7.47-7.26 (7H, m), 6.43-6.41 (2H, m), 5.77 (2H, s), 4.56-4.54 (4H, m), 2.16 (2H, s), 1.90 (2H, s) **(Figure**

37). ^{13}C NMR (100MHz, MeOD) δ 167.81, 167.24, 164.87, 161.42, 161.07, 159.77, 159.69, 152.70, 152.27, 144.45, 140.90, 140.85, 135.11, 135.04, 128.19, 127.98, 127.93, 125.96, 124.48, 117.22, 116.12, 116.07, 108.23, 108.17, 106.18, 67.44, 60.83, 51.25, 27.91, 26.82 **(Figure 77).** ESI (+ve) m/z calculated for $C_{35}H_{29}N_7O_6$ [$(M+H)^+$] 644.65, found 644.43 **(Figure 110).**

2-(4-hydroxy-3-methoxyphenyl)-3-((1-(4-(2-(4-hydroxy-3-methoxyphenyl)-4-oxoquinazolin-3(4H)-yl)butyl)-1H-1,2,3-triazol-4-yl)methyl)quinazolin-4(3H)-one (10C). 7N (0.10 g, 0.2938 mM) and **4N** (0.09 g, 0.2938 mM) were solubilized in DMF followed by addition of sodium ascorbate (0.034 g, 0.1762 mM) and $CuSO_4$ (0.036 g, 0.1469 mM) and reacted as per **2.2.9** to yield 0.05 g (25 % yield). Theoretical yield: 0.197 g. ^{1}H NMR (400MHz, MeOD) δ 8.24-8.20 (1H, m), 8.09-8.04 (4H, m), 7.88-7.72 (5H, m), 7.53-7.44 (2H, m), 6.98-6.90 (2H, m), 5.81 (2H, s), 4.63-4.57 (2H, m), 4.14-4.09 (2H, m), 3.97 (6H, s), 2.23-2.19 (2H, m), 1.98-1.92 (2H, m) **(Figure 38).** ^{13}C NMR (100MHz, MeOD) δ 165.04, 164.63, 157.86, 157.63, 150.37, 150.31, 149.74, 149.40, 142.95, 142.28, 142.16, 134.29, 134.18, 133.67, 133.45, 126.37, 126.16, 125.71, 125.56, 124.38, 122.40, 121.59, 120.91, 113.39, 113.31, 111.94, 65.77, 55.67, 55.63, 50.09, 42.42, 26.23, 25.01 **(Figure 78).**

3-(4-oxo-3,4-dihydroquinazolin-2-yl)phenyl sulfate (1S). 1L (0.05 g, 0.2098 mM), was solubilized in 3 ml acetonitrile followed by addition of triethylamine (0.18 ml, 1.2592 mM) and SO_3Me_3N (0.175 g, 1.2592 mM) and allowed to react as per **2.2.10** to yield 0.05 g (75 % yield). Theoretical yield: 0.066 g. ^{1}H NMR (400MHz, D_2O) δ 7.89-7.87 (1H, m), 7.69-7.63 (3H, m), 7.56-7.52 (1H, m), 7.48-7.45 (2H, m), 7.36 (1H, t, *J* = 7.8) **(Figure**

39). ^{13}C NMR (100MHz, D_2O) δ 151.41, 135.56, 133.50, 130.56, 127.52, 125.74, 125.40, 124.97, 120.78, 119.42 **(Figure 79).** ESI (-ve) m/z calculated for $C_{14}H_9N_2O_5S^-$ [$(M)^-$] 317.30, found 317.17 **(Figure 111).**

5-(4-oxo-3,4-dihydroquinazolin-2-yl)-1,3-phenylene bis(sulfate) (2S). 1M (0.05 g, 0.1966 mM), was solubilized in 3 ml acetonitrile followed by addition of triethylamine (0.32 ml, 2.3599 mM) and SO_3Me_3N (0.328 g, 2.3599 mM) and allowed to react as per **2.2.10** to yield 0.06 g (74 % yield). Theoretical yield: 0.081 g. ^{1}H NMR (400MHz, D_2O) δ 8.13-8.11 (1H, m), 7.86-7.82 (1H, m), 7.72-7.68 (3H, m), 7.54 (1H, t, *J* = 8), 7.48 (1H, t, *J* = 2.16) **(Figure 40).** ^{13}C NMR (100MHz, D_2O) δ 152.17, 135.76, 134.72, 127.81, 125.96, 118.56, 118.31 **(Figure 80).** ESI (-ve) m/z calculated for $C_{14}H_8N_2O_9S_2^{-2}$ [$(M+Na)^+$] 435.35, found 435.10 **(Figure 112).**

2-methoxy-4-(4-oxo-3,4-dihydroquinazolin-2-yl)phenyl sulfate (3S). 1N (0.05 g, 0.1863 mM), was solubilized in 3 ml acetonitrile followed by addition of triethylamine (0.16 ml, 1.1182 mM) and SO_3Me_3N (0.15 g, 1.1182 mM) and allowed to react as per **2.2.10** to yield 0.05 g (80 % yield). Theoretical yield: 0.064 g. ^{1}H NMR (400MHz, D_2O) δ 7.96 (1H, d, *J* = 8), 7.71 (1H, t, *J* = 7.76), 7.53 (1H, d, *J* = 8.2), 7.47-7.35 (4H, m), 3.90 (3H, s) **(Figure 41).** ^{13}C NMR (100MHz, D_2O) δ 151.45, 142.88, 135.63, 130.40, 127.48, 125.86, 122.82, 120.64, 119.49, 112.57, 56.27 **(Figure 81).** ESI (-ve) m/z calculated for $C_{15}H_{11}N_2O_6S^-$ [$(M)^-$] 347.32, found 347.16 **(Figure 113).**

2-methoxy-5-(4-oxo-3,4-dihydroquinazolin-2-yl)phenyl sulfate (4S). 1O (0.05 g, 0.1863 mM), was solubilized in 3 ml acetonitrile followed by addition of triethylamine (0.16 ml, 1.1182 mM) and SO_3Me_3N (0.15 g, 1.1182 mM) and allowed to react as per

2.2.10 to yield 0.045 g (70 % yield). Theoretical yield: 0.064 g. ^{1}H NMR (400MHz, D_2O) δ 7.70-7.68 (1H, m), 7.60-7.54 (2H, m), 7.45-7.42 (1H, m), 7.34 (1H, d, *J* = 8.12), 7.24-7.20 (1H, m), 6.95 (1H, d, *J* = 8.8), 3.78 (3H, s) **(Figure 42).** ^{13}C NMR (100MHz, D_2O) δ 154.27, 139.79, 135.42, 127.07, 126.69, 125.60, 123.91, 121.70, 118.89, 113.17, 56.08 **(Figure 82).** ESI (-ve) m/z calculated for $C_{15}H_{11}N_2O_6S^-$ [$(M)^-$] 347.32, found 347.16 **(Figure 114).**

2,6-dimethoxy-4-(4-oxo-3,4-dihydroquinazolin-2-yl)phenyl sulfate (5S). 1P (0.05 g, 0.1676 mM), was solubilized in 3 ml acetonitrile followed by addition of triethylamine (0.14 ml, 1.0056 mM) and SO_3Me_3N (0.14 g, 1.0056 mM) and allowed to react as per **2.2.10** to yield 0.035 g (55 % yield). Theoretical yield: 0.063 g. ^{1}H NMR (400MHz, D_2O) δ 7.90 (1H, d, *J* = 0.92), 7.65 (1H, t, *J* = 1.36), 7.63 (1H, d, *J* = 1.36), 7.36 (1H, t, *J* = 7.24), 7.04 (2H, s), 3.86 (6H, s) **(Figure 43).** ^{13}C NMR (100MHz, D_2O) δ 154.24, 135.52, 132.18, 129.95, 127.47, 125.74, 119.42, 105.18, 56.44 **(Figure 83).** ESI (-ve) m/z calculated for $C_{16}H_{13}N_2O_7S^-$ [$(M)^-$] 377.35, found 377.17 **(Figure 115).**

4-(4-oxo-3,4-dihydroquinazolin-2-yl)-1,3-phenylene bis(sulfate) (6S). 1Q (0.05 g, 0.1966 mM), was solubilized in 3 ml acetonitrile followed by addition of triethylamine (0.32 ml, 2.3599 mM) and SO_3Me_3N (0.328 g, 2.3599 mM) and allowed to react as per **2.2.10** to yield 0.06 g (74 % yield). Theoretical yield: 0.081 g. ^{1}H NMR (400MHz, D_2O) δ 7.94 (1H, s), 7.79-7.72 (2H, m), 7.52-7.38 (4H, m) **(Figure 44).** ^{13}C NMR (100MHz, D_2O) δ 154.18, 149.45, 135.61, 131.95, 127.73, 126.00, 125.85, 119.45, 116.27, 55.61, 42.50, 38.73 **(Figure 84).** ESI (-ve) m/z calculated for $C_{14}H_8N_2O_9S_2^{-2}$ [$(M+Na)^+$] 435.35, found 435.16 **(Figure 116).**

2-(4-oxo-3,4-dihydroquinazolin-2-yl)benzene-1,3,5-triyl tris(sulfate) (7S). 1R (0.05 g, 0.1850 mM), was solubilized in 3 ml acetonitrile followed by addition of triethylamine (0.46 ml, 3.3303 mM) and SO_3Me_3N (0.463 g, 3.3303 mM) and allowed to react as per **2.2.10** to yield 0.06 g (53 % yield). Theoretical yield: 0.093 g. ^{1}H NMR (400MHz, D_2O) δ **(Figure 45).** ^{13}C NMR (100MHz, D_2O) δ 163.47, 162.28, 155.63, 154.40, 143.92, 135.33, 126.61, 125.27, 123.44, 118.05, 98.16, 55.58 **(Figure 85).**

3-(3-(4-(4-((2-(3-acetoxyphenyl)-4-oxoquinazolin-3(4H)-yl)methyl)-1H-1,2,3-triazol-1-yl)butyl)-4-oxo-3,4-dihydroquinazolin-2-yl)phenyl sulfate (CS2). C2 (0.05 g, 0.0765 mM), was solubilized in 3 ml acetonitrile followed by addition of triethylamine (0.04 ml, 0.4592 mM) and SO_3Me_3N (0.063 g, 0.4592 mM) and allowed to react as per **2.2.10** to yield 0.05 g (89 % yield). Theoretical yield: 0.056 g. ^{1}H NMR (400MHz, D_2O) δ 8.39-8.37 (1H, m), 8.33 (1H, s), 8.26 (1H, t, *J* = 1.92), 8.20 (1H, t, *J* = 1.96), 8.16-8.15 (1H, m), 8.02 (2H, d, *J* = 8.16), 7.89-7.82 (4H, m), 7.55-7.50 (3H, m), 7.41-7.30 (2H, m), 7.24-7.21 (1H, m), 5.76 (2H, s), 4.61 (2H, t, *J* = 6.4), 4.64 (2H, t, *J* = 6.96), 2.07-2.03 (2H, m), 1.84 (2H, s) **(Figure 46).** ^{13}C NMR (100MHz, D_2O) δ 169.29, 166.11, 165.81, 158.70, 157.85, 153.85, 151.10, 150.82, 142.04, 138.84, 138.36, 134.40, 134.11, 129.69, 128.81, 127.58, 127.38, 126.98, 125.46, 124.80, 124.22, 123.27, 123.20, 123.16, 122.95, 121.29, 120.44, 114.51, 114.50 **(Figure 86).** ESI (-ve) m/z calculated for $C_{37}H_{30}N_7O_8S^-$ [$(M)^-$] 732.74, found 732.38 **(Figure 117).**

3-(3-((1-(4-(2-(3-phenylsulfate)-4-oxoquinazolin-3(4H)-yl)butyl)-1H-1,2,3-triazol-4-yl)methyl)-4-oxo-3,4-dihydroquinazolin-2-yl)phenyl sulfate (CS3). C3 (0.09 g, 0.1308 mM), was solubilized in 3 ml acetonitrile followed by addition of triethylamine (0.2ml,

1.5706 mM) and SO_3Me_3N (0.2 g, 1.5706 mM) and allowed to react as per **2.2.10** to yield 0.08 g (70 % yield). Theoretical yield: 0.113 g. ^{1}H NMR (400MHz, D_2O) δ 7.53-6.53 (16H, m), 5.11 (2H, s), 4.24 (2H, s), 3.62 (2H, s), 1.65 (2H, s), 1.26 (2H, s) **(Figure 47).** ^{13}C NMR (100MHz, D_2O) δ 154.62, 151.52, 151.37, 151.02, 149.67, 149.38, 145.07, 142.68, 142.42, 138.21, 138.08, 136.39, 134.55, 133.70, 133.54, 130.28, 129.57, 127.21, 126.54, 126.31, 125.64, 125.31, 125.07, 124.33, 123.18, 122.26, 122.08, 121.17, 120.83, 119.94, 118.94, 113.42, 113.32, 65.92, 59.25, 55.53, 50.04, 39.56, 26.28, 25.00 **(Figure 87).** ESI (-ve) m/z calculated for $C_{35}H_{27}N_7O_{10}S_2^{-2}$ [(M+Na)] 792.76, found 792.36 **(Figure 118).**

3-(3-((1-(4-(2-(3-acetoxy-5-phenylsulfate)-4-oxoquinazolin-3(4H)-yl)butyl)-1H-1,2,3-triazol-4-yl)methyl)-4-oxo-3,4-dihydroquinazolin-2-yl)phenyl sulfate (CS4). C4 (0.06 g, 0.0895 mM), was solubilized in 3 ml acetonitrile followed by addition of triethylamine (0.15 ml, 1.0751 mM) and SO_3Me_3N (0.150 g, 1.0751 mM) and allowed to react as per **2.2.10** to yield 0.05 g (64 % yield). Theoretical yield: 0.074 g. ^{1}H NMR (400MHz, D_2O) δ 7.97 (1H, s), 7.87 (1H, s), 7.58-7.53 (2H, m), 7.24-6.99 (9H, m), 6.74-6.59 (3H, m), 5.25 (2H, s), 4.33 (2H, t, *J* = 5.96), 3.70-3.65 (2H, m), 2.23 (3H, s), 1.72 (2H, s), 1.32 (2H, s) **(Figure 48).** ^{13}C NMR (100MHz, D_2O) δ 172.29, 165.30, 165.09, 157.94, 157.09, 151.76, 151.51, 150.50, 149.65, 149.31, 142.83, 139.07, 138.07, 133.82, 129.67, 126.72, 125.74, 125,64, 125.30, 123.59, 122.46, 122.17, 120.87, 118.43, 118.24, 116.86, 113.57, 113.47, 65.96, 59.15, 55.49, 50.14, 26.23, 25.01, 20.54 **(Figure 88).** ESI (-ve) m/z calculated for $C_{37}H2_9N_7O_{12}S_2^{-2}$ [(M+Na)] 850.80, found 850.39 **(Figure 119).**

5-(3-(4-(4-((2-(3-phenylsulfate)-4-oxoquinazolin-3(4H)-yl)methyl)-1H-1,2,3-triazol-1-yl)butyl)-4-oxo-3,4-dihydroquinazolin-2-yl)-1,3-phenylene bis(sulfate) (CS5). C5 (0.05 g, 0.0792 mM), was solubilized in 3 ml acetonitrile followed by addition of triethylamine (0.2 ml, 1.4263 mM) and SO_3Me_3N (0.2 g, 1.4263 mM) and allowed to react as per **2.2.10** to yield 0.055 g (80 % yield). Theoretical yield: 0.068 g. ^{1}H NMR (400MHz, D_2O) δ 8.52-8.50 (2H, m), 8.33-8.31 (3H, m), 8.02-7.97 (2H, m), 7.83-7.77 (4H, m), 7.48-7.44 (5H, m), 5.77 (2H, s), 4.62-4.57 (4H, m), 2.20-2.14 (2H, m), 1.96-1.91 (2H, m) **(Figure 49).** ^{13}C NMR (100MHz, D_2O) δ 167.93, 167.39, 160.51, 159.86, 156.45, 154.71, 152.91, 152.73, 144.29, 141.07, 135.32, 135.23, 135.12, 130.83, 128.62, 128.35, 128.28, 128.02, 126.18, 124.58, 124.53, 122.06, 118.89, 118.09, 116.27, 115.90, 67.63, 61.01, 28.13, 26.93 **(Figure 89).** ESI (-ve) m/z calculated for $C_{35}H_{26}N_7O_{14}S_3^{-3}$ [$(M-SO_3^-)$] 786.82, found 786.33 **(Figure 120).**

5-(3-((1-(4-(2-(3-acetoxy-5-phenylsulfate)-4-oxoquinazolin-3(4H)-yl)butyl)-1H-1,2,3-triazol-4-yl)methyl)-4-oxo-3,4-dihydroquinazolin-2-yl)-1,3-phenylene bis(sulfate) (CS7). C7 (0.01 g, 0.0178 mM), was solubilized in 3 ml acetonitrile followed by addition of triethylamine (0.04 ml, 0.3215 mM) and SO_3Me_3N (0.44 g, 0.3215 mM) and allowed to react as per **2.2.10** to yield 0.006 g (50 % yield). Theoretical yield: 0.012 g. ^{1}H NMR (400MHz, MeOD) δ 8.62 (1H, s), 8.45 (2H, d, *J* = 2.16), 8.34 (1H, t, *J* = 1.52), 8.14-8.04 (3H, m), 7.92-7.82 (4H, m), 7.57 (2H, m), 7.38 (1H, t, *J* = 2.16), 7.25 (1H, t, *J* = 2.16), 5.84 (2H, s), 4.66-4.58 (4H, m), 2.33 (3H, s), 2.22-2.17 (2H, m), 1.95-1.91 (2H, m) **(Figure 50).** ^{13}C NMR (100MHz, MeOD) δ 171.02, 168.11, 167.48, 159.77, 159.72, 154.78, 152.97, 152.70, 141.29, 140.82, 135.22, 135.11, 128.72, 128.57, 128.38, 128.30,

124.68, 124.54, 119.83, 119.11, 118.59, 118.28, 118.02, 116.42, 116.37, 67.66, 28.11, 26.86, 21.01 **(Figure 90).** ESI (-ve) m/z calculated for $C_{37}H2_9N_7O_{13}S_2^{-2}$ [(M-2SO_3-1H+)] 764.80, found 764.37 **(Figure 121).**

5-(3-((1-(4-(2-(3,5-dihydroxyphenyl)-4-oxoquinazolin-3(4H)-yl)butyl)-1H-1,2,3-triazol-4-yl)methyl)-4-oxo-3,4-dihydroquinazolin-2-yl)-1,3-phenylene bis(sulfate) (CS8). C8 (0.01 g, 0.0162 mM), was solubilized in 3 ml acetonitrile followed by addition of triethylamine (0.05 ml, 0.3898 mM) and SO_3Me_3N (0.054 g, 0.3898 mM) and allowed to react as per **2.2.10** to yield 0.006 g (40 % yield). Theoretical yield: 0.015 g. ^{1}H NMR (400MHz, MeOD) δ 8.61 (1H, s), 8.47 (2H, d, *J* = 2.2), 8.35 (2H, d, *J* = 2.2), 8.19-8.10 (2H, m), 7.95-7.85 (2H, m), 7.57 (2H, t, *J* = 7.48), 7.44 (1H, t, *J* = 2.2), 7.37 (1H, t, *J* = 2.2), 5.87 (2H, s), 4.72 (2H, t, *J* = 6.32), 4.61 (2H, t, *J* = 6.92), 2.25-2.21 (2H, m), 1.99-1.93 (2H, m) **(Figure 51).** ^{13}C NMR (100MHz, MeOD) δ 168.12, 167.53, 160.10, 159.82, 154.84, 154.64, 153.03, 152.85, 143.93, 141.06, 140.84, 135.28, 135.10, 128.77, 128.63, 128.36, 128.32, 127.18, 124.60, 118.96, 118.54, 118.19, 118.00, 116.42, 116.40, 67.71, 60.67, 28.24, 26.93, 24.99 **(Figure 91).** ESI (-ve) m/z calculated for $C_{35}H_{25}N_7O_{18}S_4^{-4}$ [(M-3SO_3-1H+)] 722.87, found 722.30 **(Figure 122).**

4-(3-((1-(4-(2-(4-hydroxy-3-methoxyphenyl)-4-oxoquinazolin-3(4H)-yl)butyl)-1H-1,2,3-triazol-4-yl)methyl)-4-oxo-3,4-dihydroquinazolin-2-yl)-2-methoxyphenyl sulfate (CS9). (0.03 g, 0.0446 mM), was solubilized in 3 ml acetonitrile followed by addition of triethylamine (0.08 ml, 0.5359 mM) and SO_3Me_3N (0.074 g, 0.5359 mM) and allowed to react as per **2.2.10** to yield 0.02 g (54 % yield). Theoretical yield: 0.037 g. ^{1}H NMR (400MHz, MeOD) δ 7.86 (1H, s), 7.38-7.07 (10H, m), 6.86-6.70 (3H, m), 5.06

(2H, s), 4.35 (2H, s), 3.62 (6H, d, *J* = 6.44), 1.73 (2H, s), 1.36 (2H, s) **(Figure 52).** ^{13}C NMR (100MHz, MeOD) δ 165.04, 164.63, 157.86, 157.63, 150.37, 150.31, 149.74, 149.40, 142.95, 142.28, 142.16, 134.29, 134.18, 133.67, 133.45, 126.16, 125.71, 125.56, 124.38, 122.40, 121.59, 120.91, 113.39, 113.31, 111.94, 55.67, 55.63, 50.09, 42.42, 26.23, 25.01 **(Figure 92).** ESI (-ve) m/z calculated for $C_{35}H_{25}N_7O_{18}S_4^{-4}$ [(M+Na)] 852.81, found 852.40 **(Figure 123).**

Chapter 3 Results and Discussion

3.1 Dimerization of quinazolinones using click chemistry

A number of different approaches have been tried to dimerize molecules. Some of the most popular methods are: 1. Ulmann coupling of halogenated monomers, 2. metal-catalyzed cross coupling, 3. phenol oxidative coupling and 4. nucleophilic substitution.

Ulmann coupling is probably one of the oldest dimerization methods. It is a copper catalyzed coupling of aryl halides. However, high reaction temperatures (260-300 °C) and poor yields (20-30%) **(Scheme 4)**.[60] Metal catalyzed cross coupling reactions is another way which has been used extensively. It consists of two main type of reactions, Stille coupling and Suzuki coupling. Stille reaction is a coupling reaction in which an organotin compound is coupled with an sp^2 hybridized organohalide catalyzed by palladium **(Scheme 5)**.[61] The high cost of the palladium catalyst, the need for an extremely oxygen free environment and the high probability of side reactions are the major drawbacks associated with such chemistry.[62] Suzuki is again a palladium catalyzed reaction between the aryl, vinyl boronic acid with aryl or vinyl halide **(Scheme 6)**.[63] This is an excellent option if the boronic acid derivative is commercially available as the point of contention is synthesis of the boronic acid derivative of the required starting material since it is problematic. Nucleophilic substitution is the simplest approach which can be

used for dimerization. In this case, dihaloalkanes, dihaloalkenes, dihalophenyls can be used as linkers in a S_N2 type reaction **(Scheme 7)**.[59] Thus, in spite of a large number of options being available, none of the above reactions satisfy the requirements needed in a reaction for the purpose of synthesizing a library.

Scheme 4 **General scheme for Ulmann Coupling**

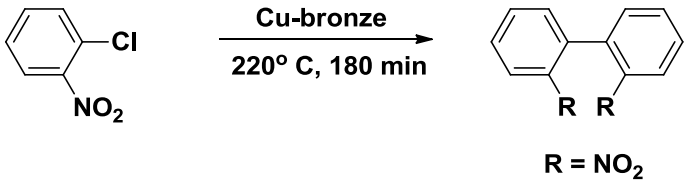

Scheme 5 **General scheme for Stille Coupling**

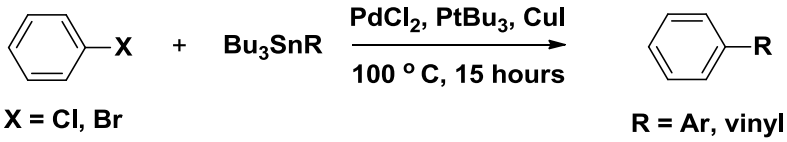

Scheme 6 **General scheme for Suzuki Coupling**

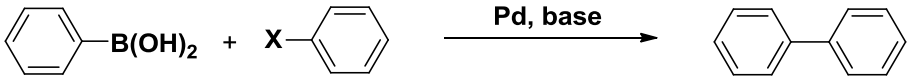

Scheme 7 **General scheme for Nucleophilic Substitution**

Despite the drawbacks of the above mentioned reactions, synthesizing a library of small organic molecules either by dimerization or any other method has been pursued and mastered in the last decade. From the years 2005 to 2009 alone, in excess of 2200 libraries of small molecules each containing hundreds of molecules of varying scaffolds have been generated.[72-76] Different approaches like solid-support chemistry, combinatorial chemistry, multicomponent reactions etc. have been used for achieving this feat.[15] Production of small molecule libraries via high-throughput extraction, purification and characterization has also gained popularity in recent times.[77] However, in this huge collection of small molecules, there in not a single library which contains molecules that can mimic heparin. In other words, creating a library of non-saccharide sulfated small molecules has never been attempted before.

The production of such a library of small sulfated molecules is necessary as it would probably unravel important information about heparin-protein interactions. Thus, the first aim of this thesis project was thus, to try and establish a protocol for dimerization of the quinazolinone monomers using reactions which have the following qualities: no protection-deprotection strategies, mild reaction conditions, high yields and easy purifications. It was decided to take the click chemistry approach considering high yields, mild conditions and easy purification are one of the main characteristics of this reaction. Another advantage of this reaction is that there is no stereochemical complication. Using copper sulfate ($CuSO_4$) as a catalyst at room temperature affords exclusively the 1,4-regioisomer.[71] This 1,4-regioisomer was confirmed using NMR spectroscopy as mentioned in the experimental section. After careful optimization and manipulation of the

solvent systems and catalyst, the reaction was calibrated to afford maximum yields. Thus, it was now possible to dimerize molecules with free hydroxyl groups. Monomers having a variety of functional groups, i.e. hydroxyl, acetyl and methoxy were tested to ensure the compatibility of this reaction with these functional groups. Monomers with up to two hydroxyl groups were successfully dimerized to the product having four free hydroxyl groups. This was achieved at yields ranging from 60-80 %. Unlike Suzuki reaction, where the coupling reaction is very efficient but preparation of the desired monomers is difficult, in this case preparation of the monomers for the click reaction was relatively easy consisting of S_N2 reactions at room temperature, quantitative yields and easy purification. Since, this protocol is now well established, efforts are on in our lab to increase the number and diversity of these hydroxyl groups with the aim of having dimers with greater structural diversity.

3.2 Non-aqueous purification of sulfated molecules

As mentioned previous, the major hurdle in synthesizing a library of small sulfated molecules was the considerable loss of yield and time due to the aqueous purification process like size exclusion chromatography. Because of extremely dilute chromatographic fractions, to overcome the limit of detection, the sample size for purification had to be in excess of 200 mg. This might not seem like a lot but if the synthetic scheme involves a large number of steps before sulfation, most often than not the first step has to be performed in multi-gram quantities to end up with the required amount. This results in rise in expense, not only due to the high amounts of starting

material used, but also in terms of the solvents and keeping the cost per reaction low is a very important parameter for the synthesis of such a library. For size exclusion chromatography to be performed, the column needs to be washed with the chromatographic vehicle, that is water for 12 hours. This is then followed by loading the sample and eluting it for the next 12 hours. The fractions containing the compound of interested are pooled together and lyophilized, which takes approximately 24 hours before it can be subjected to cation exchange. Thus, the total time required for such purifications is in excess of 48 hours. We had hypothesized earlier that considering the highly lipophilic backbone, if the charge of the sulfate is masked in some way, it would allow non-aqueous means to be employed for purification. The sulfation reaction was carried out in sulfur trioxide complexed with triethyl amine. The triethyl amine counter ion is sufficiently lipophilic to mask the charge of the sulfate. As expected, when subjected to normal phase silica gel column chromatography, using dichloromethane and methanol (0-20 %) as the solvent system, the dimers with as many as four sulfate groups could be easily chromatographed. With the success of this technique, such purifications were tried using a flash chromatography using the same solvent system, aiming to further reduce the purification time and further reducing the minimum sample size required for purification. This method was extremely successful and dimers with as many as four sulfate groups could be easily purified. The phenomenally low purification time (15 minutes) and low sample size requirements (15 mg) has made this a very valuable development towards the synthesis of libraries of small sulfated molecules.

Table 6 The following table gives a comparison between the different aspects of aqueous and non-aqueous chromatography.

Parameters	**Aqueous**	**Non-aqueous**
Eluent	Water	DCM : MeOH (0-20 %)
Separation media	Sephadex G-10	Silica gel
Time	~ 48 hrs.	~ 0.25 hrs.
Minimum sample size	200 mg	15 mg

3.3 Screening against coagulation enzymes

The synthesized compounds were screened against factor Xa, thrombin and factor XIa, the most important targets for anticoagulant agents. The synthesized molecules were first screened against each enzyme at 500 μM concentration and the residual enzyme activity calculated. If any compound showed 0 % residual enzyme activity, i.e. it completely inhibits the enzyme at this concentration, then its IC50 was calculated.

Figure 124 Factor Xa inhibition. Compounds present at 500 μM. Standard error in this experiment was less than 10 %.

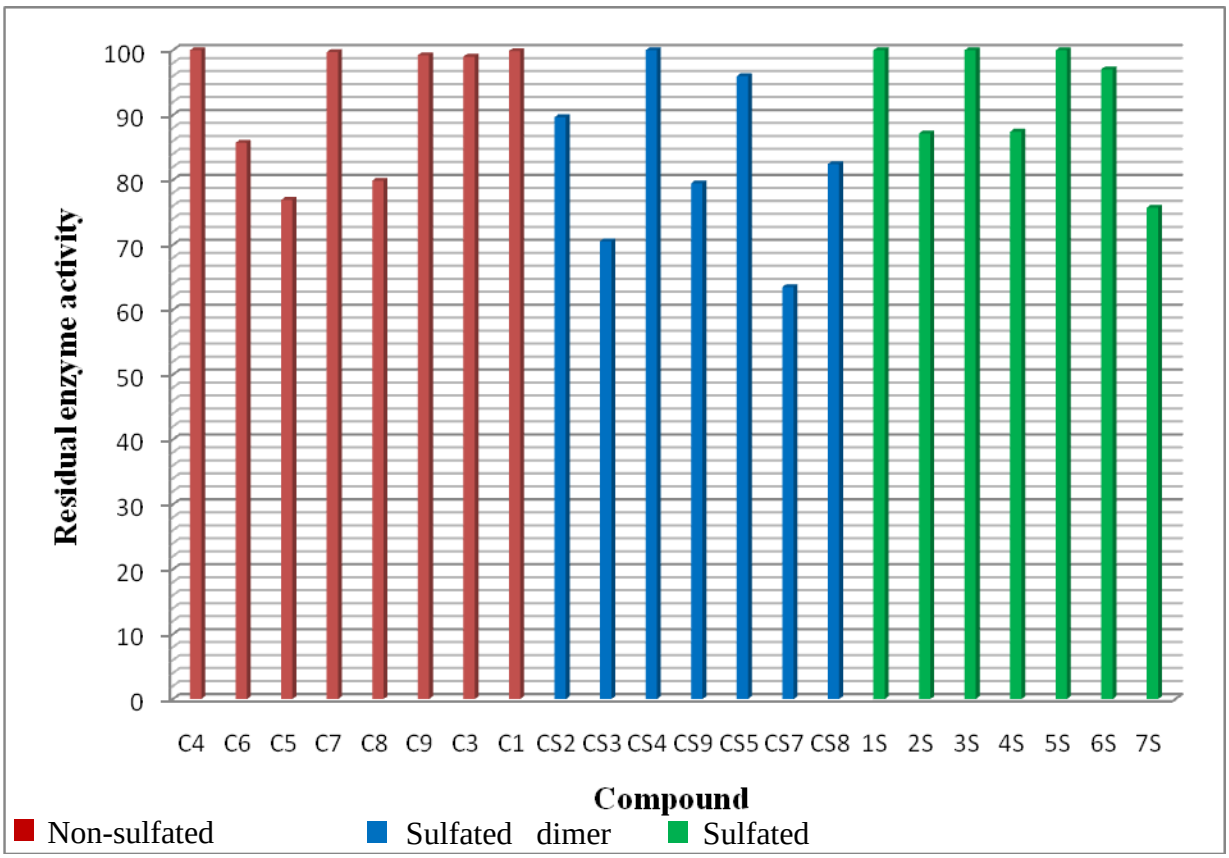

Thus, the residual enzyme activity for each compound was greater than 50 % indicating that these molecules do not have much inhibitory effects on factor Xa.

Firgure 125 Thrombin inhibition. Compounds present at 500 μM. Standard error in this experiment was less than 10 %.

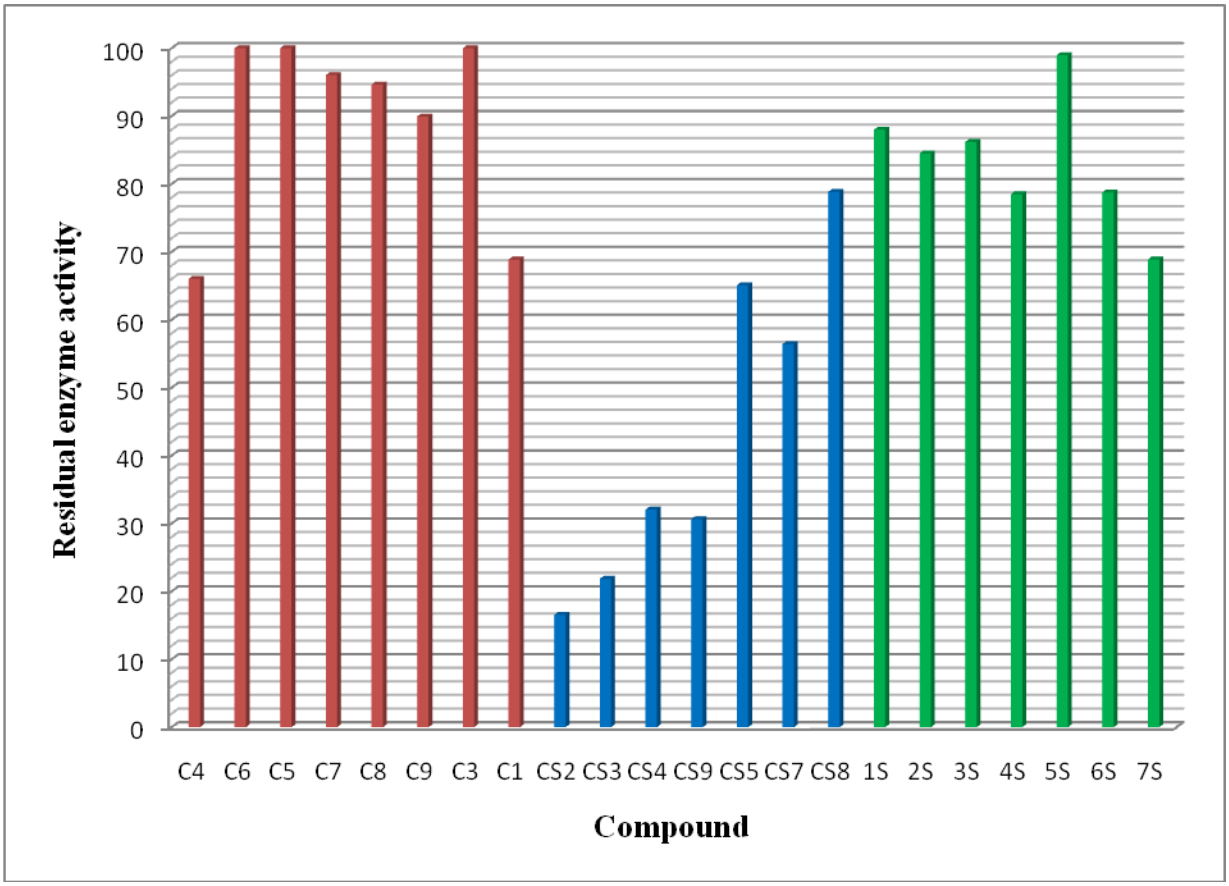

In case of thrombin, the non-sulfated dimers were found to be inactive with the residual enzyme active for each compound not going below 50 %. The same was observed for the sulfated monomers. However, in case of the sulfated dimers, a clear trend is evident. 'CS2' has one sulfate group, 'CS3' has two sulfates, 'CS4' and 'CS9' also have two sulfates but with additional acetyl and methoxy groups respectively. 'CS5', 'CS7' have three sulfates and 'CS8' has four sulfate groups **(Figure 3)**. Thus, as the number of sulfate group increases from 1-4 the inhibitory activity with respect to thrombin decreases.

Figure 126 Structures of the sulfated dimers CS2, CS3, CS4, CS5, CS7, CS8, CS9.

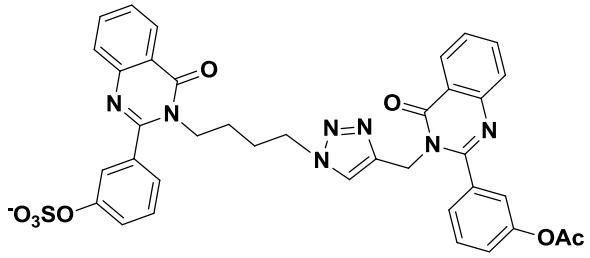

CS2

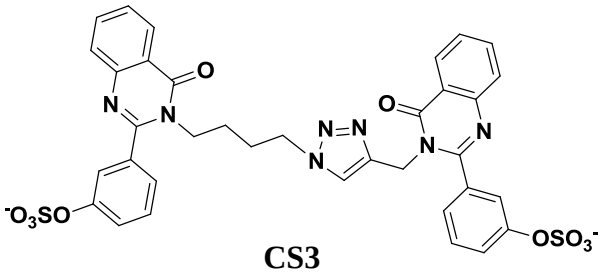

CS3

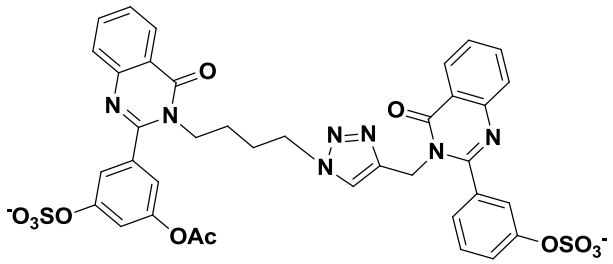

CS9

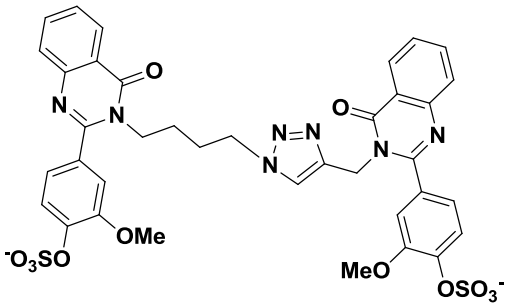

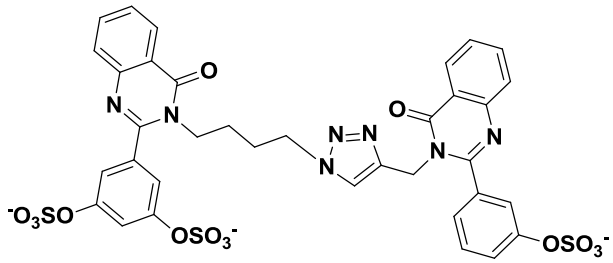

CS5

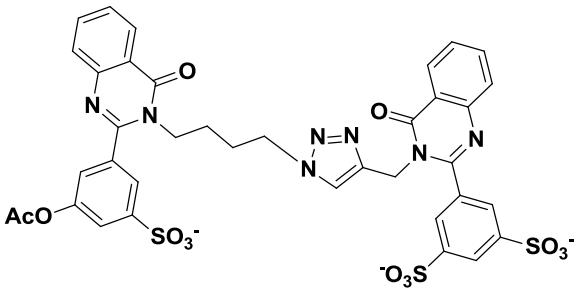

CS7

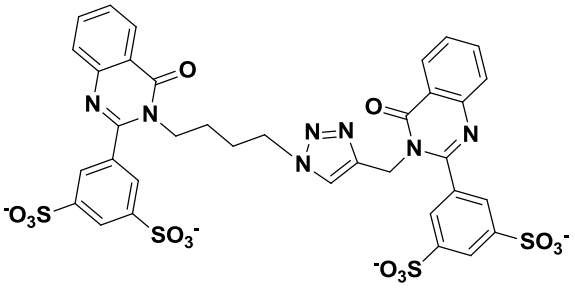

CS8

Figure 127 Factor XIa inhibition. Compounds present at 500 µM. Standard error in this experiment was less than 10 %.

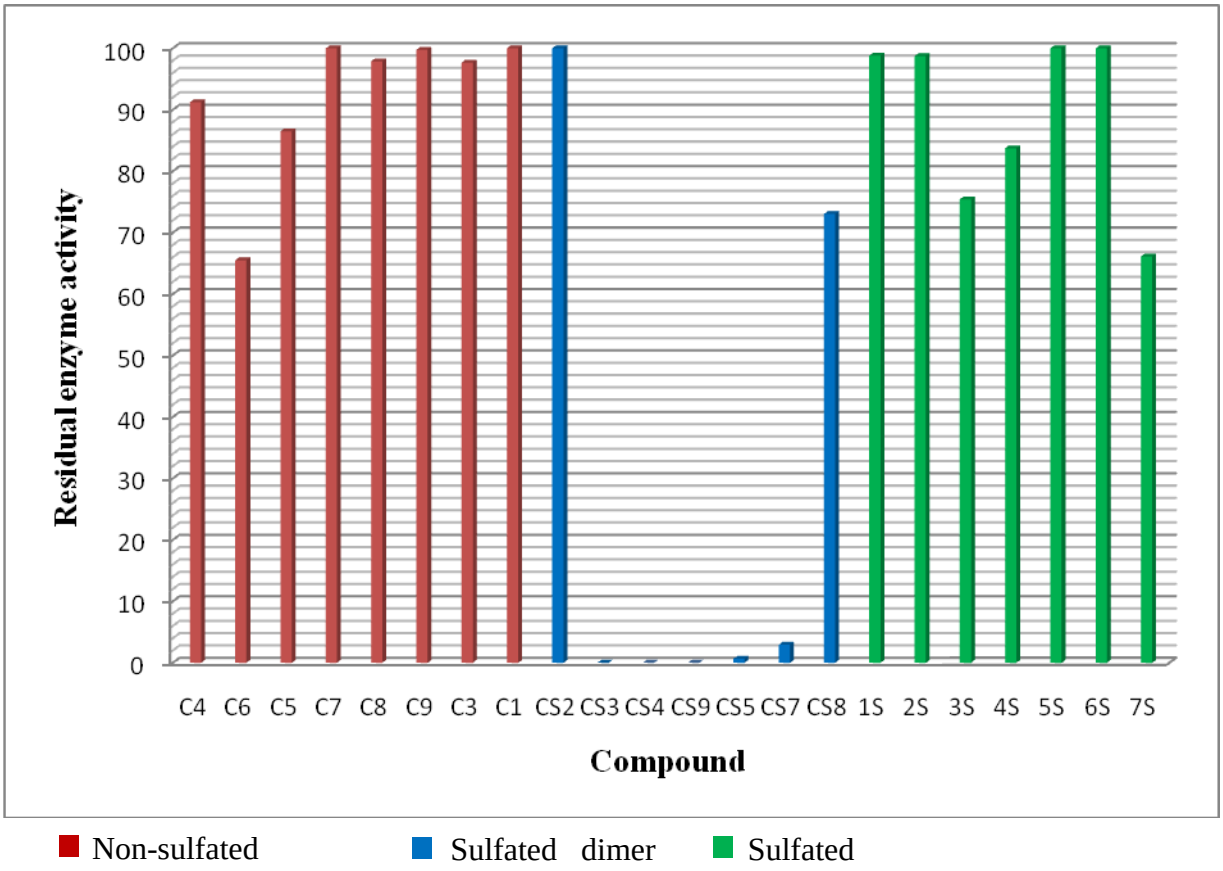

For factor XIa, yet again the non-sulfated dimers did not show any substantial inhibition. However, for sulfated dimers, again there is an interesting trend which is present. The mono-sulfated molecule 'CS2' was completely inactive. The compounds containing 2 and 3 sulfates viz. CS3, CS4, CS5, CS7 and CS9 almost completely inhibited the enzyme at 500 µM. While 'CS8' which has 4 sulfates was again inactive. In order to make a better comparison between CS3, CS4, CS5, CS7 and CS9 their IC50's were determined.

Figure 128 IC50 curve for CS3

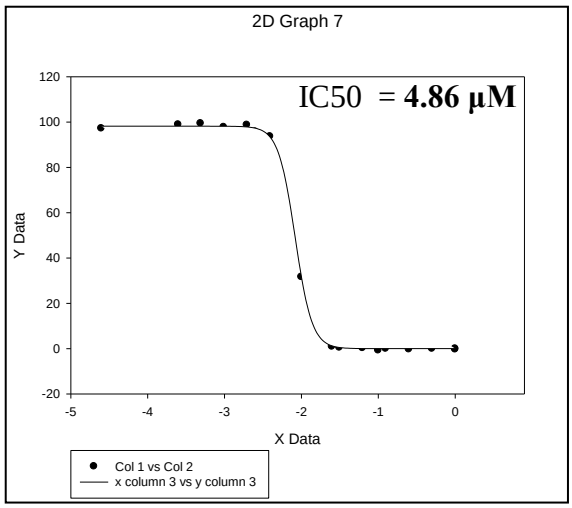

	Coefficient	Std. Error	t	P
logIC50	-2.0817	0.0052	-403.315	<0.0001
Ym	98.1641	0.3262	300.9777	<0.0001
Yo	1.81E-09	0.2564	7.07E-09	1
HS	3.9574	0.1881	21.0357	<0.0001

Figure 129 IC50 curve for CS4

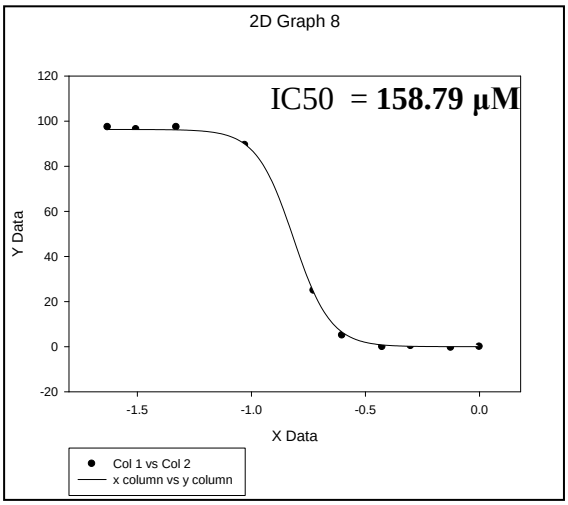

	Coefficient	Std. Error	t	P
logIC50	-0.8159	0.007	-116.8752	<0.0001
Ym	96.2958	0.6338	151.9312	<0.0001
Yo	5.58E-09	0.5984	9.33E-09	1
HS	5.3502	0.3011	17.7659	<0.0001

Figure 130 IC50 curve for CS9

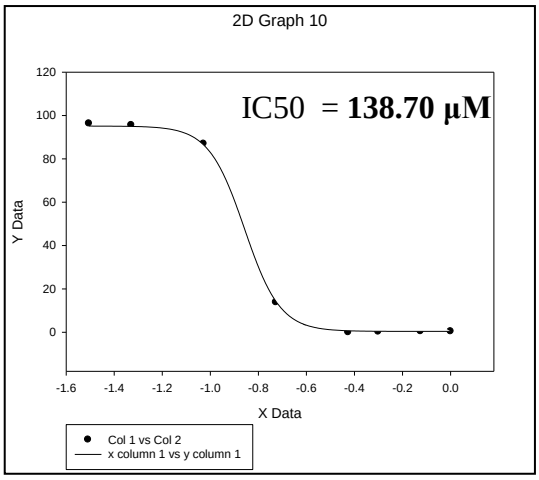

	Coefficient	Std. Error	t	P
logIC50	-0.8579	0.008	-106.6184	<0.0001
Ym	95.1395	0.783	121.5022	<0.0001
Yo	4.18E-01	0.6098	6.86E-01	0.5185
HS	5.85	0.31	18.8724	<0.0001

Figure 131 IC50 curve for CS5

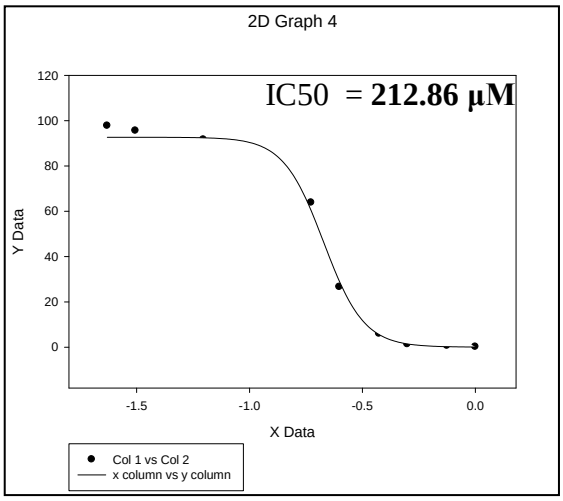

	Coefficient	Std. Error	t	P
logIC50	-0.6719	0.0114	-59.0696	<0.0001
Ym	92.6748	1.4844	62.4327	<0.0001
Yo	5.30E-02	1.9056	2.78E-02	0.9785
HS	4.8683	0.6124	7.9492	<0.0001

Figure 132 IC50 curve for CS7

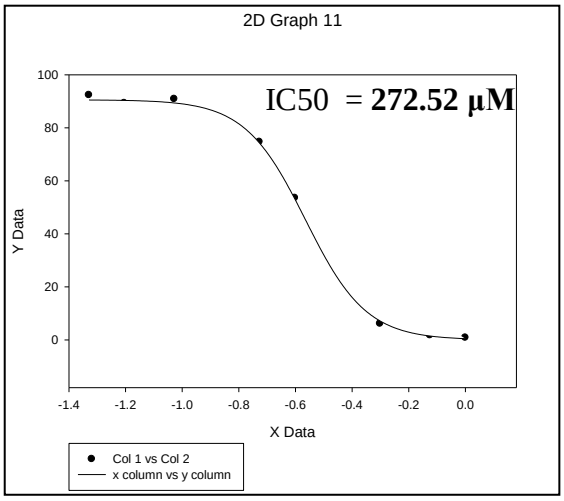

	Coefficient	Std. Error	t	P
logIC50	-0.5646	0.0094	-60.0924	<0.0001
Ym	90.5654	1.0855	83.4344	<0.0001
Yo	3.11E-10	0.9839	3.16E-10	1
HS	4.0509	0.3327	12.1744	<0.0001

Thus, summarizing the above results, the simplest structure **CS3** having just two sulfates is the most potent with an IC50 of 4.86 µM. As the substitutions increase, as in the case of **CS4** and **CS9** the IC50 goes up to 152.79 and 138.70 µM respectively. Both **CS5** and **CS7** have 3 sulfates and their IC50's are 212.86 and 272.52 respectively. Hence, as the number of sulfates increases from 2 to 3 the potency decreases.

Even more interesting is the level of specificity of these interactions. From the above results, it is evident that by changing the number of sulfates present in the molecule, there are subtle changes in the specificity for different enzymes. While the monosulfated **CS2** is the most potent compound in case of thrombin, it is completely inactive in case of factor XIa and factor Xa. Similarly, **CS3** which has an IC50 of 4.86

μM for factor XIa, is inactive for factor Xa and weakly interacts with thrombin (residual enzyme activity 22 % at 500 μM). **Figure 10** provides a comparison of this sulfate mediate selectivity for different enzymes.

Figure 133 Residual enzyme activity comparison between factor Xa, thrombin and factor XIa for sulfated dimers CS2, CS3, CS4, CS9, CS5, CS7, CS8. The x-axis depicts the compound number followed by the substitution pattern.

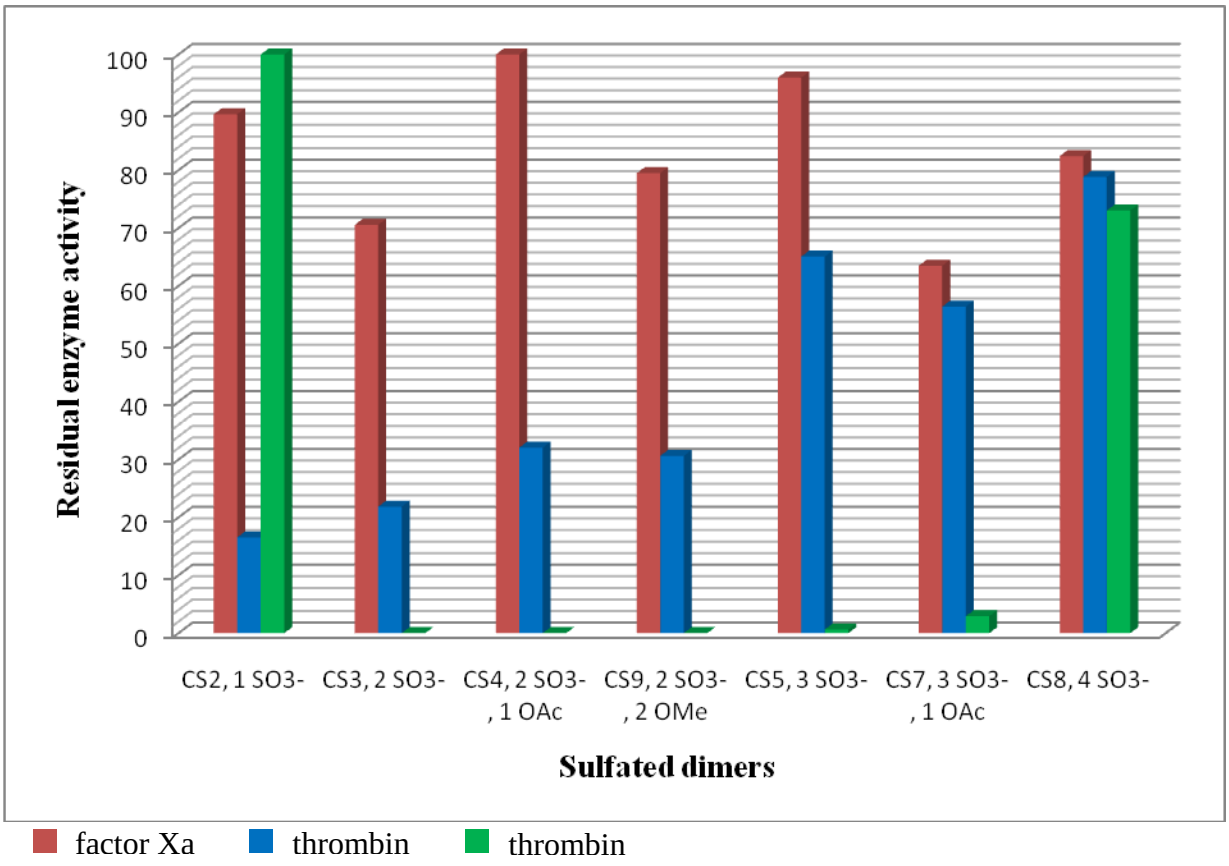

Further, the next graph is a plot of the IC 50 for factor XIa giving a better idea of the structural requirements for factor XIa inhibition.

Figure 134 Plot of IC 50 of sulfated dimers CS2, CS3, CS4, CS9, CS5, CS7, CS8. X-axis represents the important functional groups present on each compound.

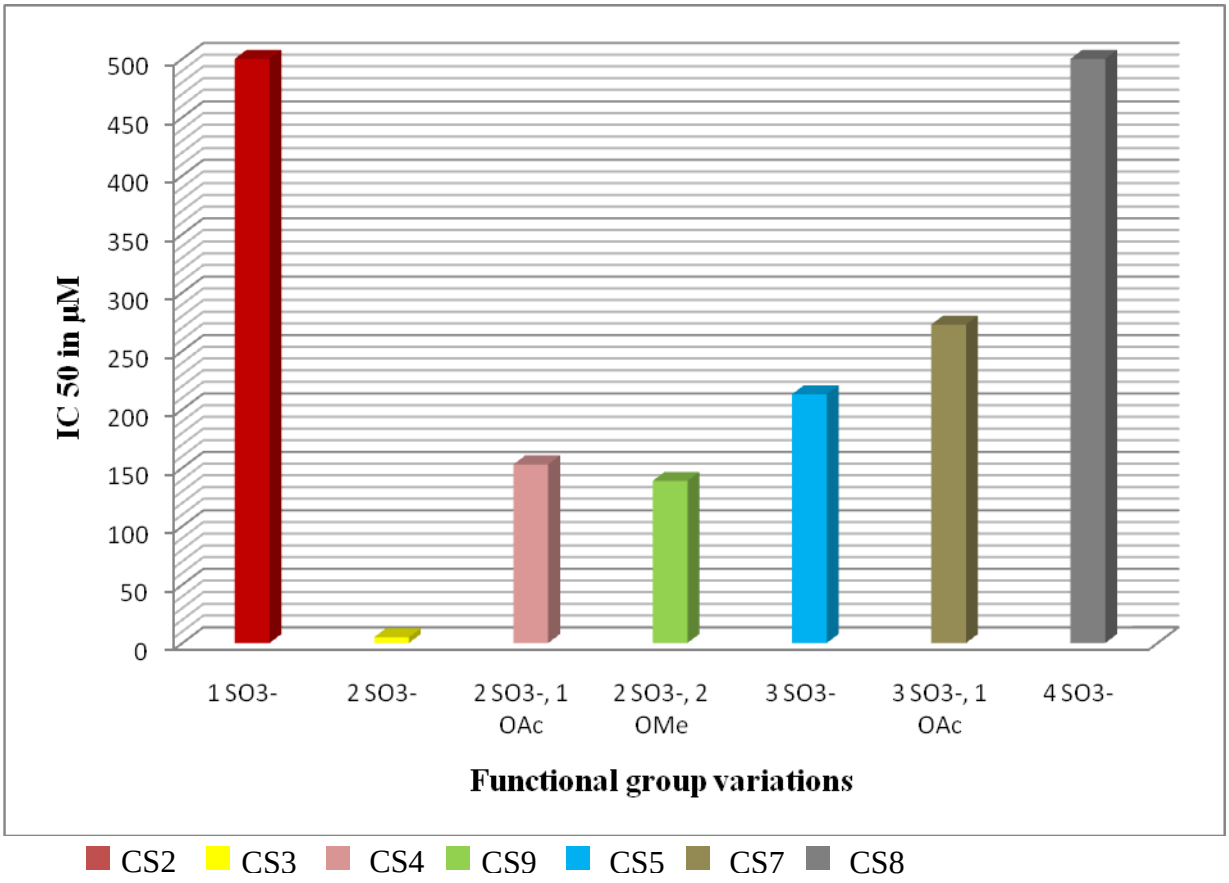

Thus, as expected, small change in the charge density can lead to a considerable change in the activity. The best molecule 'CS3' is very interesting as it is considerably potent towards factor XIa inhibition (IC 50 = 4.86 µM), considerably selective for this enzyme and hence, can be used as a lead for developing a better more selective molecule.

3.4 Advantages of targeting factor XIa

The pathway for thrombus formation involves mainly two phases, the initiation phase and amplification phase.[6] Tissue factor (TF) is present on the cell surface and upon vascular injury this TF is exposed. This exposed TF, activates factor VII (to VIIa) and forms a TF-VIIa complex. This complex, further activates factor IX (to IXa) and factor X (to Xa). Factor Xa ultimately activates prothrombin to thrombin. Tissue factor pathway inhibitor (TFI) and antithrombin normally inhibit this thrombin generation rapidly. However, small amounts of residual thrombin can activate fator XI (to XIa) which subsequently activates platelet bound factor IX (to IXa). This is the beginning of the amplification phase. The factor XIa then generates thrombin via factor Xa mediated activation which results in localized thrombus formation at the sites of injury.[65] **Figure 12** gives a schematic representation of the above mentioned phases. Its well known that LMWH, UFH and warfarin, target multiple coagulation factors due to which this therapy is associated with bleeding complications and a narrow therapeutic window. Although, fairly selectively thrombin and factor Xa inhibitors are available, since these act on the initiation phase, they affect the normal hemostasis and thus create opportunities for bleeding complications. Also, being fairly new, their clinical efficacy and safety are still being studied.[66] Conversely, since factor XIa is a part of the amplification phase, targeting factor XIa will reduce thrombus formation and since this will not affect the initiation phase, it would not affect the hemostasis and thus, should not present any bleeding complications. Further proof of the safety in targeting factor XIa was provided by Hanson and Gruber. They demonstrated using a baboon thrombosis model, that

inhibition of factor XIa using a anti factor XIa antibody, did not prevent thrombus initiation, yet it reduced the intraluminal thrombus growth to a significant extent. Even more significantly, this antibody, did not prolong the bleeding time.[67] Thus, targeting factor XIa seems like a promising strategy in order to develop safe as well as efficacious drugs.

Figure 135 Schematic representation of the initiation and amplification phases in the coagulation cascade. (Figure adapted from Gailani, D.; Renne, T. Intrinsic pathway of coagulation and arterial thrombosis. *Arterioscler. Thromb. Vasc. Biol.* **2007**, *27*, 2507-2513.)

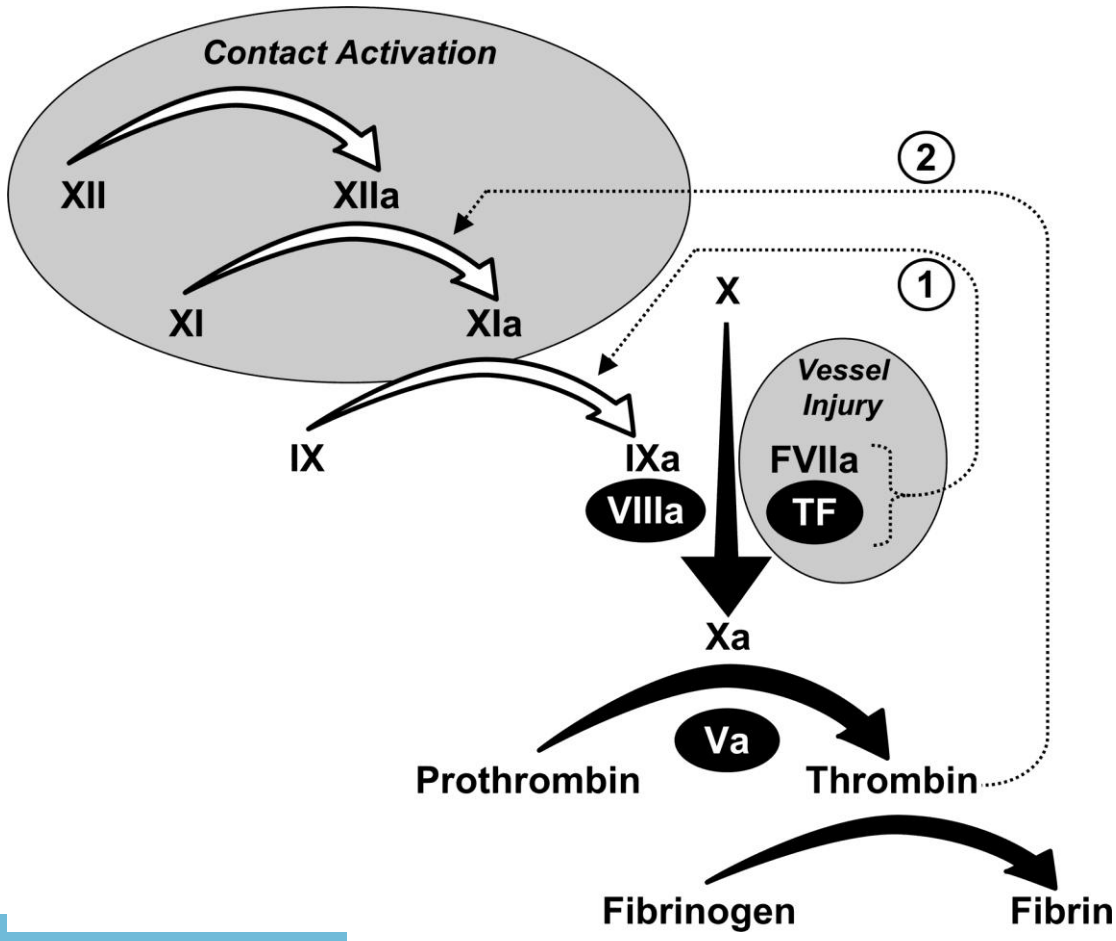

3.5 Probable binding site

Factor XIa, a serine protease, exists as a disulfide linked homodimer having a molecular mass of approximately 160 kDa. Within each monomer, the N-terminal heavy chain contains four 'apple domains' which are basically repeating loops of 90-91 amino acids. Natural ligands such as factor XI and other platelet glycoproteins bind at this site.[68] The C-terminal of each monomer contains the catalytic domain.[69] The binding sites for heparin are located in two areas, the apple-3 domain, where the basic residues present interact with heparin and the catalytic domain.[70] Since, **CS3** is designed to mimic heparin, it is possible that it binds to the apple-3 domain. Another observation that also suggests binding of **CS3** to apple-3 is the observed selectivity. All serine protease share similar homology, especially at the active site. Thus, it is extremely difficult to achieve selectivity for an active-site inhibitor. However, there might be considerable difference at other sites. Heparin exploits the basic residues at allosteric sites, leading to a conformation change, finally causing inhibition. At this point, the data suggests that **CS3** also binds at an allosteric site, which could most probably be the apple-3 domain, however this can be readily verified by performing Michaelis-Menten kinetics experiment. If this is the case, then it will be significantly easy to maximize the affinity while maintaining or even improving the selectivity.

3.6 Summary

Thus, it is evident that subtle changes in structure can lead to enormous changes in affinity, selectivity etc. towards different proteins. Before beginning this study, the main

aim was to establish a protocol for dimerization and non-aqueous purification of sulfated molecules with the final aim of making the synthesis of a library of small sulfated molecules a possibility. The need was this library was emphasized in the beginning and the outcome of testing this small library has supported our claim. However, a larger library would provide us with even more information and hopefully, it will one day be possible to predict the effect of a sulfated molecule on a protein. Also, from the results of the biological screening, the importance of sulfation is clear, with all the unsulfated molecules being inactive. Further, the sulfated monomers also were inactive or weakly active, indicating the need for making dimers and possibly in the future, trimers and tetramers. The aim and focus of our lab has been to understand this complex system, as drug discovery and design is only a byproduct of this understanding.

Chapter 4 Future Directions

'CS3' seems like a promising lead, having an IC 50 of 4.86 μM against factor XIa with considerable selectivity. However, further studies will enable us to optimize the design and attain better activity as well as selectivity. A 'two-pronged' approach consisting of synthetic exploration and biochemical studies might be a good way to further explore this lead and optimize its structure.

4.1 Synthetic exploration

The structure of **CS3** leaves great room for making further modifications with a view of achieving maximum inhibitory potential. Since the non-sulfated analogue of **CS3** was found to be inactive, the importance of the sulfate group for activity is well established. However, the position of the sulfate group can be modified further to check for any effect on activity **(Table 7)**. The chain length for the azide as well as propargyl linker can also undergo substantial exploration to optimize the chain length. The best way to do this efficiently would be to reduce one carbon from the azide side first and depending on the outcome of this chain length reductions further modifications can be made **(Table 8)**. Once the optimum structure is established, the 1,5-regioisomer of that analogue can be synthesized to analyze the effect of this subtle change in geometry **(Figure 137)**.

Figure 136 Possible structural modifications

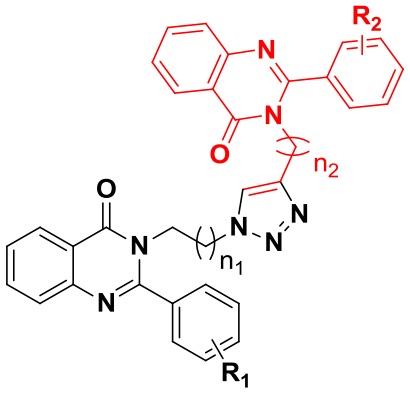

Table 1 Modification of R_1 and R_2 (Color red represents substitution pattern of CS3)

R1	R2
3-SO_3^-	3-SO_3^-
2-SO_3^-	2-SO_3^-
4-SO_3^-	4-SO_3^-
2-SO_3^-	H
3-SO_3^-	H
4-SO_3^-	H
H	2-SO_3^-
H	3-SO_3^-
H	4-SO_3^-

Table 2 Modifications of n1 and n2 (Color red represents substitution pattern of CS3)

n1	n2
4	1
3	1
2	1
4	2
4	2
3	2
2	2
3	3

Figure 137 1,5-regioisomer of the optimized structure

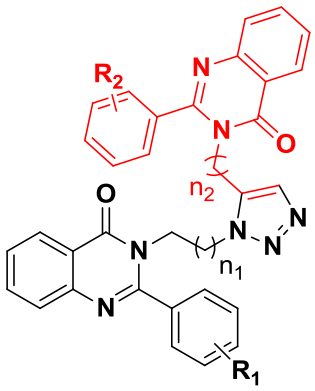

4.2 Biochemical studies and x-ray crystallography

Since these molecules are synthesized as heparin analogues, it is hypothesized that they bind to the heparin binding site on factor XIa. However, this needs to be confirmed by doing several biochemical experiments. The simplest experiment which would give us an

idea if it is binding to a site other than the active site is the Michaelis-Menten kinetics experiment. This experiment will also provide information about the inhibition, whether competitive, non-competitive or uncompetitive.

If the above mentioned experiment indicates allosteric binding, then competitive studies with heparin would provide further insight about the binding site of the molecule. Further, crystallization of the optimized inhibitor with factor XIa (human or bovine) would provide conclusive evidence about the binding site and more important binding mode of the molecule. This will also provide the interacting amino acids and thus broaden the scope to optimize the interactions and thus attain its maximum inhibitory potential.

Literature Cited

Literature Cited

(1) Wardrop, D.; Keeling D. The story of discovery of heparin and warfarin. *Br. J. Heamatol.* **2008**, *141,* 757-763.

(2) Capila, I.; Linhardt, R. J. Heparin-protein interactions. *Angew. Chem. Int. Ed.* **2002,** *41,* 390-412.

(3) Charles, A. F.; Todd, A. R. Observation on the structure of the barium salt of heparin. *Biochem. J.* **1940,** *34,* 112-118.

(4) Perlin, A. S.; Mazurek, M.; Jaques, L. B.; Kavanaugh, L. W. A proton magnetic resonance study of heparin, L-iduronic acid residues in commercial heparins. *Carbohydr. Res.* **1968,** *7,* 369-379.

(5) Best, C. H. Preparation of heparin and its use in the first clinical cases. *Circulation* **1959,** *19,* 79-86.

(6) Rodden, L.; Feingold, D. S. A vintage year for Jorpes, Crafoord, and heparin. *Trends Biochem. Sci.* **1985,** *10,* 407-409.

(7) Fareed, J.; Hoppensteadt, D. A.; Bick, R. L. An update on heparins at the beginning of the new millennium. *Semin. Thromb. Hemostasis* **2000,** *26,* 5-21.

(8) Rubin, H. Serine protease inhibitors: Where mechanism meets medicine. *Nat. Med.* **1996,** *2,* 632-633.

(9) Bjork, I.; Olson, S. T. Antithrombin. A bloody important serpin. *Adv. Exp. Med. Biol.* **1997,** *425,* 17-33.

(10) Dementiev, A.; Petitou, M.; Herbert, J. M.; Gettins, P. G. The ternary complex of antithrombin-anhydrothrombin-heparin reveals the basis of inhibitor specificity. *Nat. Struct. Biol.* **2004,** *11,* 863-867.

(11) Olson, S. T.; Swanson, R.; Raub-Segall, E.; Bedsted, T.; Sadri, M.; Petitou, M.; Herault, J. P.; Herbert, J. M.; Bjork, I. Accelerating ability of synthetic oligosaccharides on antithrombin inhibition of proteinases of clotting and fibrinolytic systems. Comparison with heparin and low-molecular weight heparin. *Thromb. Haemost.* **2004,** *92,* 929-939.

(12) Olson, S. T.; Bjork, I.; Sheffer, R.; Craig, P. A.; Shore, J. D.; Choay, J. Role of the antithrombin binding pentasaccharide in heparin acceleration of antithrombin proteinase reactions. Resolution of antithrombin conformational changes contributing to heparin rate enhancement. *J. Biol. Chem.* **1992,** *267,* 12528-12538.

(13) Olson, S. T.; Bjork, I. Predominant contribution of surface approximation to the mechanism of heparin acceleration of the antithrombin-thrombin reaction. Elucidation from salt concentration effects. *J.Biol. Chem.* **1991,** *266,* 6353-6364.

(14) Burgess, W. H.; Maciag, T. The heparin binding (fibroblast) growth factor family of proteins. *Annu. Rev. Biochem.* **1989,** *58,* 575-606.

(15) Clowes, A. W.; Karnowsky, M. J. Supression by heparin of smooth muscle cell proliferation in injured artries. *Nature* **1977,** *265,* 625-626.

(16) Shing, Y.; Folkman, J.; Sullivan, R.; Butterfield, C.; Murray, J. et al. Heparin affinity: purification of tumor-derived capillary endothelial growth factor. *Science* **1984,** *223,* 1296-1299.

(17) Schlessinger, J.; Plotnikov, A. N.; Ibrahimi, O. A.; Eliseenkova, A. V.; Yeh, B. K.; Yayon, A.; Linhardt, R. J.; Mohommadi, M. *Mol. Cell* **2000,** *6,* 743-750.

(18) Gitay-Goren, H.; Soker, S.; Vlodavsky, I.; Neufeld, G. The binding of vascular endothelial growth factor to its receptors is dependent on cell surface-associated heparin like molecules. *J. Biol. Chem.* **1992,** *267,* 6093-6098.

(19) Higashiyama, S.; Abraham, J. A.; Klagsbrun, M. Heparin-binding EGF-like growth factor stimulation of smooth muscle cell migration: dependence on interactions with cell surface heparan sulfate. *J. Cell Biol.* **1993,** *122,* 933-940.

(20) Castellot, J. J. Jr.; Wong, K.; Herman, B.; Hoover, R. L.; Albertini, D. F. et al. Binding and internalization of heparin by vascular smooth muscle cells. *J. Cell Physiol.* **1985,** *124,* 13-20.

(21) Sasisekharan, R.; Shriver, Z.; Venkataraman, G.; Narayanasami, U. Roles of heparan sulfate glycosaminoglycans in cancer. *Nat. Rev. Cancer* **2002,** *2,* 521-528.

(22) Bussolino, F.; DiRenzo, M. F.; Ziche, M.; Bocchietto, E.; Olivero, M.; Naldini, L.; Guadino, G.; Tamagnone, L.; Coffer, A.; Comoglio, P. M. *J. Cell Biol.* **1992,** *119,* 629-641.

(23) Mousa, S. A. Comparative efficacy of different low-molecular weight heparins (LMWHs) and drug interactions with LMWH: implications for management of vascular disorders. *Semin. Thromb. Hemost.* **2000,** *26 Suppl 1,* 39-46.

(24) Tyrell, D. J.; Horne, A. P.; Holme, K. R.; Preuss, J. M.; Page, C. P. Heparin in inflammation: potential therapeutic applications beyond anticoagulation. *Adv. Pharmacol.* **1999,** *46*, 151-208.

(25) Tyrell, D. J.; Kilfeather, S.; Page, C. P. Therapeutic uses of heparin beyond its traditional role as an anticoagulant. *Trends Pharmacol. Sci.* **1995,** *16*, 198-204.

(26) Lantz, M.; Thysell, H.; Nilsson, E.; Olsson, I. On the binding of tumor necrosis factor (TNF) to heparin and the release in vivo of the TNF-binding protein I by heparin. *J. Clin. Invest.* **1991,** *88*, 2026-2031.

(27) Hiebert, L. M.; Liu, J. M. Heparin protects cultured arterial endothelial cells from damage by toxic oxygen metabolites. *Atherosclerosis* **1990,** *83*, 47-51.

(28) Matzner, Y.; Marx, G.; Drexler, R.; Eldor, A. The inhibitory effect of heparin and related glycosaminoglycans on neutrophil chemotaxis. *Thromb. Haemostat.* **1984,** *52*, 134-137.

(29) Gaffney, P. R.; O'Leary, J. J.; Doyle, C. T.; Gaffney, A.; Hogan, J. et al. Response to heparin in patients with ulcerative colitis. *Lancet* **1991,** *337*, 192-195.

(30) Prajapati, D. N.; Newcomer, J. R.; Emmons, J.; Abu-Hajir, M.; Binion, D. G. Successful treatment of an acute flare of steroid-resistant Chron's colitis during pregnancy with unfractionated heparin. *Inflamm. Bowel Dis.* **2002,** *8*, 192-195.

(31) Bernfield, M.; Kokeyesi, R.; Kato, M.; Hinkes, M. T.; et al. Biology of the syndecans: A family of the transmembrane heparan sulfate proteoglycans. *Annu. Rev. Cell Biol.* **1992,** *8*, 365-393.

(32) WuDunn, D.; Spear, P. G. Initial interaction of herpes simplex virus with cells is binding to heparan sulfate. *J. Virol.* **1989,** *63,* 52-58.

(33) Harrop, H. A.; Coombe, D. R.; Rider, C. C. Heparin specifically inhibits binding of V3 loop antibodies to HIV-1 gp120, an effect potentiated by CD4 binding. *AIDS* **1994,** *8,* 183.

(34) Shukla, D.; Spear, P. G. Herpesviruses and heparan sulfate: an intimate relationship in aid of viral entry. *J. Clin. Invest.* **2001,** *108,* 503-510.

(35) Raghuraman, A.; Tiwari, V.; Zhao, Q.; Shukla, D.; Debnath, A. S.; Desai, U. R. Viral inhibition studies on sulfated lignin, a chemically modified biopolymer and a potential mimic of heparan sulfate. *Biomacromolecules* **2007,** *8,* 1759-1763.

(36) Cardin, A. D.; Weintraub, H. J. Molecular modeling of protein-glycosaminoglycan interactions. *Arteriosclerosis* **1989,** *217,* 21-32.

(37) Sobel, M.; Soler, D. F.; Kermode, J. C.; Harris, B. R. Localization and characterization of a heparin binding domain peptide of human Von Willebrand Factor. *J. Biol. Chem.* **1992,** *267,* 8857-8862.

(38) Lindahl, U.; Backstrom, G.; Thunberg, L.; Leder, I. G. Evidence of 3-*O*-sulfated D-glucosamine residue in the antithrombin bindingsequence of heparin. *Proc. Natl. Acad. Sci. USA* **1980**, *77,* 6551-6555.

(39) Faham, S.; Linhardt, R. J.; Rees, D. C. Diversity does make a difference: fibroblast growth factor-heparin interactions. *Curr. Opin. Struct. Biol.* **1998**, *8,* 578-586.

(40) Verghese, J.; Liang, A.; Sidhu, P. P.; Hindle, M.; Zhou, Q.; Desai, U. R. First steps in the direction of synthetic, allosteric, direct inhibitors of thrombin and factor Xa. *Bioorg. Med. Chem. Lett.* **2009**, *19*, 4126-4129.

(41) Sears, P.; Wong, C. H. Enzyme action in glycoprotein synthesis. *Cell Mol. Life Sci.* **1998**, *54*, 223-252.

(42) Sears, P.; Wong, C. H. Toward automated synthesis of oligosaccharides and glycoproteins. *Science* **2001**, *291*, 2344-2350.

(43) Seeberger, P. H.; Haase, W. C.; Solid-phase oligosaccharide synthesis and combinatorial carbohydrate libraries. *Chem. Rev.* **2000**, *100*, 4349-4393.

(44) Heidlas, J. E.; Williams, K. W.; Whitesides, G. M. Nucleoside phosphate sugars: syntheses on practical scales for use as reagents in enzymatic preparation of oligosaccharides and glycoconjugates. *Acc. Chem. Res.* **1992**, *25*, 307-314.

(45) Wong, C. H.; Haynie, S. L.; Whitesides, G. M. Enzyme catalyzed synthesis of N-acetyl lactoseamine with in situ regeneration of uridine 5'-phosphate glucose and uridine 5'-diphosphate galactose. *J. Org. Chem.* **1982**, *47*, 5416-5418.

(46) Gunnarsson, G. T.; Desai, U. R. Exploring new non-sugar sulfated molecules as activators of antithrombin. *Bioorg. Med. Chem. Lett.* **2003**, *13*, 679-683.

(47) Raghuraman, A.; Riaz, M.; Hindle, M.; Desai, U. R. Rapid and efficient microwave assisted synthesis of highly sulfated organic scaffolds. *Tetrahedron Lett.* **2007**, *48*, 6754-6758.

(48) Al-Horani, R.; Desai, U. R. Chemical sulfation of small molecules-advances and challenges. *Tetrahedron* **2010**, *66*, 2907-2918.

(49) Hoiberg, C. P.; Mumma, R. O. Preparation of sulfate esters. Reactions of various alcohols, phenols, amines, mercaptans and oximes with sulfuric acid and dicyclohexylcarbodiimide. *J. Am. Chem. Soc.* **1969**, *91*, 4273-4278.

(50) Gunnarsson, G. T.; Riaz, M.; Adams, J.; Desai, U. R. Synthesis of per-sulfated flavonoid using 2,2,2-trichloroethyl protecting group and their factor Xa inhibition potential. *Bioorg. Med. Chem. Lett.* **2005**, *13*, 1783-1789.

(51) Kanie, O.; Barresi,F.; Ding, Y.; Labbe, J.; et al. A strategy of random glycosylation for the production of oligosaccharide libraries. *Angew. Chem. Int. Ed. Engl.* **1995**, *34*, 2720-2722.

(52) Boons, J. G.; Heskamp, B.; Hout, F. Vinyl glycosides in oligosaccharide synthesis a strategy for preparation of trisaccharide libraries based on latent-active glycosylation *Angew. Chem. Int. Ed. Engl.* **1996**, *35*, 2845-2847.

(53) Zhu, T.; Boons, G. J. A two directional approach for solid-phase synthesis of trisaccharide libraries. *Angew. Chem. Int. Ed. Engl.* **1998**, *37*, 1898-1900.

(54) Noti. C.; Seeberger, P. H. Chemical approaches to define the structure-activity relationship of heparin-like glycosaminoglycans. *Chem. Biol.* **2005**, *12*, 731-756.

(55) Basten, J.; Jaurand, G.; Olde-Hanter, B.; Duchaussoy, P.; Petitoub, M.; Van Boeckel. Biologically active heparin-like fragments with a "non-glycosamino" glycan structure. *Bioorg. Med. Chem. Lett.* **1992**, *2*, 905-910.

(56) Haller, M.; Boons, G. J. Towards a modular approach for heparin synthesis. *J. Am. Chem. Soc.* **2001**, *1*, 814-822.

(57) Huang, S. X.; Powell, E.; Rajski, S. R.; et al. Discovery and total synthesis of a new estrogen receptor heterodimerizing actinopolymorphol A from *Actinopolymorpha rutilus*. *Org. Lett.* **2010**, *12*, 3525-3527.

(58) Rahman, M.; Riaz, M.; Desai, U. R. Synthesis of biologically relevant biflavanoids-A review. *Chem. Biodivers.* **2007**, *4*, 2495-2527.

(59) Rahman, M.; Riaz, M.; Desai, U. R. Synthesis of biologically relevant biflavanoids-A review. *Chem. Biodivers.* **2007**, *4*, 2495-2527.

(60) Hassan, J.; Sevignon, M.; Gozzi, C.; Schulz, E.; Lemaire, M. Aryl-aryl bond formation, one century after the discovery of the ulmann reaction. *Chem. Rev.* **2002**, *102*, 1359-1470.

(61) Milstein, D.; Stille, J. K. A general selective and facile method for ketone synthesis from acid chlorides and organotin compounds catalyzed by palladium. *J. Am. Chem. Soc.* **1978**, *100*, 3636-3638.

(62) Farina, V.; Kapadia, S.; Krishnan, B.; Wang, C.; Liebeskind, L. S. On the nature of the copper effect in stille cross coupling. *J. Org. Chem.* **1994**, *59*, 5905-5911.

(63) Suzuki, A. Recent advances in the cross-coupling reactions of organoboron derivatives with organic electrophiles, 1995-1998. *J. Organometallic Chem.* **1998**, *576*, 147-168.

(64) Bouma, B. N.; Meijers, J. C. M. Role of blood coagulation factor XI in downregulation of fibrinolysis. *Curr. Opin. Hematol.* **2000**, *7*, 266-272.

(65) Jin, L.; Pandey, P.; Babine, R. E.; et al. Crystal structures of the FXIa catalytic domain in complex with ecotin mutants reveal substrate like interactions. *J. Biol. Chem.* **2005**, *280*, 4704-4712.

(66) Hrish, J.; O'Donnell, M.; Weitz, J. I. New anticoagulants. *Blood* **2005**, *105*, 453-463.

(67) Gruber, A.; Hanson, S. R. Factor XI dependence of surface and tissue factor-initiated thrombus formation in primates. *Blood* **2011**, *102*, 953-955.

(68) Walsh, P. N. Platelets and factor XI bypass the contact system of blood coagulation. *Thromb. Haemost.* **1999**, *82*, 234-242.

(69) Davie, E. W.; Kurachi, K. Activation of human factor XI (plasma thromboplastin antecedent) by Factor XIIa (activated Hageman factor). *Biochemistry* **1977**, *16*, 5831-5839.

(70) Zhao, M.; Abdel-Razek, T.; Sun, M. F.; Gailani, D. Characterization of a heparin binding site on the heavy chain of factor XIa. *J. Biol. Chem.* **1998**, *273*, 31153-31159.

(71) Kolb, H. C.; Sharpless, K. B. The growing impact of click chemistry on drug discovery. *Drug Discov. Today* **2003**, *24*, 1128-1137.

(72) Dolle, E. R.; Bourdonnec, L. B.; Worm, K.; Morales, G. A.; Thomas, C. J.; Zhang, W. Comprehensive survey of chemical libraries for drug discovery and chemical biology:2009. *J. Comb. Chem.* **2010**, *12*, 765-806.

(73) Dolle, E. R.; Bourdonnec, L. B.; Goodman, A..; Morales, G. A.; Thomas, C. J.; Zhang, W. Comprehensive survey of chemical libraries for drug discovery and chemical biology:2008. *J. Comb. Chem.* **2009**, *11*, 739-790.

(74) Dolle, E. R.; Bourdonnec, L. B.; Goodman, A.; Morales, G. A.; Thomas, C. J.; Zhang, W. Comprehensive survey of chemical libraries for drug discovery and chemical biology:2007. *J. Comb. Chem.* **2008**, *10*, 754-802.

(75) Dolle, E. R.; Bourdonnec, L. B.; Goodman, A.; Morales, G. A.; Salvino, J. M..; Zhang, W. Comprehensive survey of chemical libraries for drug discovery and chemical biology:2006. *J. Comb. Chem.* **2007**, *9*, 855-902.

(76) Dolle, E. R.; Bourdonnec, L. B.; Morales, G. A.; Moriarty, K. J.; Salvino, J. M. Comprehensive survey of chemical libraries for drug discovery and chemical biology:2005. *J. Comb. Chem.* **2006**, *8*, 597-635.

(77) Eldridge, G. R.; Vervoort, H. C.; Lee, C. M.; et al. High-throughput method for production and analysis of large natural product libraries for drug discovery. *Anal. Chem.* **2002**, *74*, 3963-3971.

APPENDIX A

Figure 8

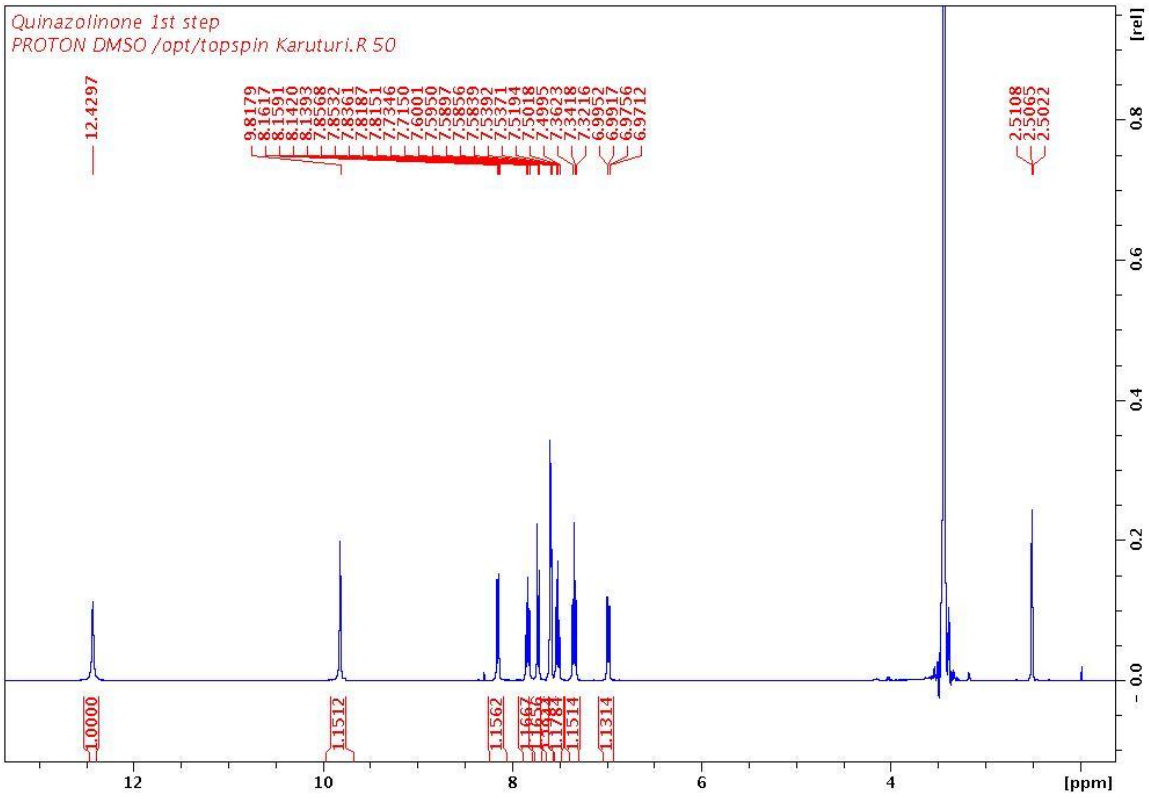

Figure 9

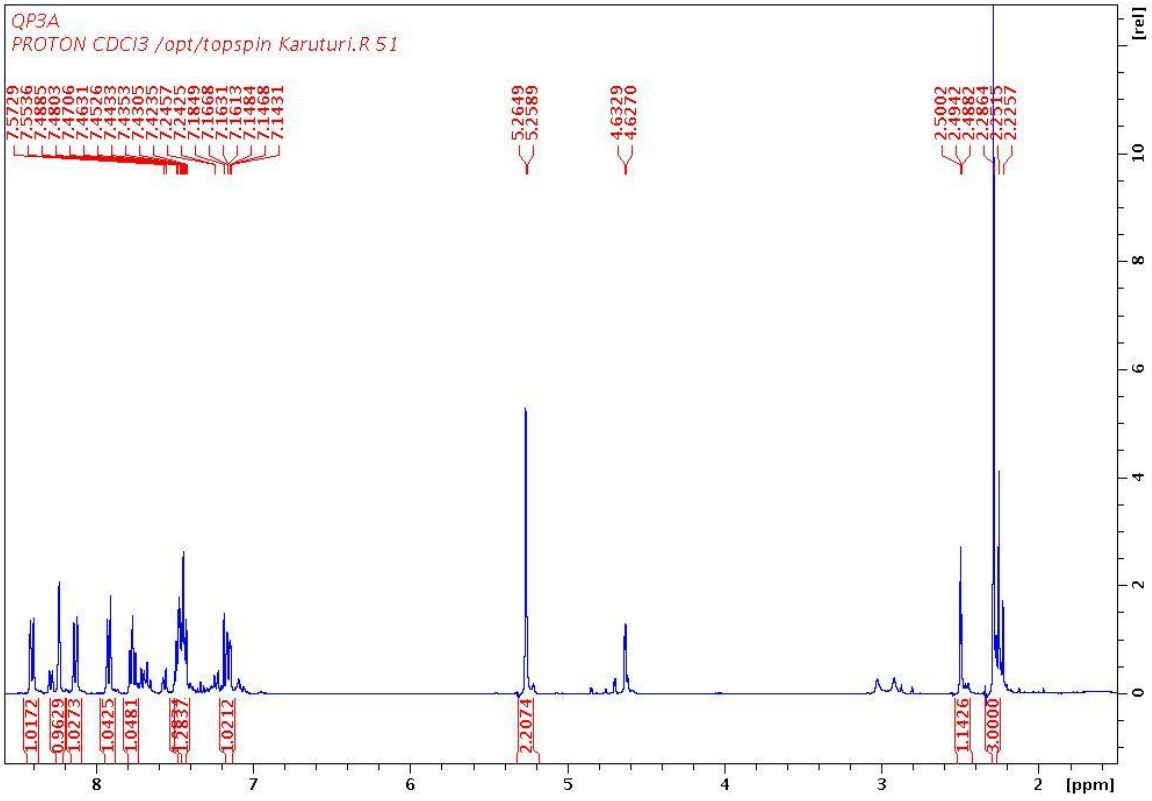

Figure 10

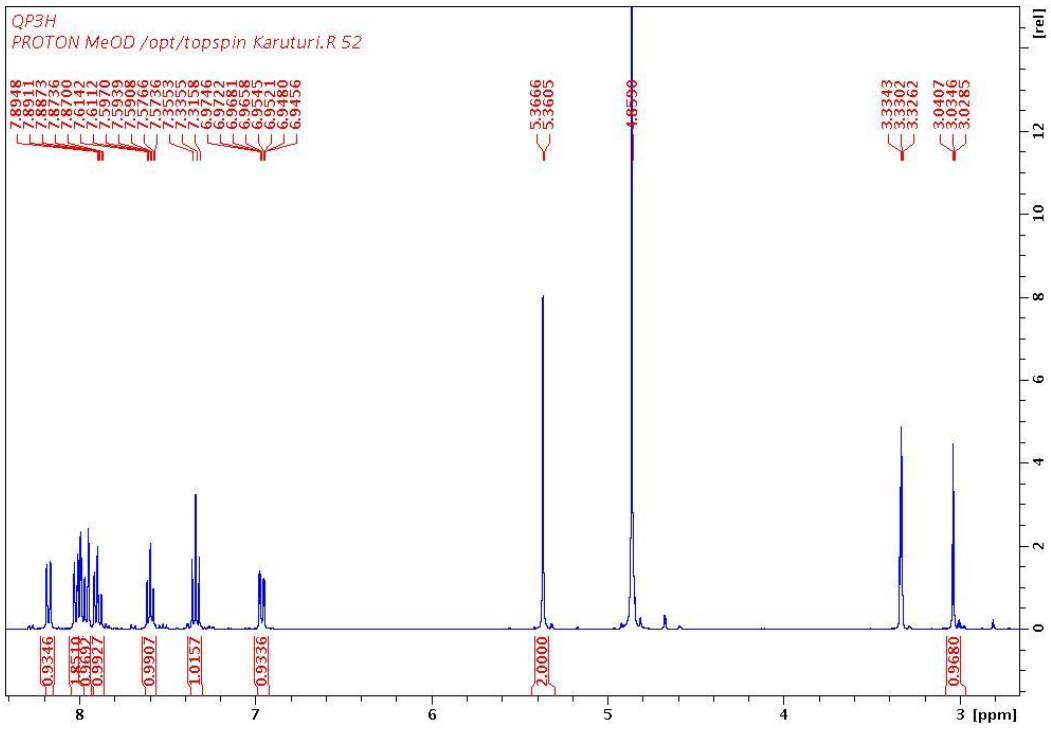

Figure 11

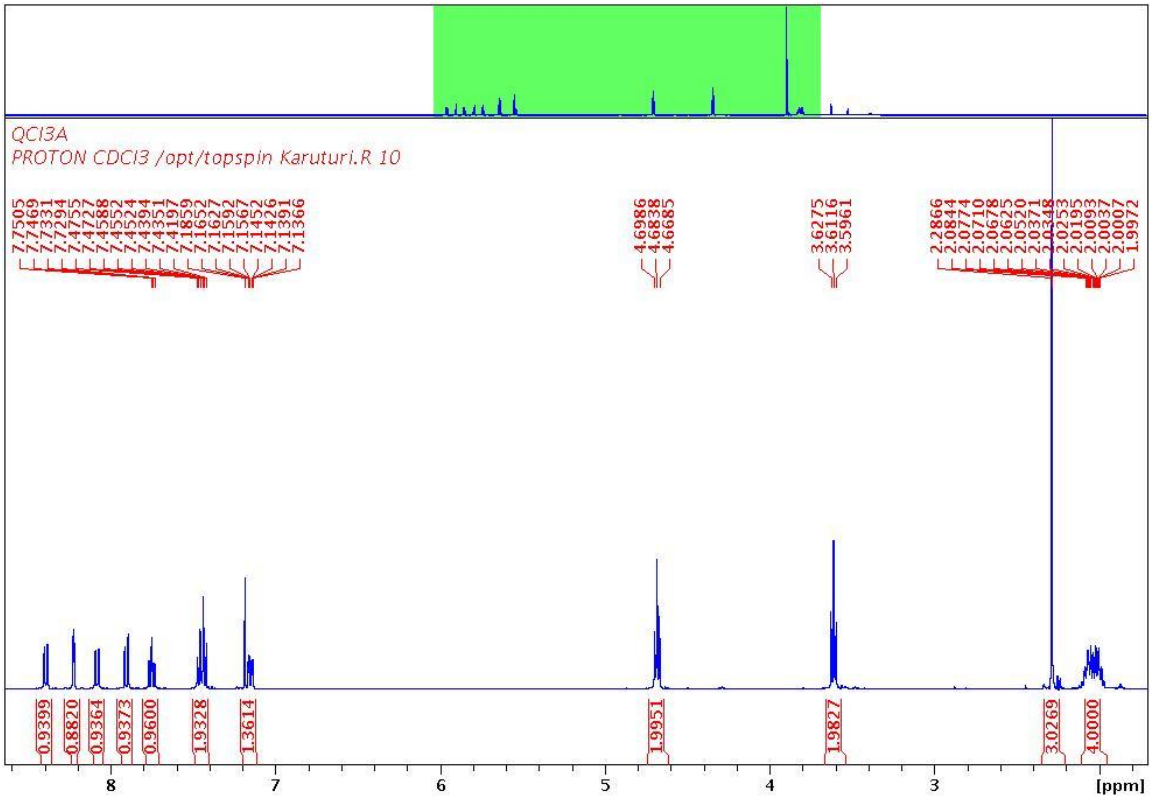

Figure 12

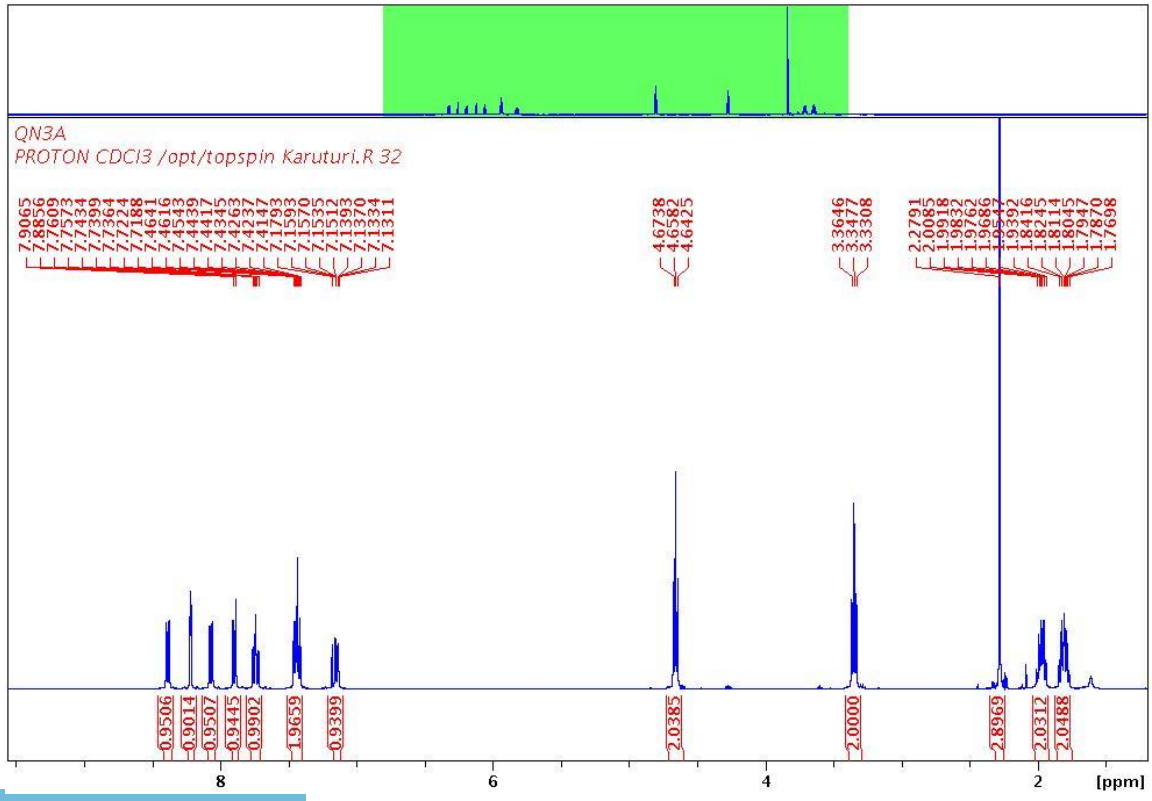

Figure 13

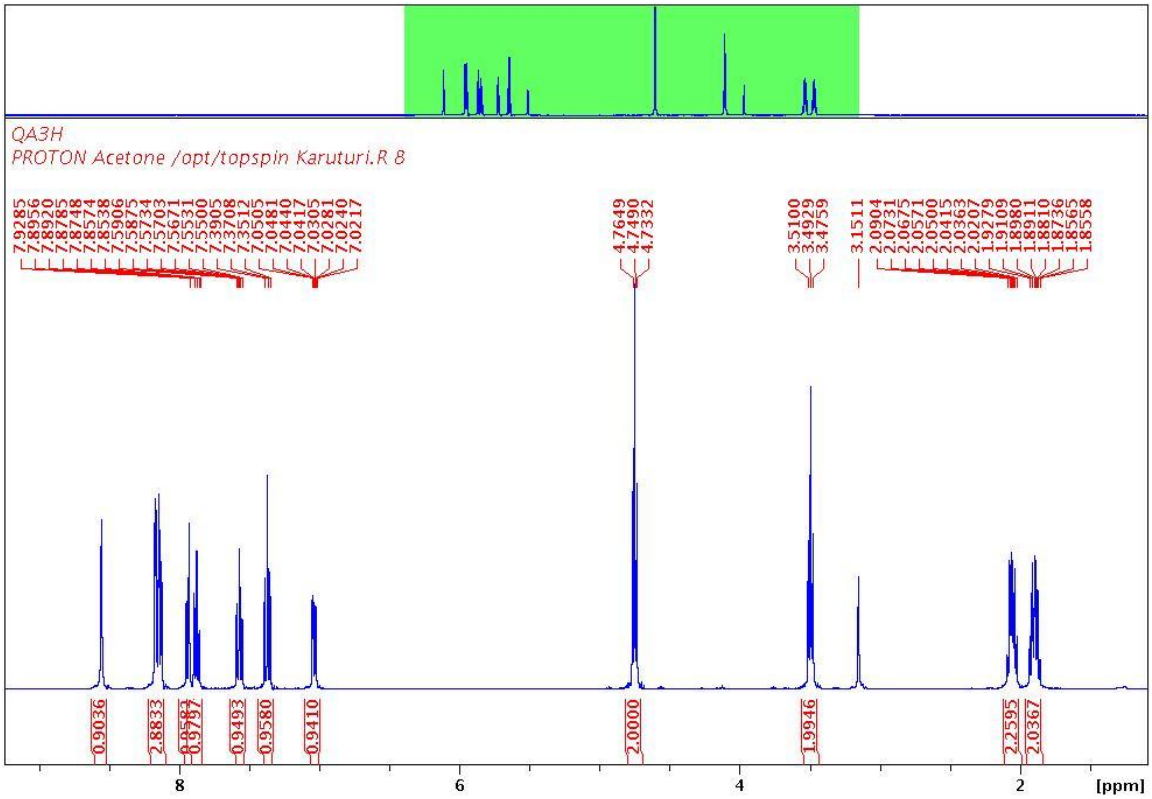

Figure 14

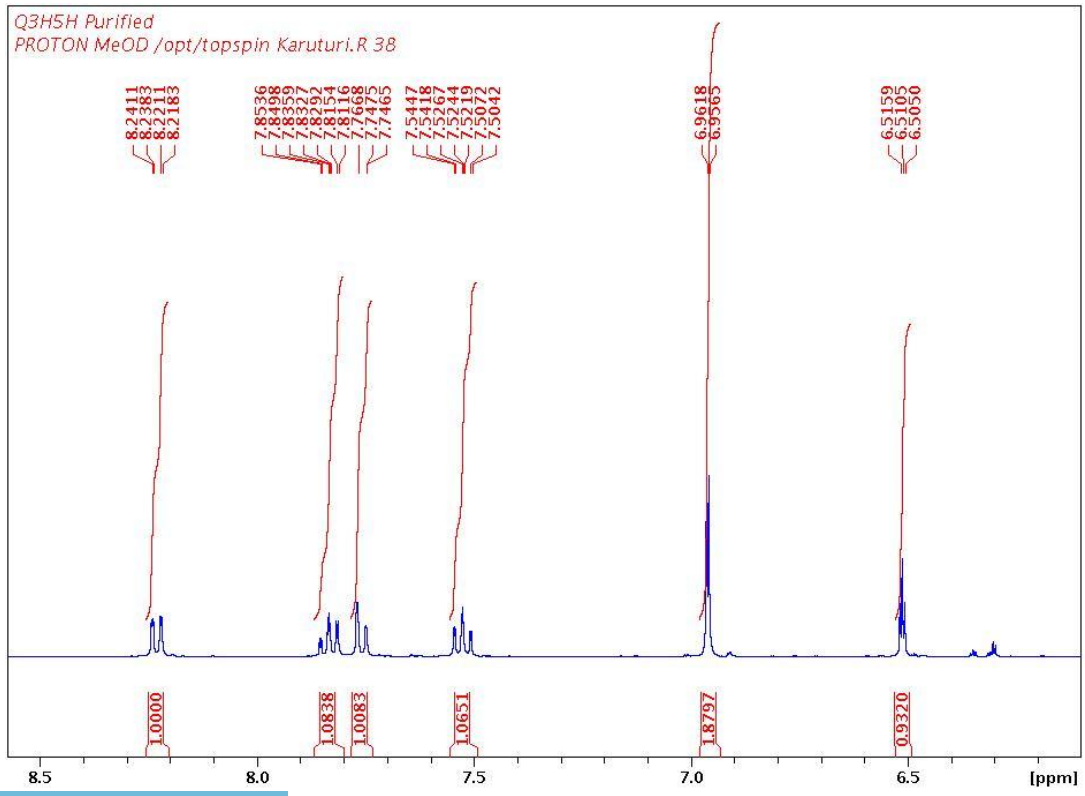

Figure 15

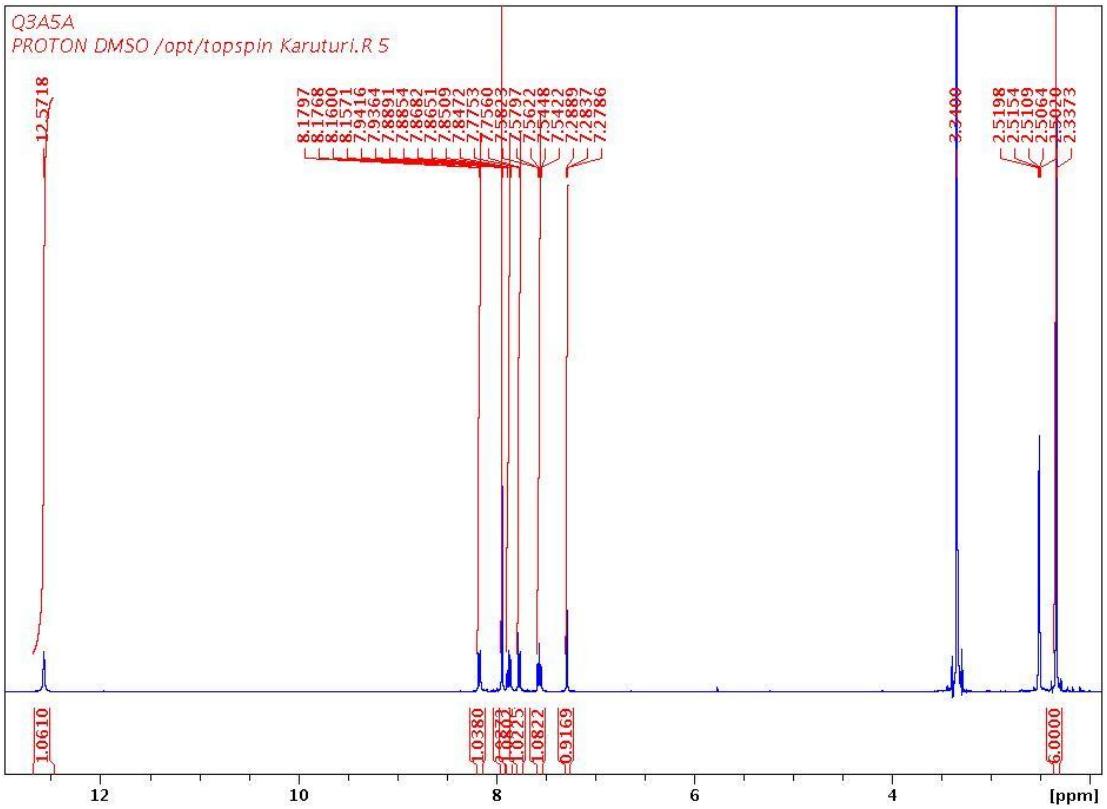

Figure 16

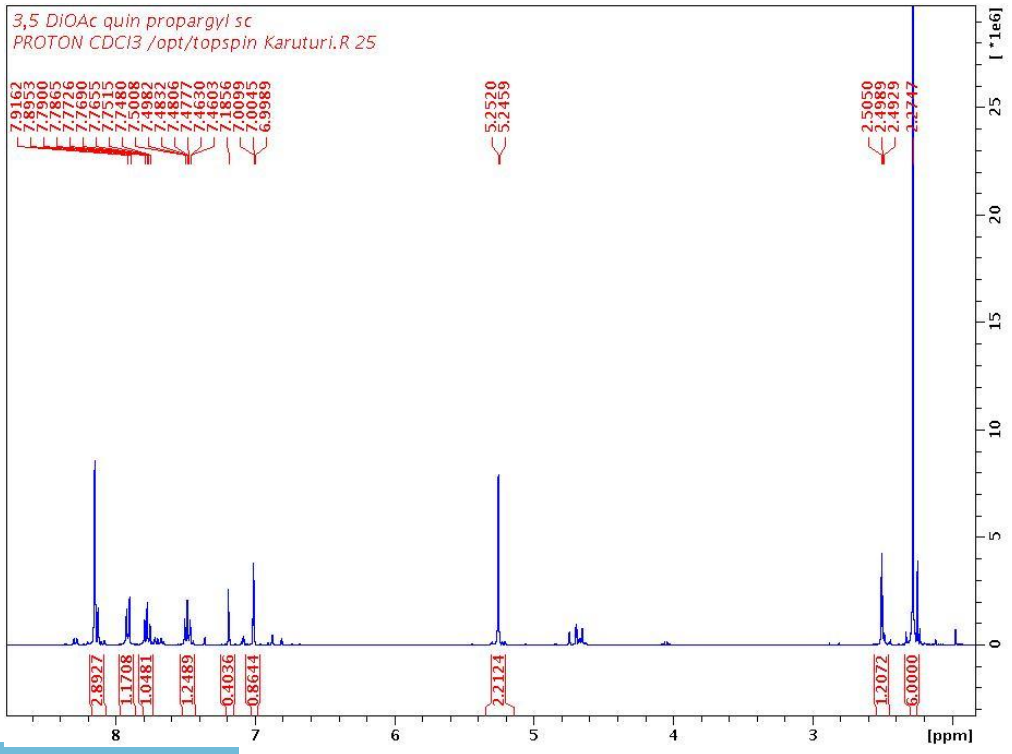

Figure 17

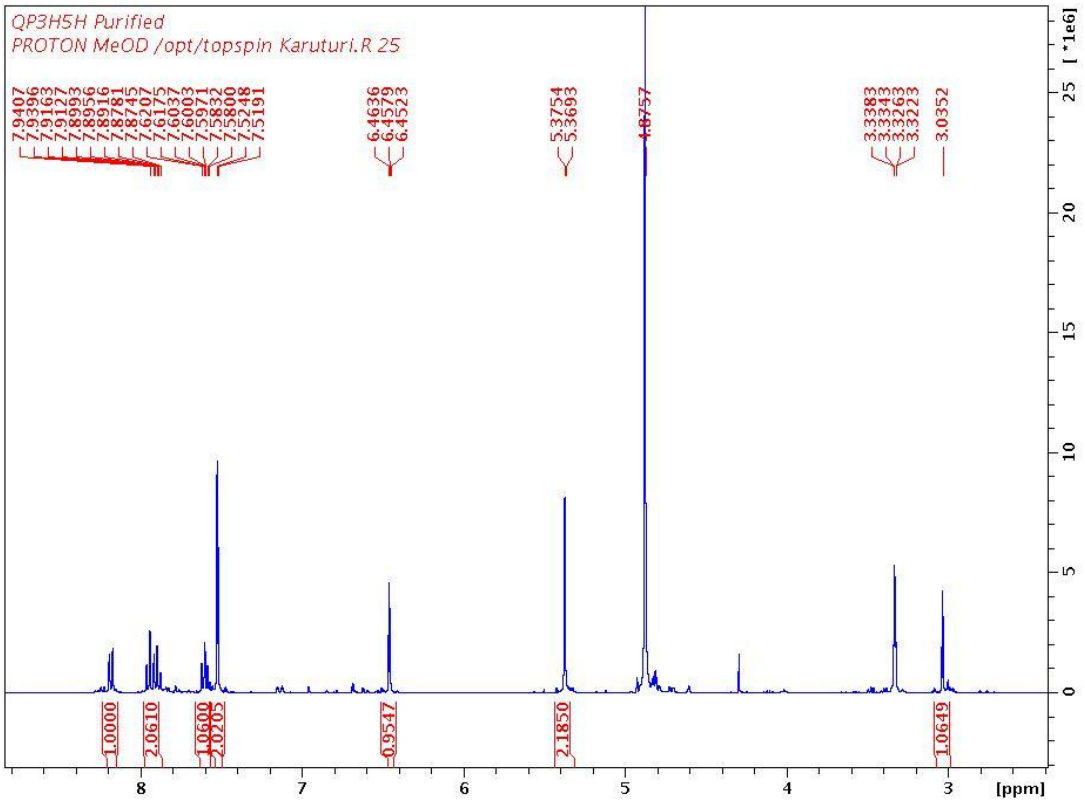

Figure 18

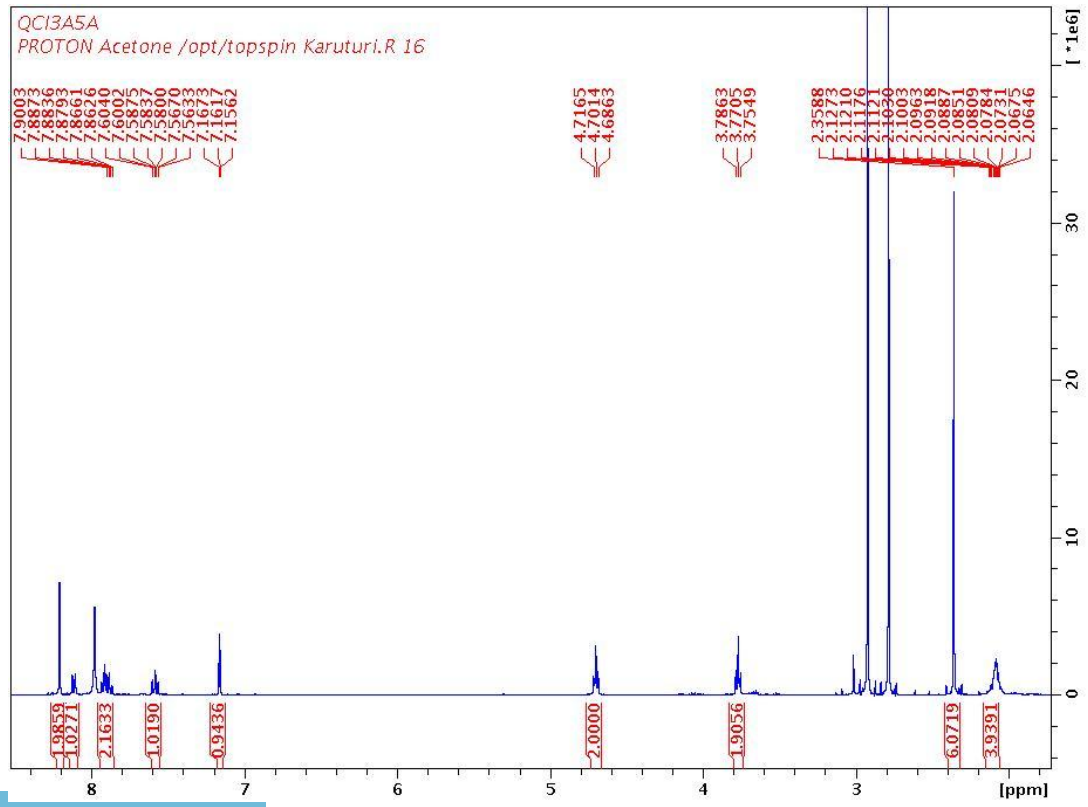

Figure 19

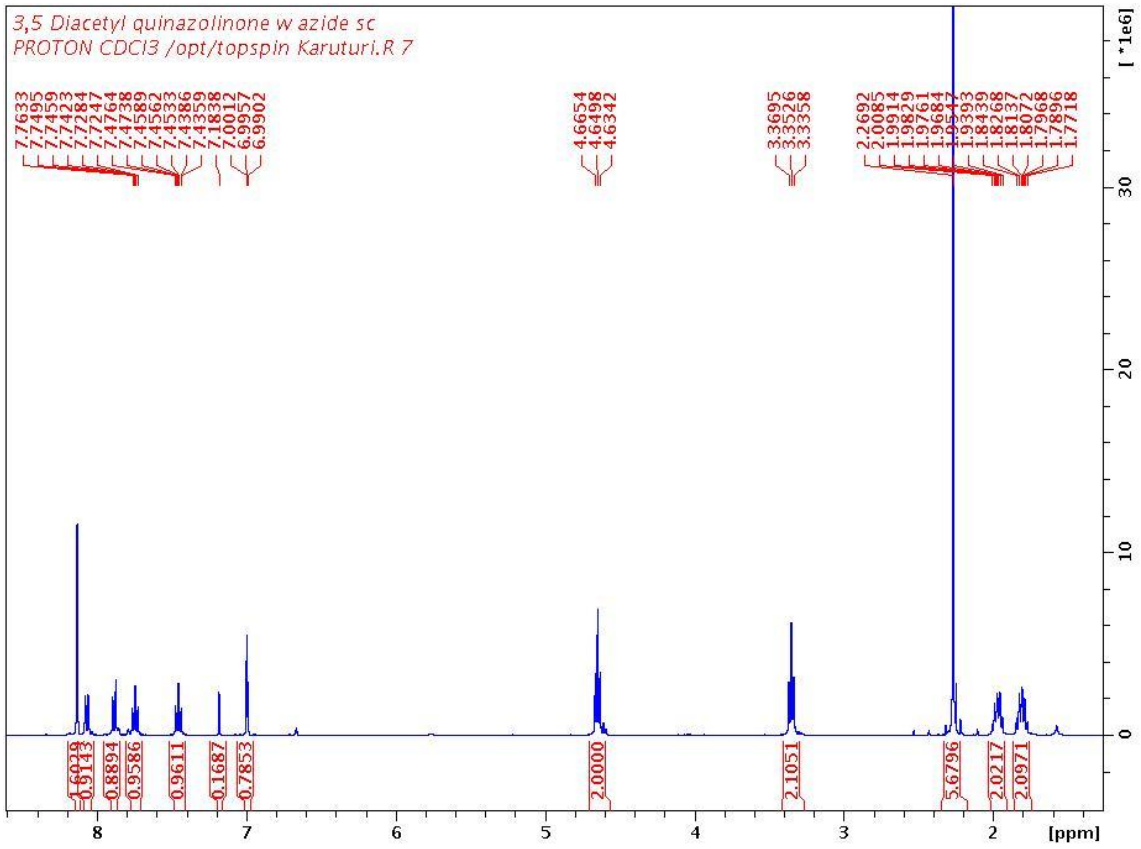

Figure 20

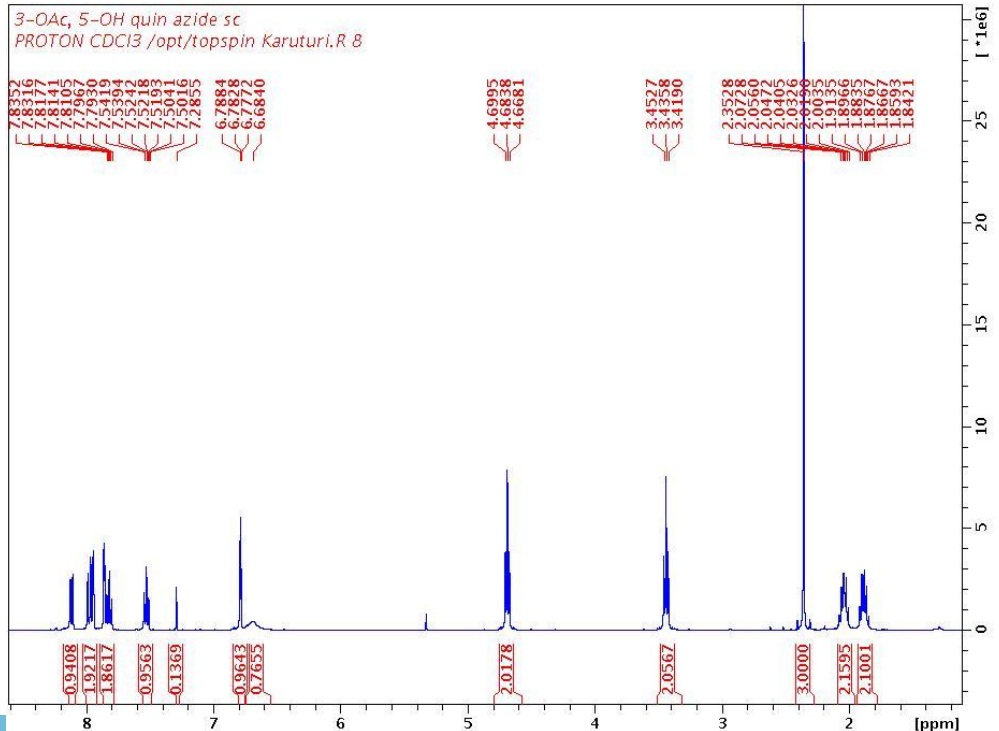

Figure 21

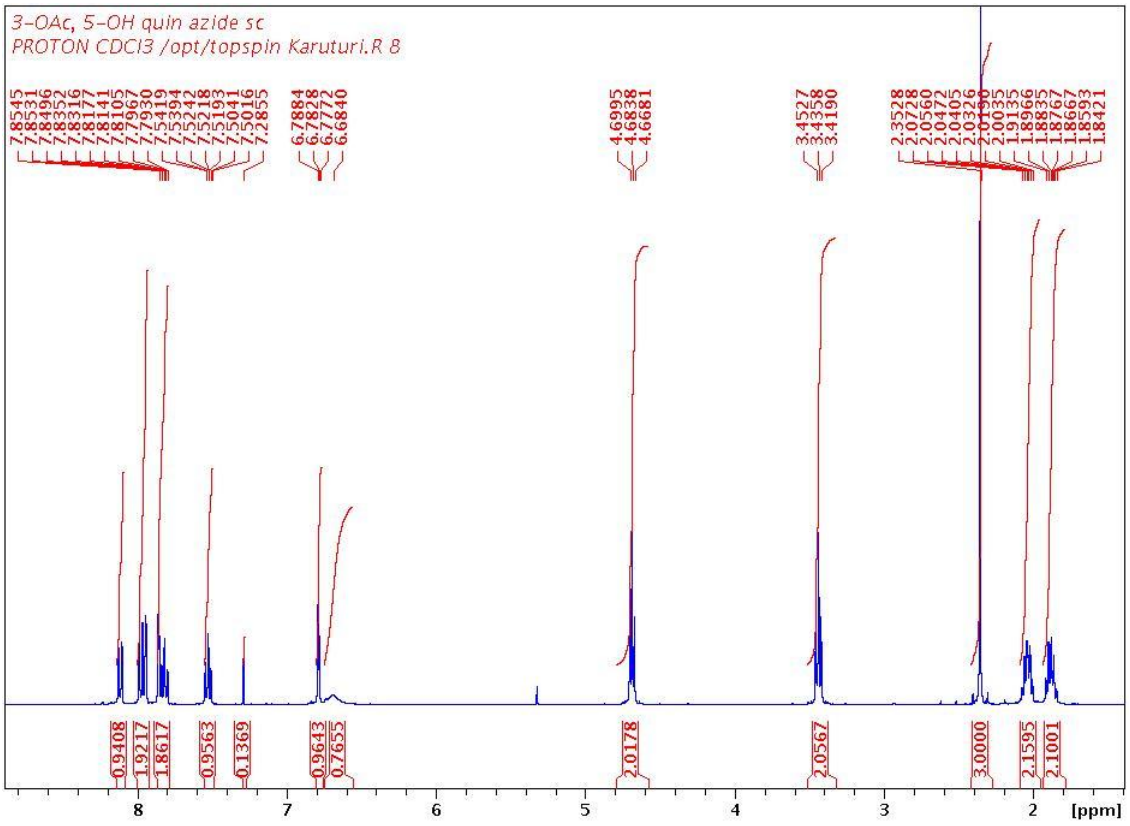

Figure 22

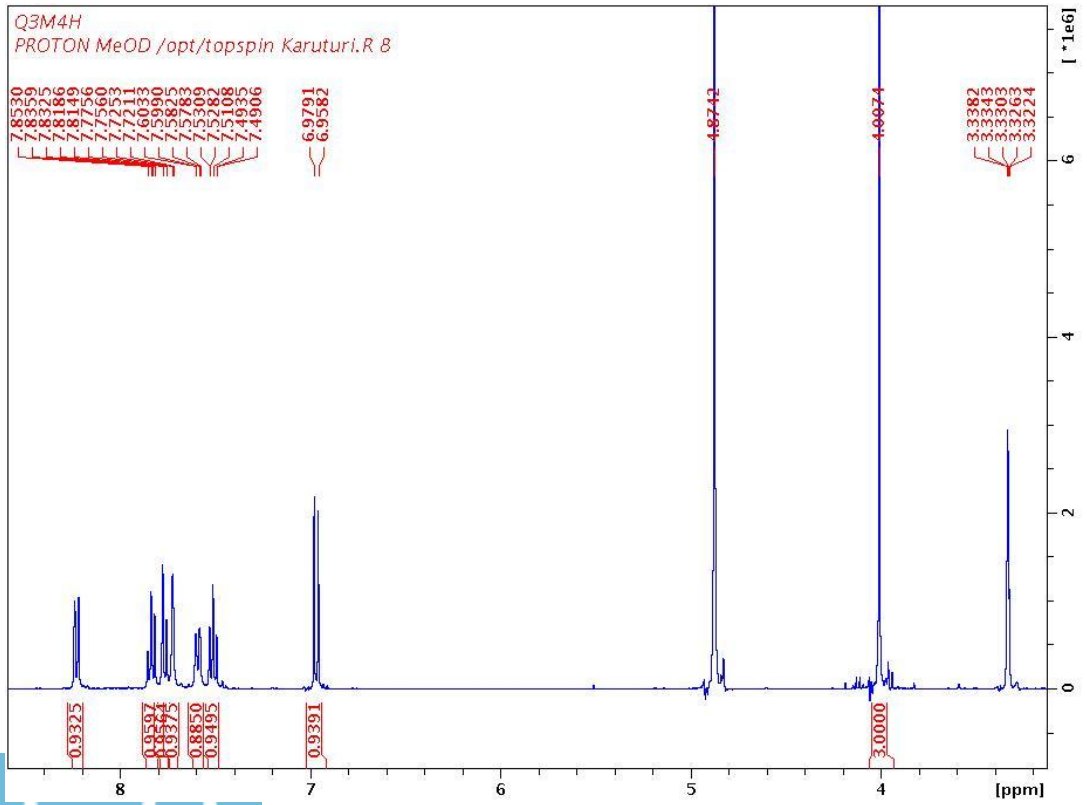

Figure 23

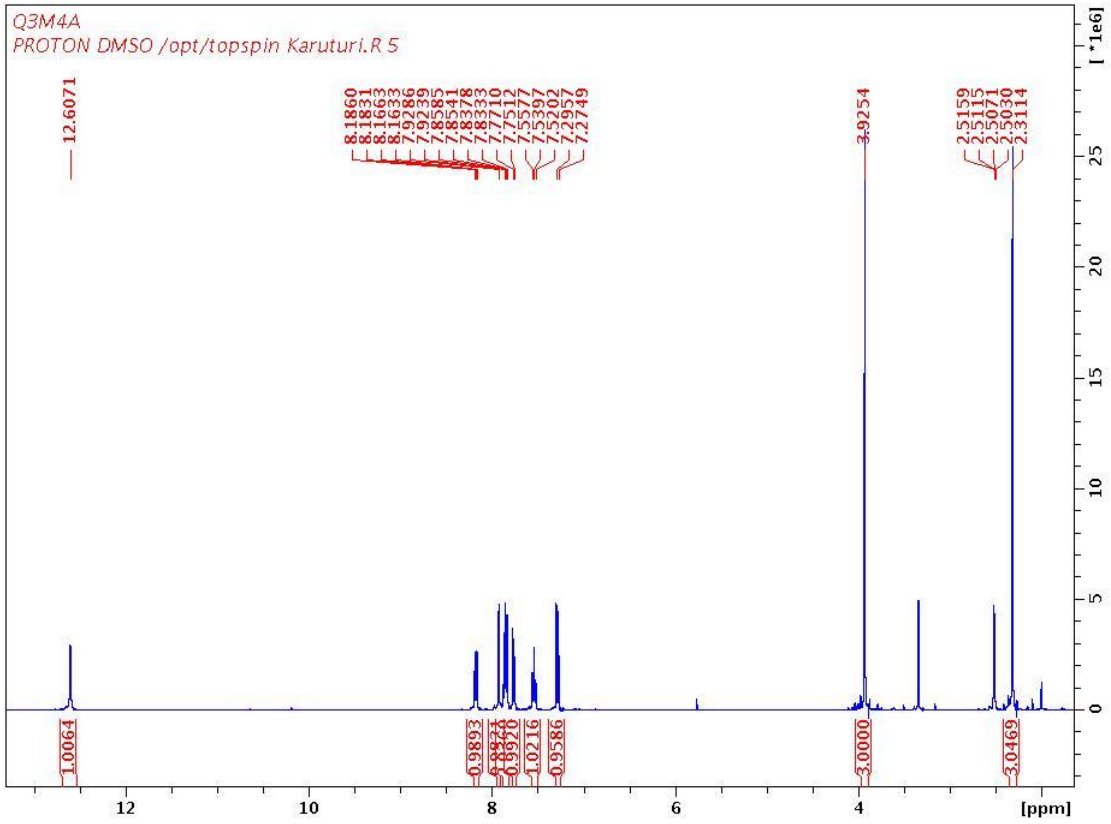

Figure 24

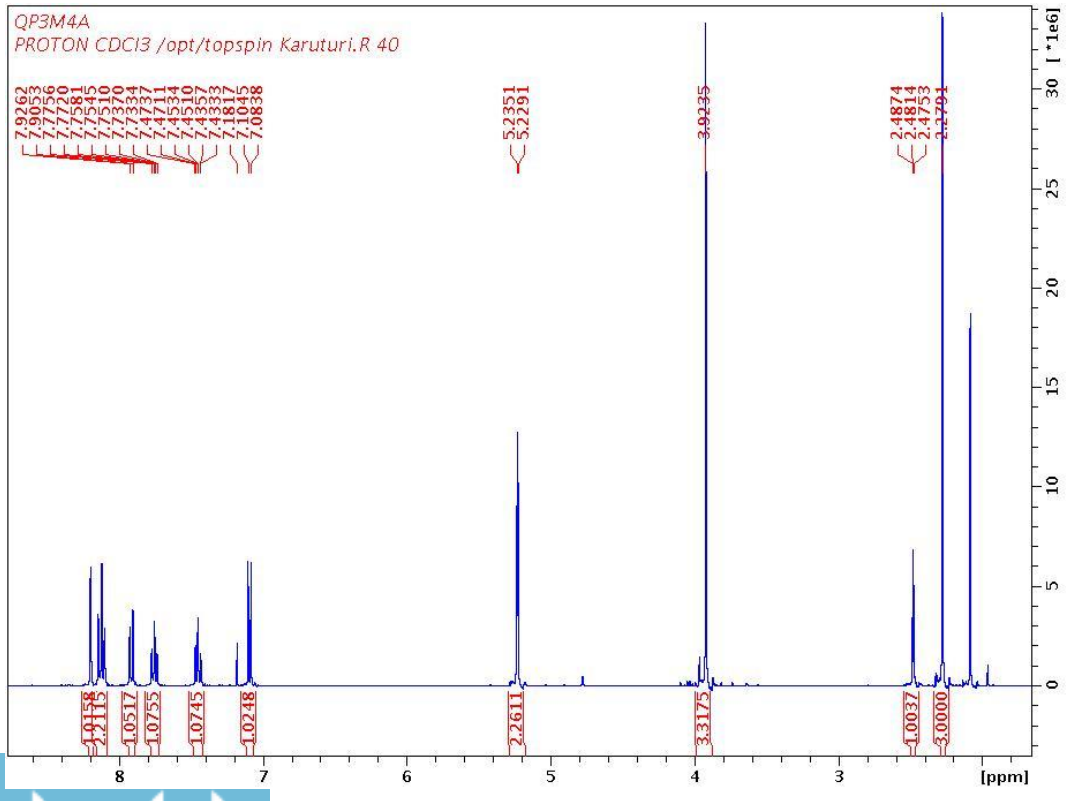

Figure 25

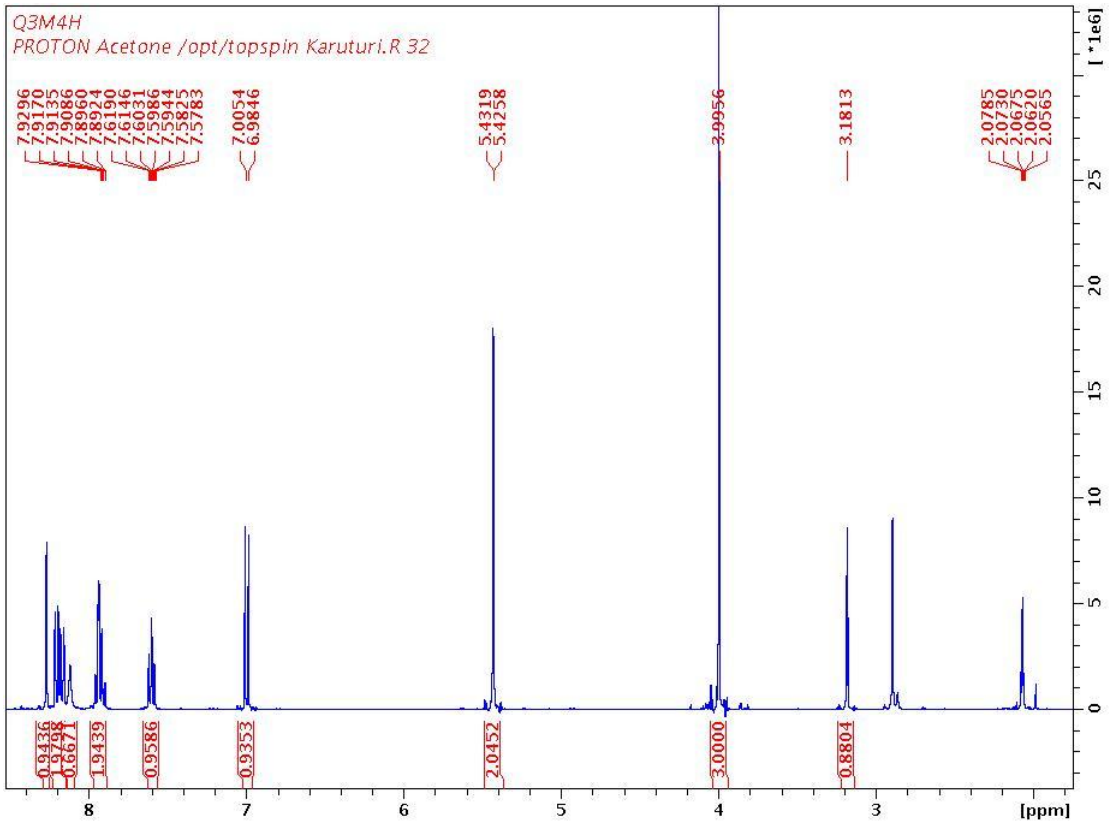

Figure 26

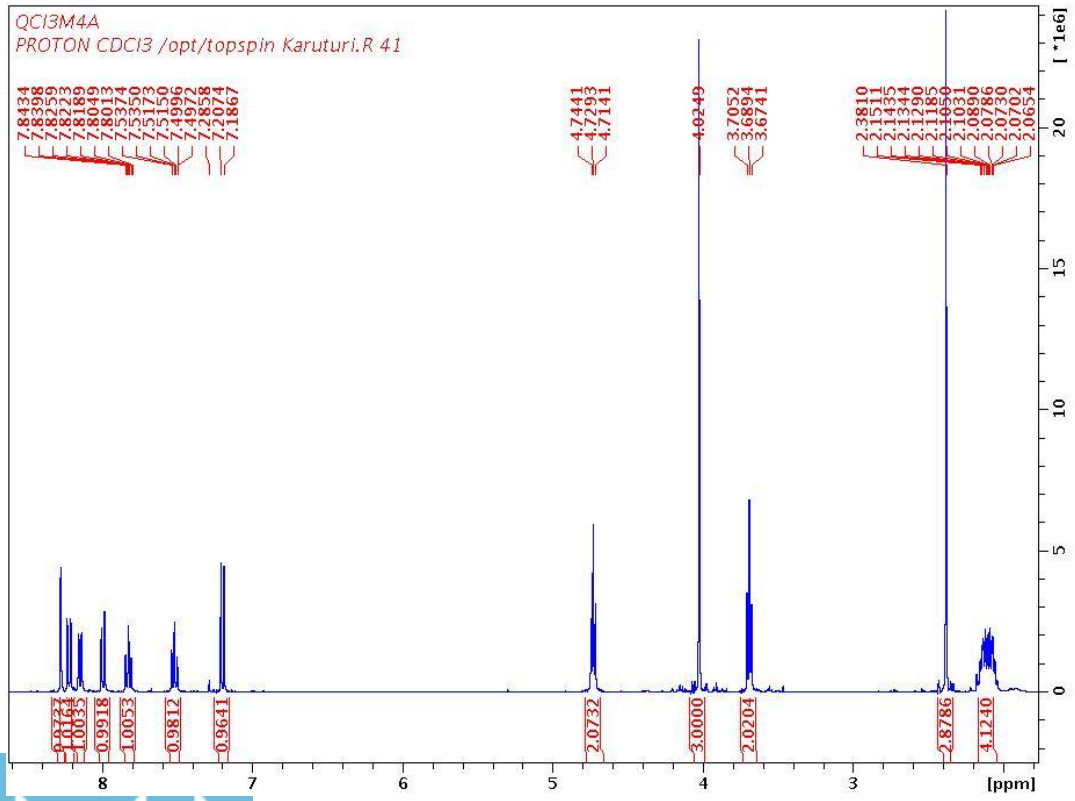

Figure 27

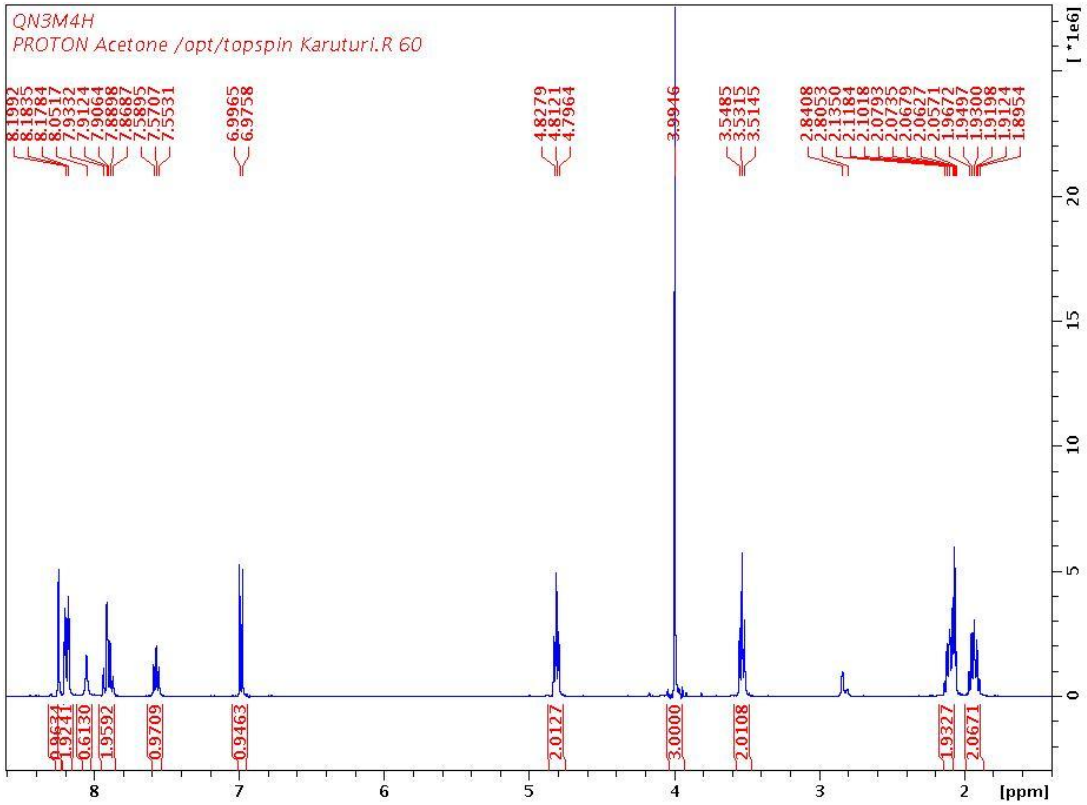

Figure 28

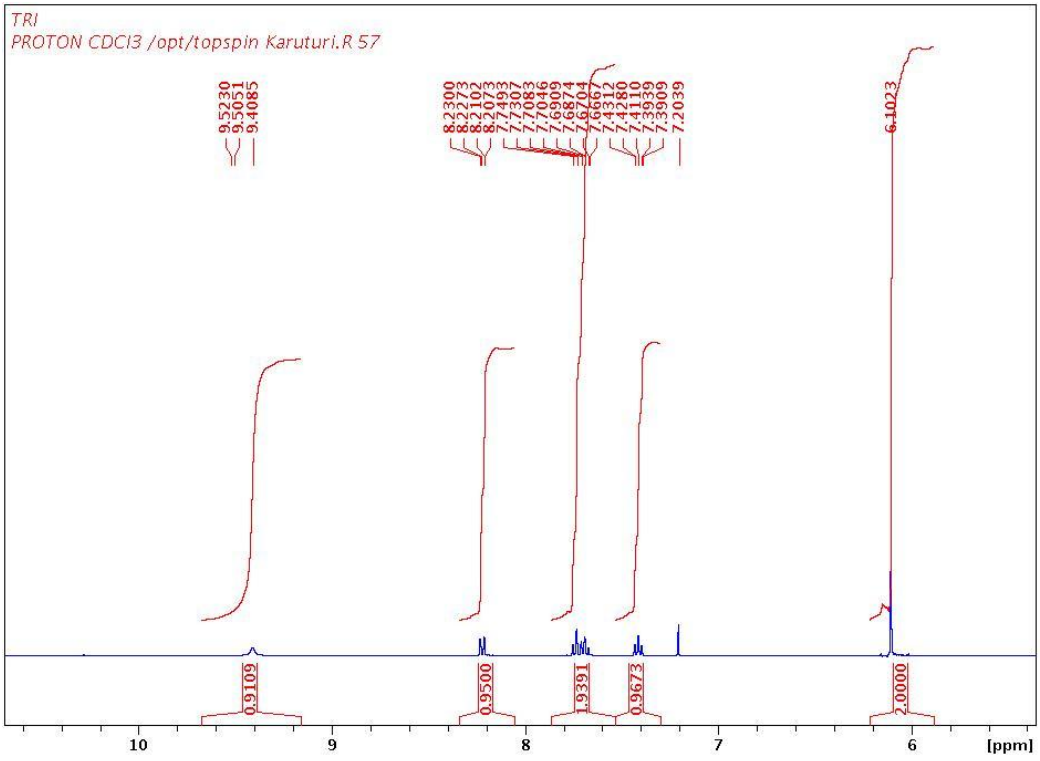

Figure 29

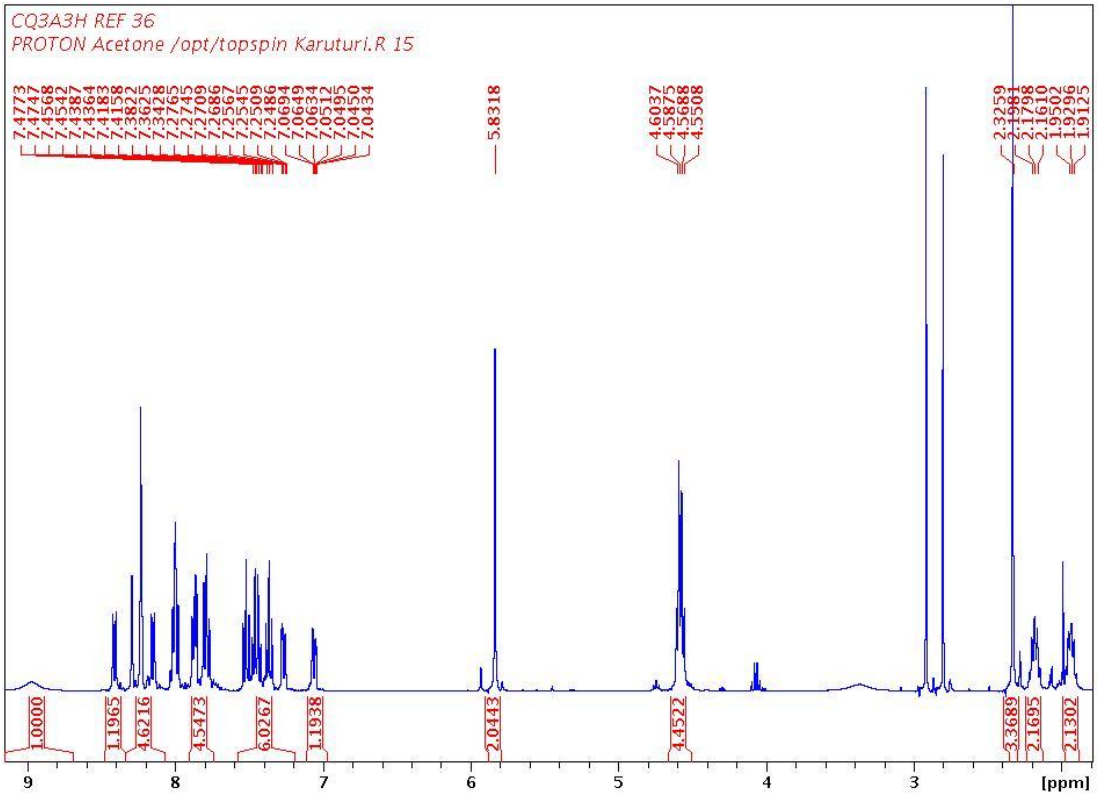

Figure 31

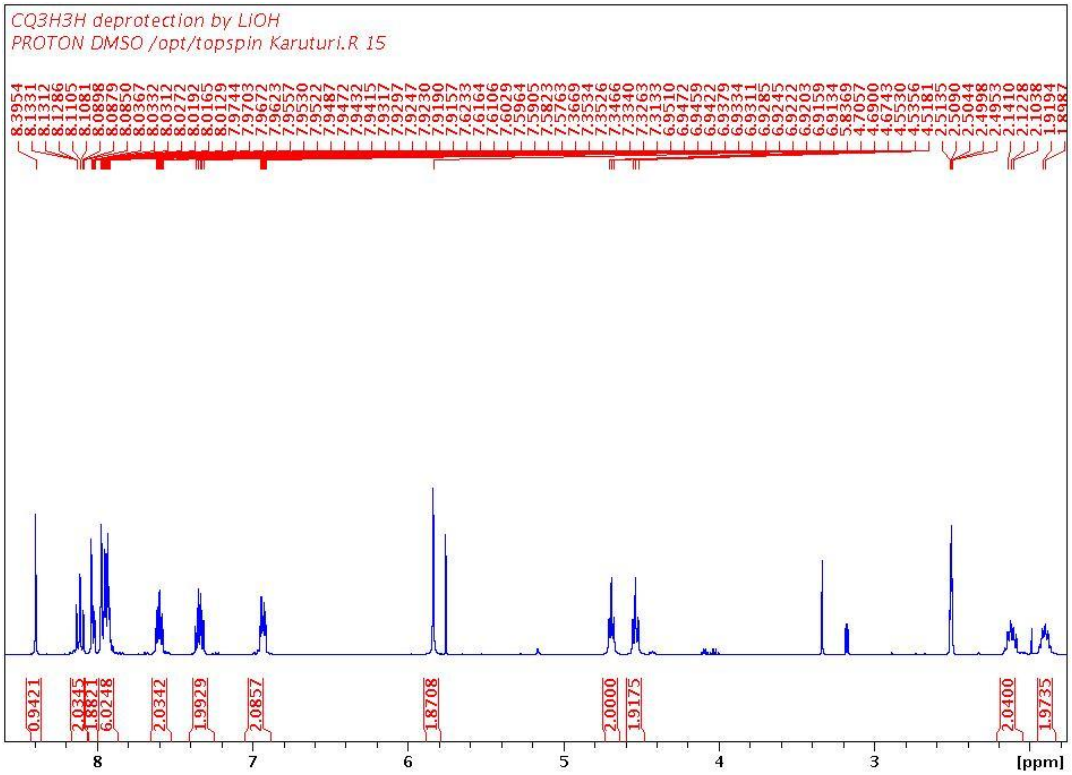

Figure 32

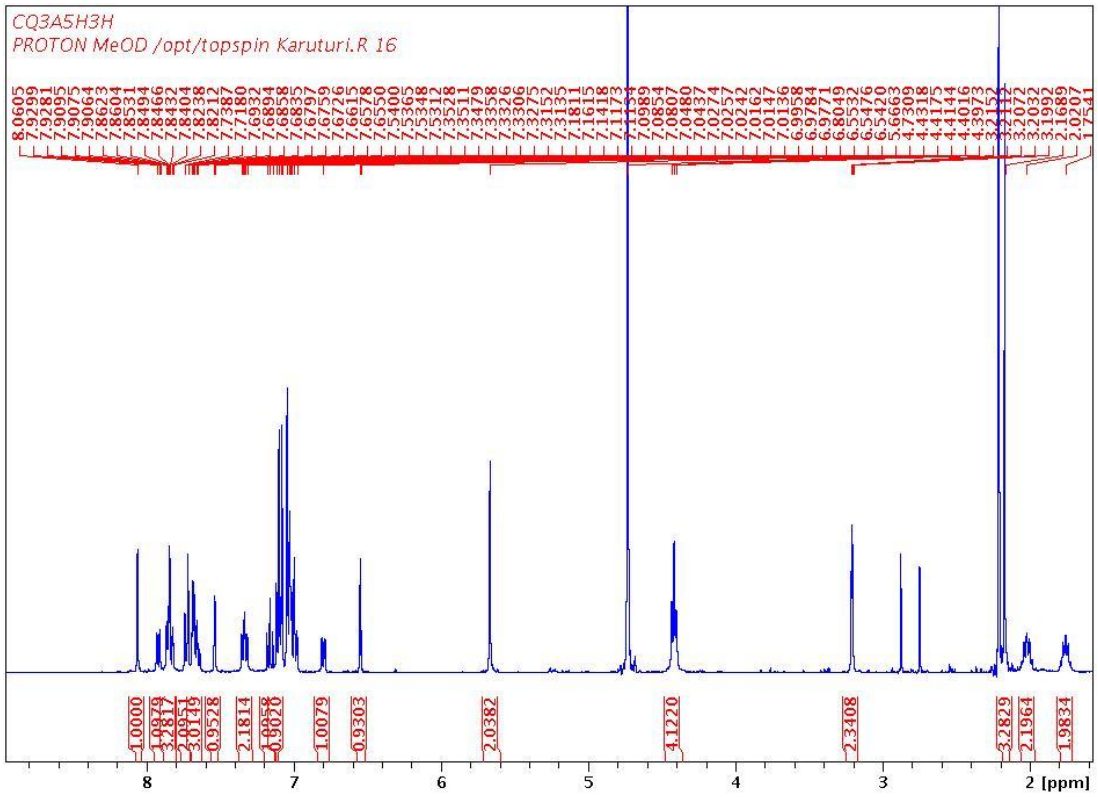

Figure 33

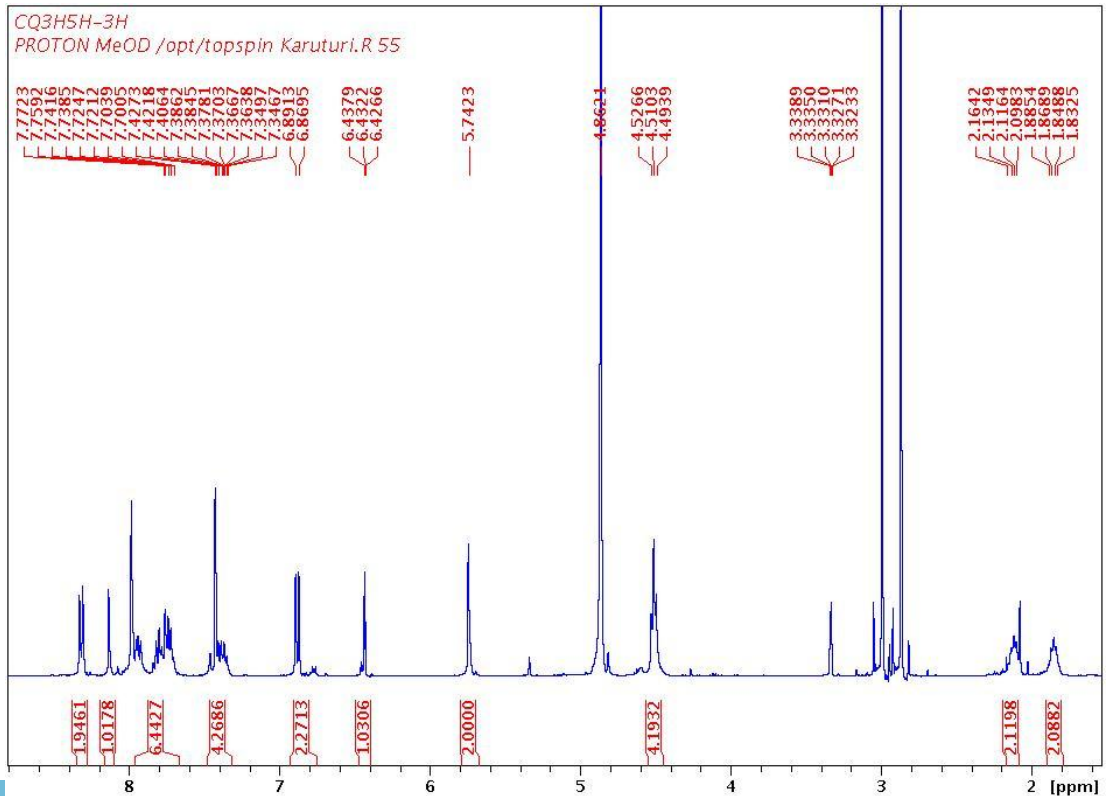

Figure 34

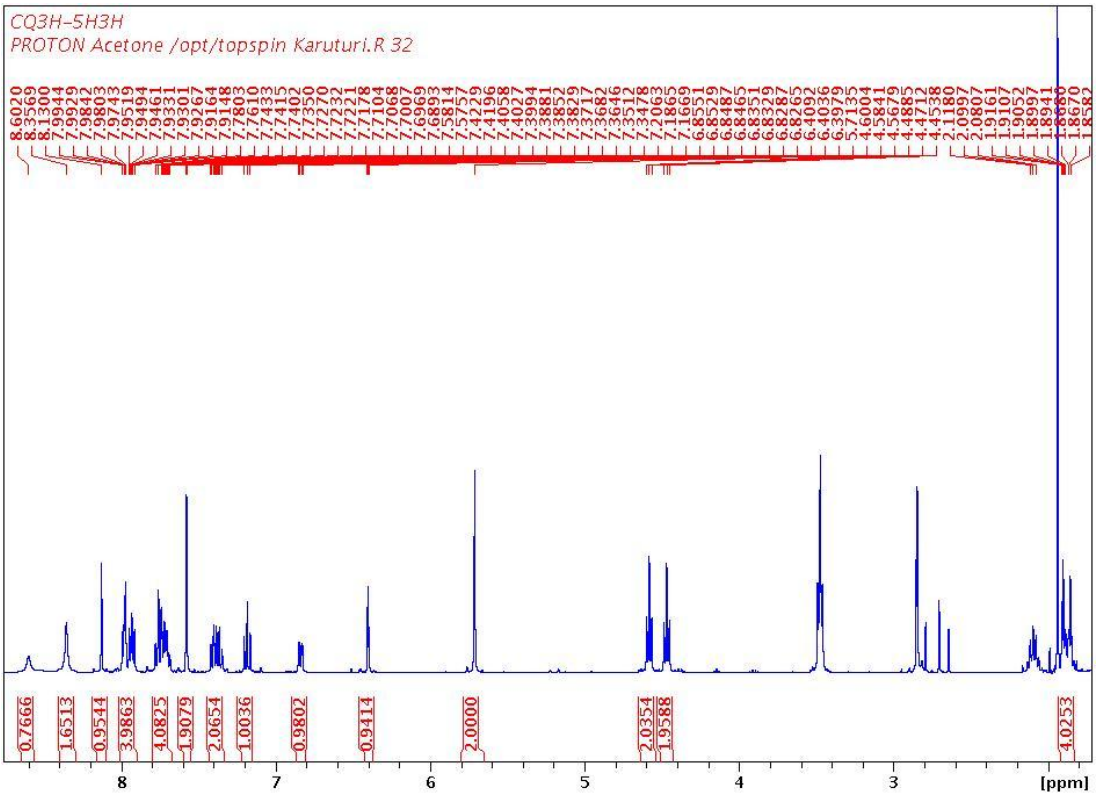

Figure 35

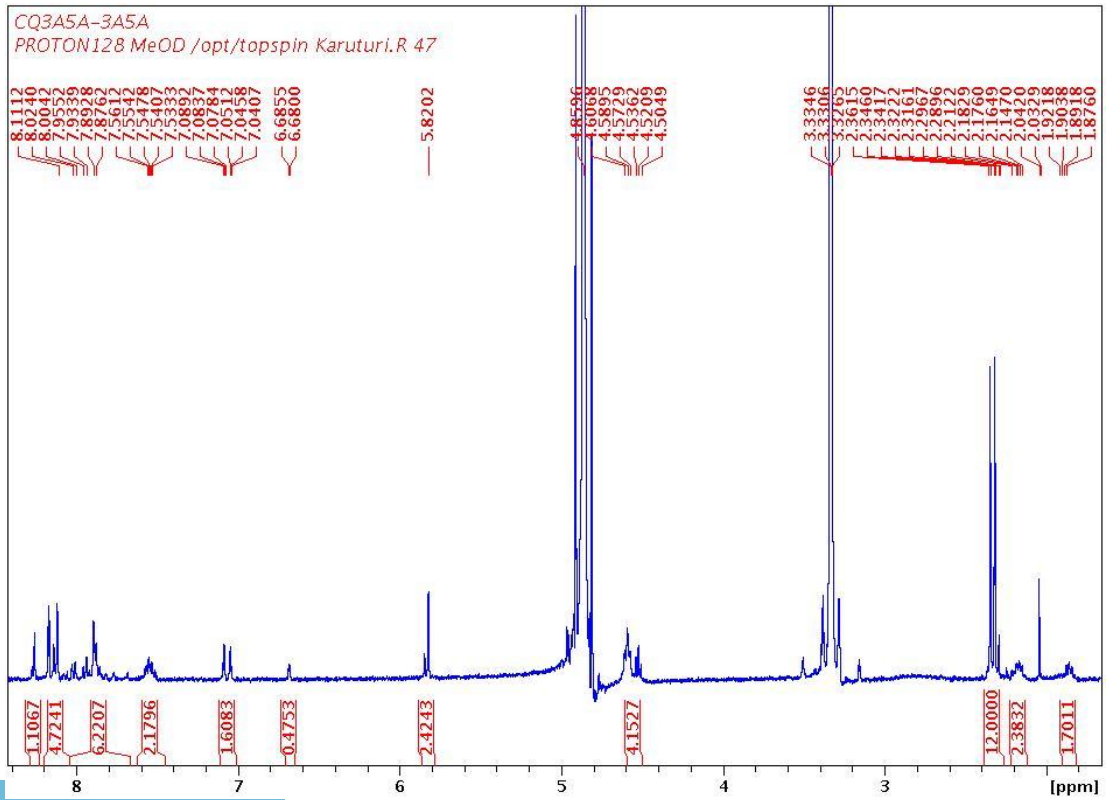

Figure 36

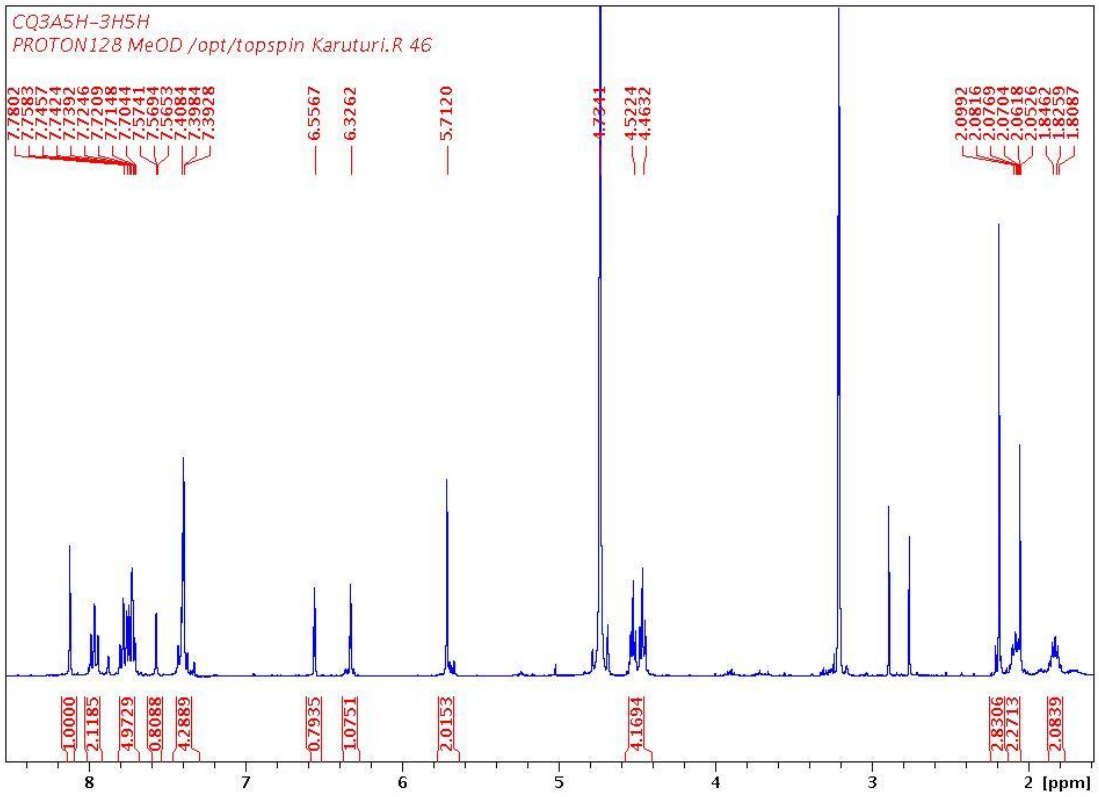

Figure 37

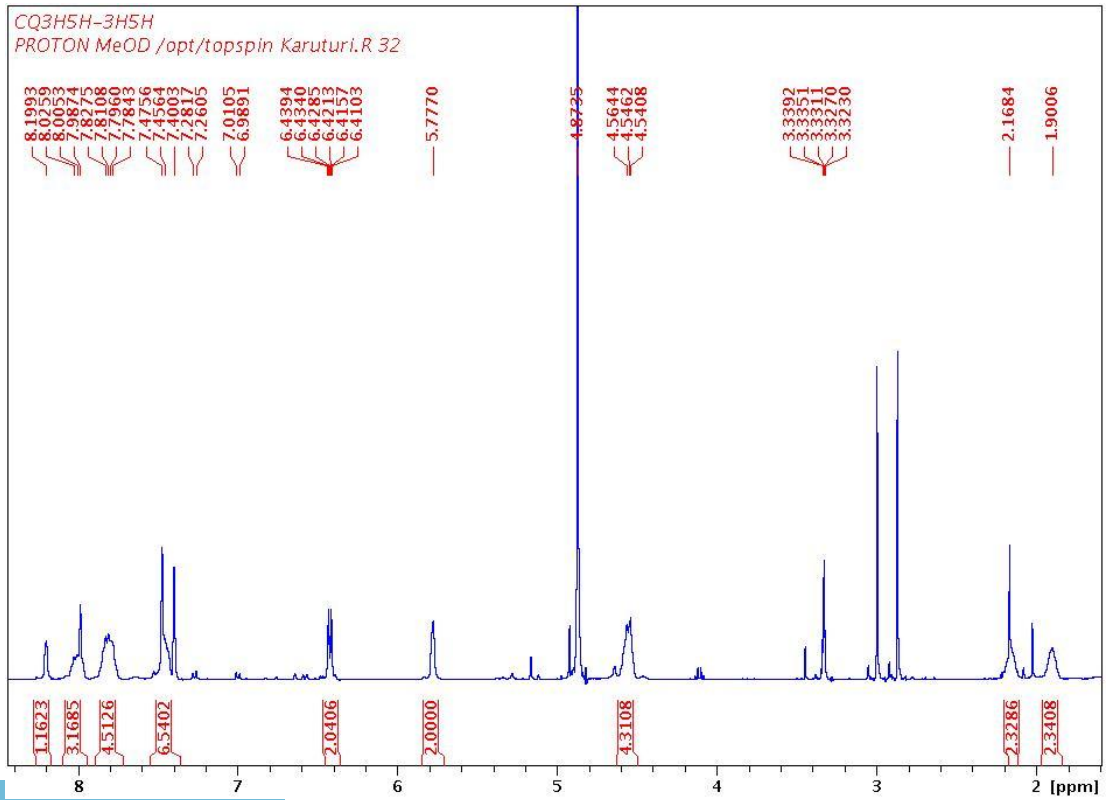

Figure 38

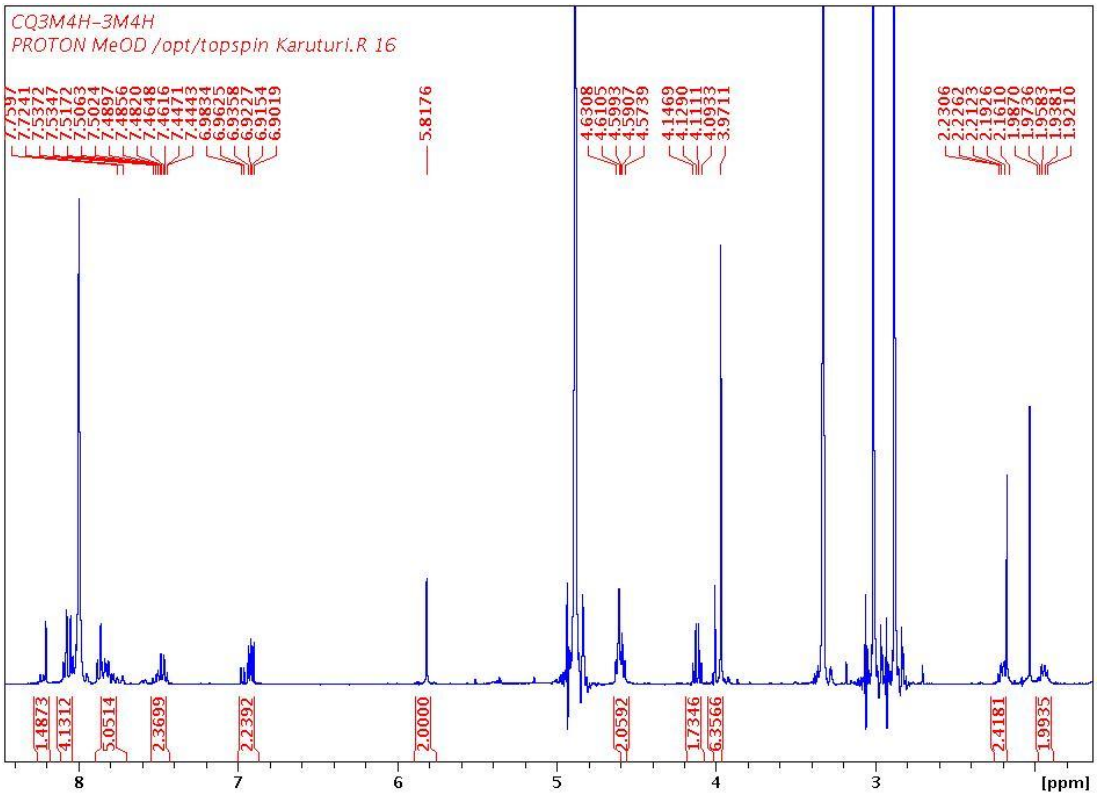

Figure 39

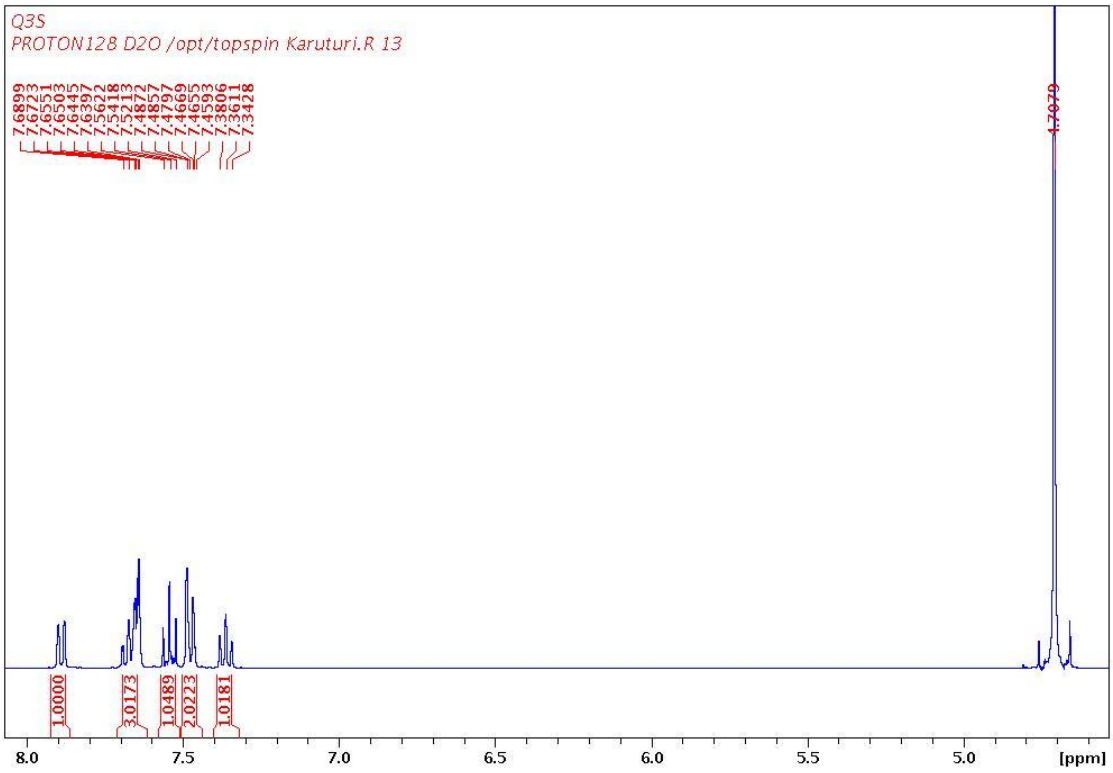

Figure 40

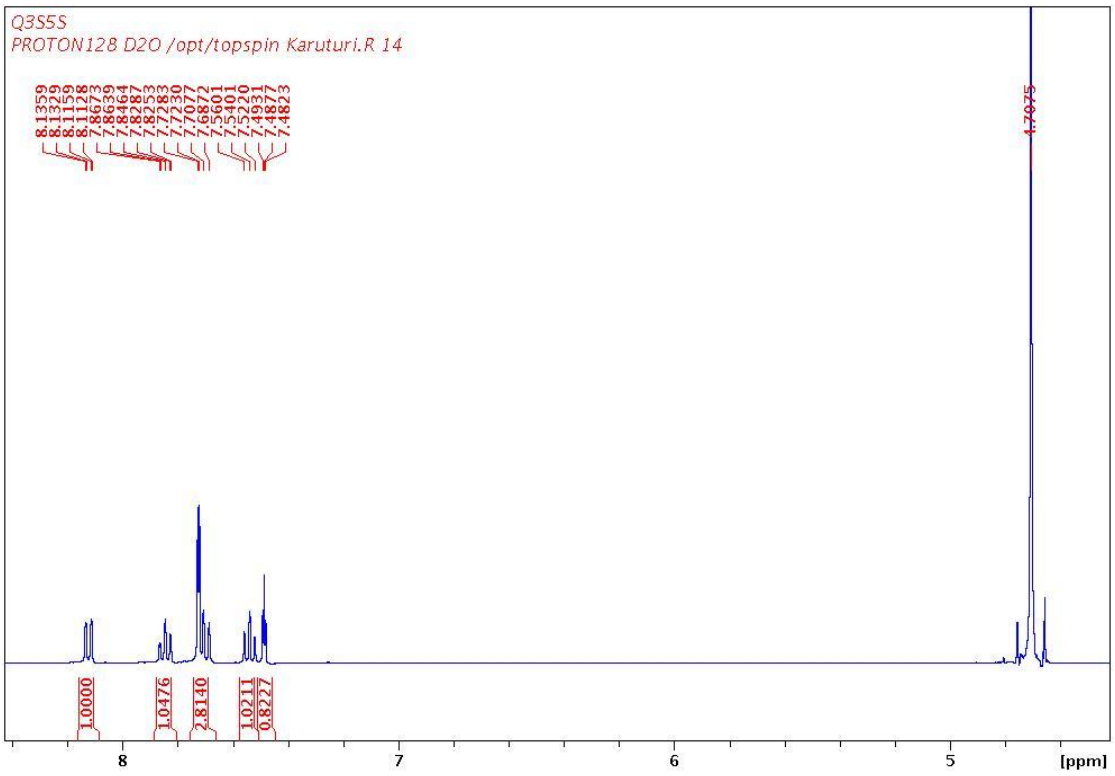

Figure 41

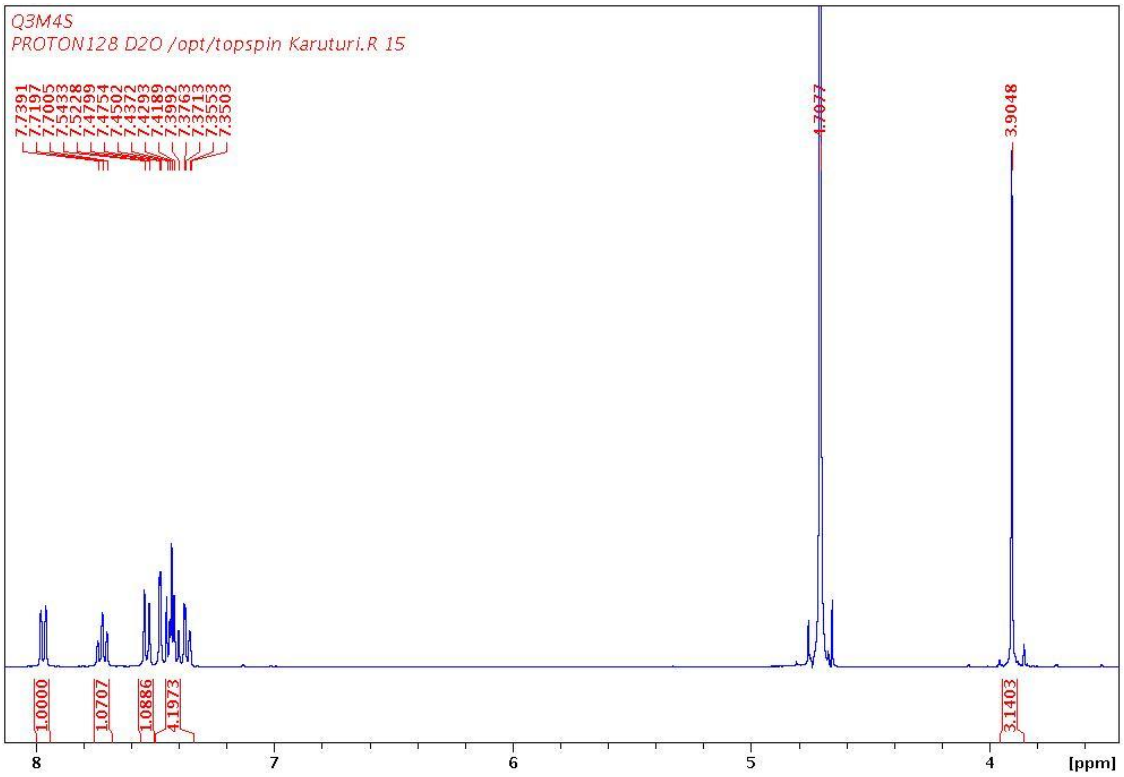

Figure 42

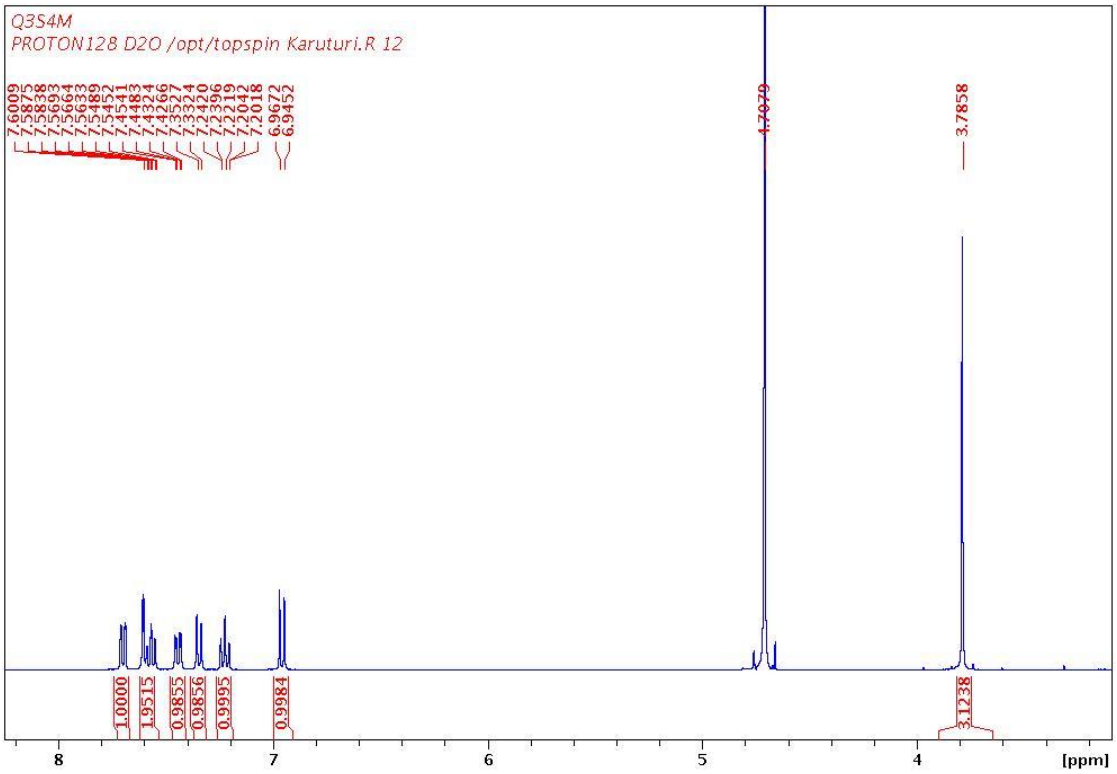

Figure 43

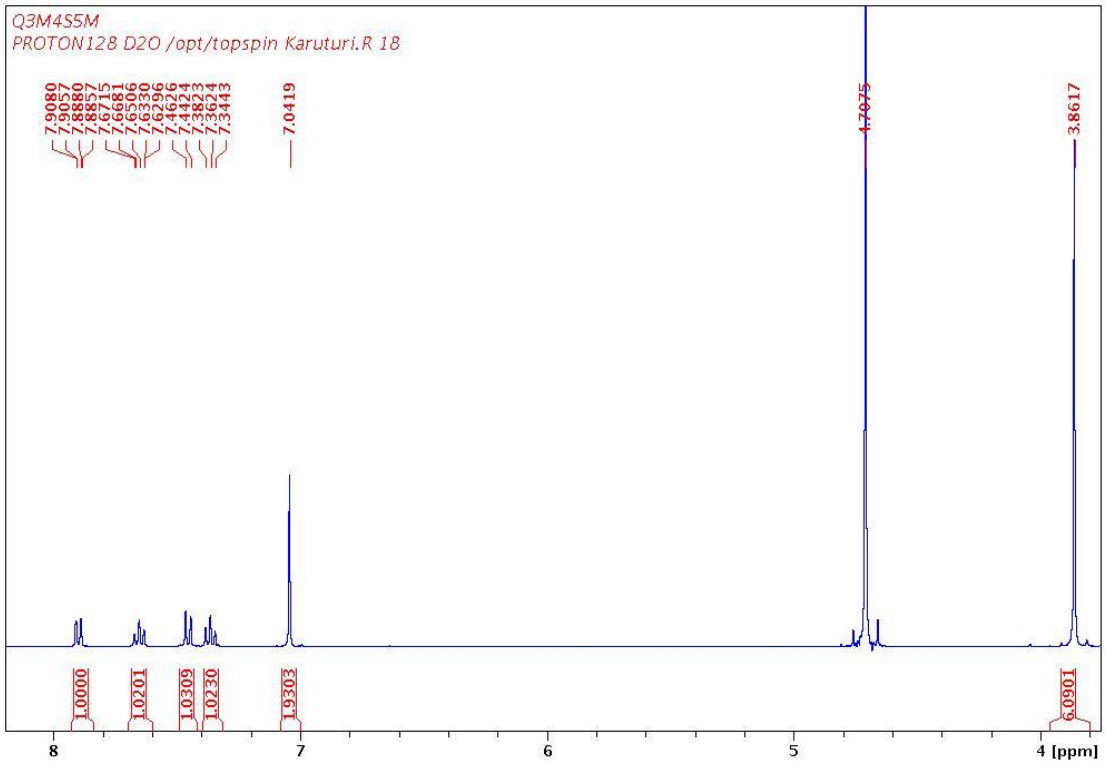

Figure 44

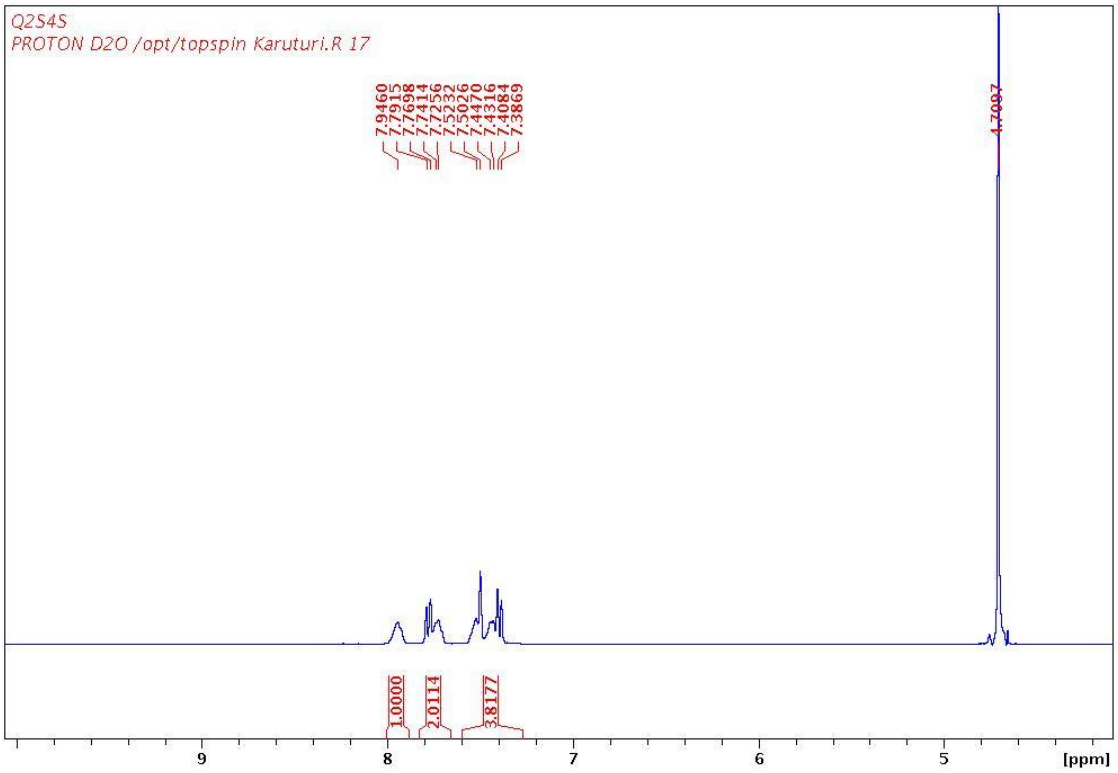

Figure 45

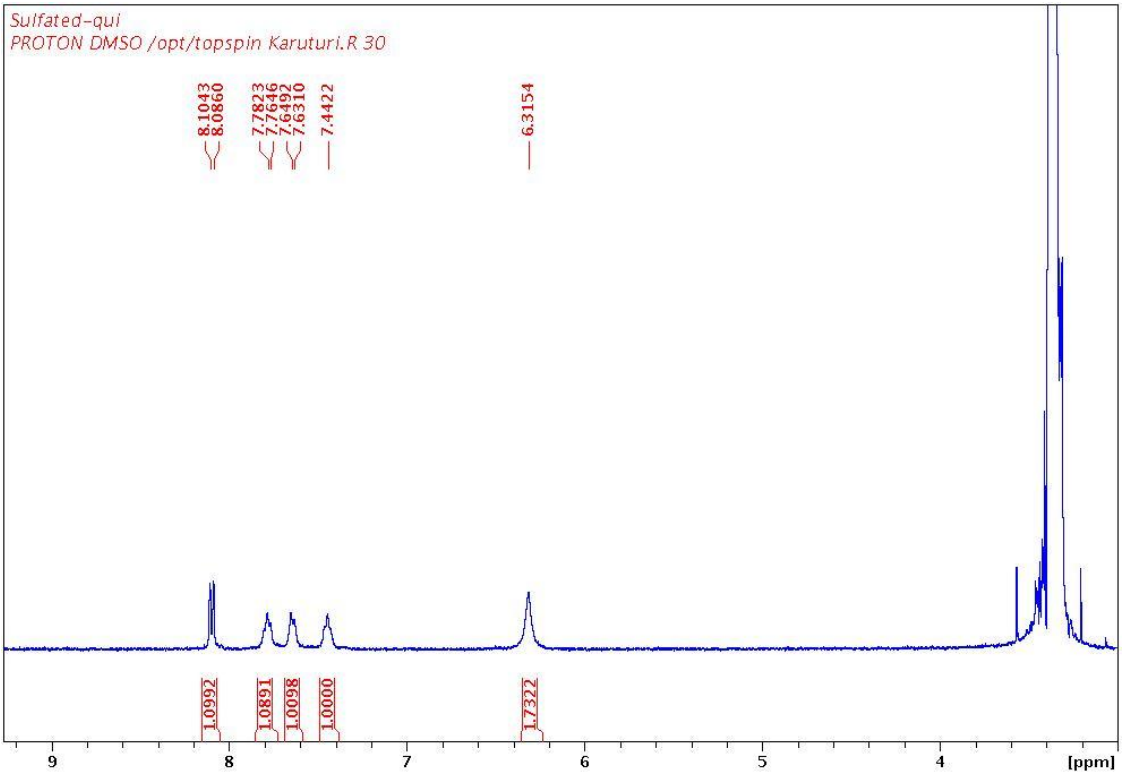

Figure 46

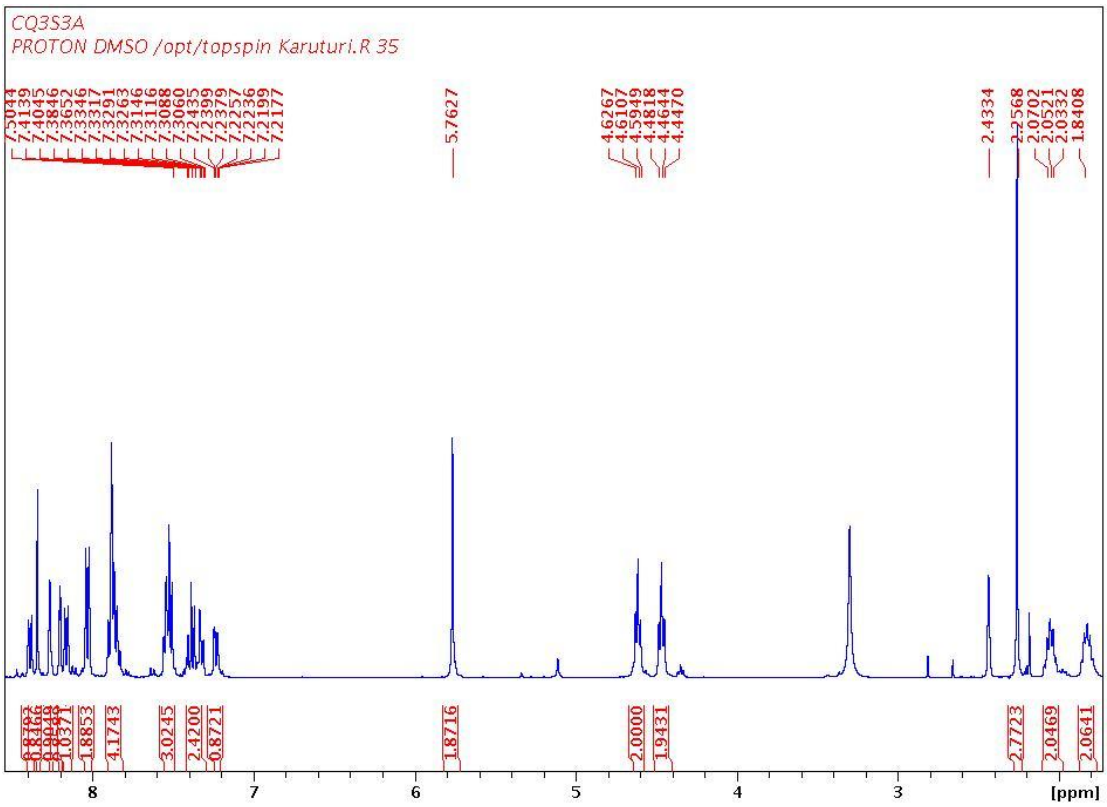

Figure 47

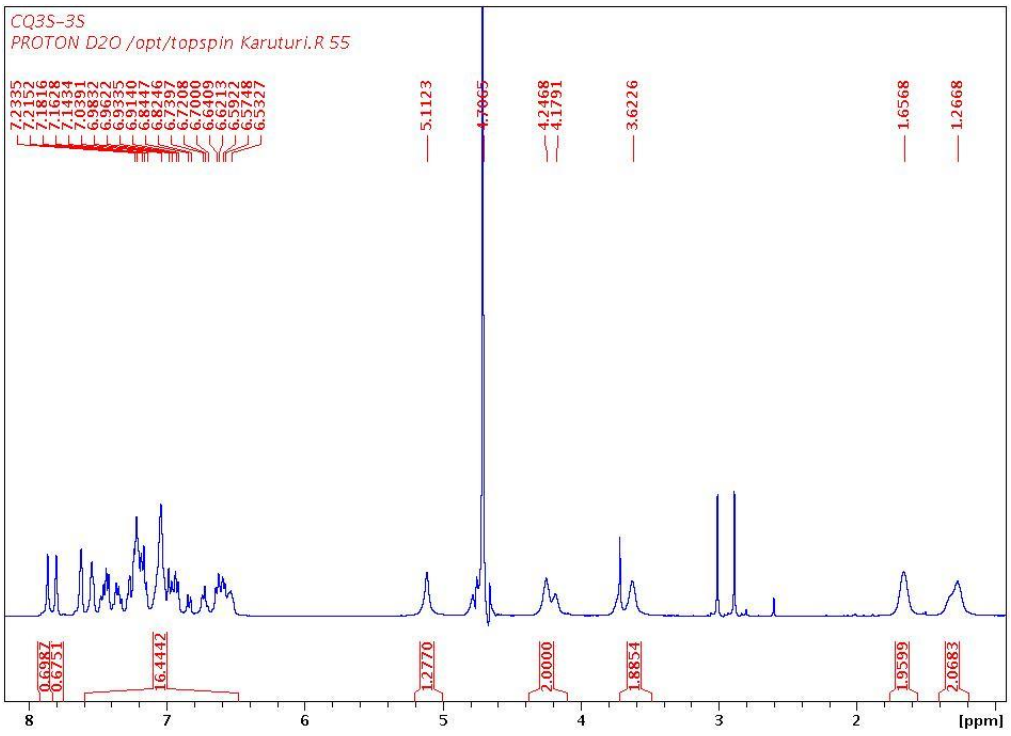

Figure 48

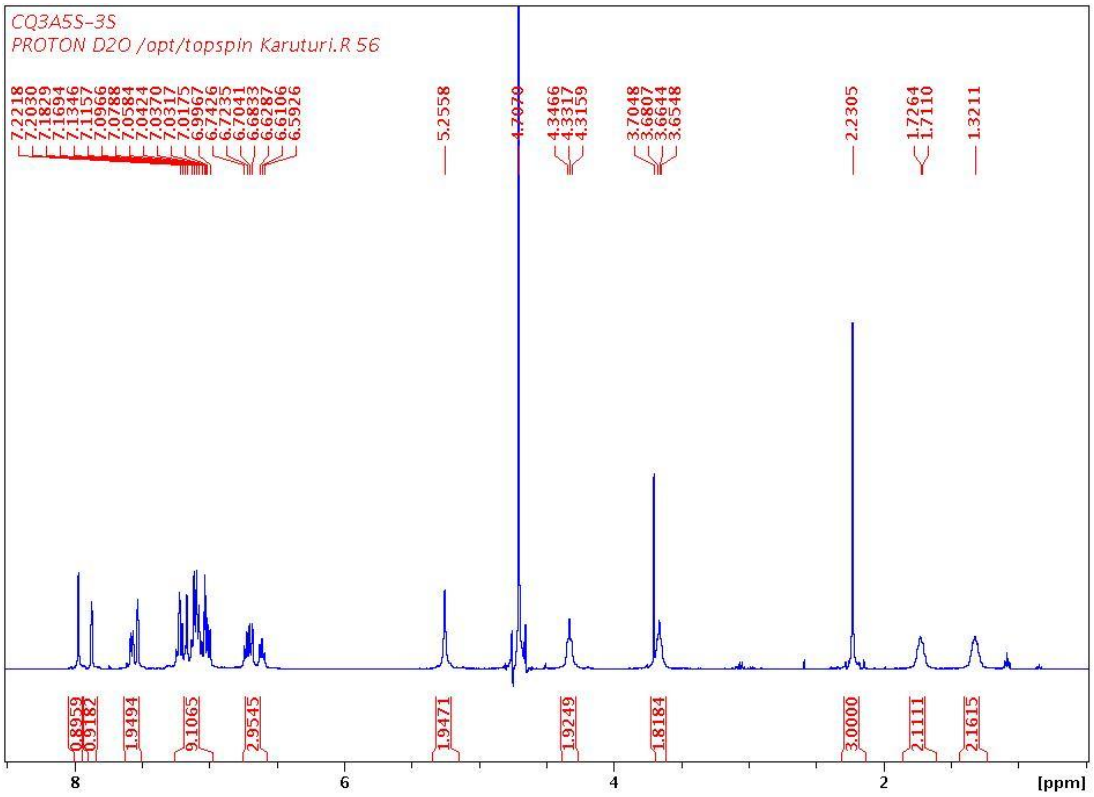

Figure 49

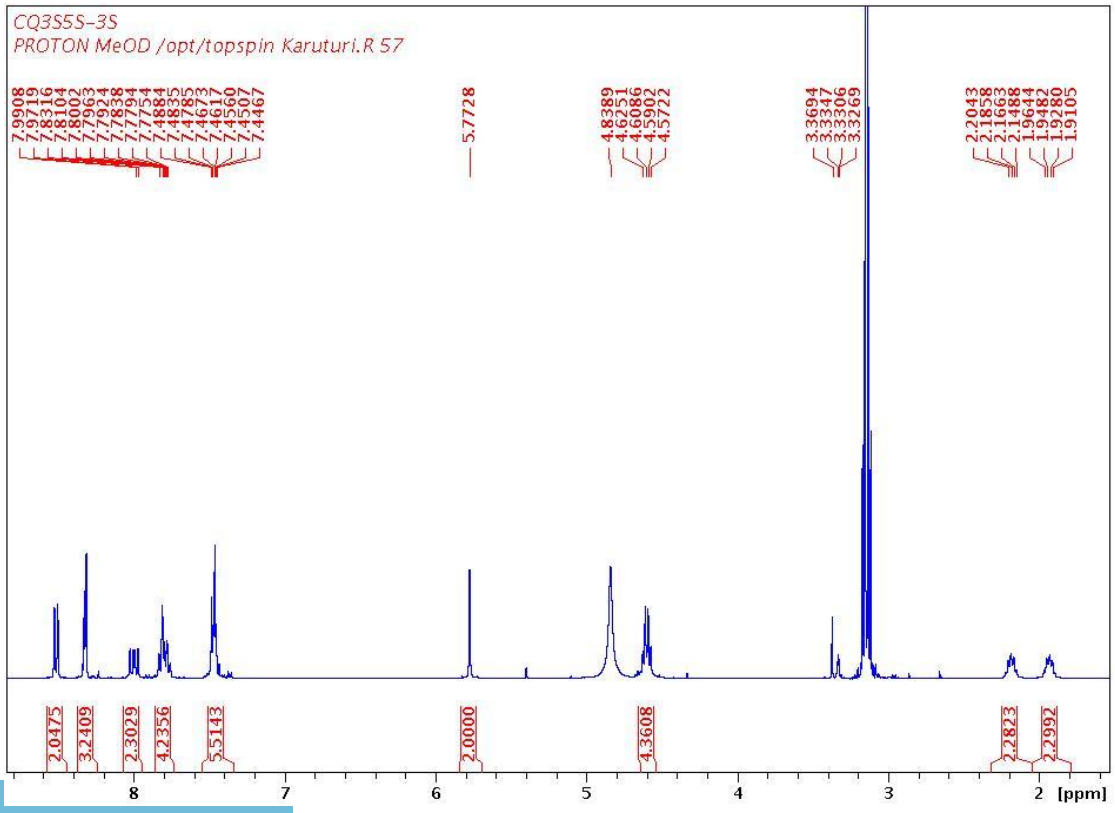

Figure 50

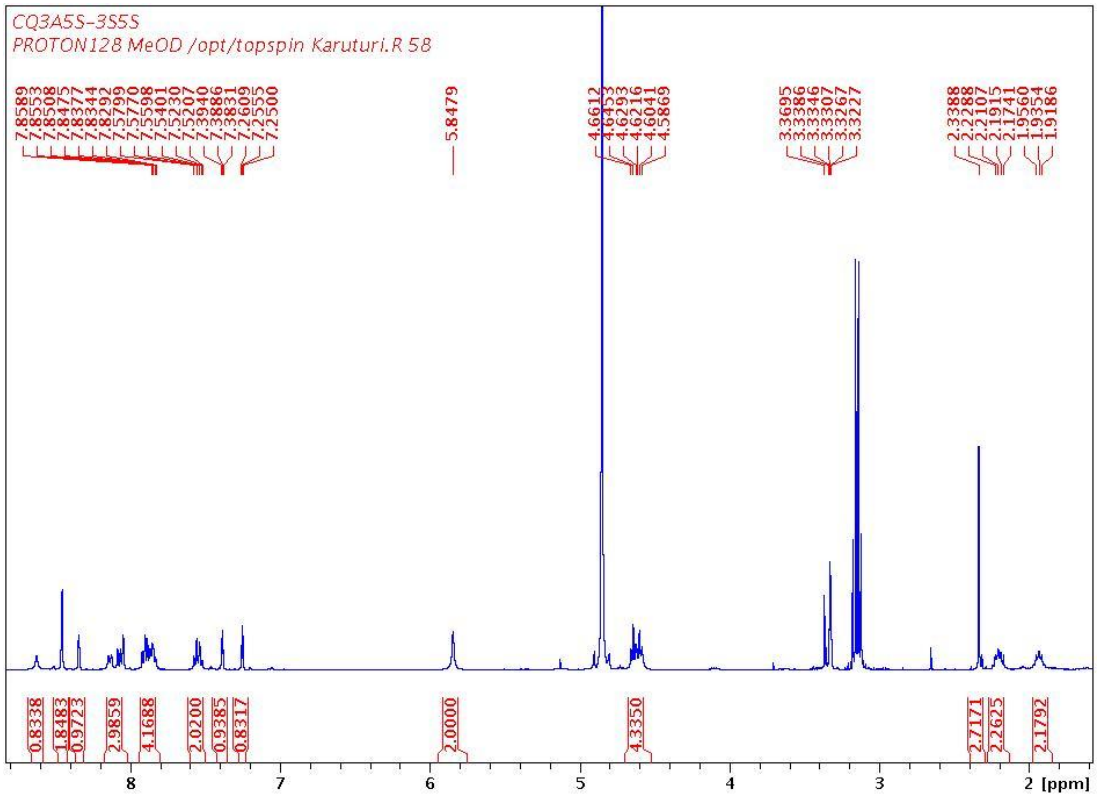

Figure 51

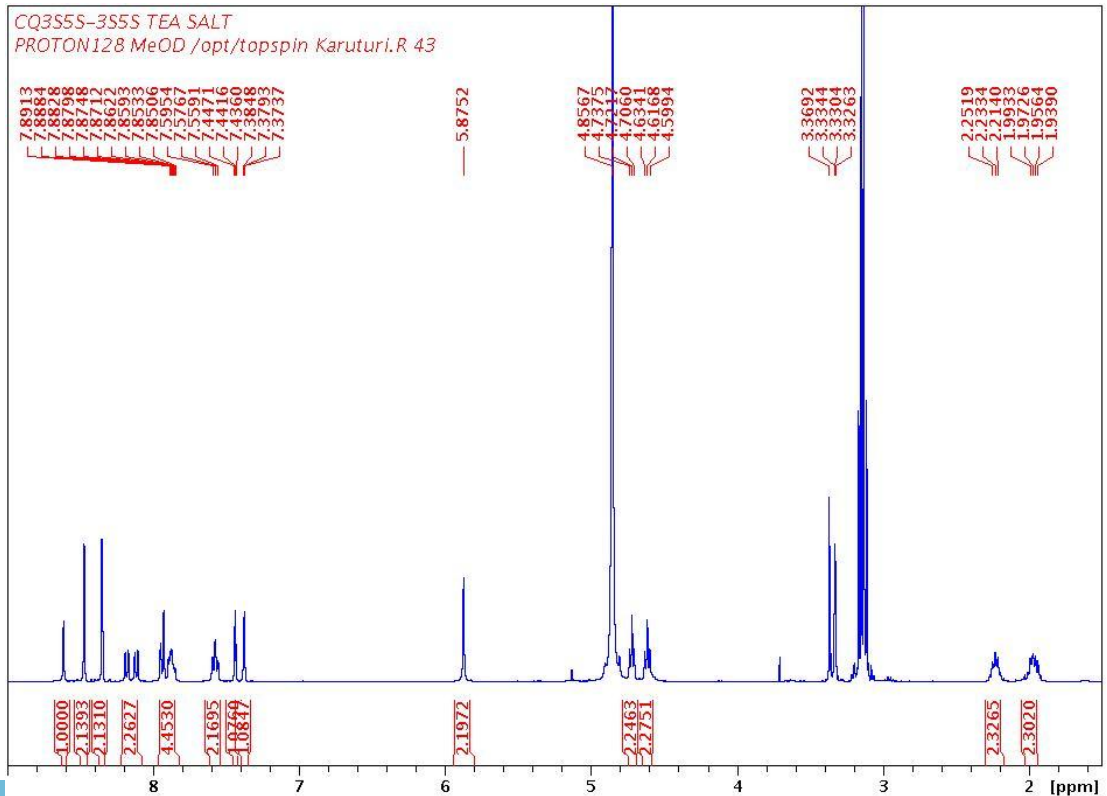

Figure 52

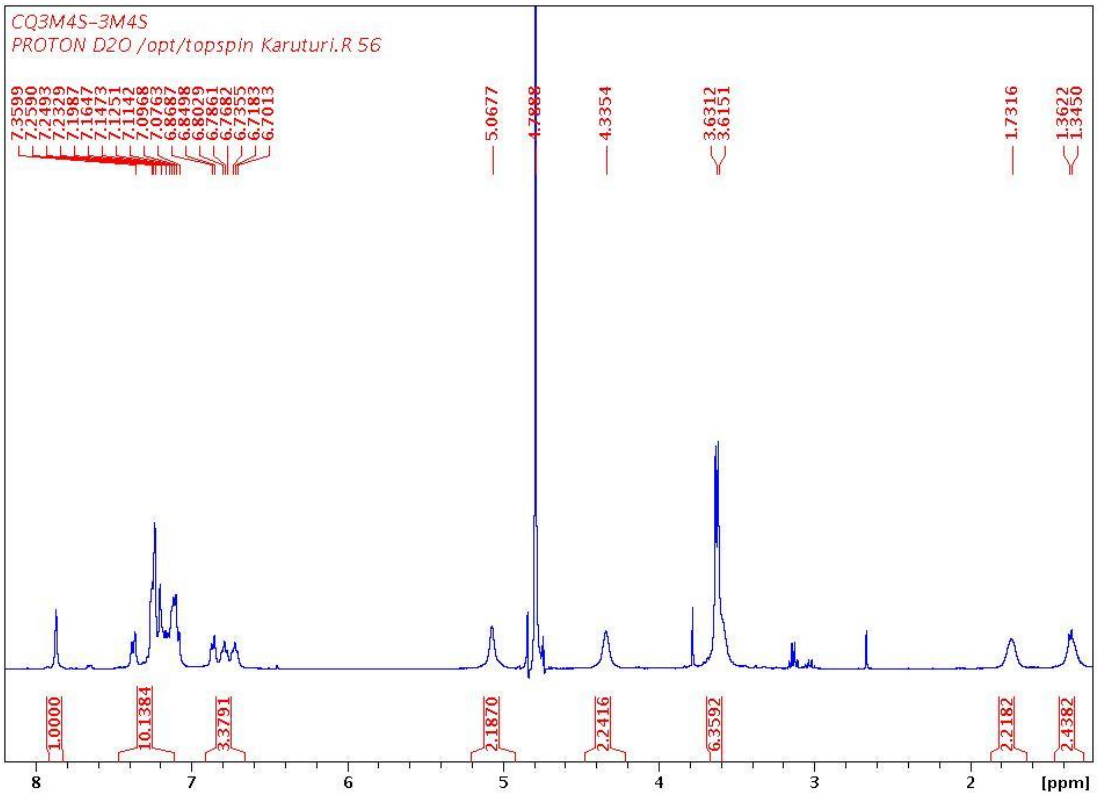

Figure 53

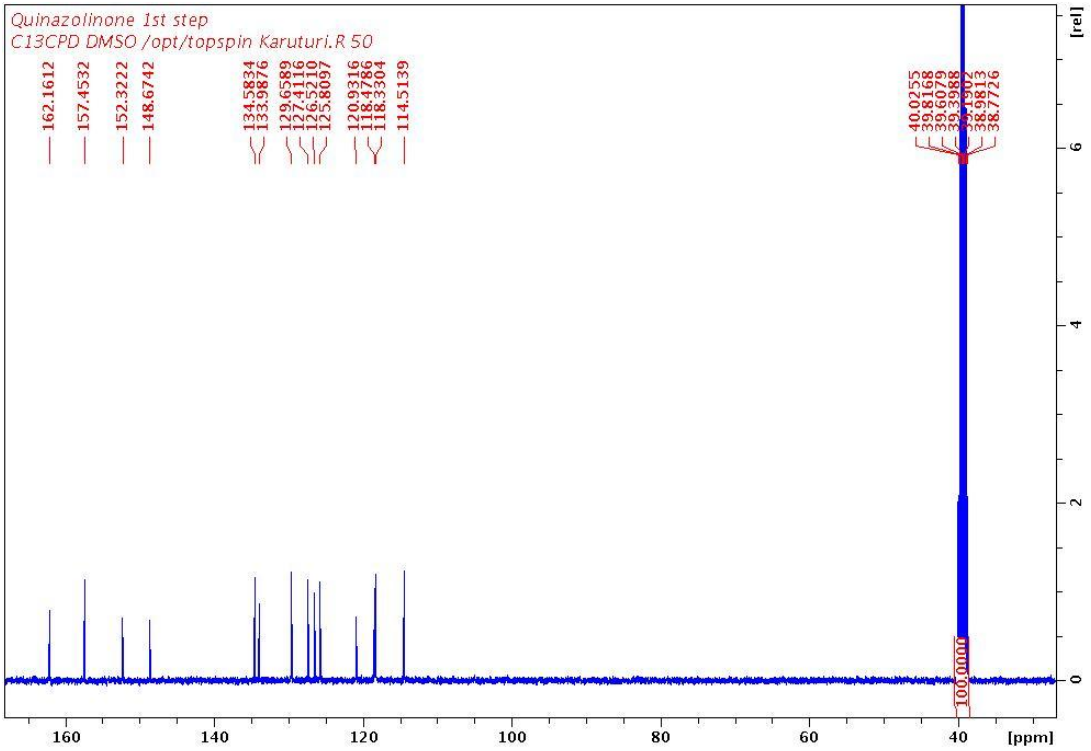

Figure 55

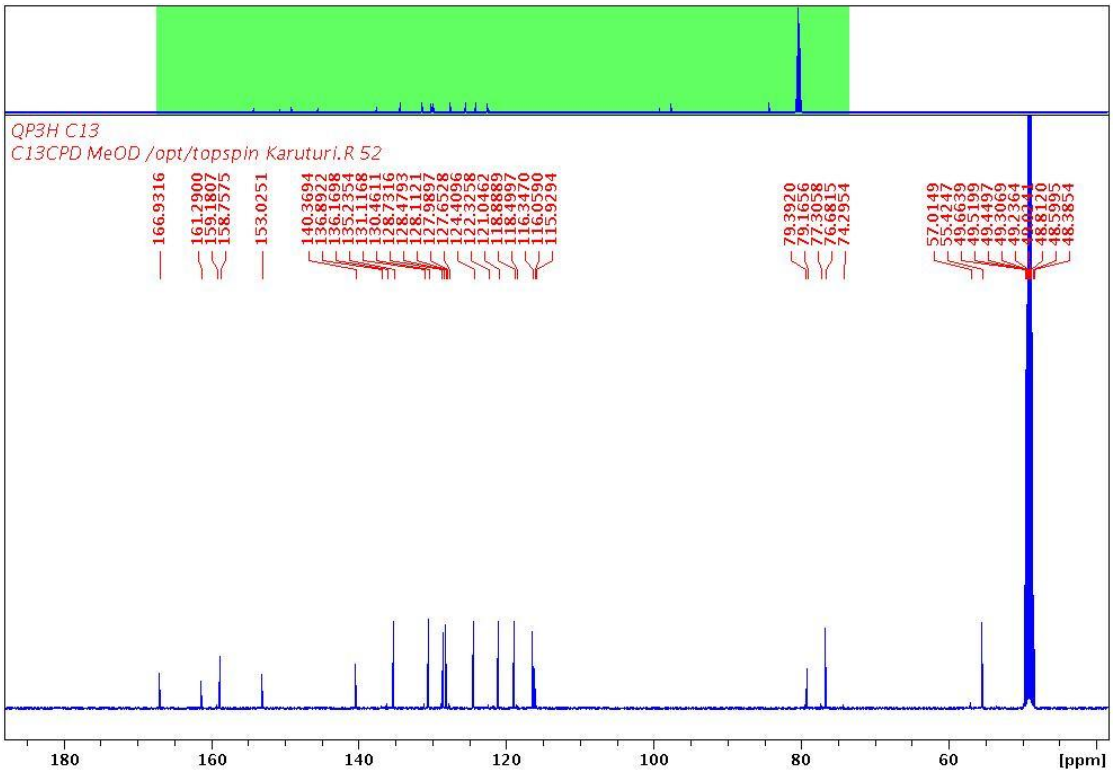

Figure 56

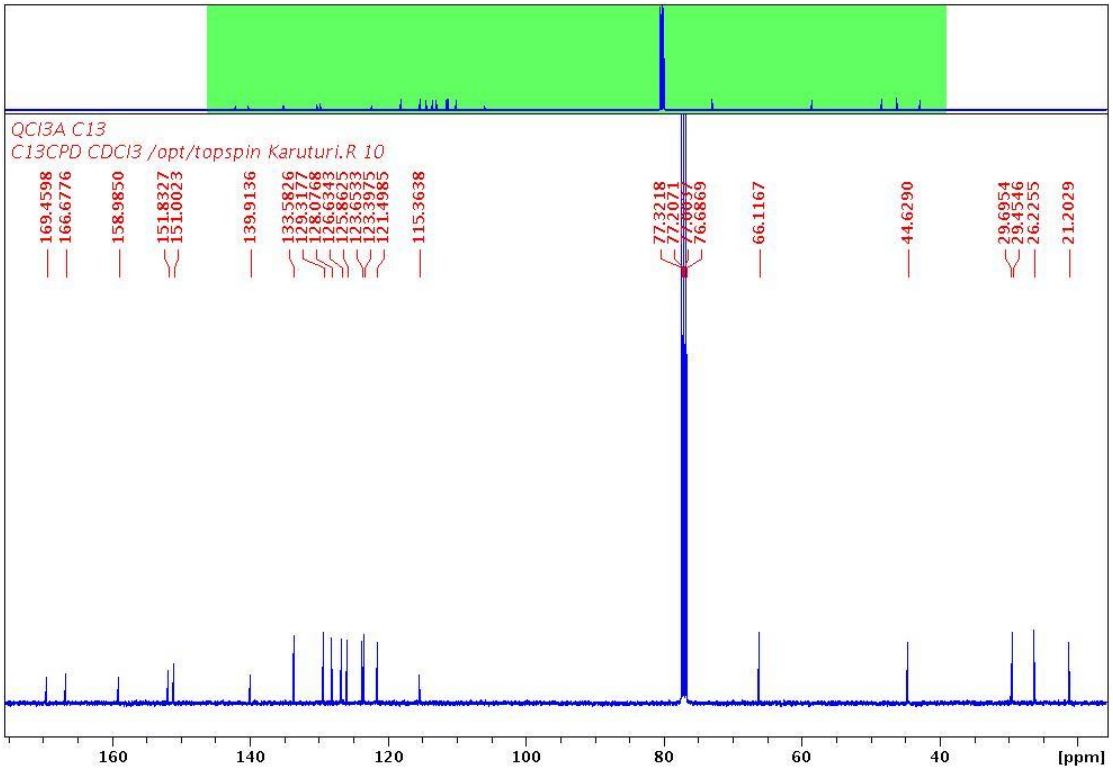

Figure 57

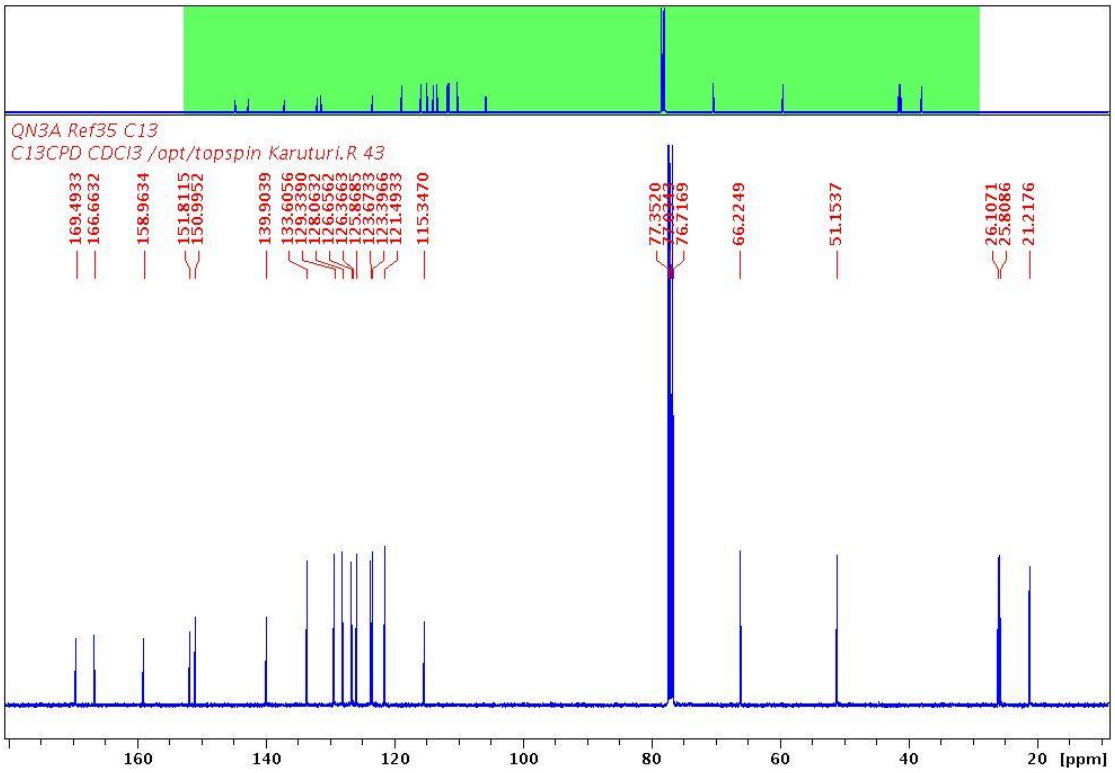

Figure 58

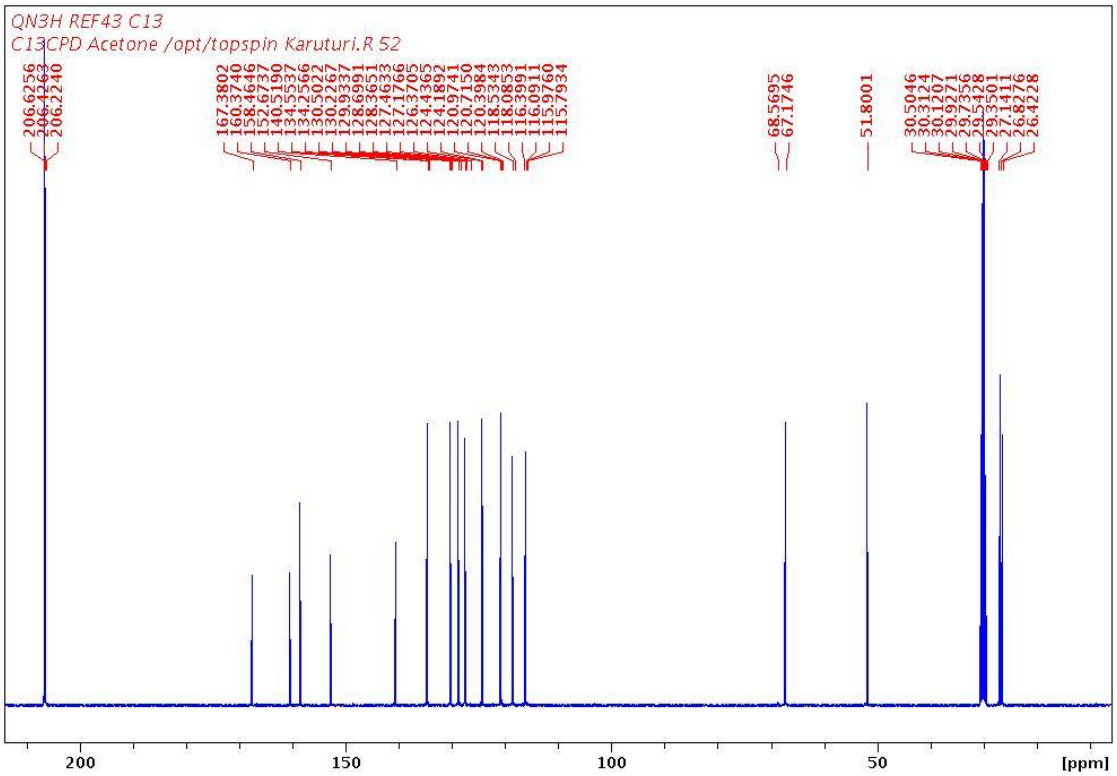

Figure 59

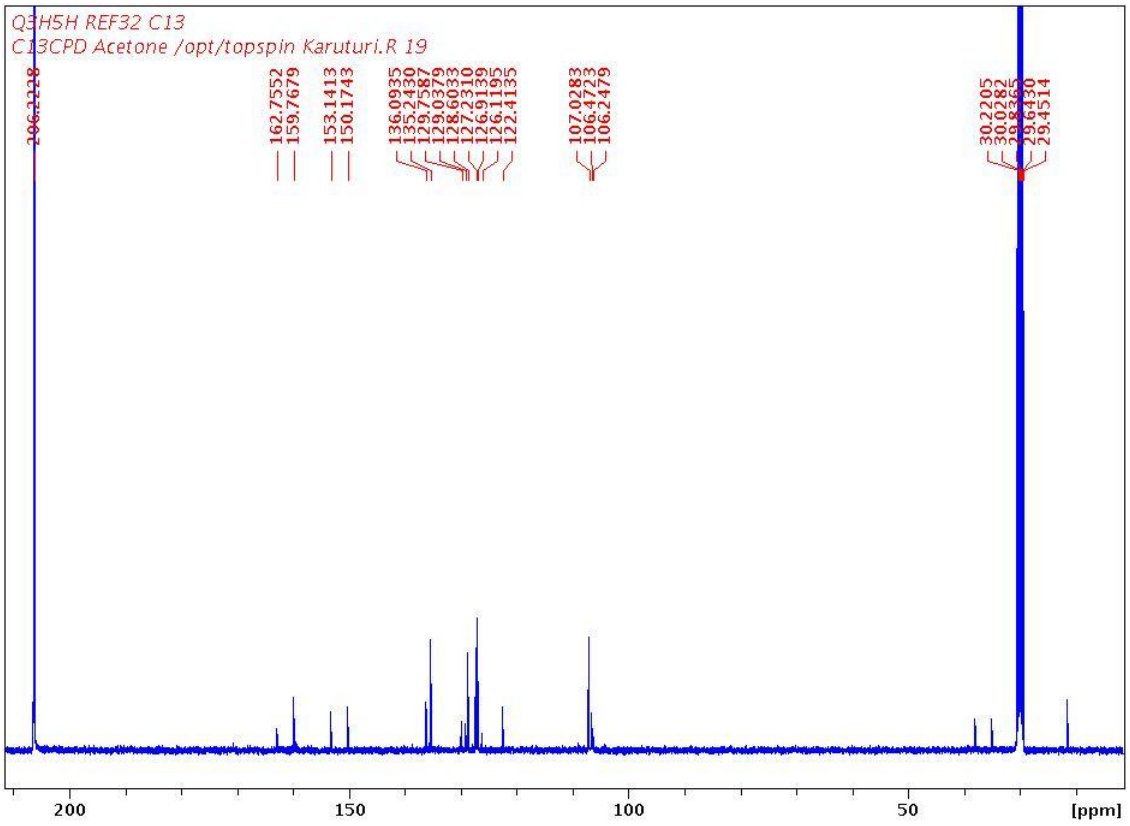

Figure 60

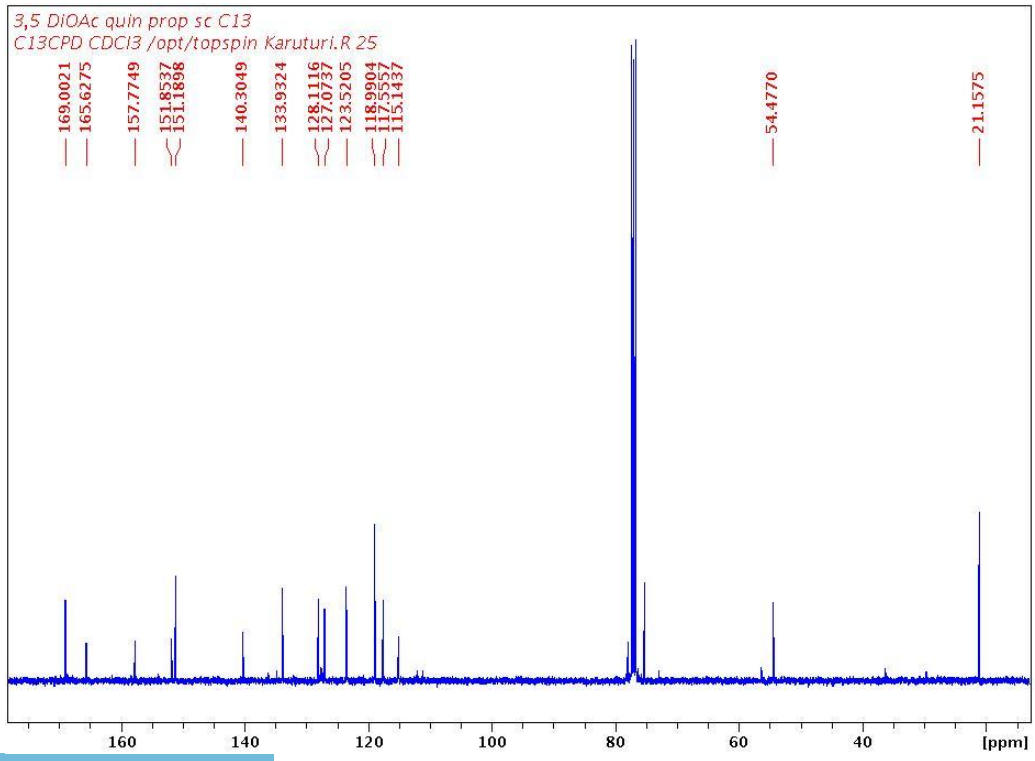

Figure 61

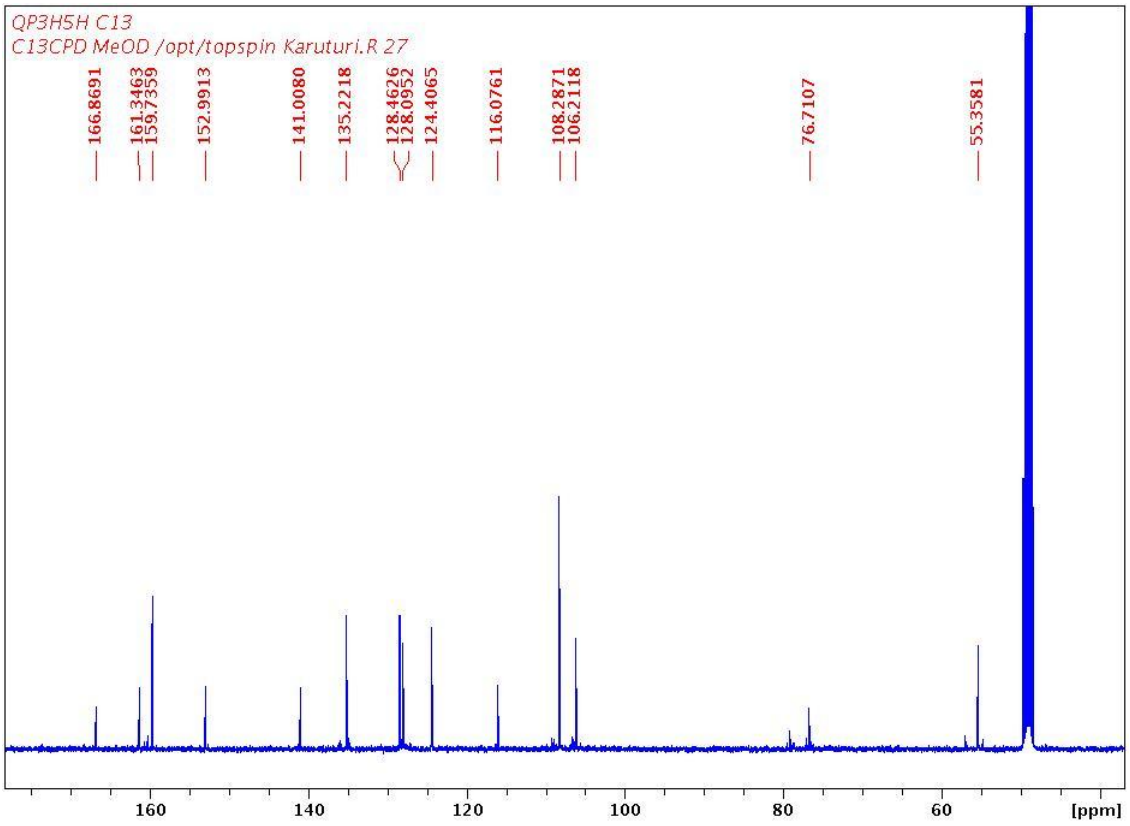

Figure 62

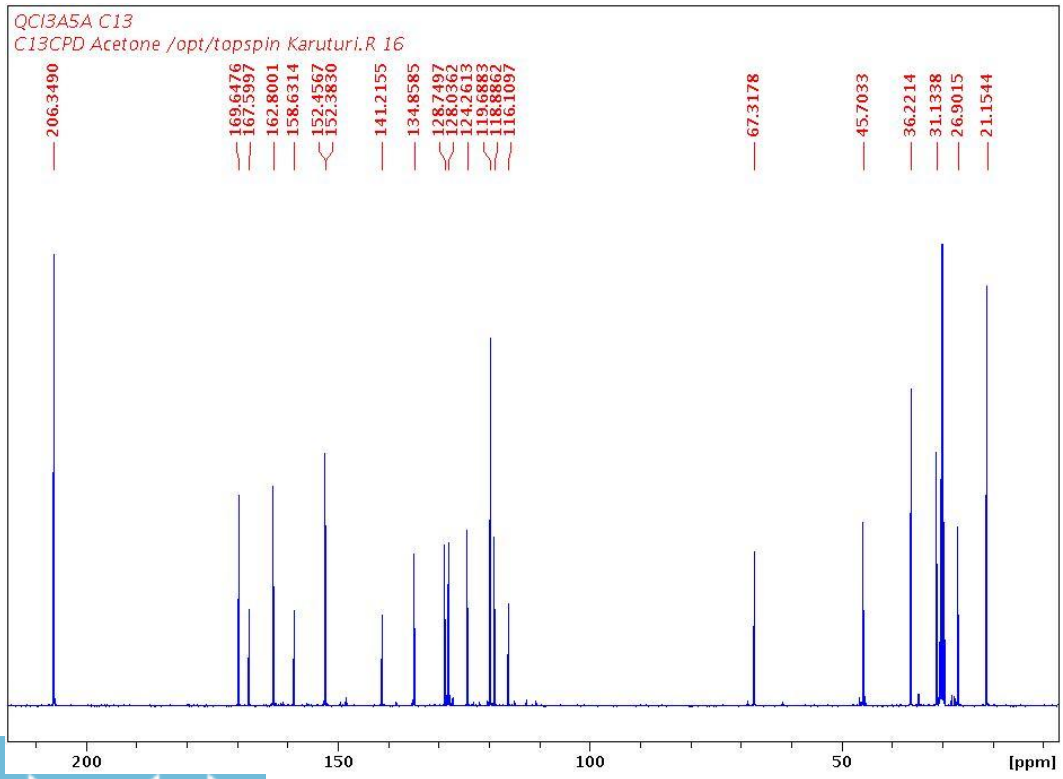

Figure 63

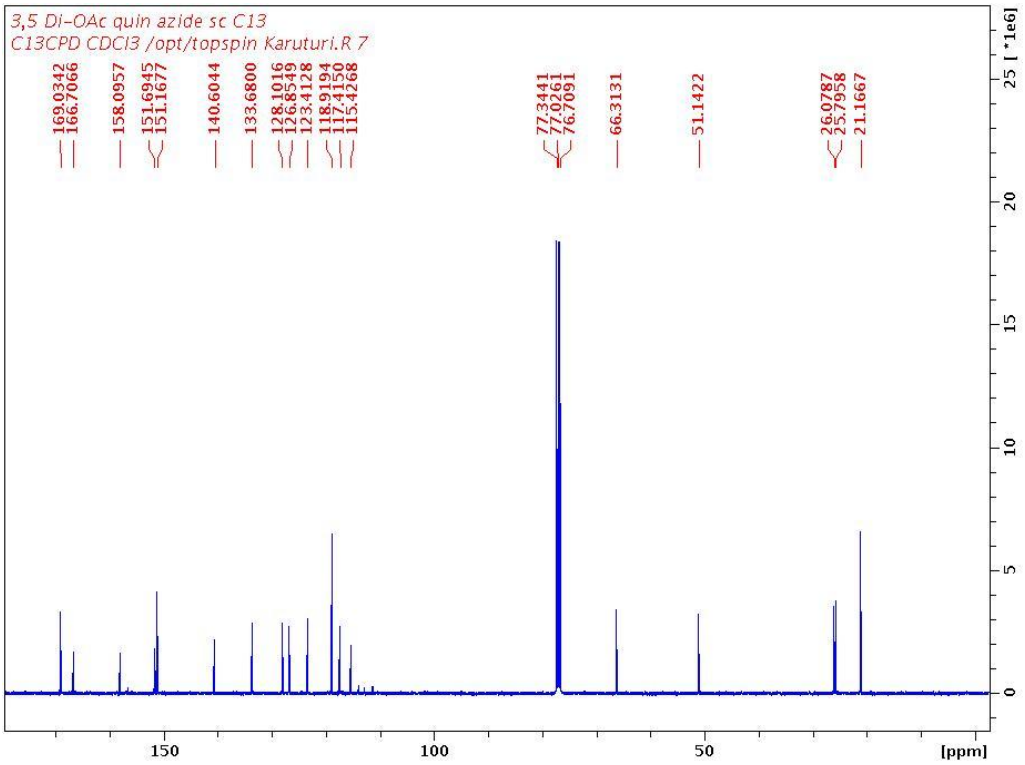

Figure 64

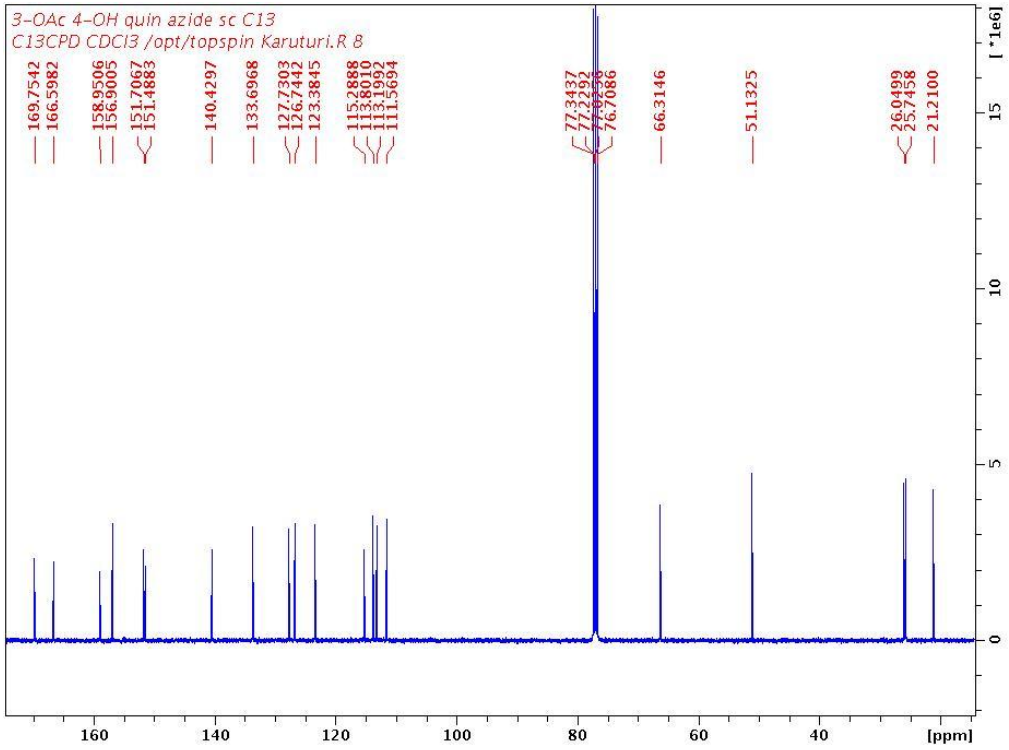

Figure 65

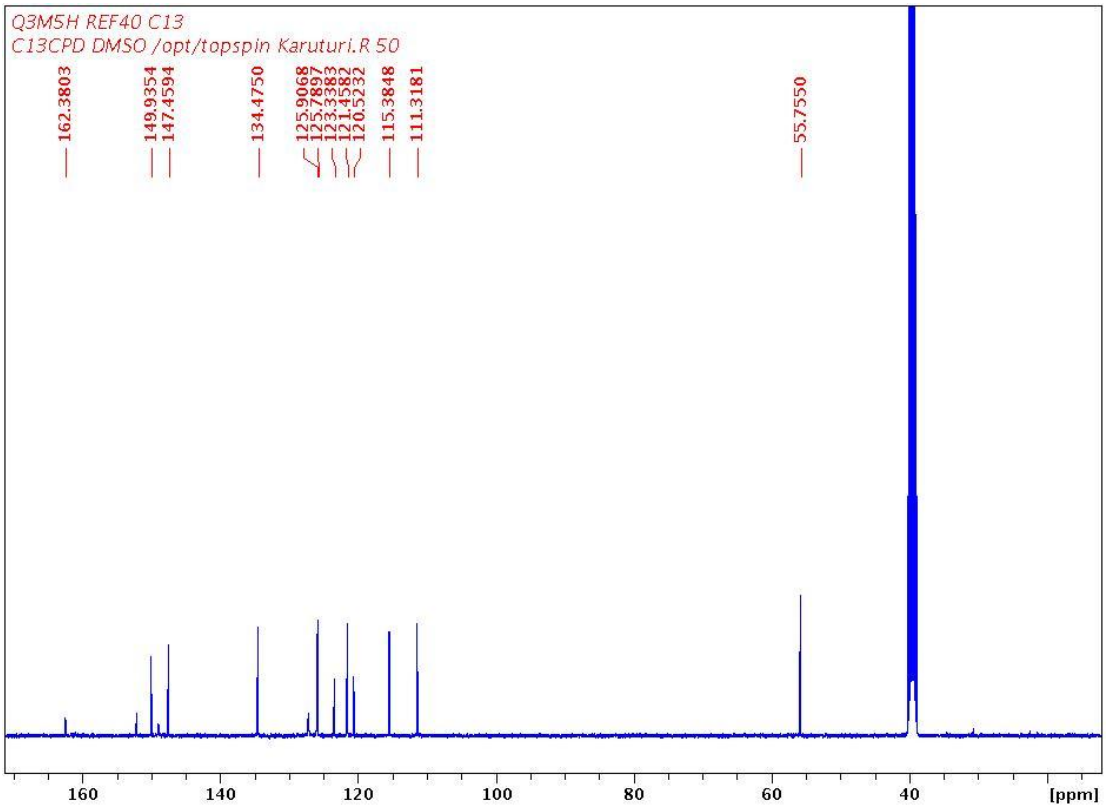

Figure 66

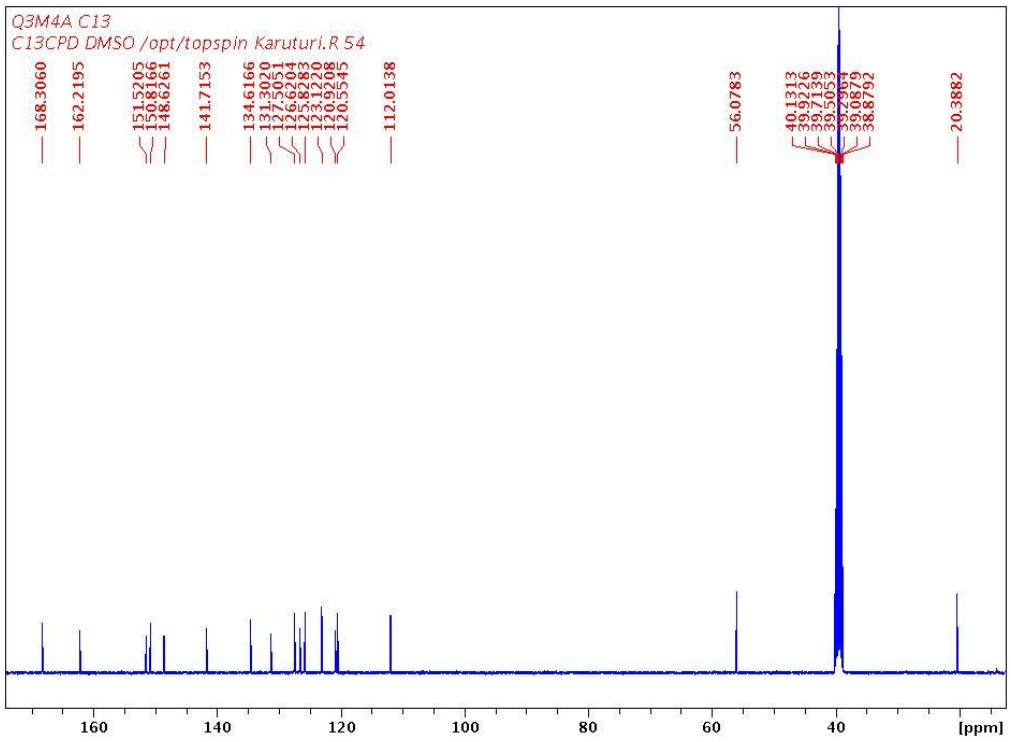

Figure 67

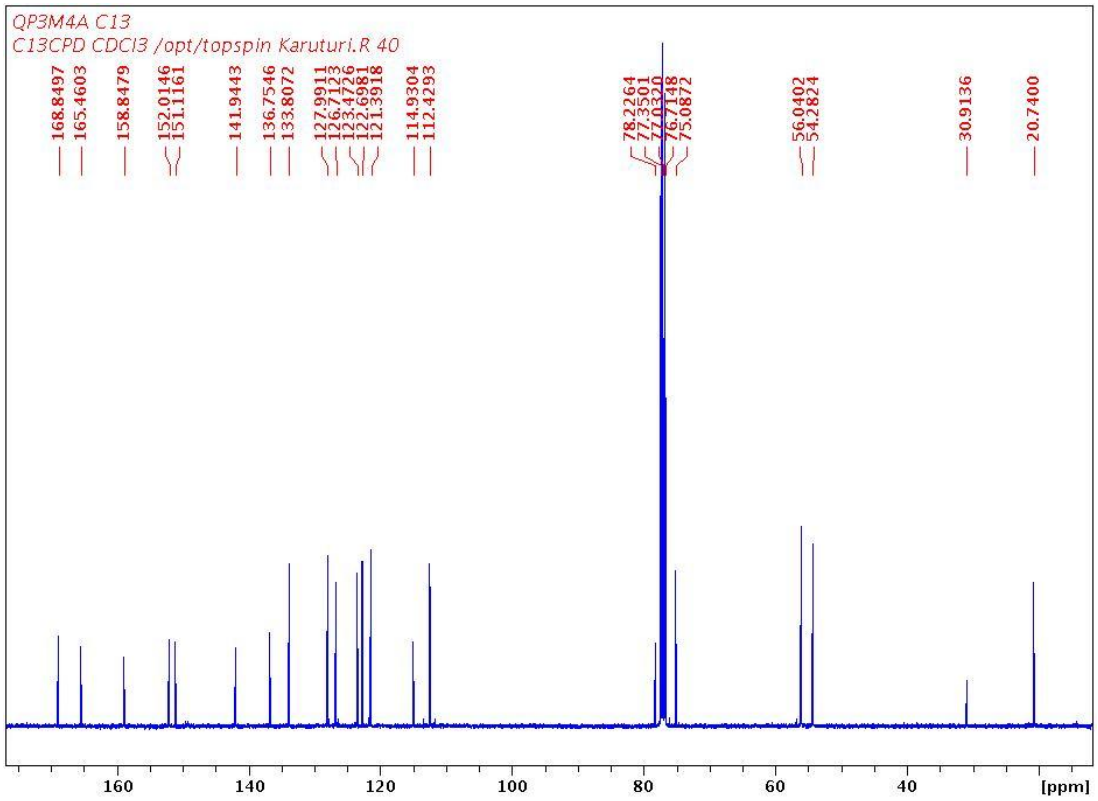

Figure 68

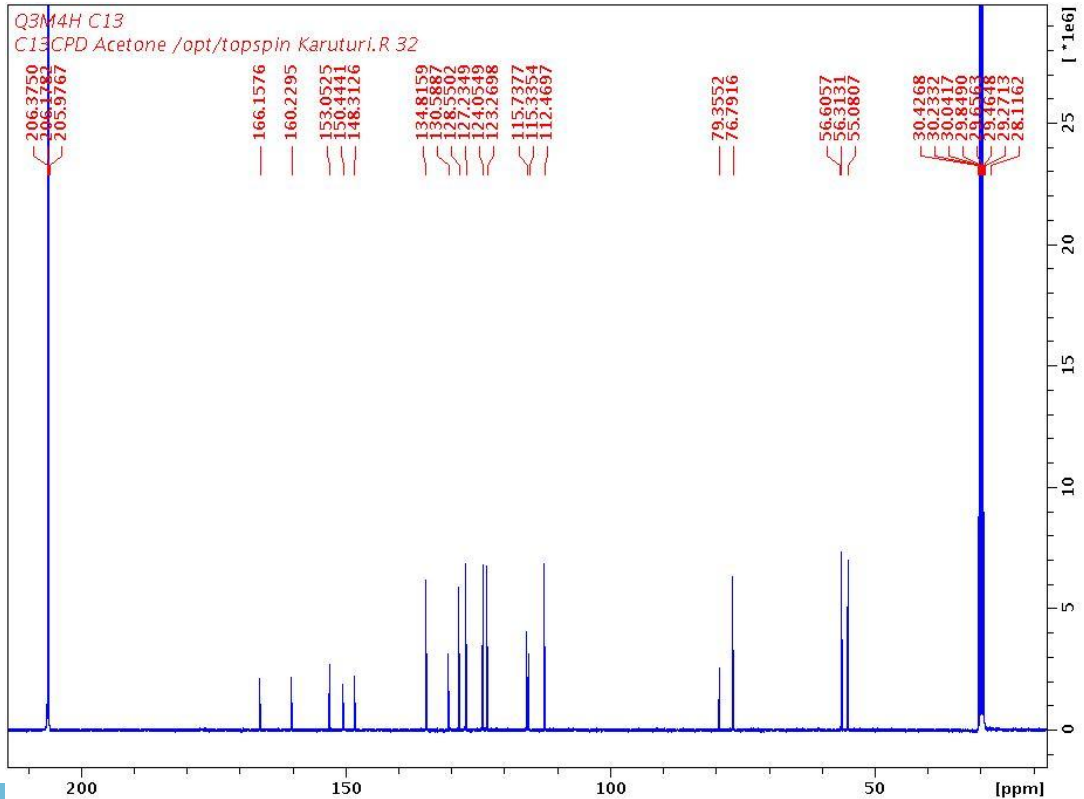

Figure 69

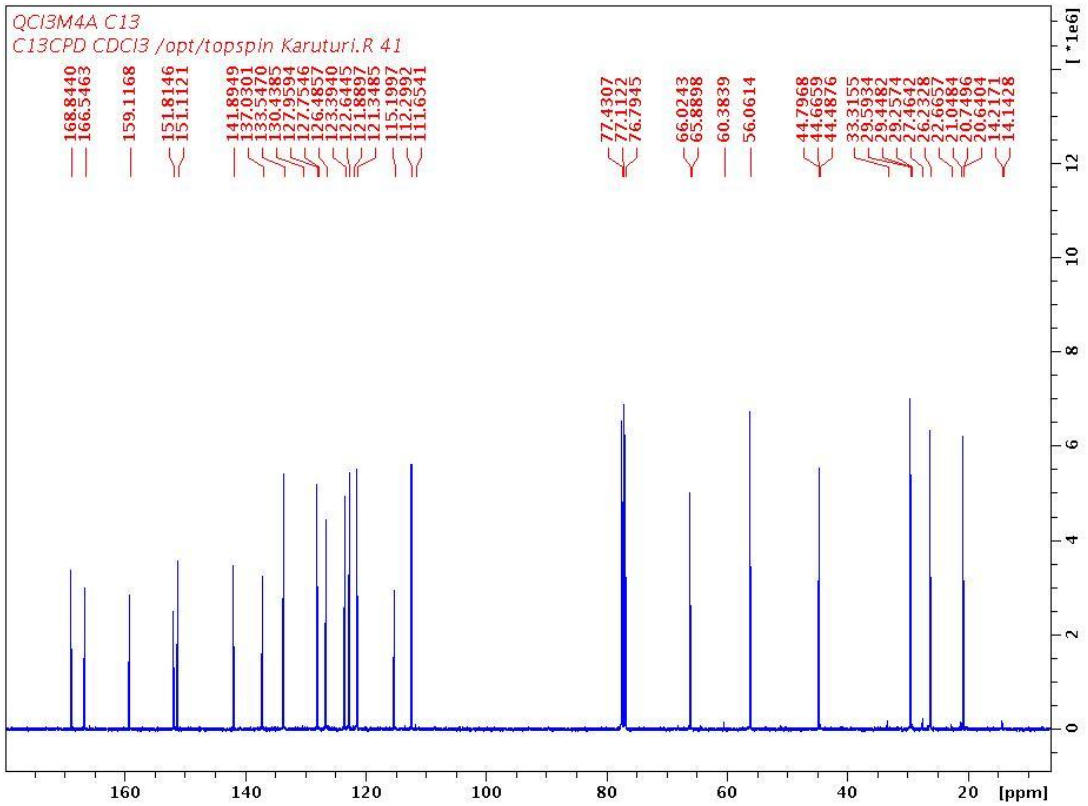

Figure 70

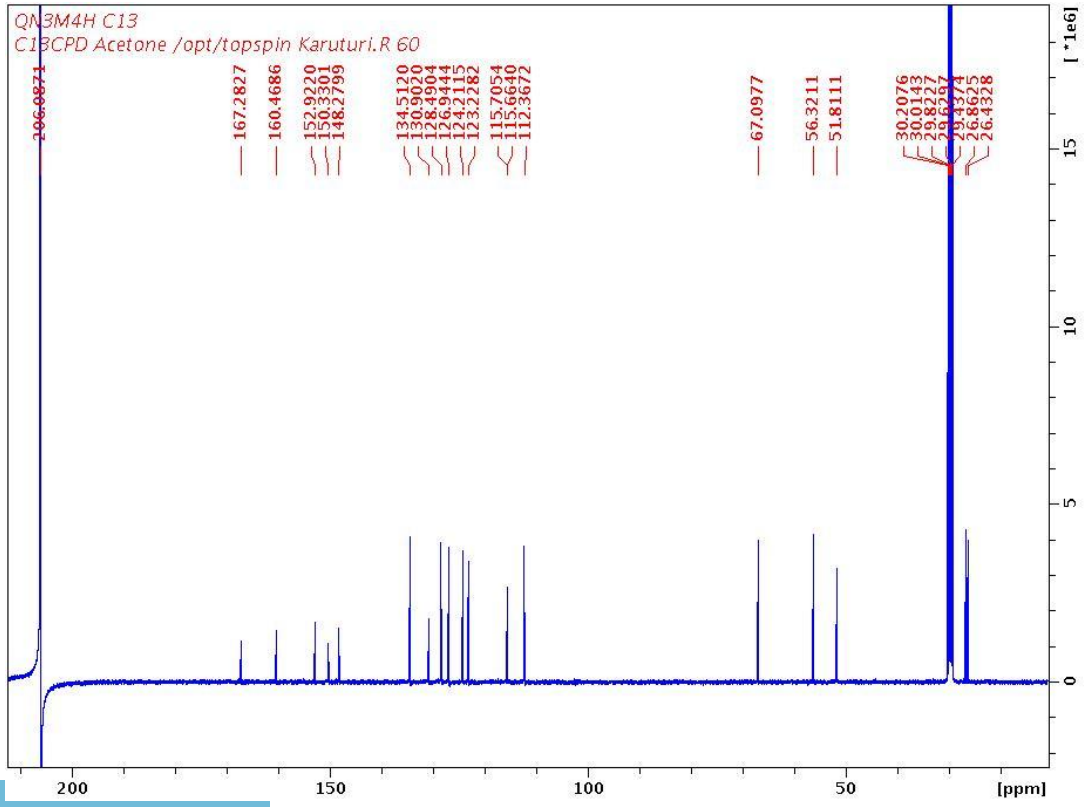

Figure 71

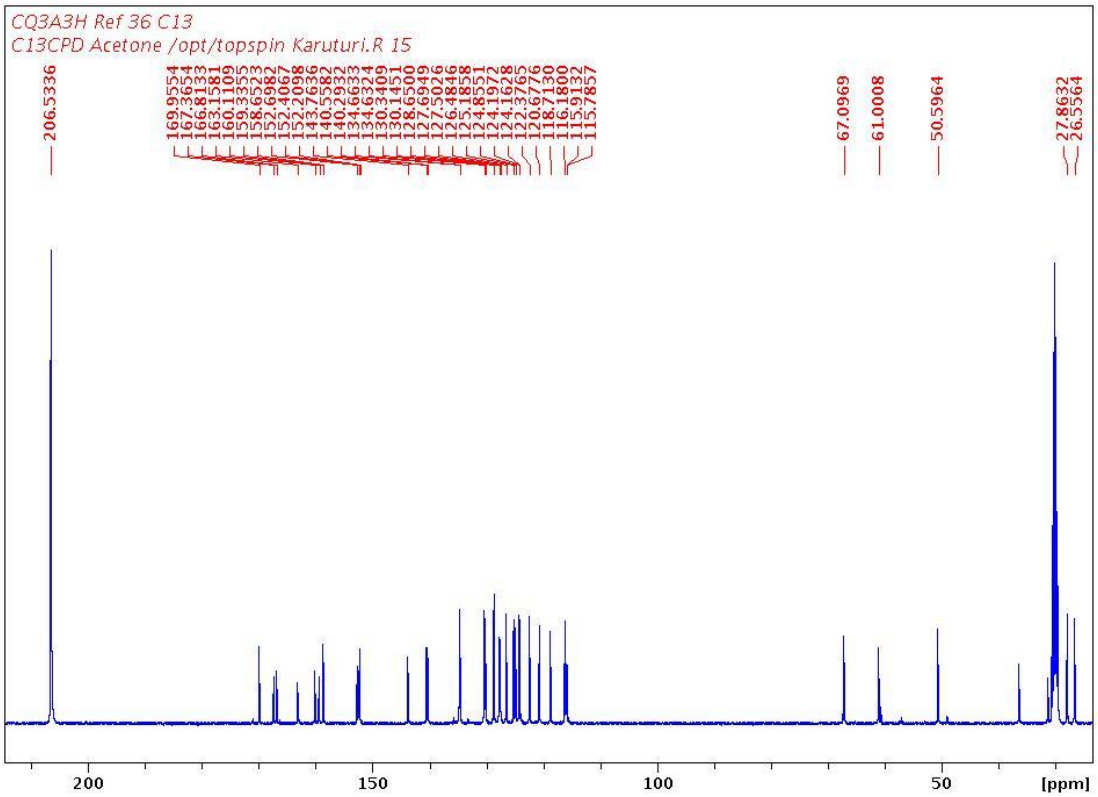

Figure 72

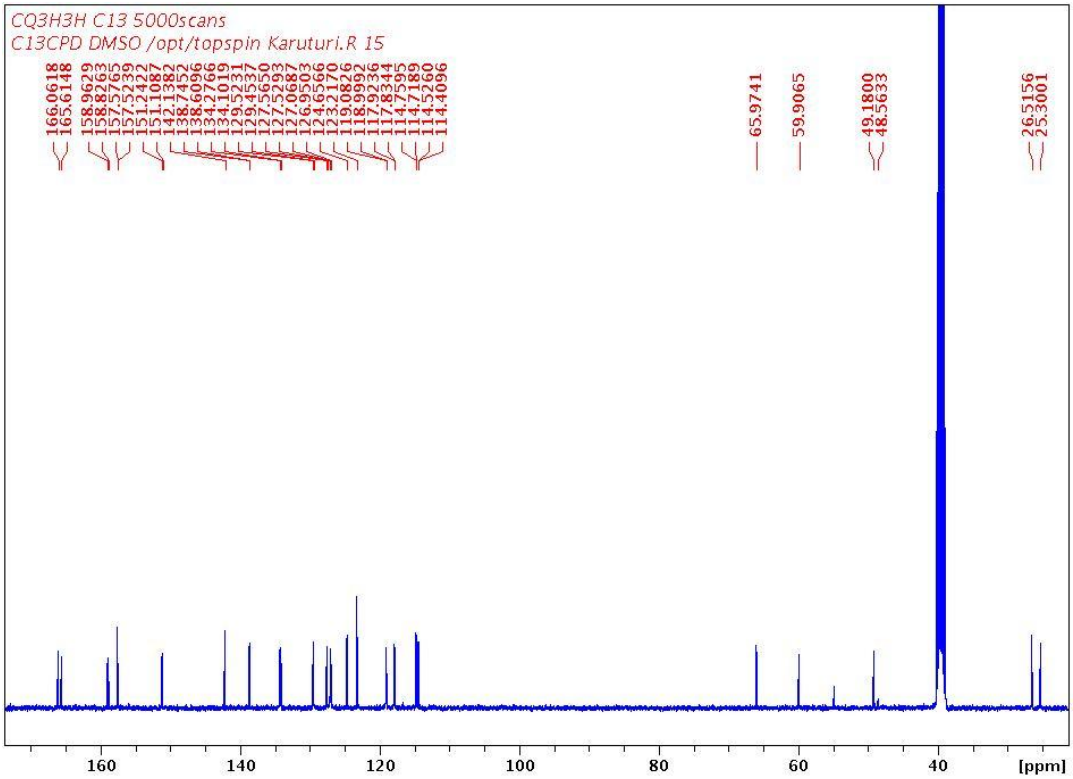

Figure 73

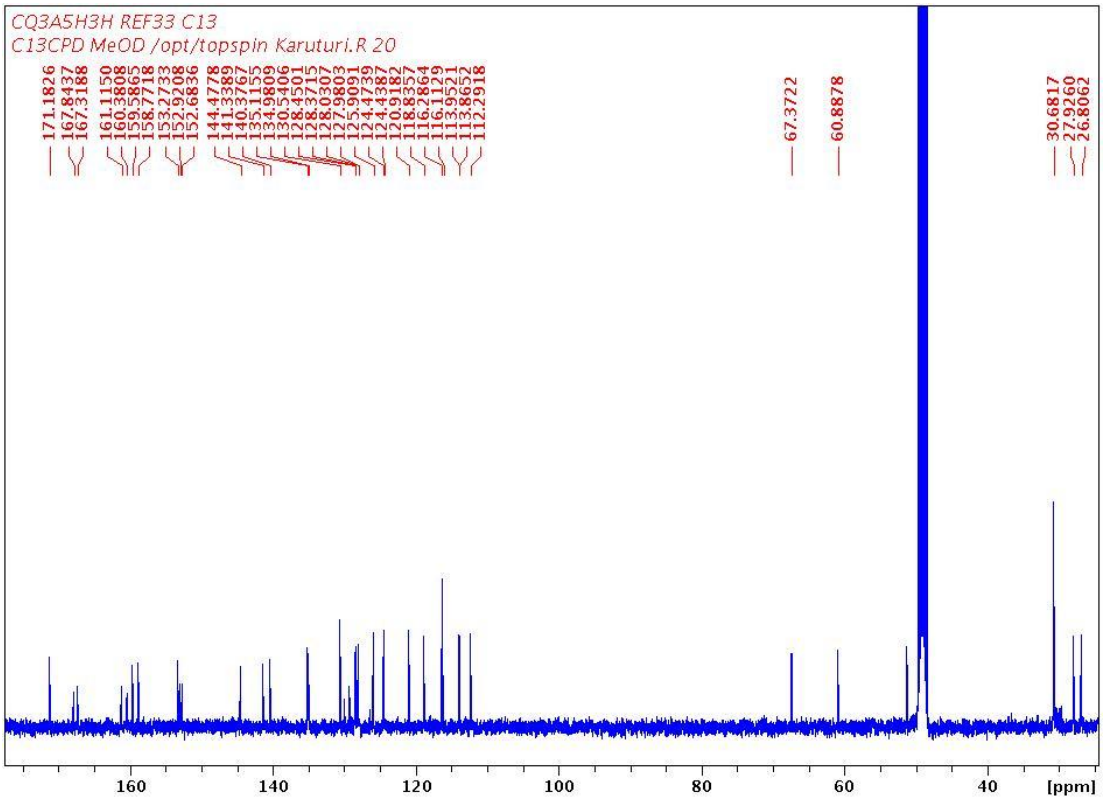

Figure 74

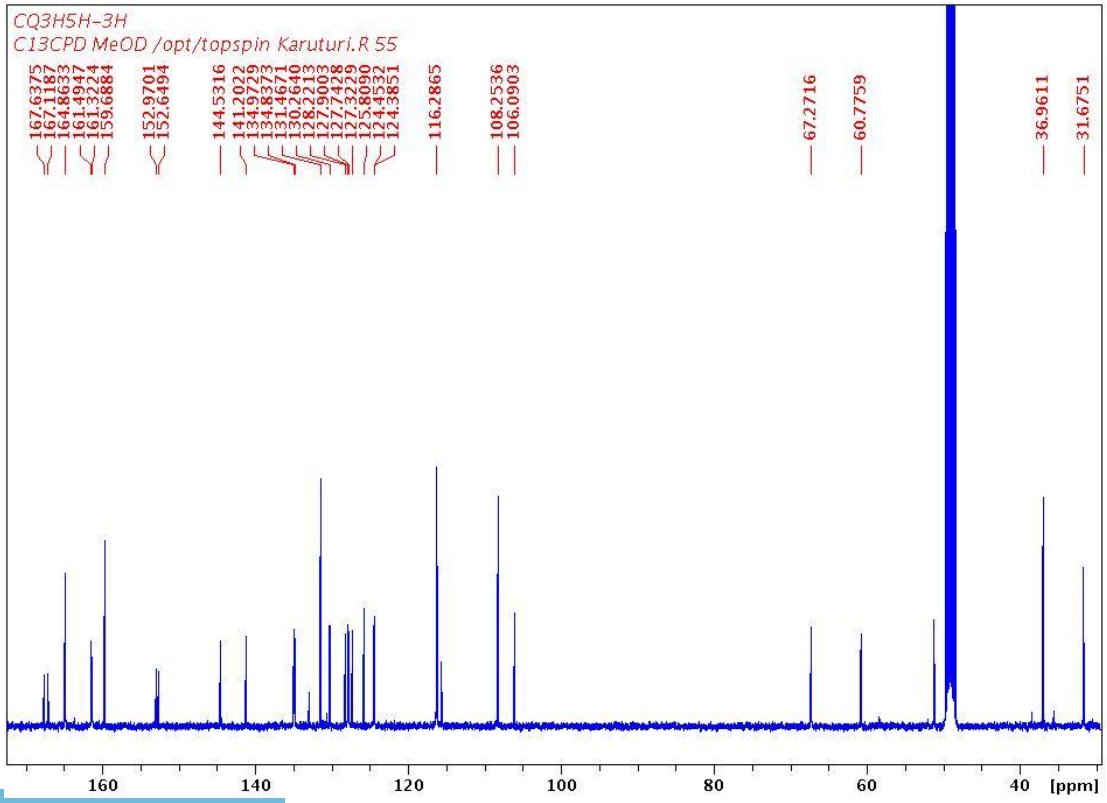

Figure 75

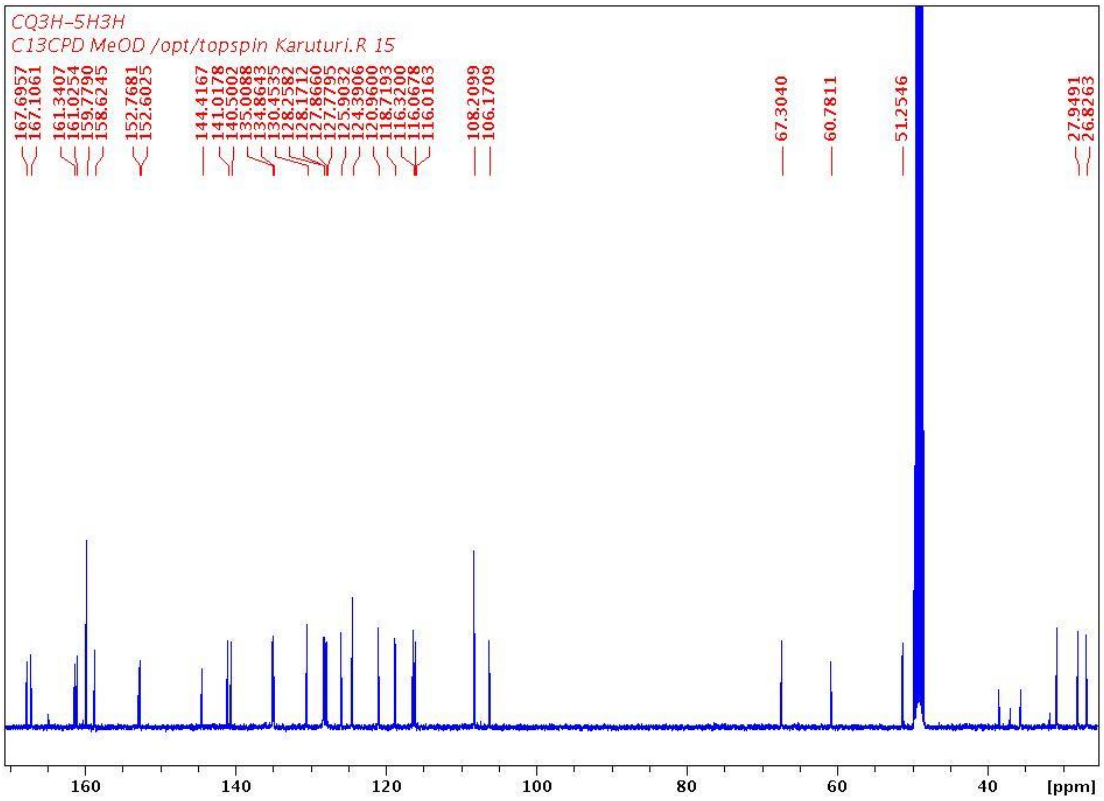

Figure 76

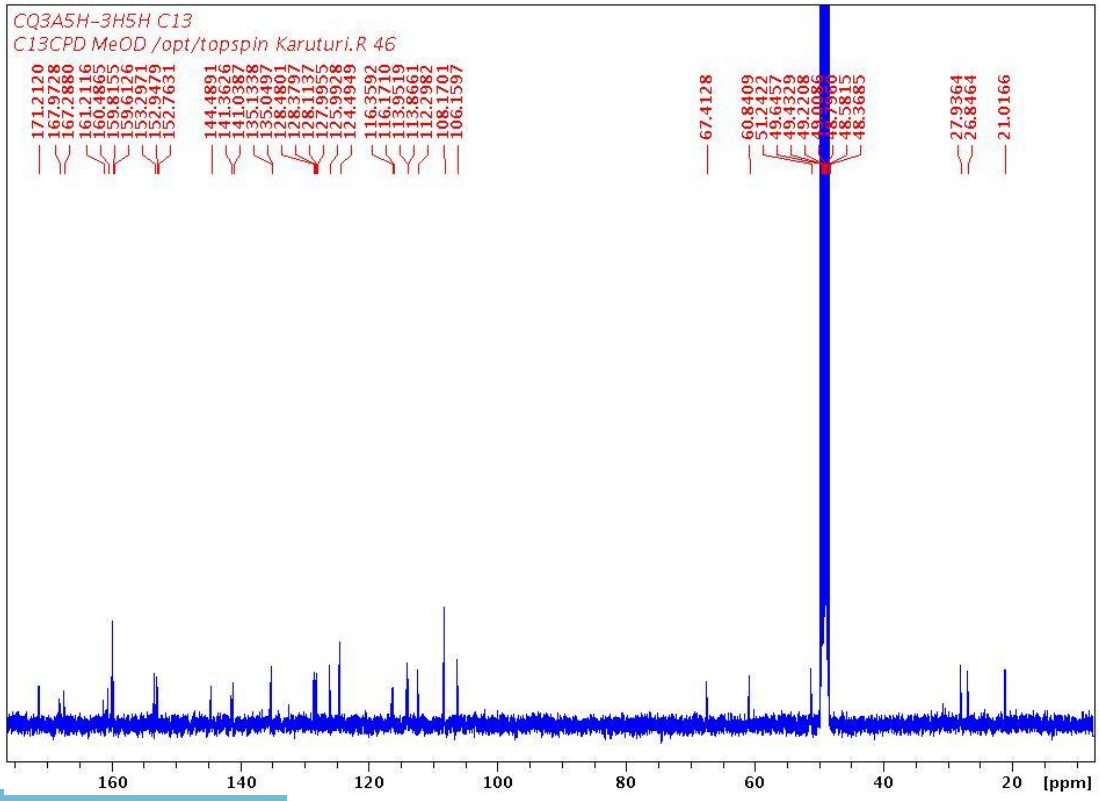

Figure 77

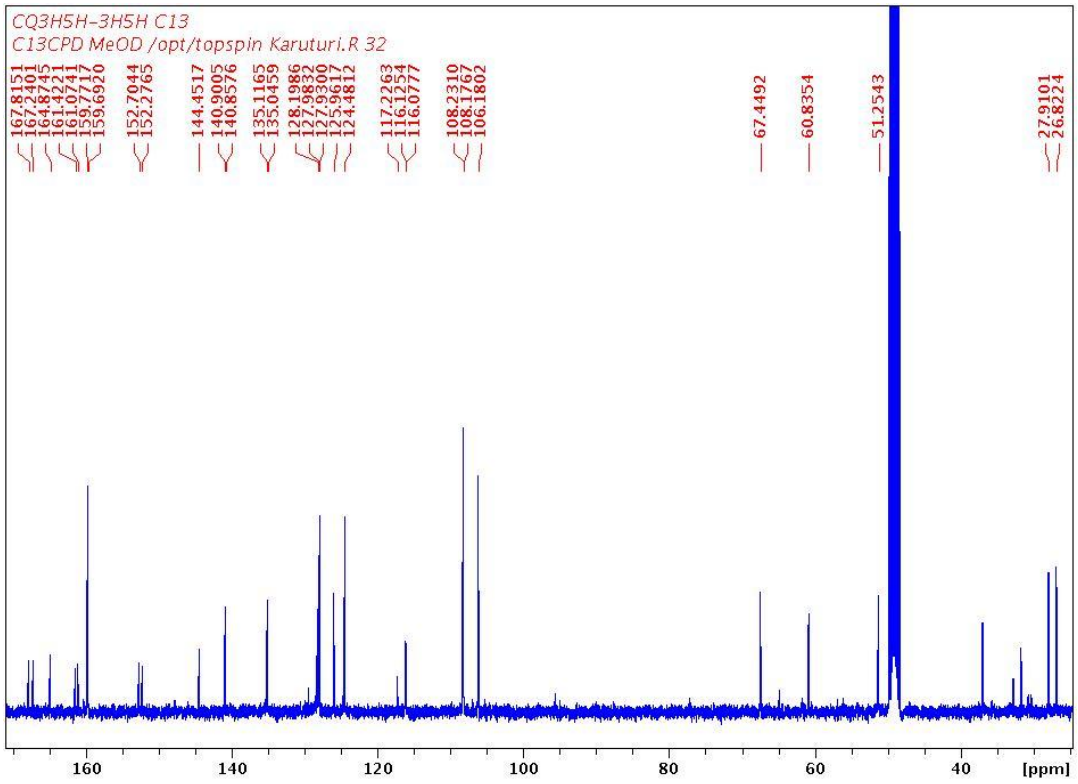

Figure 78

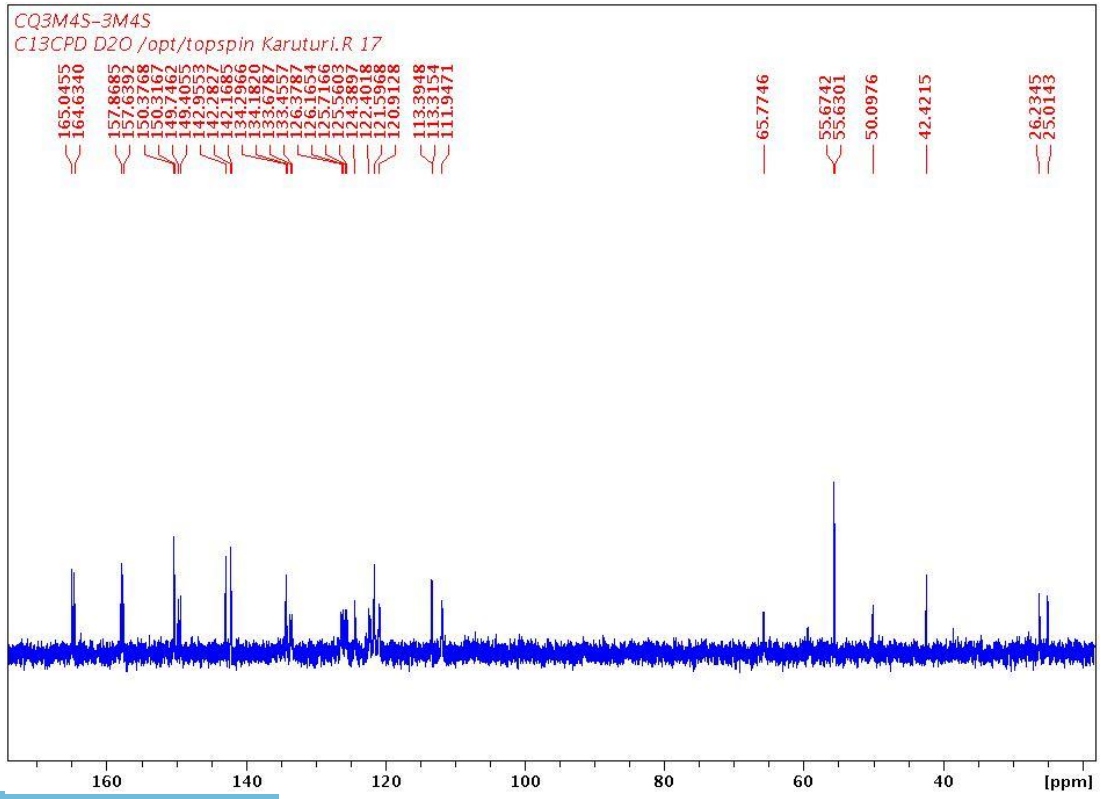

Figure 79

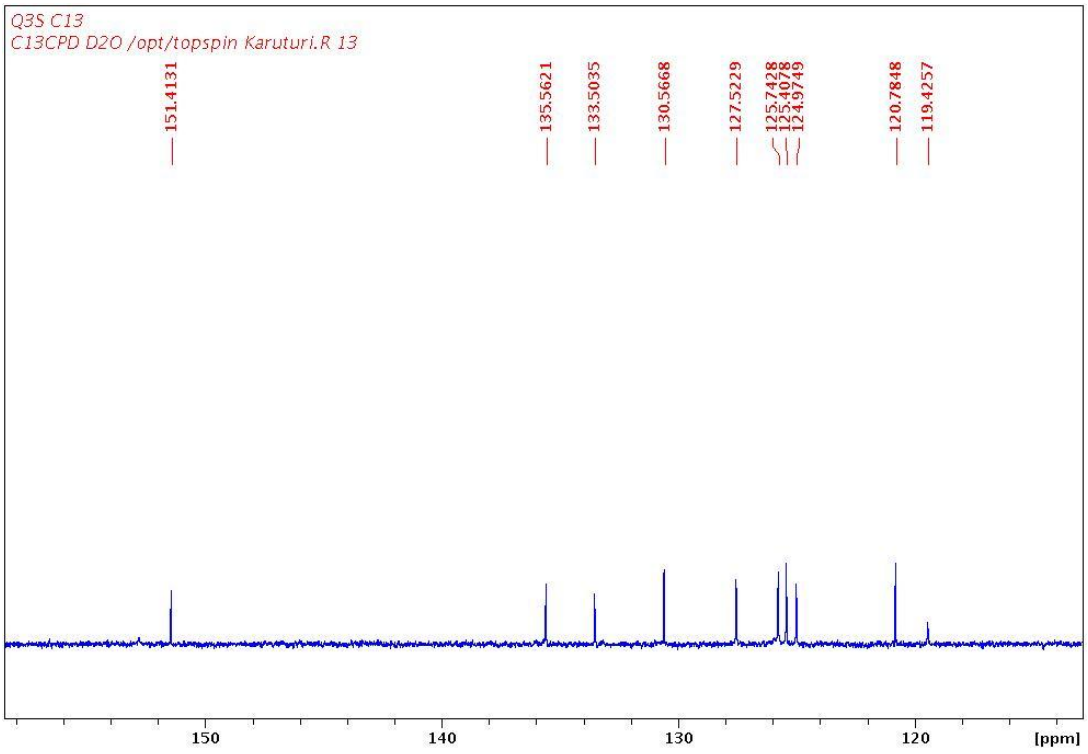

Figure 80

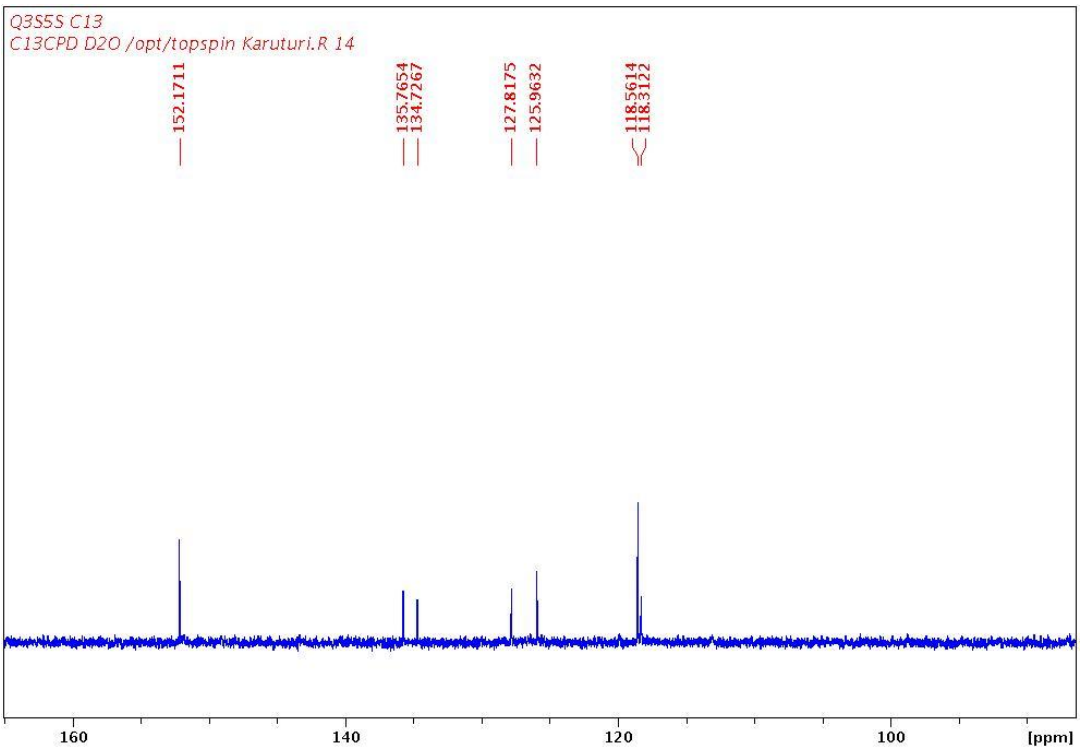

Figure 81

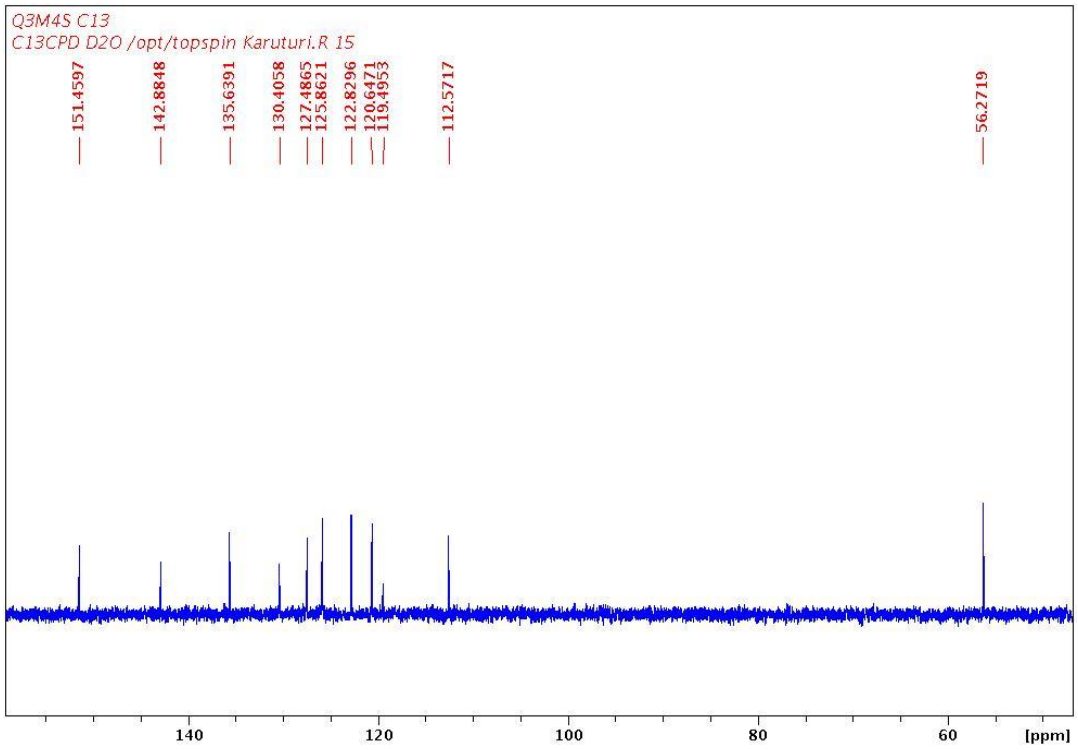

Figure 82

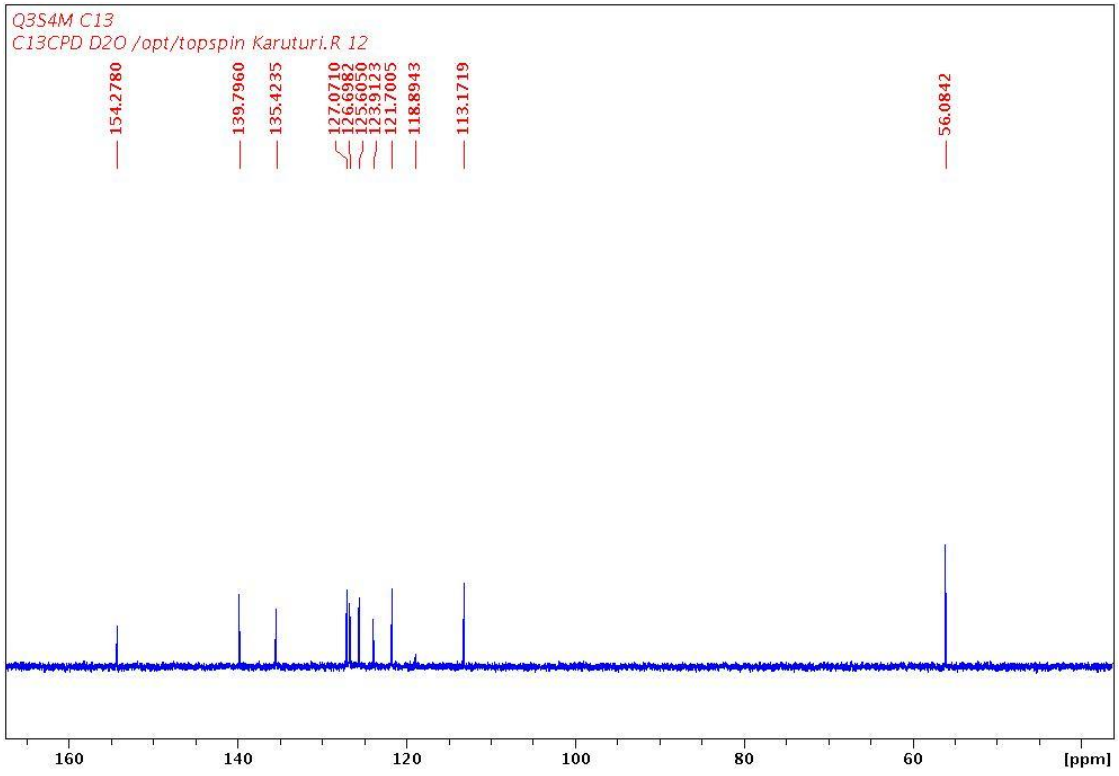

Figure 83

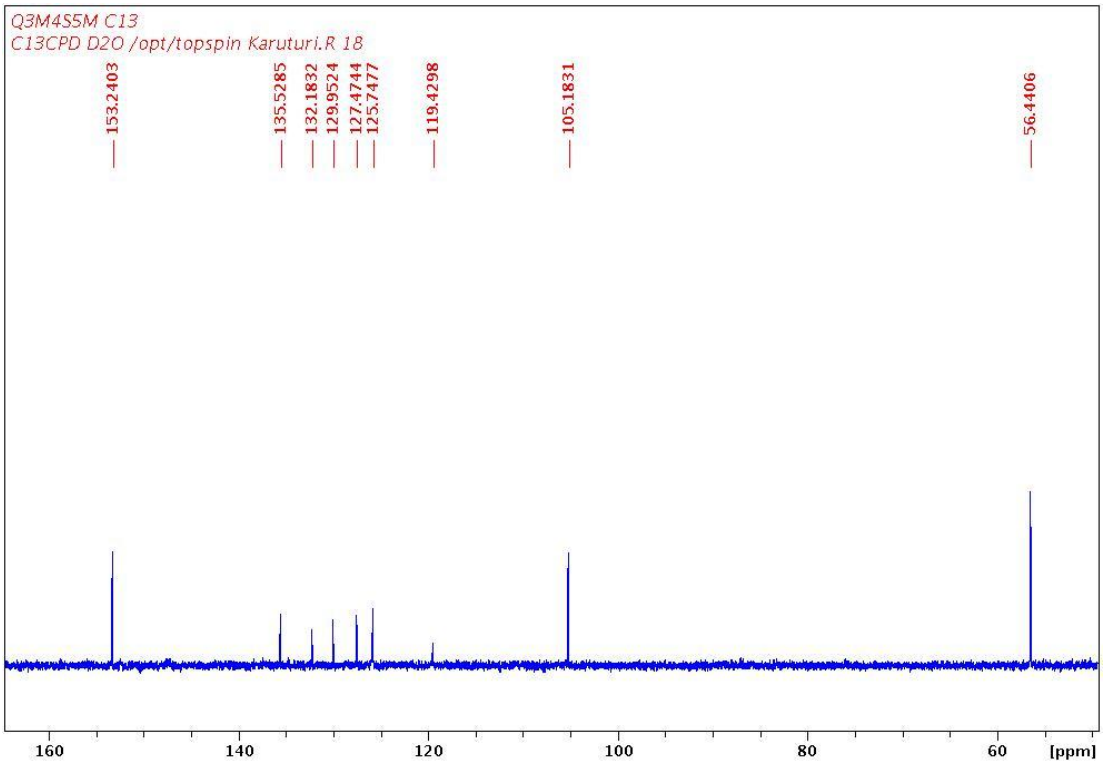

Figure 84

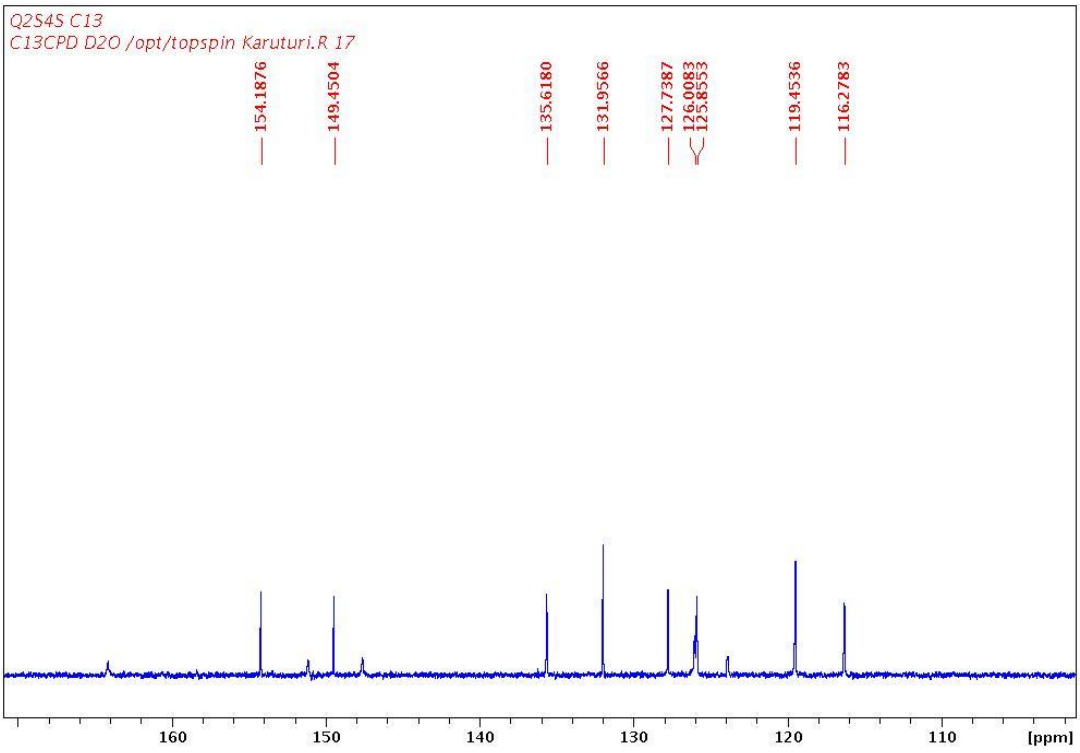

Figure 85

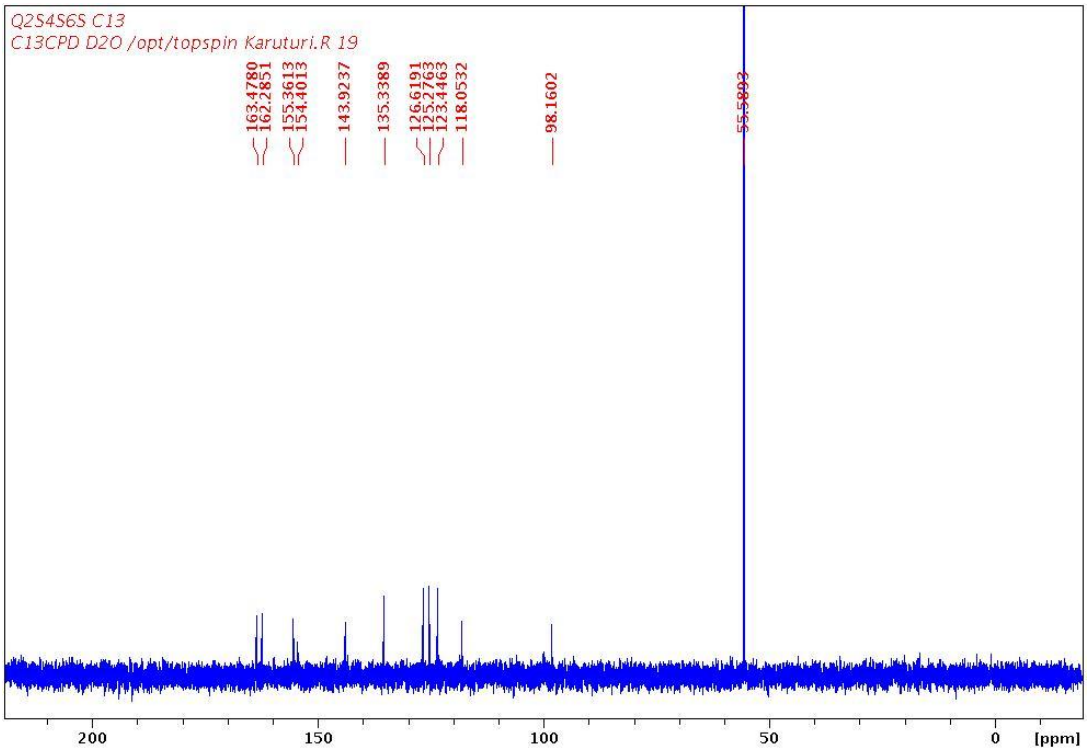

Figure 86

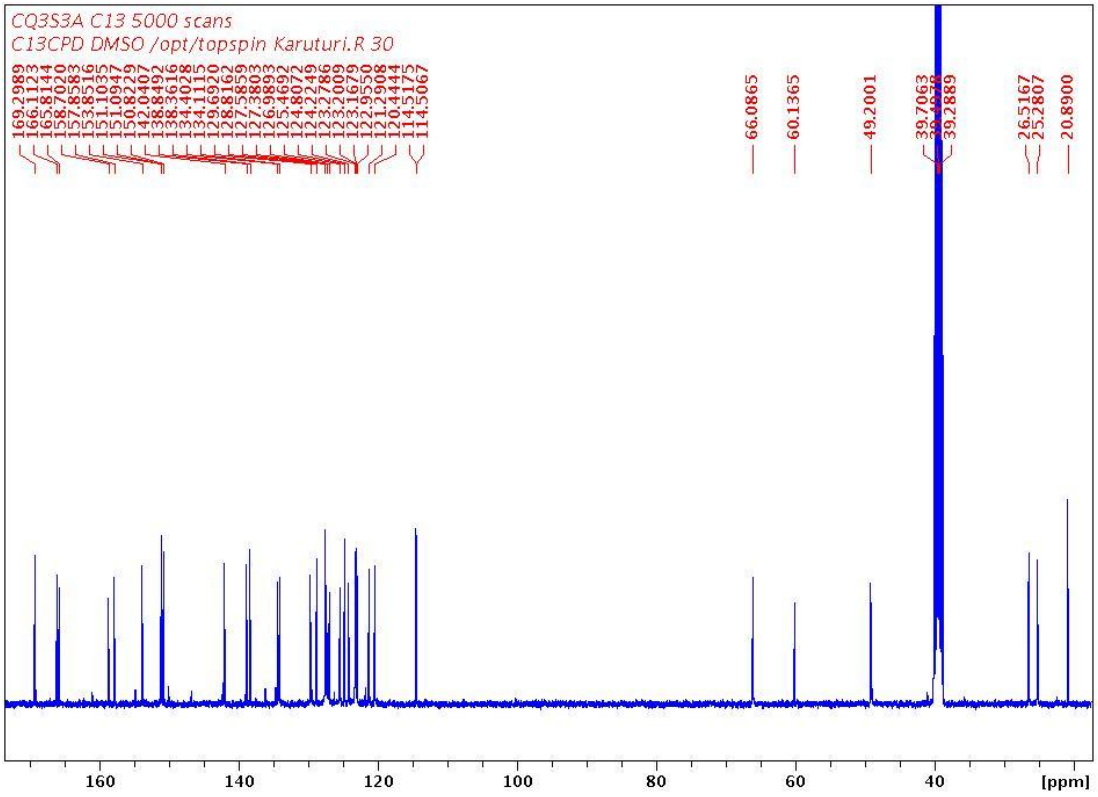

Figure 87

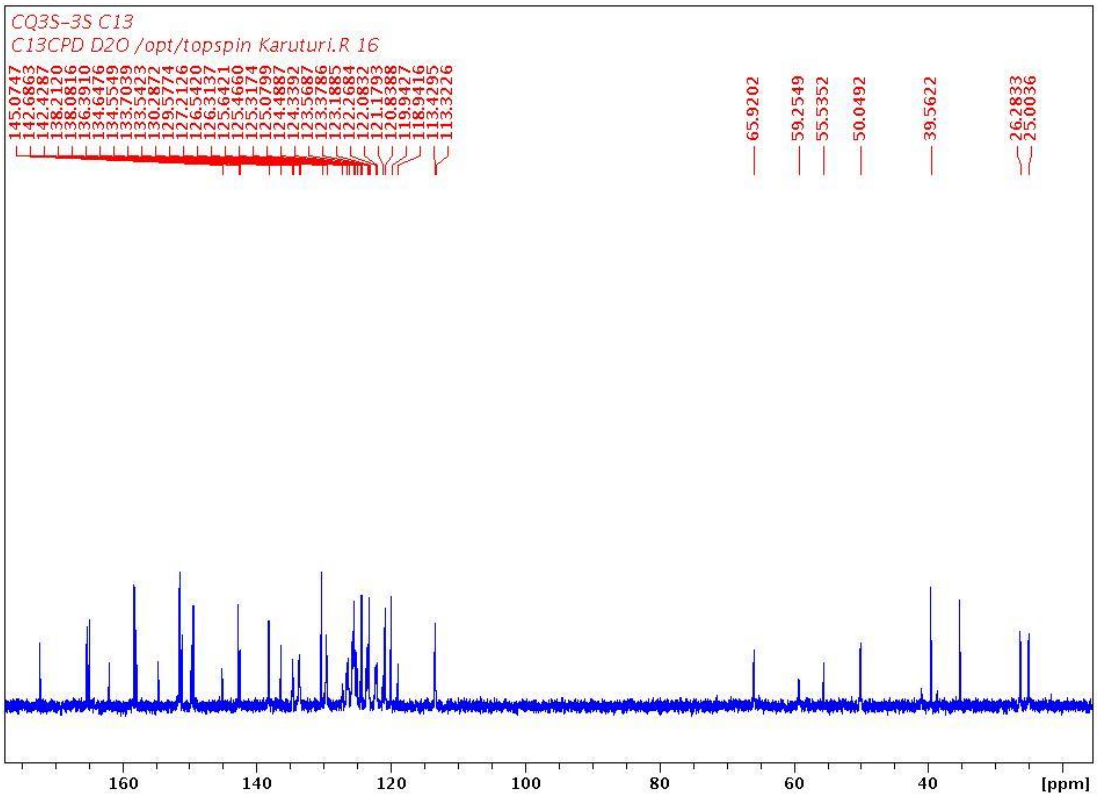

Figure 88

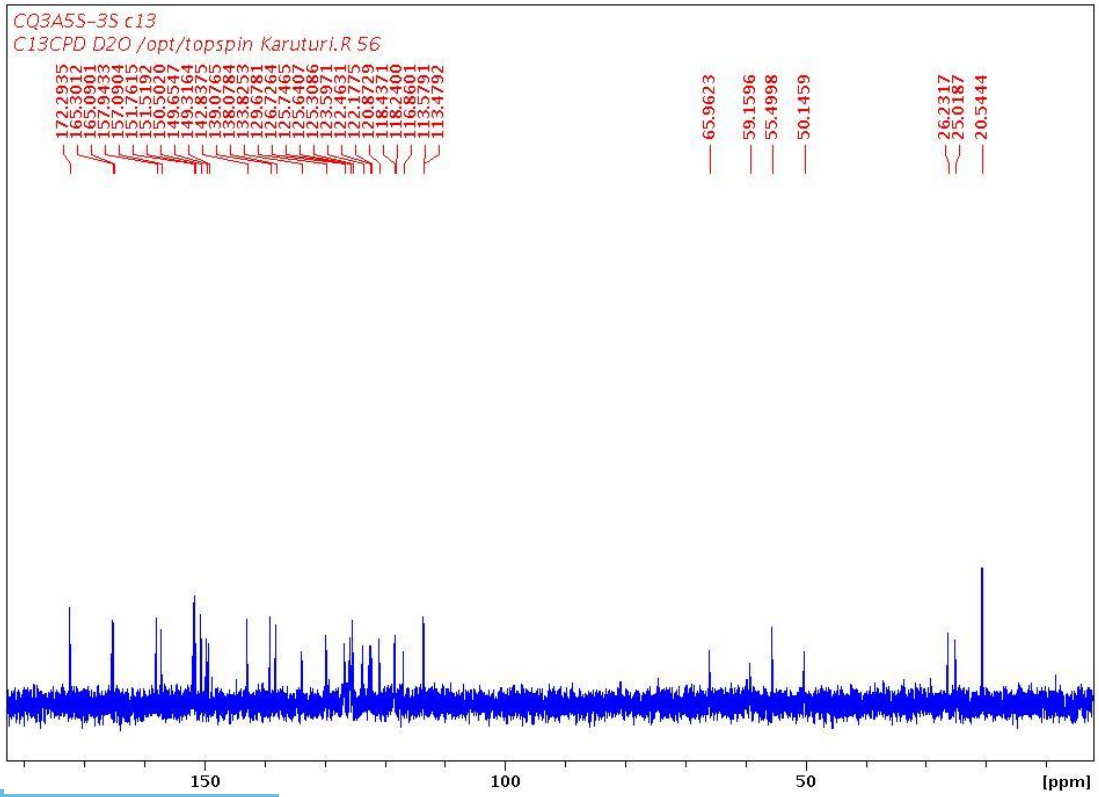

Figure 89

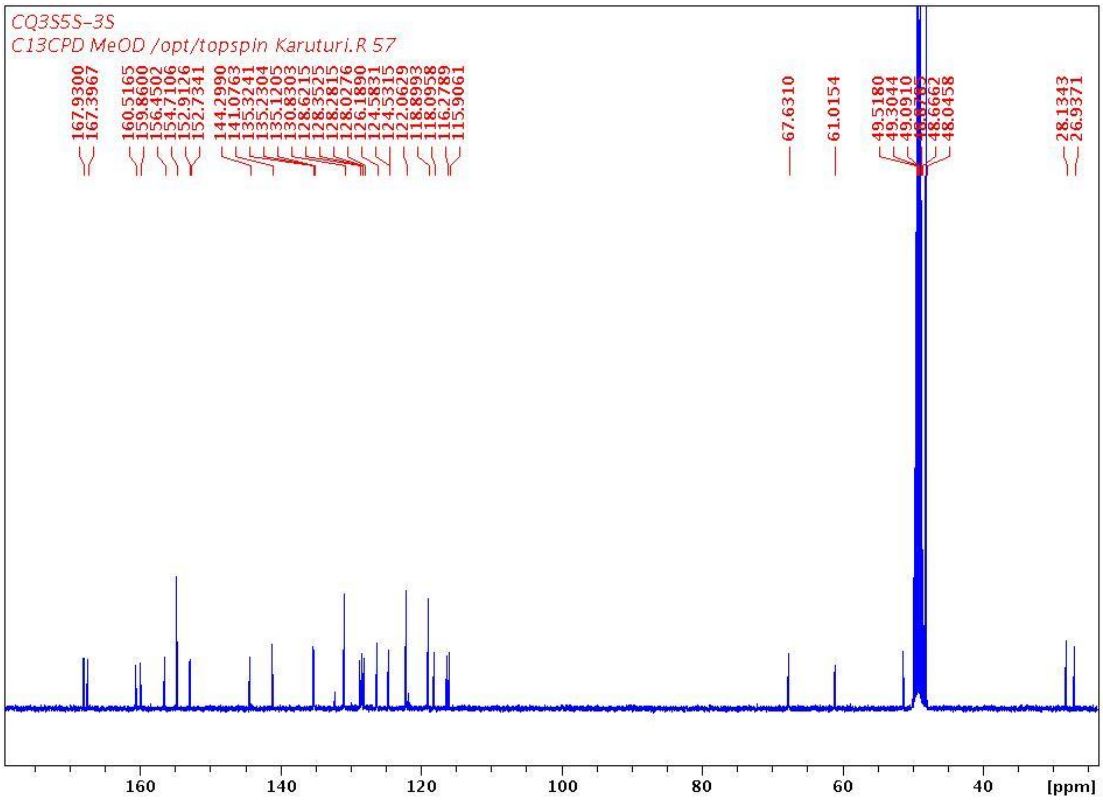

Figure 90

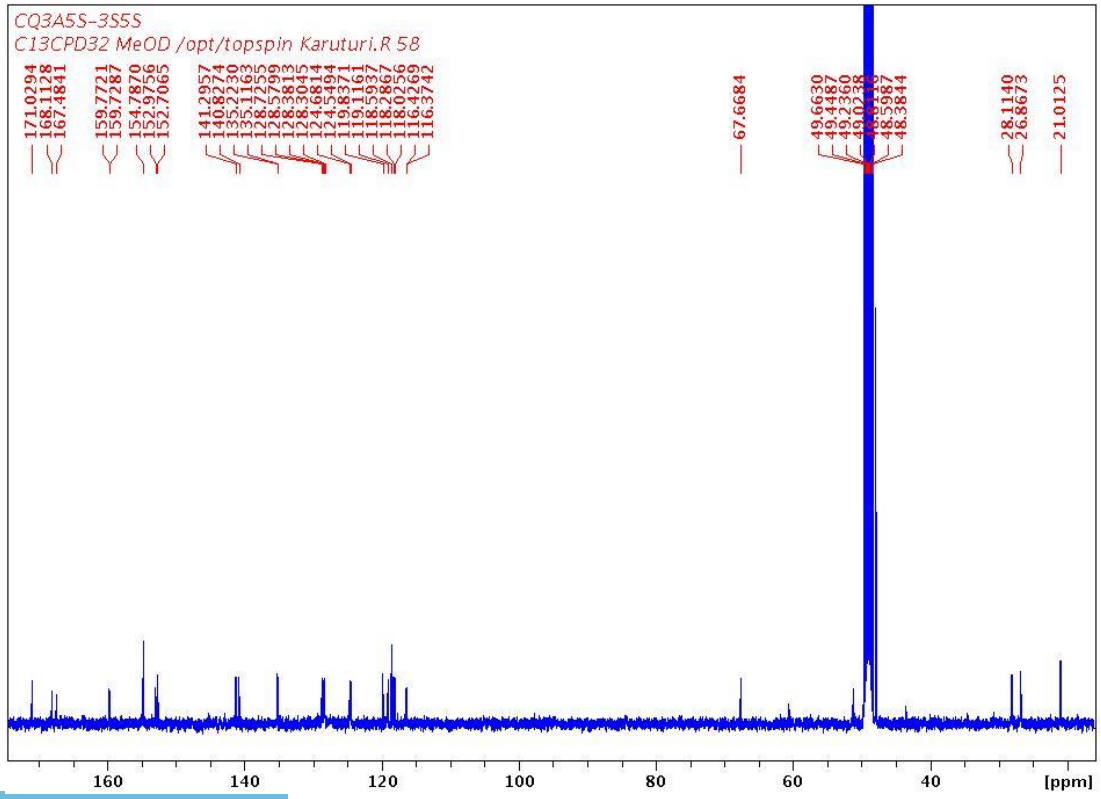

Figure 91

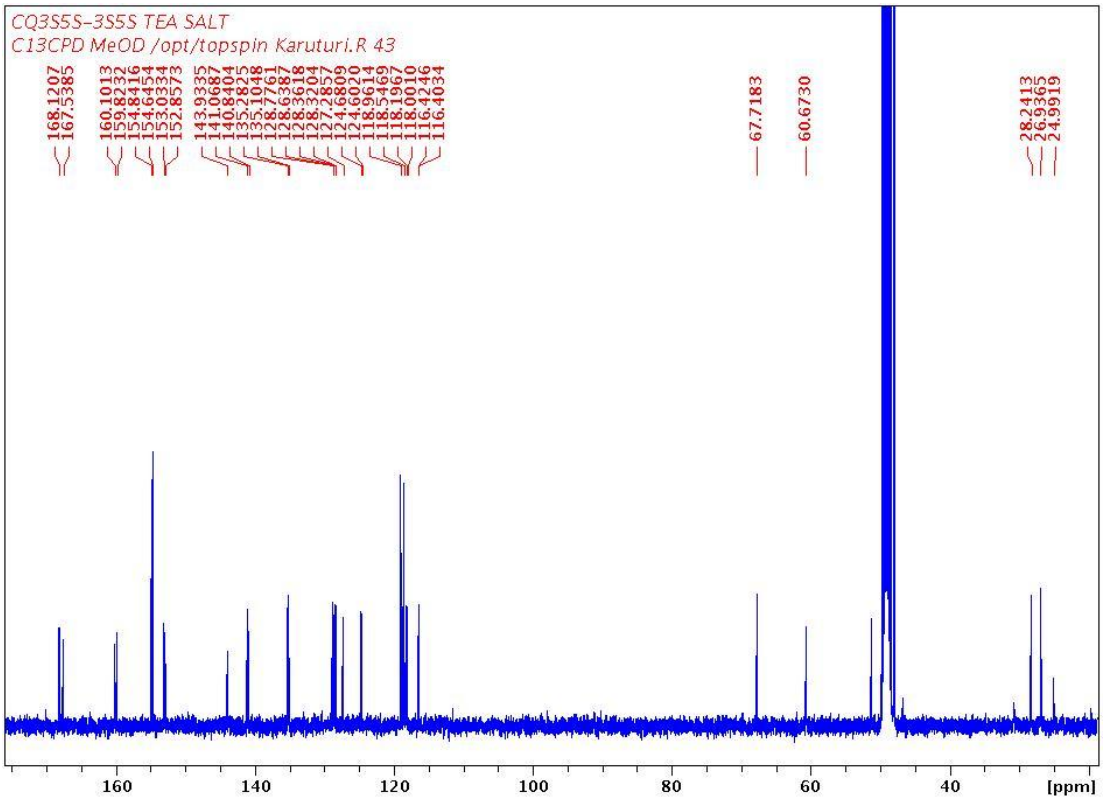

Figure 92

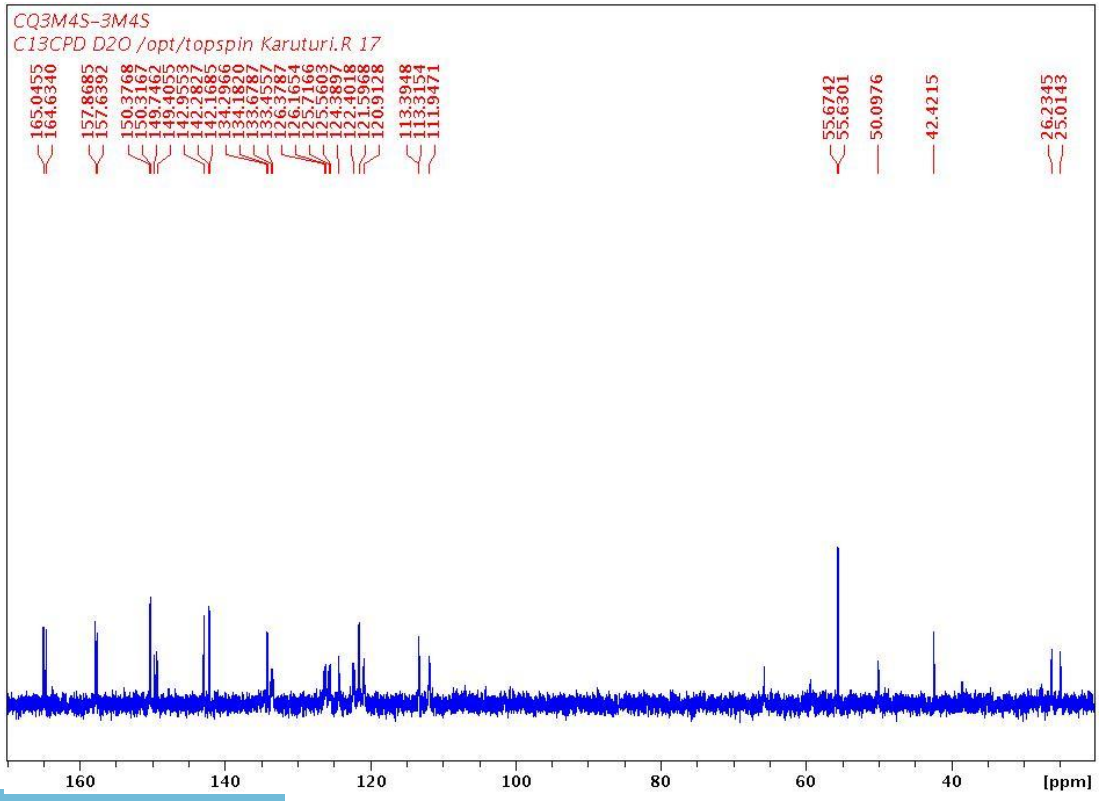

Figure 93

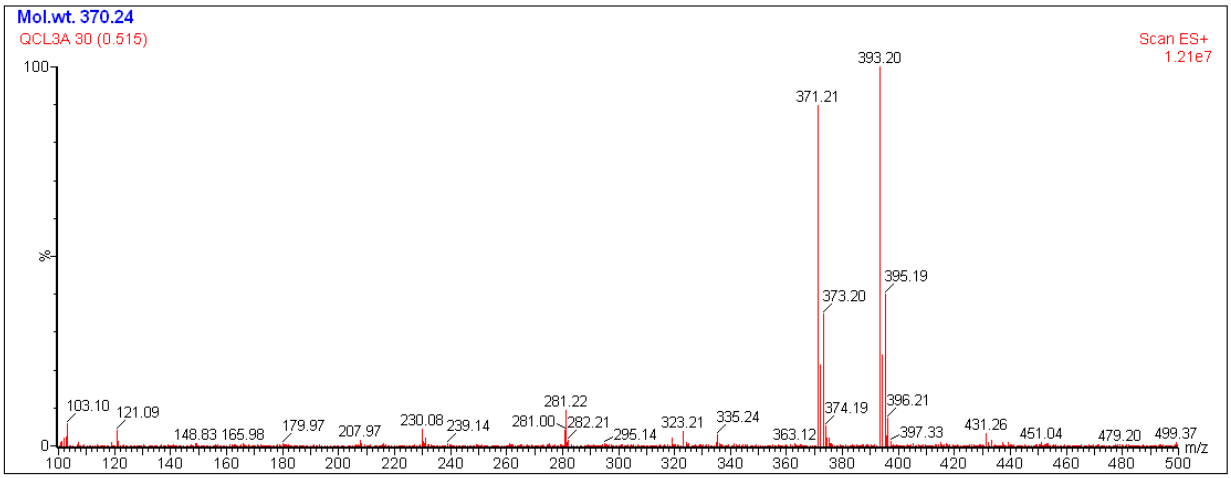

Figure 54

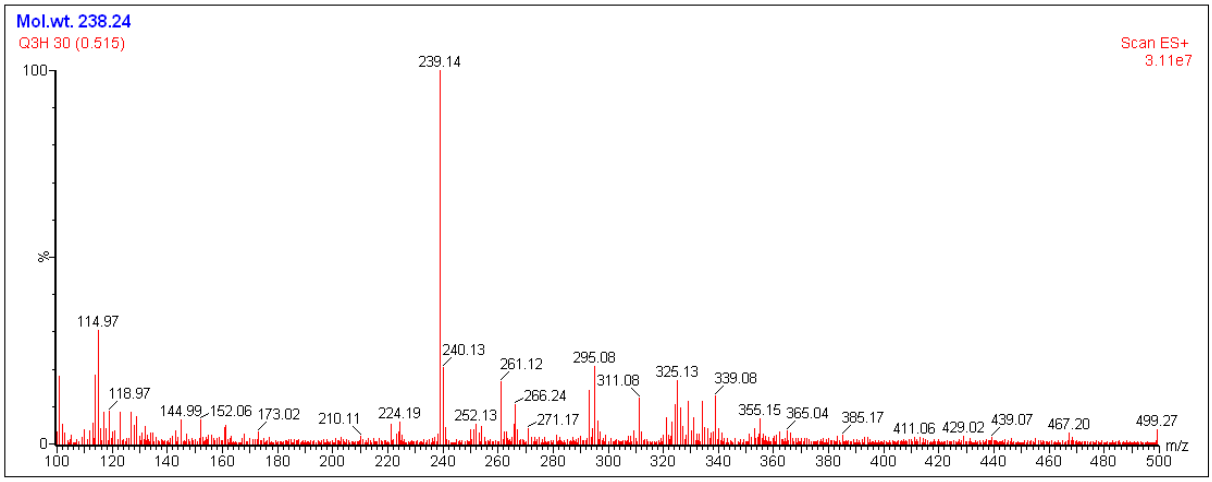

Figure 94

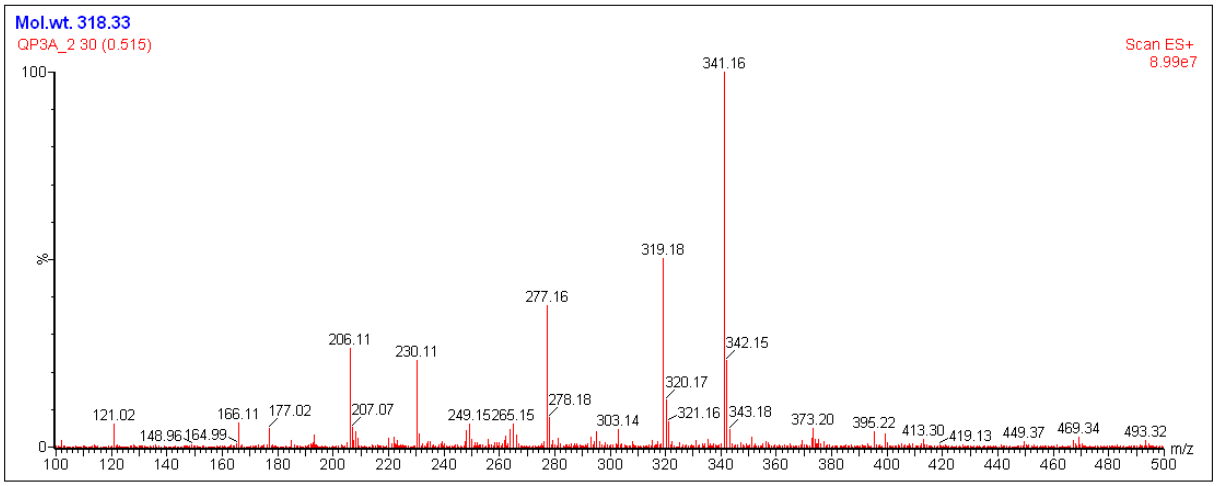

Figure 95

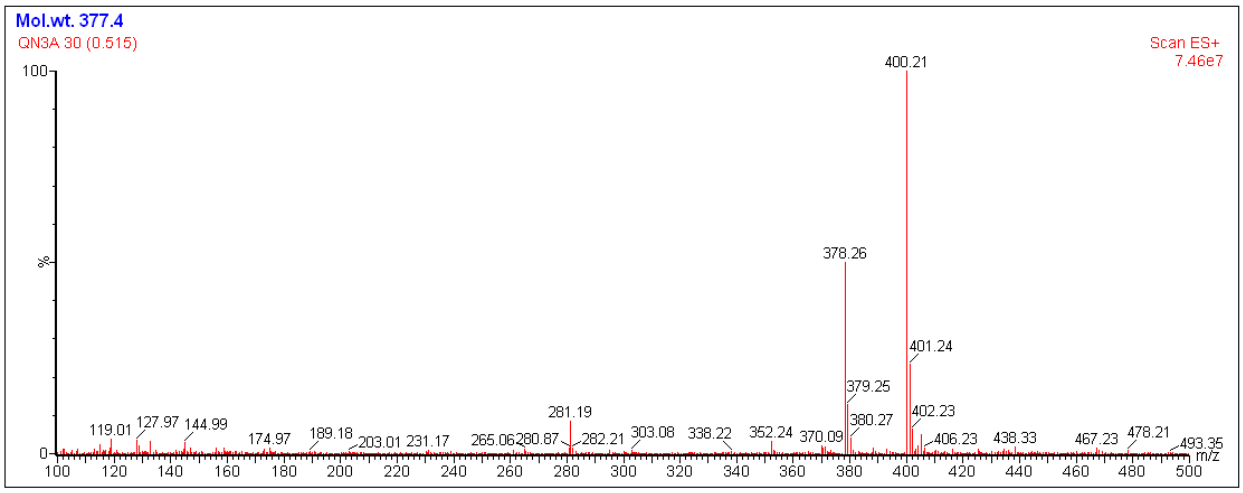

Figure 96

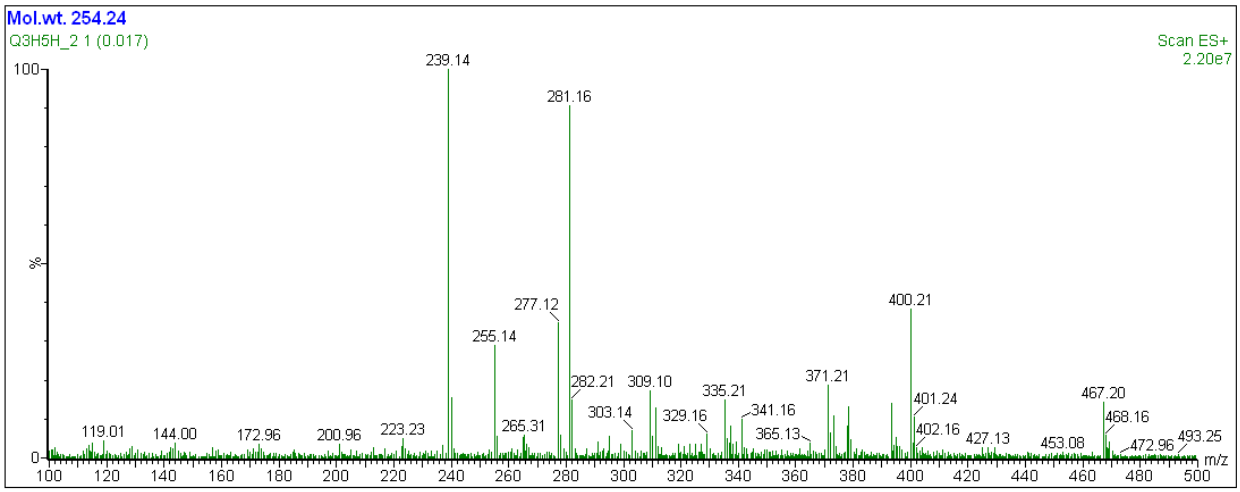

Figure 97

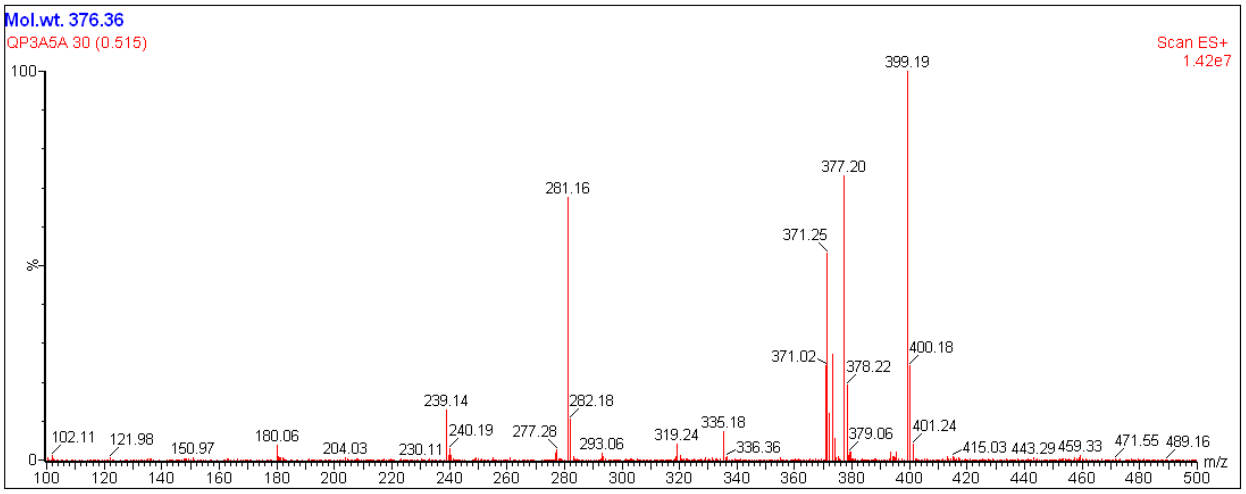

Figure 98

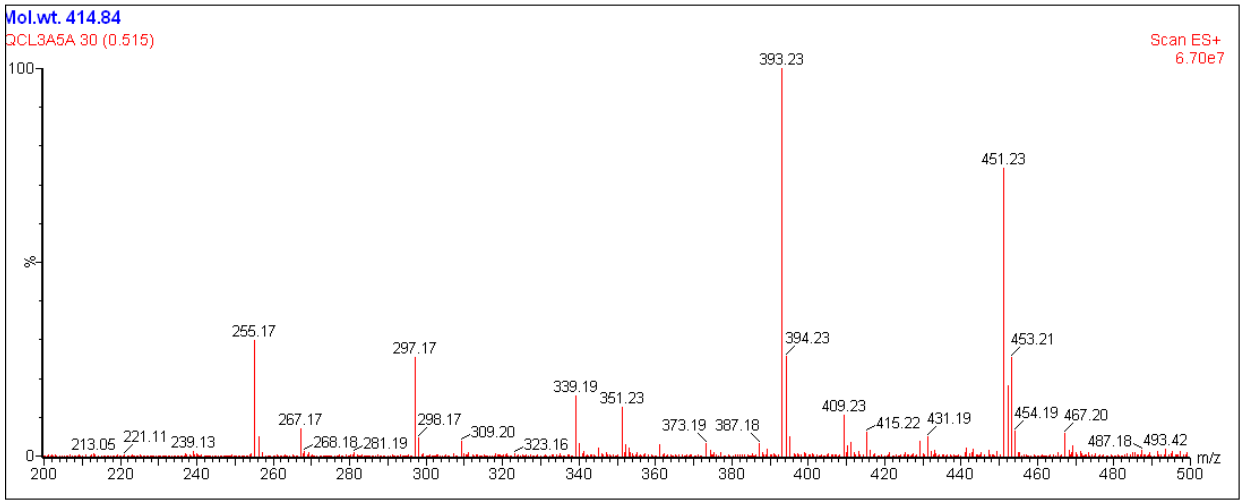

Figure 99

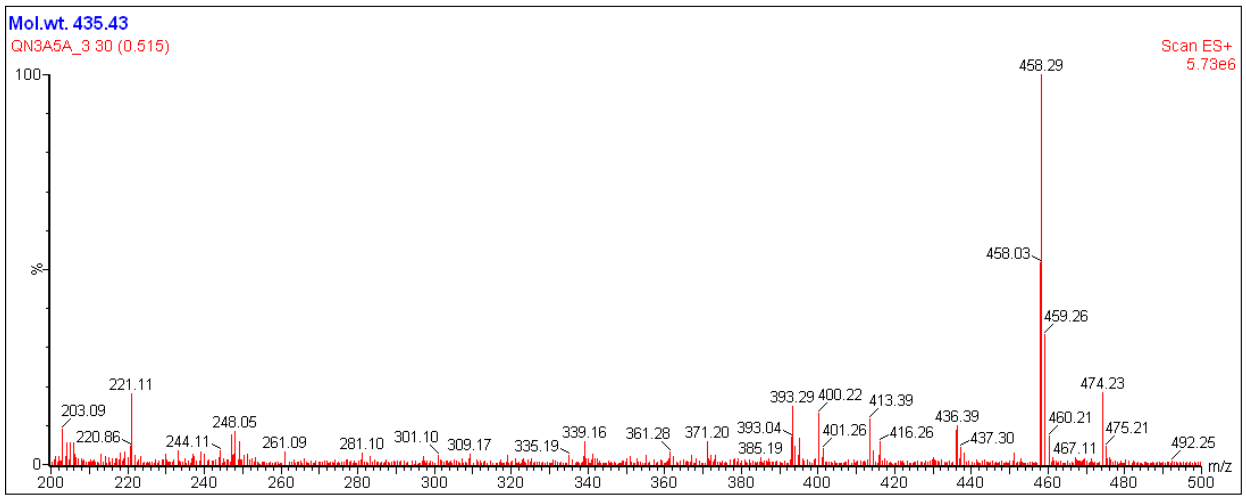

Figure 100

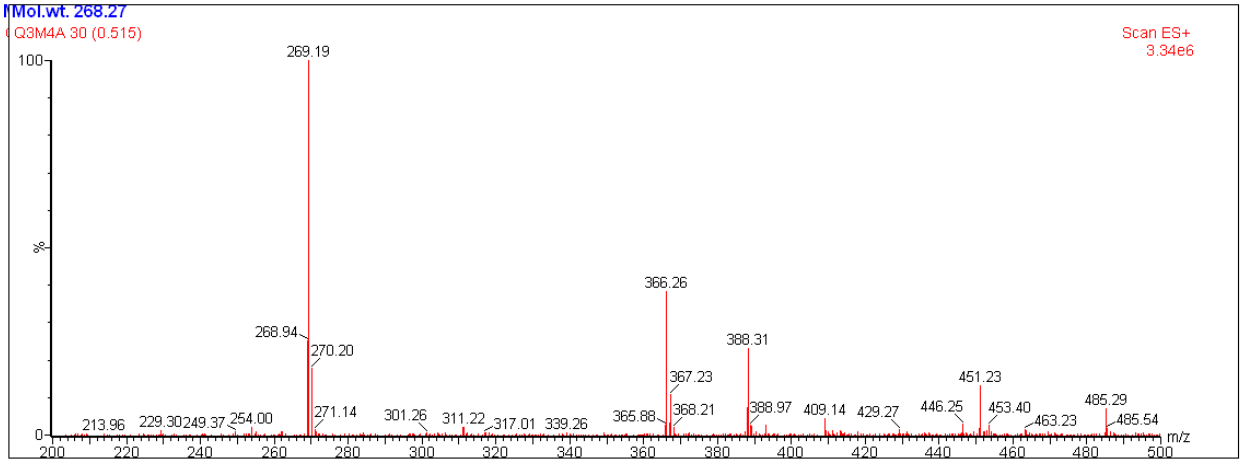

Figure 101

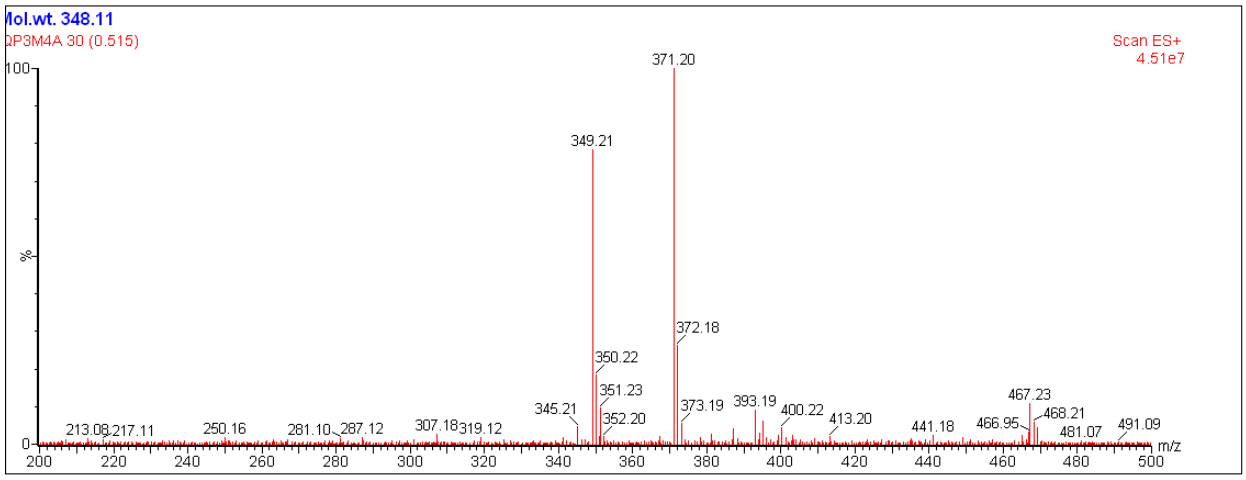

Figure 102

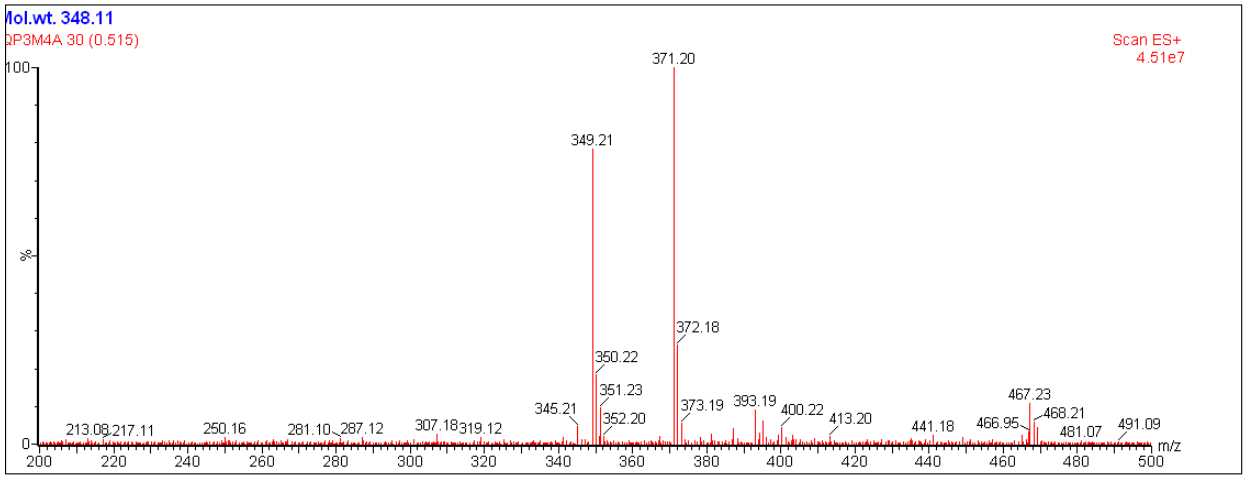

Figure 103

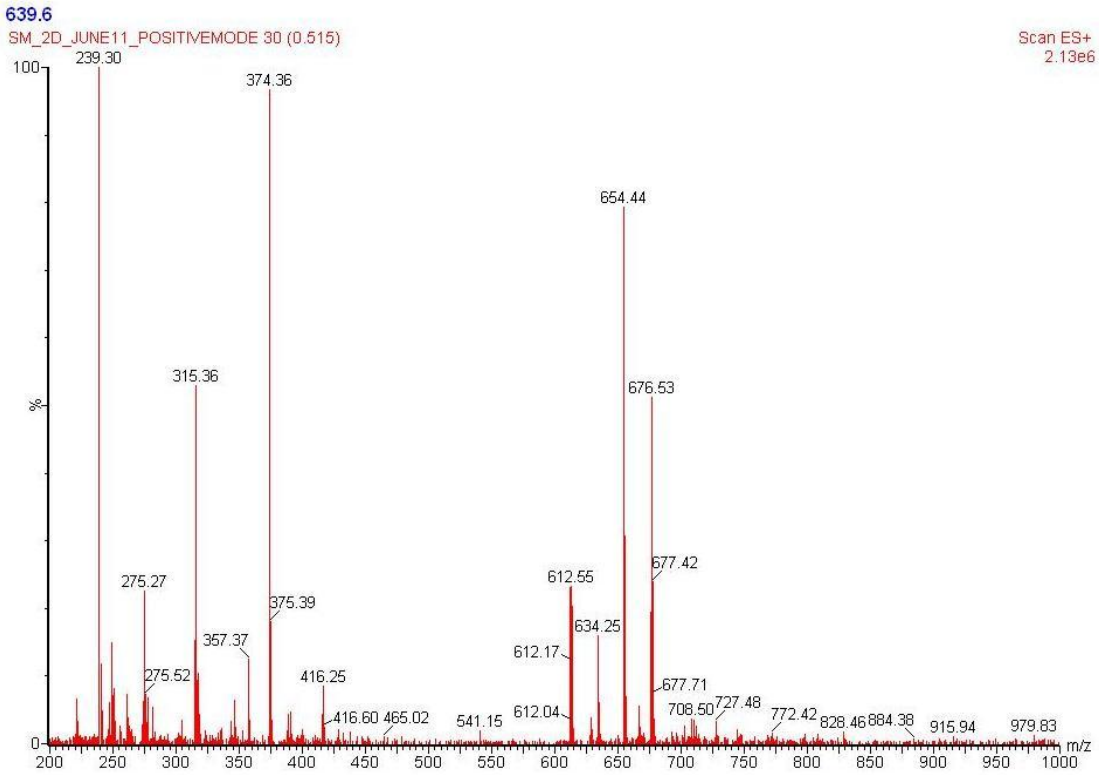

Figure 104

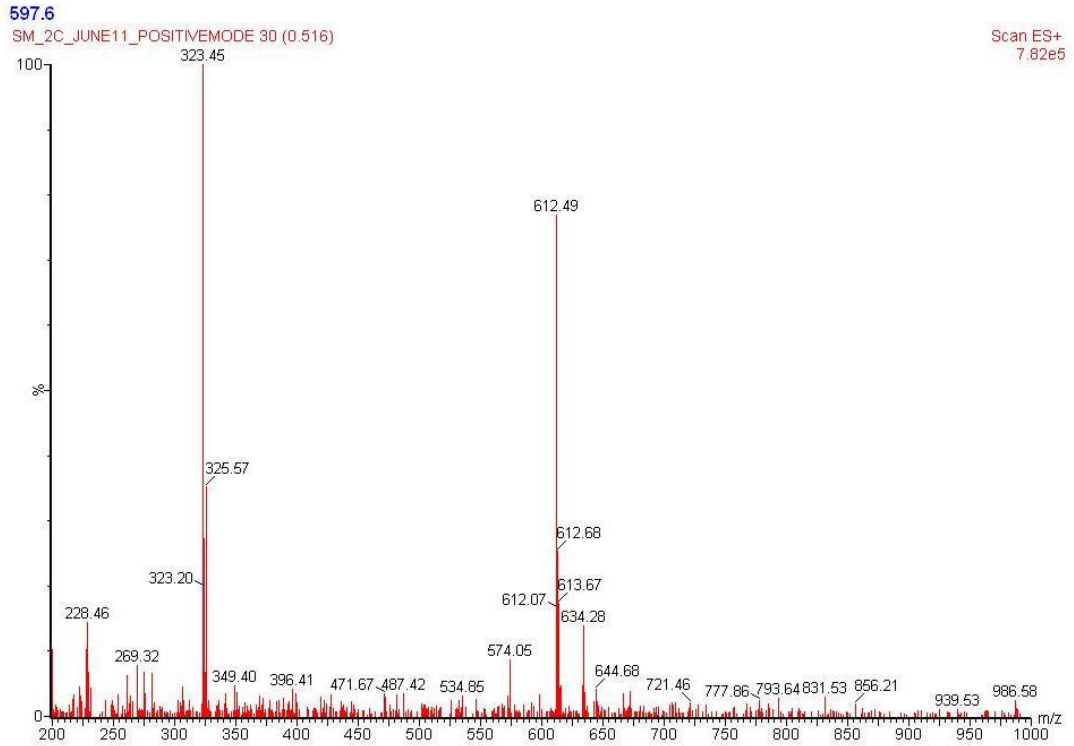

Figure 105

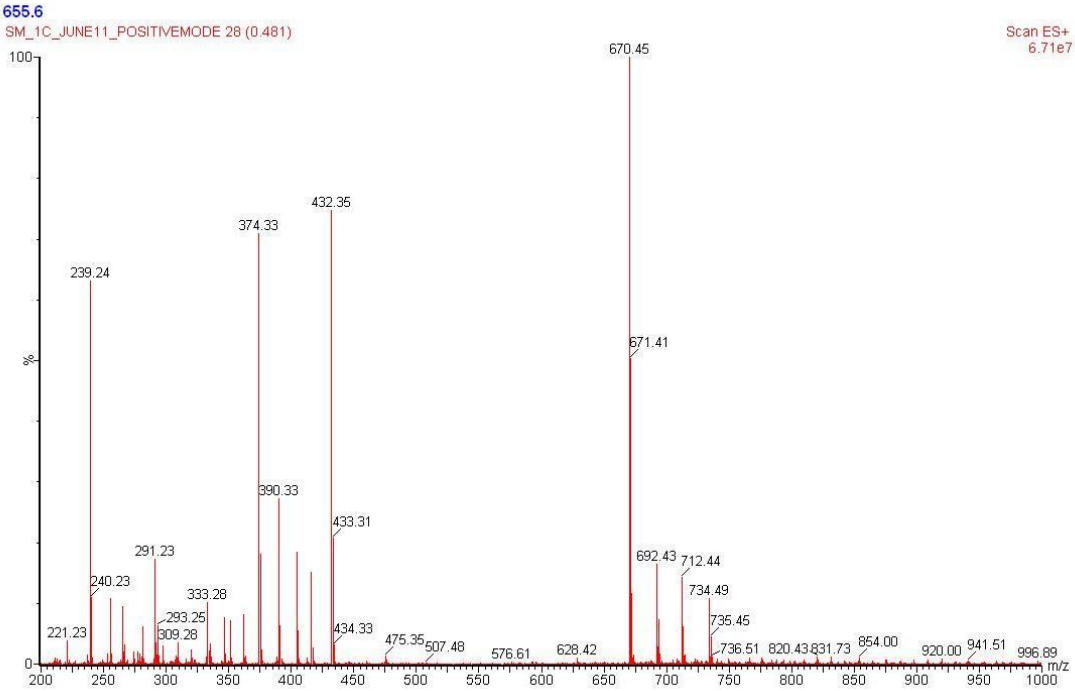

Figure 106

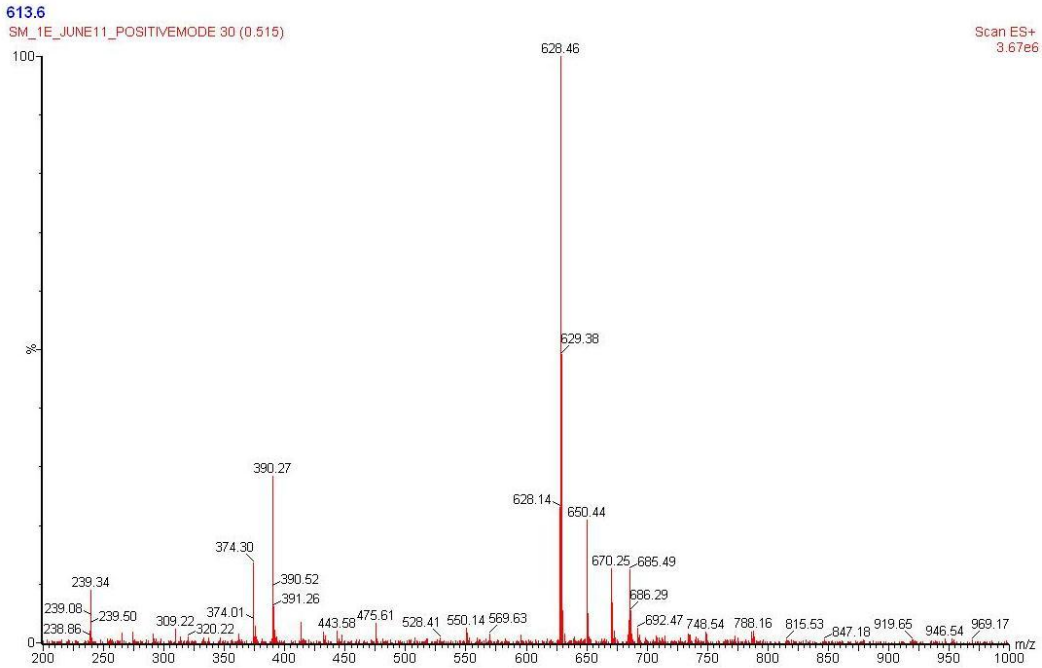

Figure 107

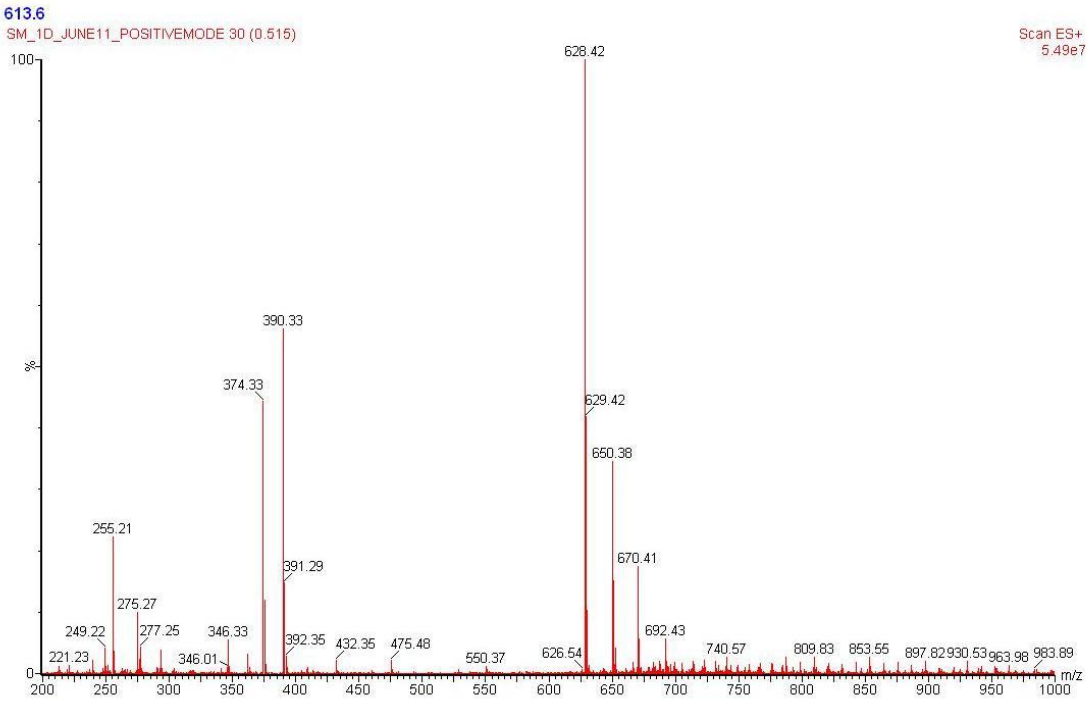

Figure 108

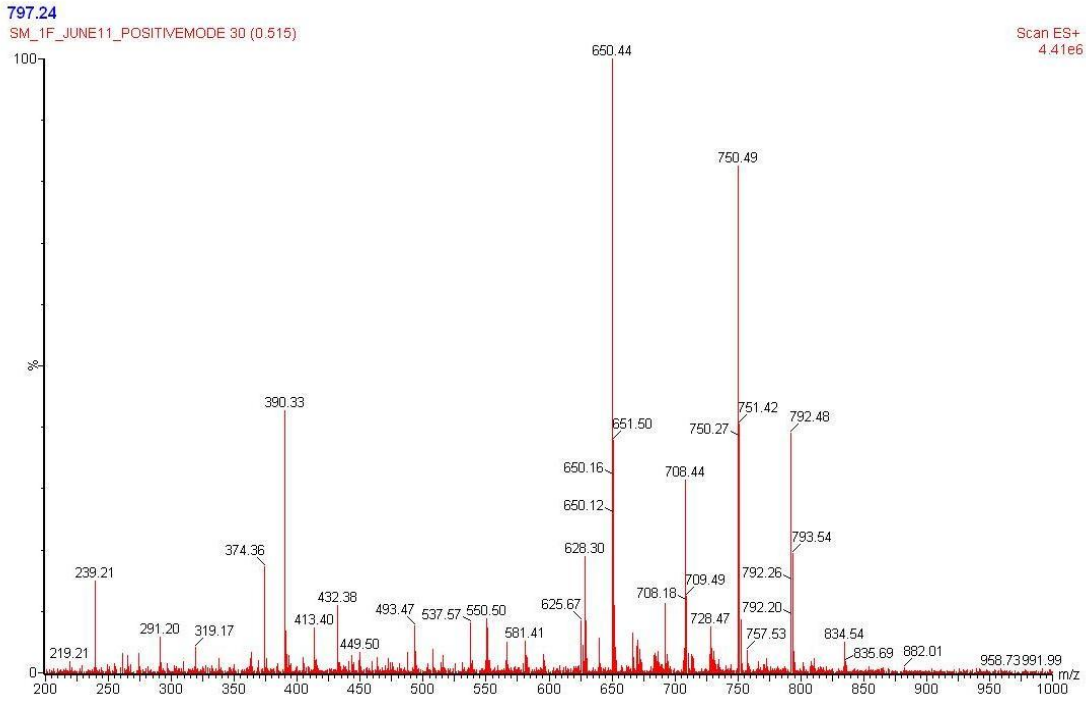

Figure 109

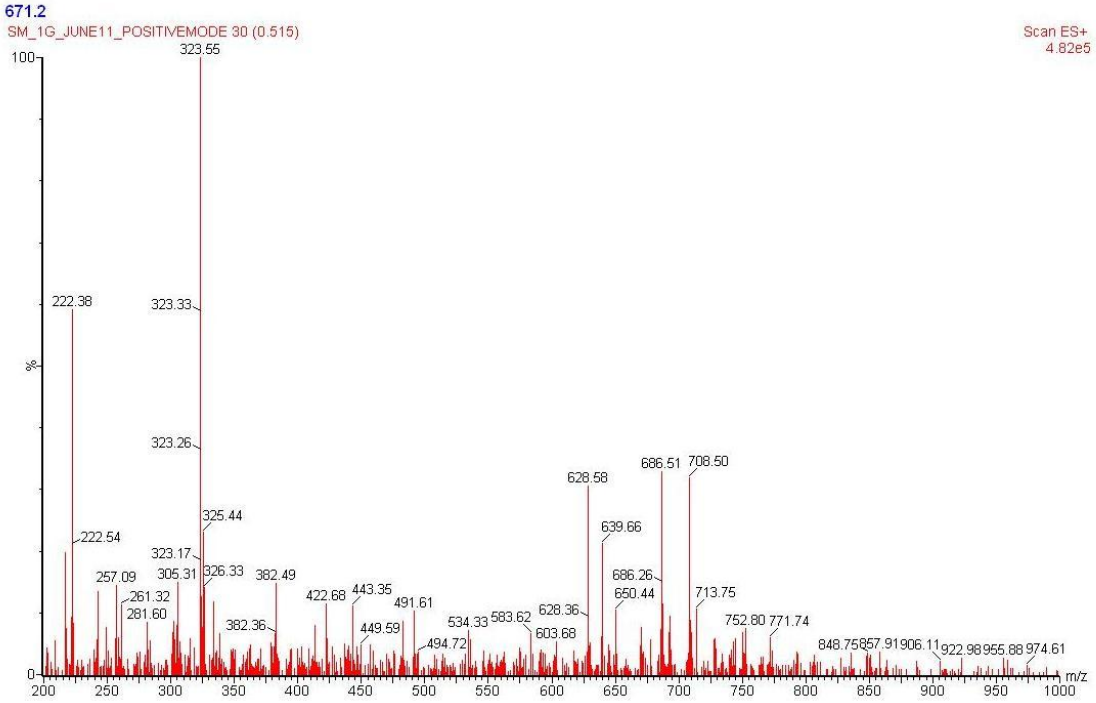

Figure 110

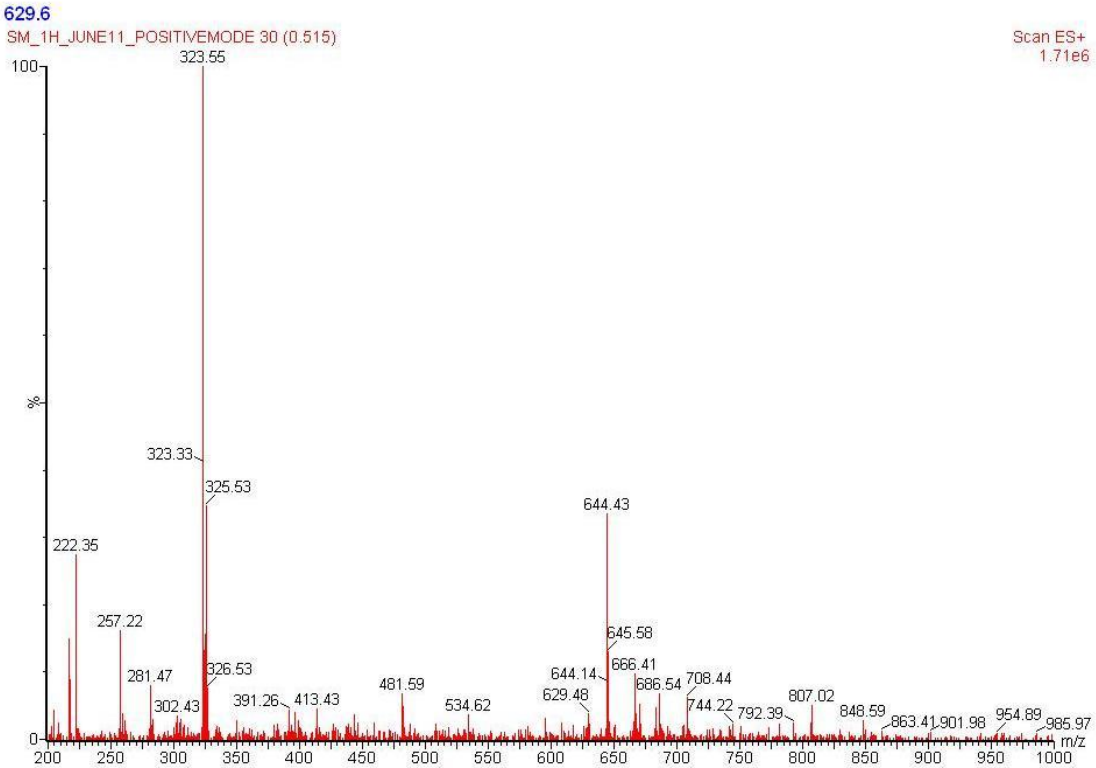

Figure 111

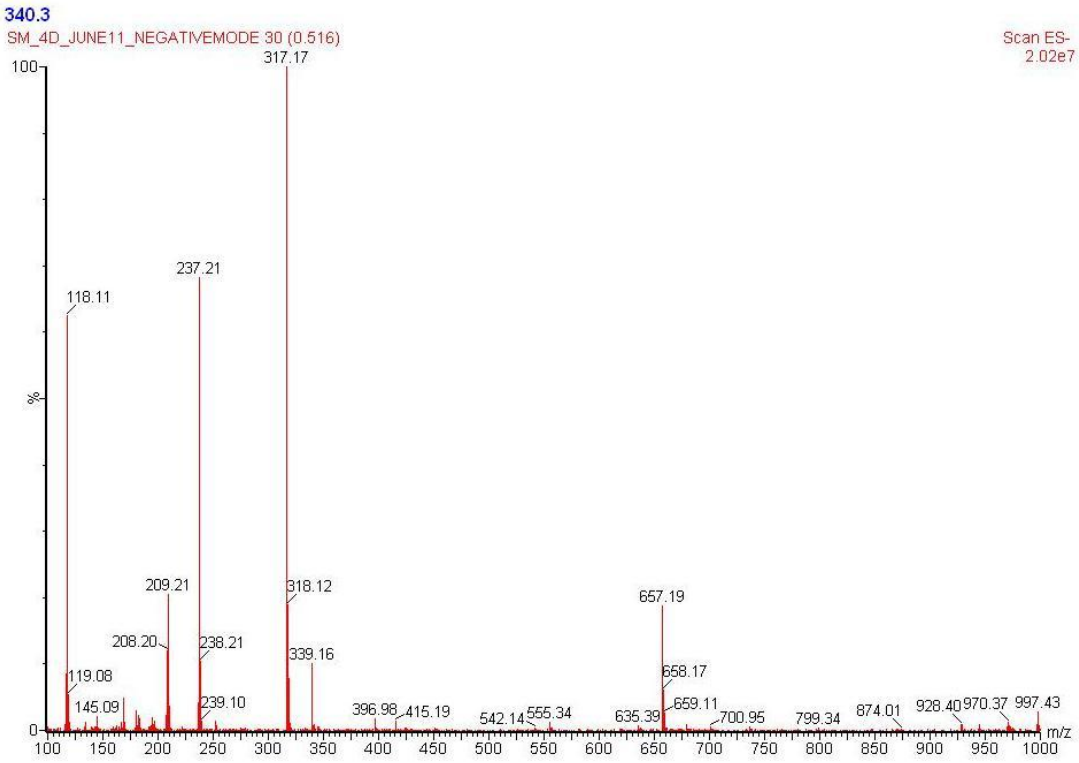

Figure 112

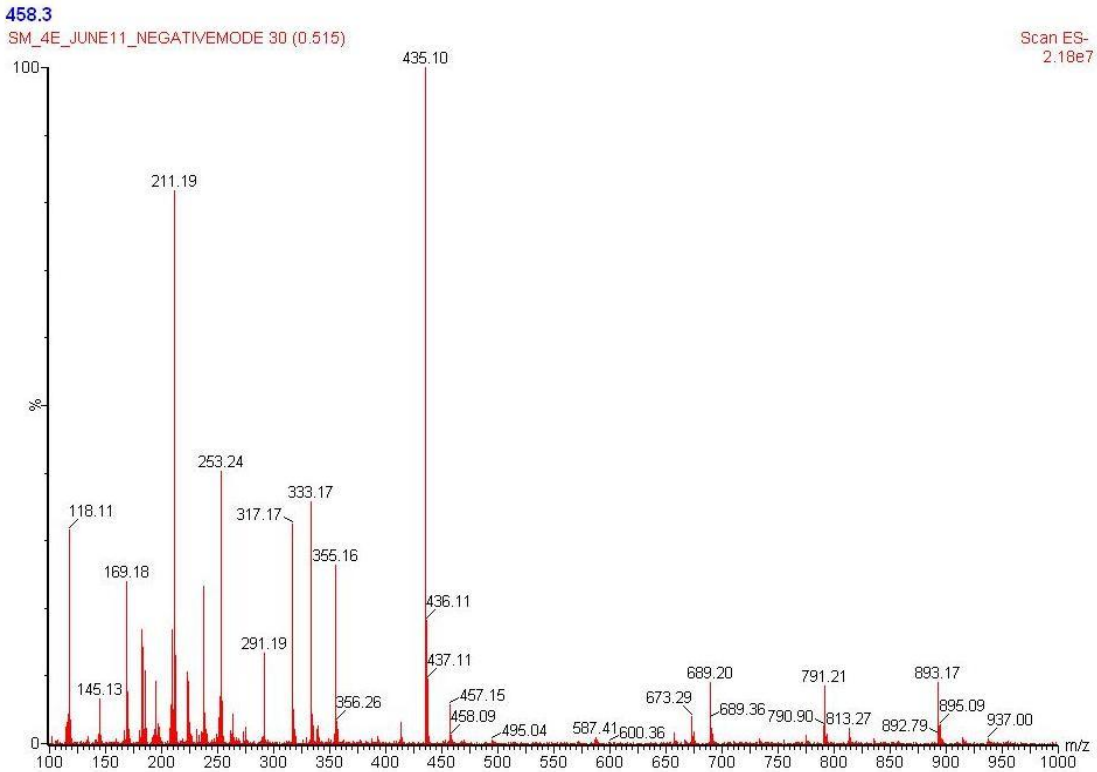

Figure 113

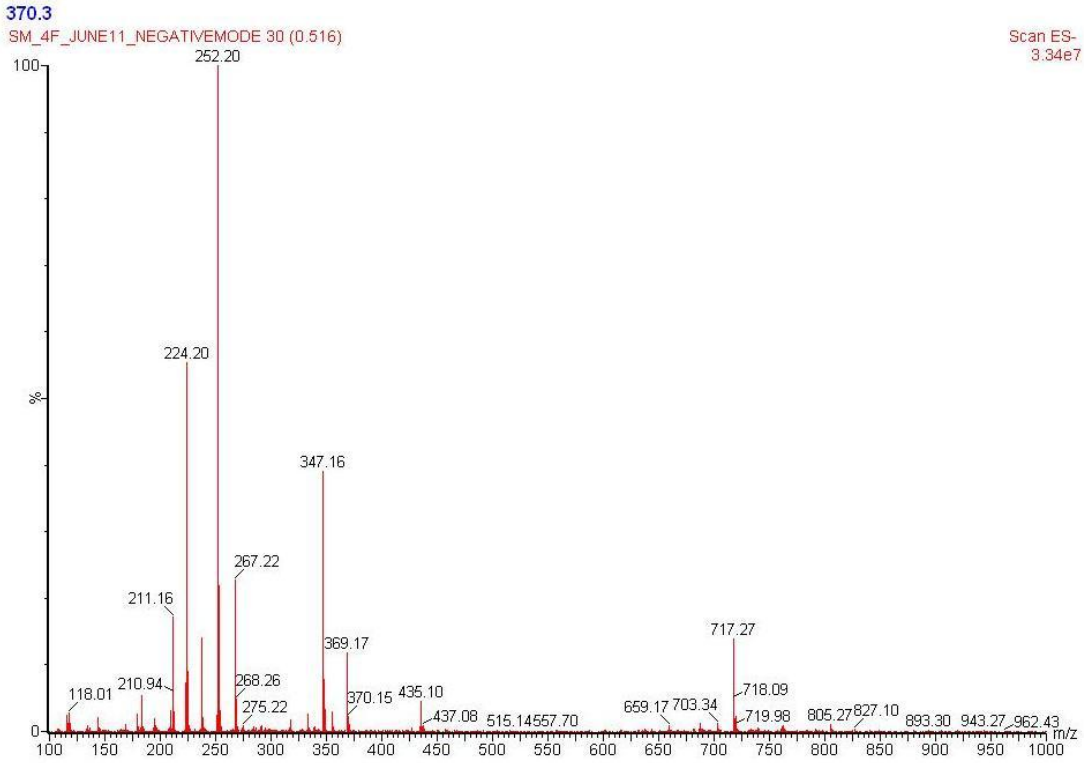

Figure 114

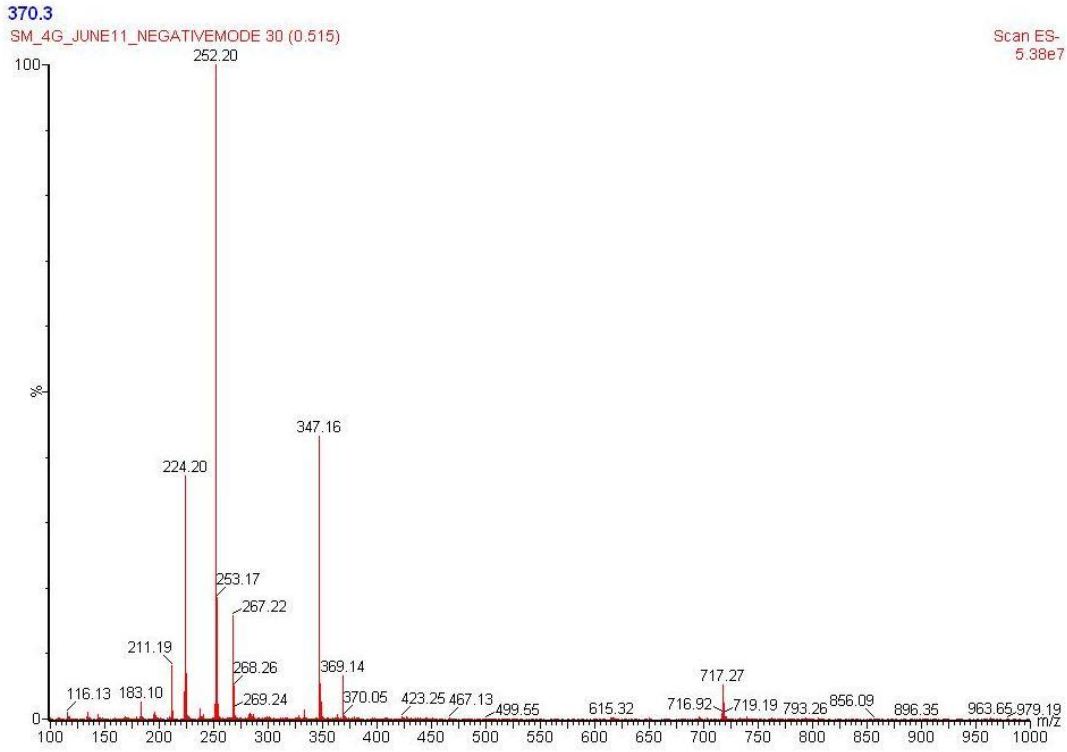

Figure 115

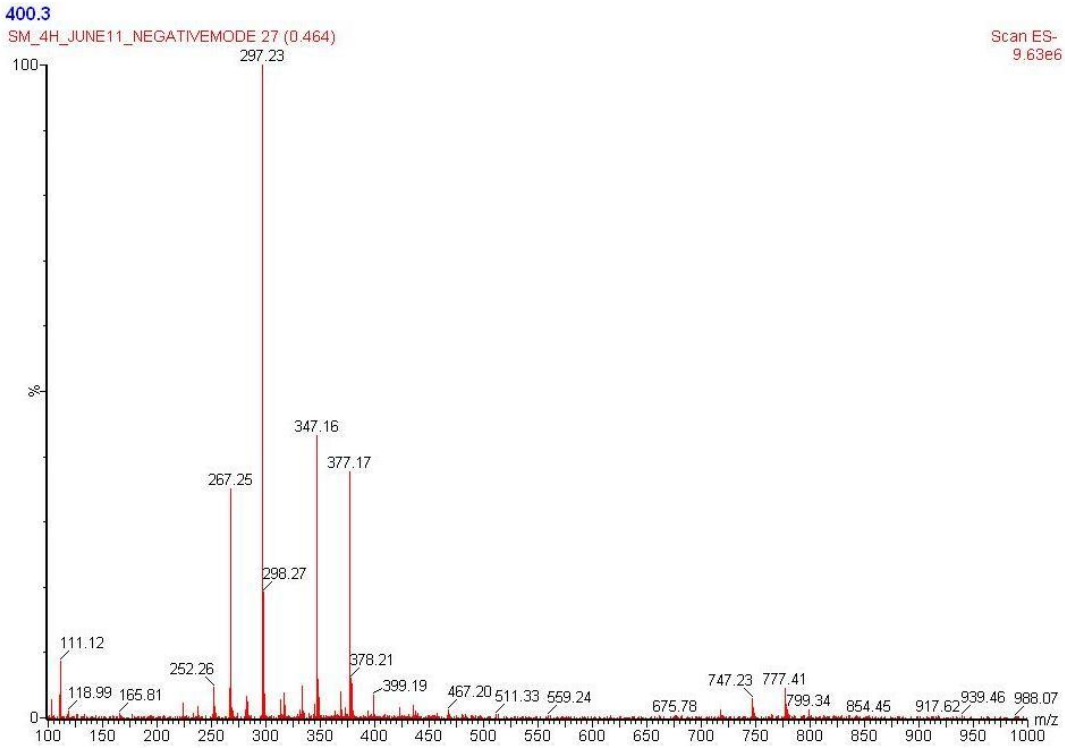

Figure 116

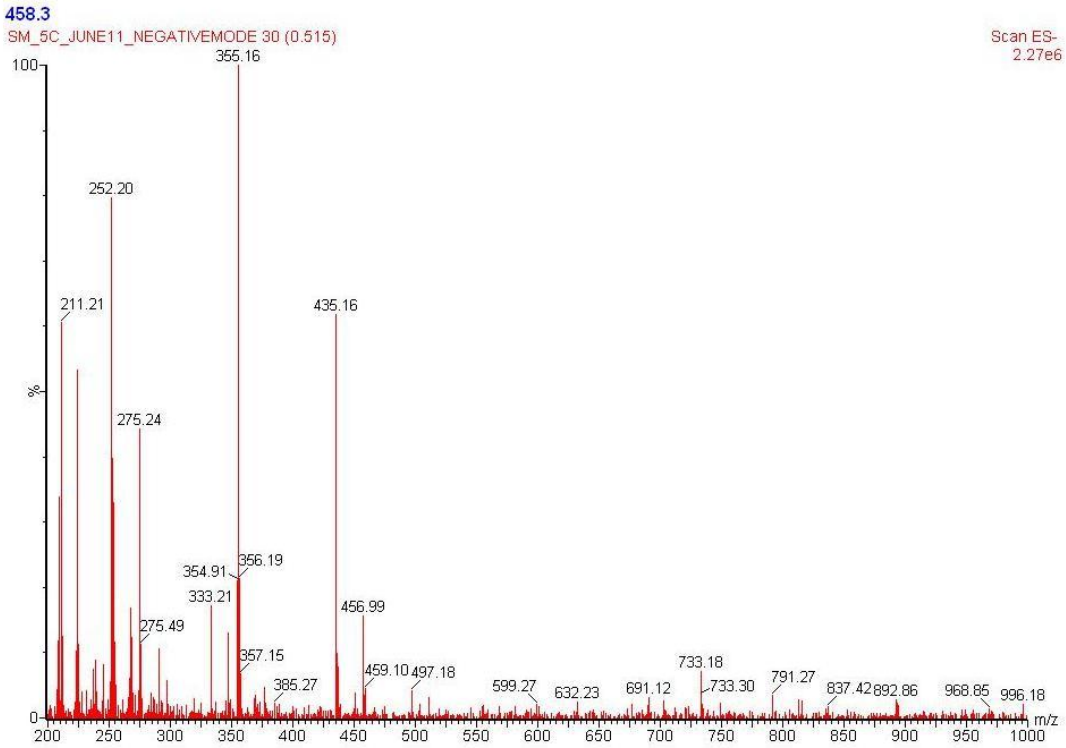

Figure 117

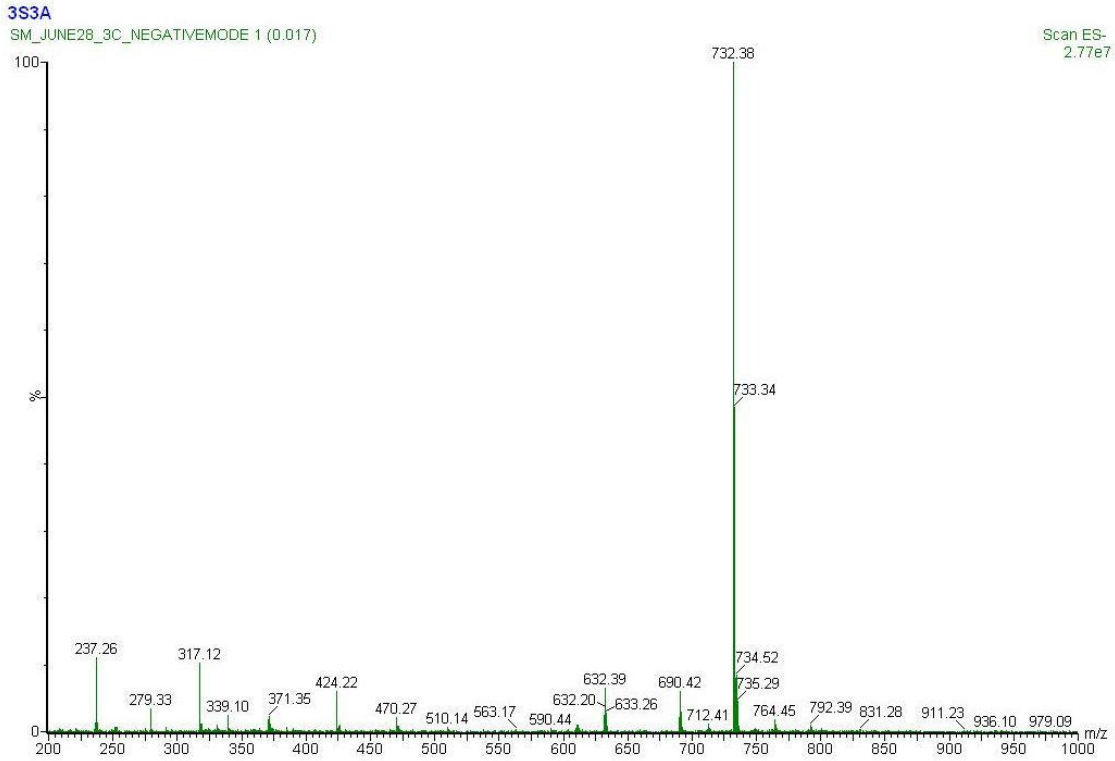

Figure 118

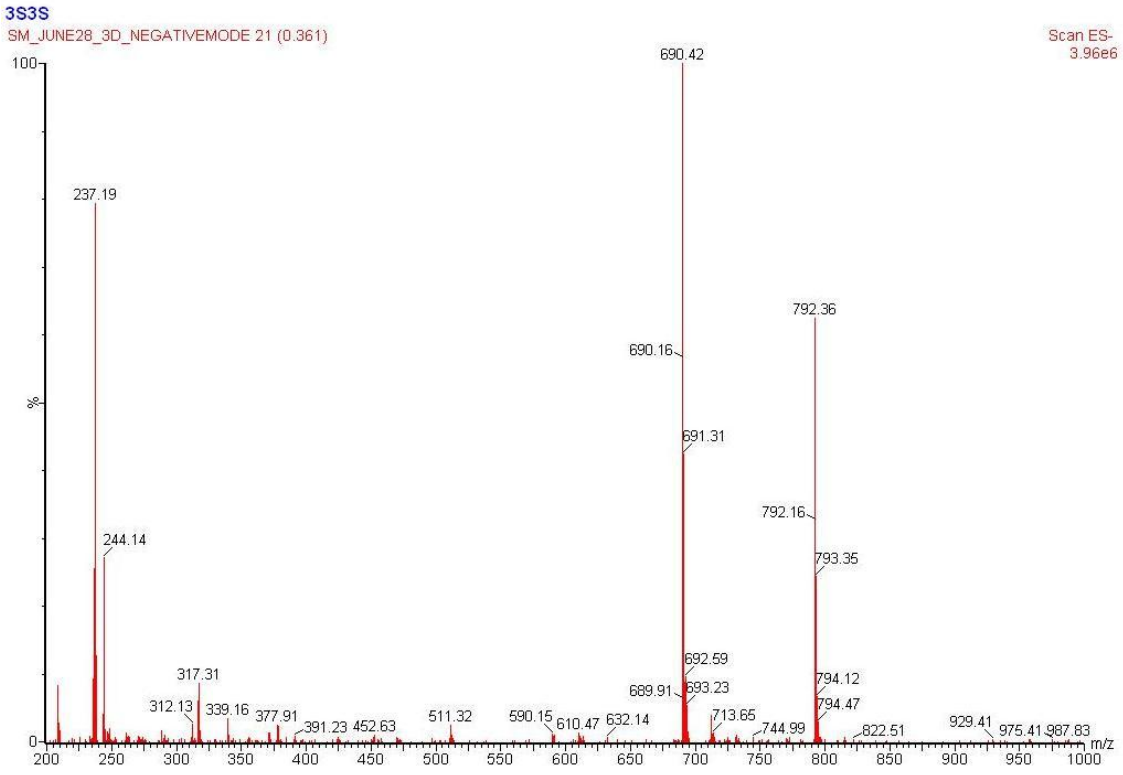

Figure 119

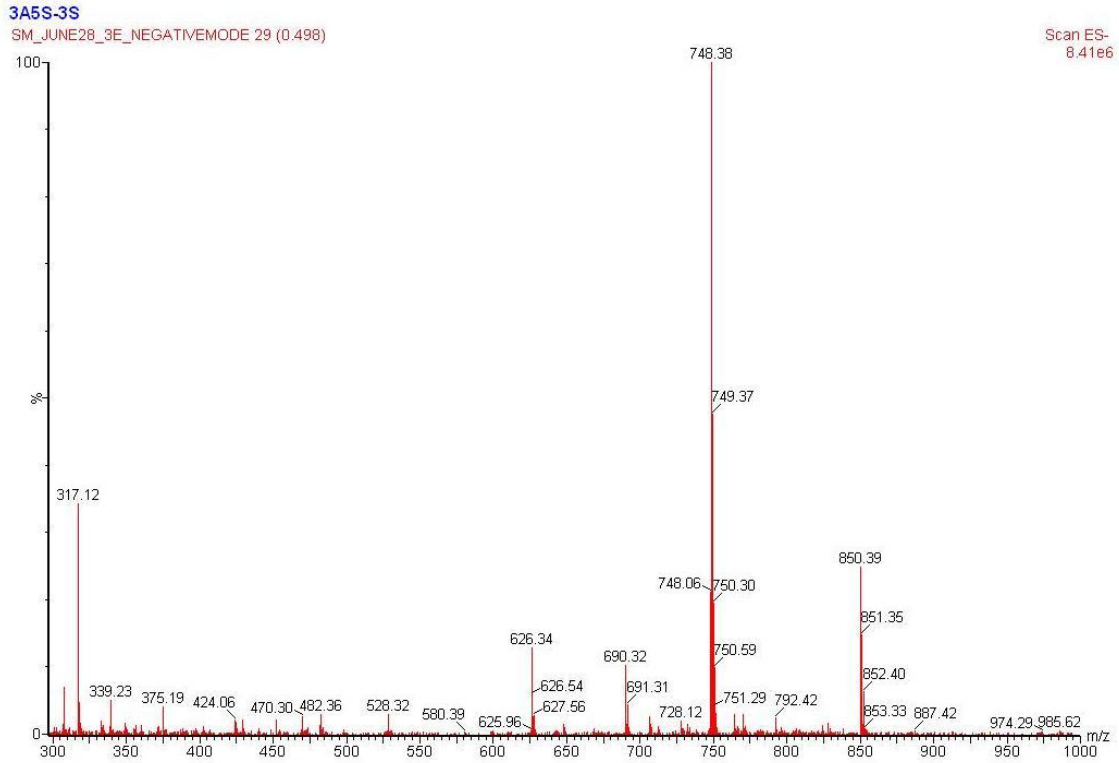

Figure 120

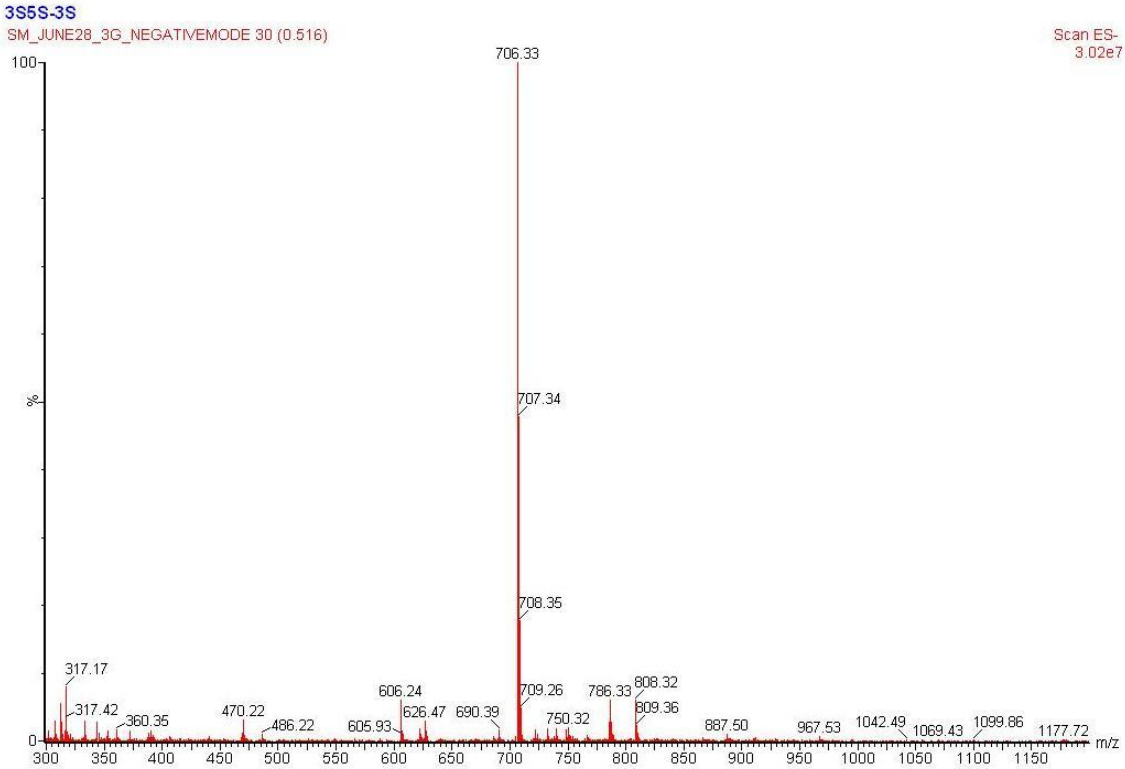

Figure 121

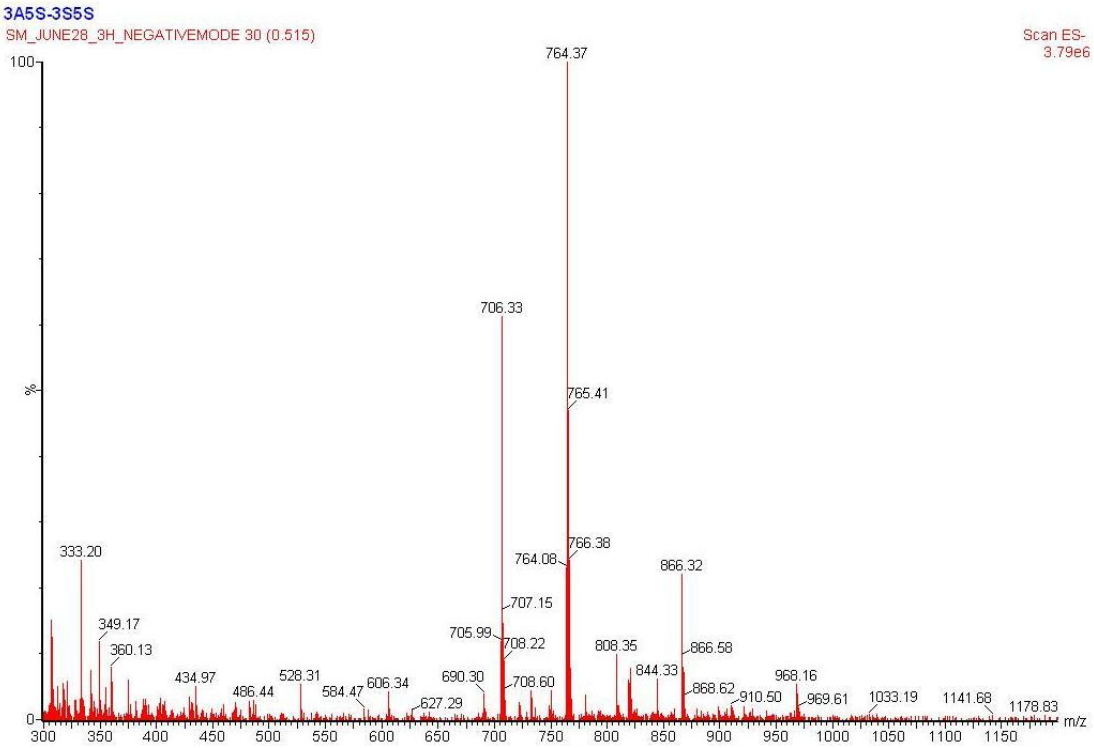

Figure 122

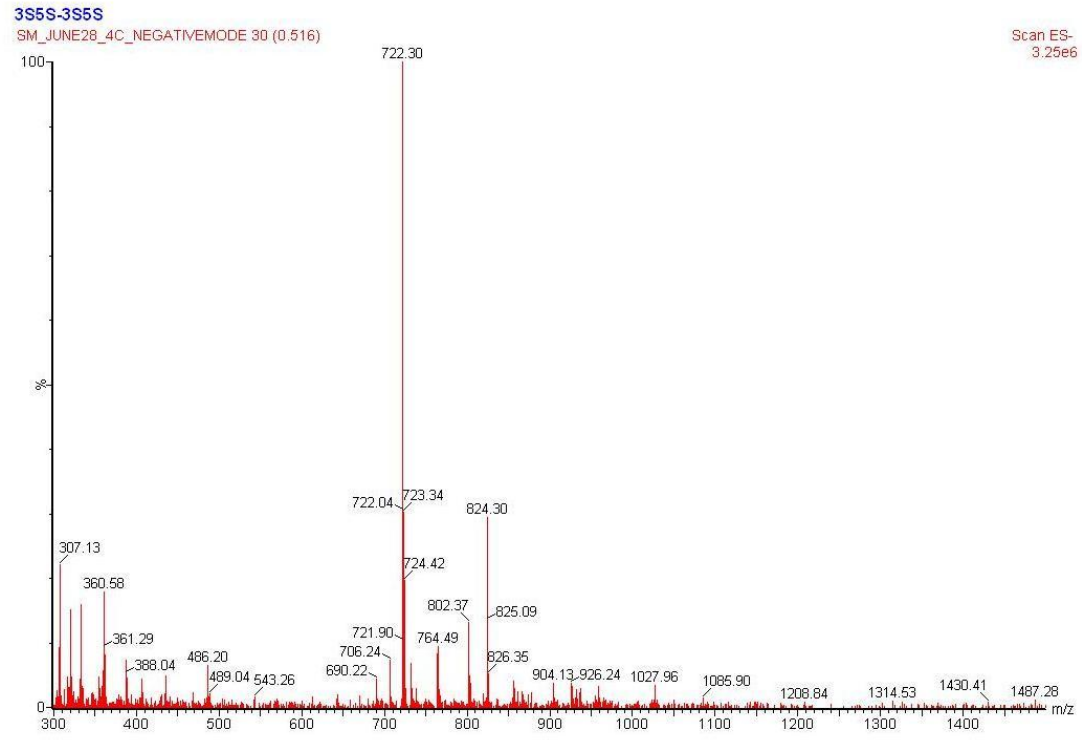

Figure 123

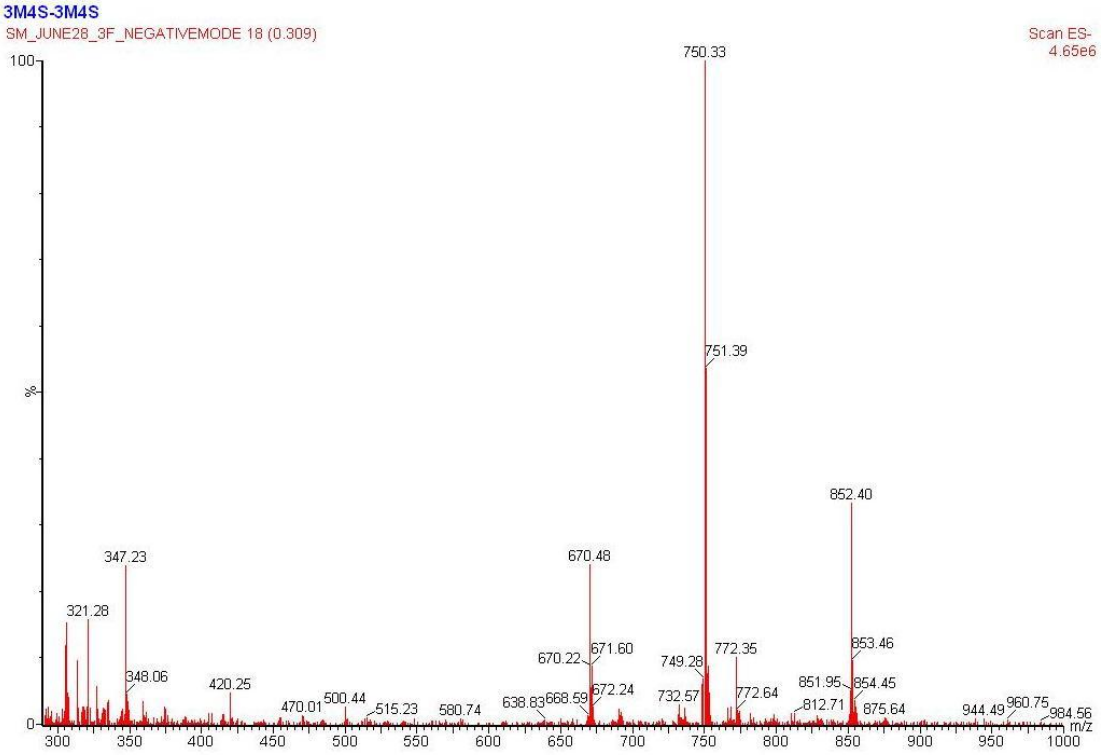

VITA

Shrenik Mehta was born on June 27, 1986 in Mumbai, India and is an Indian citizen. He obtained his Bachelor of Pharmacy degree from Mumbai Educational Trust Institute of Pharmacy in 2009. He began graduate studies in Department of Medicinal Chemistry at Virginia Commonwealth University, Richmond, Virginia, USA in August 2009.